69907

SYNCHRONOUS METEOROLOGICAL SATELLITE SYSTEM DESCRIPTION DOCUMENT

VOLUME 3

DECEMBER 1971

GSFC

GODDARD SPACE FLIGHT CENTER

GREENBELT, MARYLAND

SYNCHRONOUS METEOROLOGICAL SATELLITE SYSTEM

DESCRIPTION DOCUMENT

Volume 3

Prepared by

F. B. Pipkin
Project Coordinator

December 1971

GODDARD SPACE FLIGHT CENTER
Greenbelt, Maryland

CONTENTS

Section 5

SUBSYSTEM DESCRIPTION

CONTENTS (continued)

CONTENTS (continued)

CONTENTS (continued)

CONTENTS (continued)

CONTENTS (continued)

ILLUSTRATIONS

ILLUSTRATIONS (continued)

ILLUSTRATIONS (continued)

ILLUSTRATIONS (continued)

ILLUSTRATIONS (continued)

ILLUSTRATIONS (continued)

ILLUSTRATIONS (continued)

TABLES

TABLES (continued)

TABLES (continued)

Section 5

SUBSYSTEM DESCRIPTION

5.1 SPACECRAFT DESIGN AND INTEGRATION

5.1.1 INTRODUCTION

This section contains detailed descriptions of the structural design and analysis and mechanical integration of the SMS spacecraft system, as well as the structural design requirements.[1]

5.1.2 SPACECRAFT DESCRIPTION

The SMS spacecraft design is basically a 75-inch-diameter cylinder with a 49.5-inch-long body-mounted solar array. An electrically despun communications antenna array, optimized for RF performance and testable as a separate assembly, is attached to the spacecraft to form an extension of the cylindrical body.

The VISSR scanner is situated on the spacecraft spin axis and is provided with the required field of view through the solar array. The spacecraft is launched with the apogee boost motor (ABM) down, and with the motor case dome adjacent to the VISSR radiative cooler cover. The visible and infrared spin scan radiometer (VISSR) is supported with a three-point mount; and there are no other structural connections except for the radiative cooler protective cover.

The magnetometer sensor and the telemetry and command antennas are located above the VISSR on the opposite end from the radiative cooler aperture and communications antenna array. Holes are provided in the solar array as required for the remaining space environment monitor (SEM) sensors, attitude sensors, and the radial thrusters associated with the auxiliary propolusion (AP) subsystem.

The interface with the launch vehicle is the same as the standard 37-inch-diameter attach fitting. The resulting weight allocation for the spacecraft and apogee boost motor is 1325 pounds, not including the attach fitting.

Because the combination of spacecraft and apogee boost motor adapter is unstable (spin to transverse inertia ratio of approximately 0.40), active nutation damping is required prior to jettisoning of the apogee boost motor and its adapter. Following that event, the spacecraft is inherently stable with an effective inertia ratio of approximately 1.05 without fuel, at end of life.

An exploded view of the principal elements of spacecraft and adapter is shown in Figure 5-1.

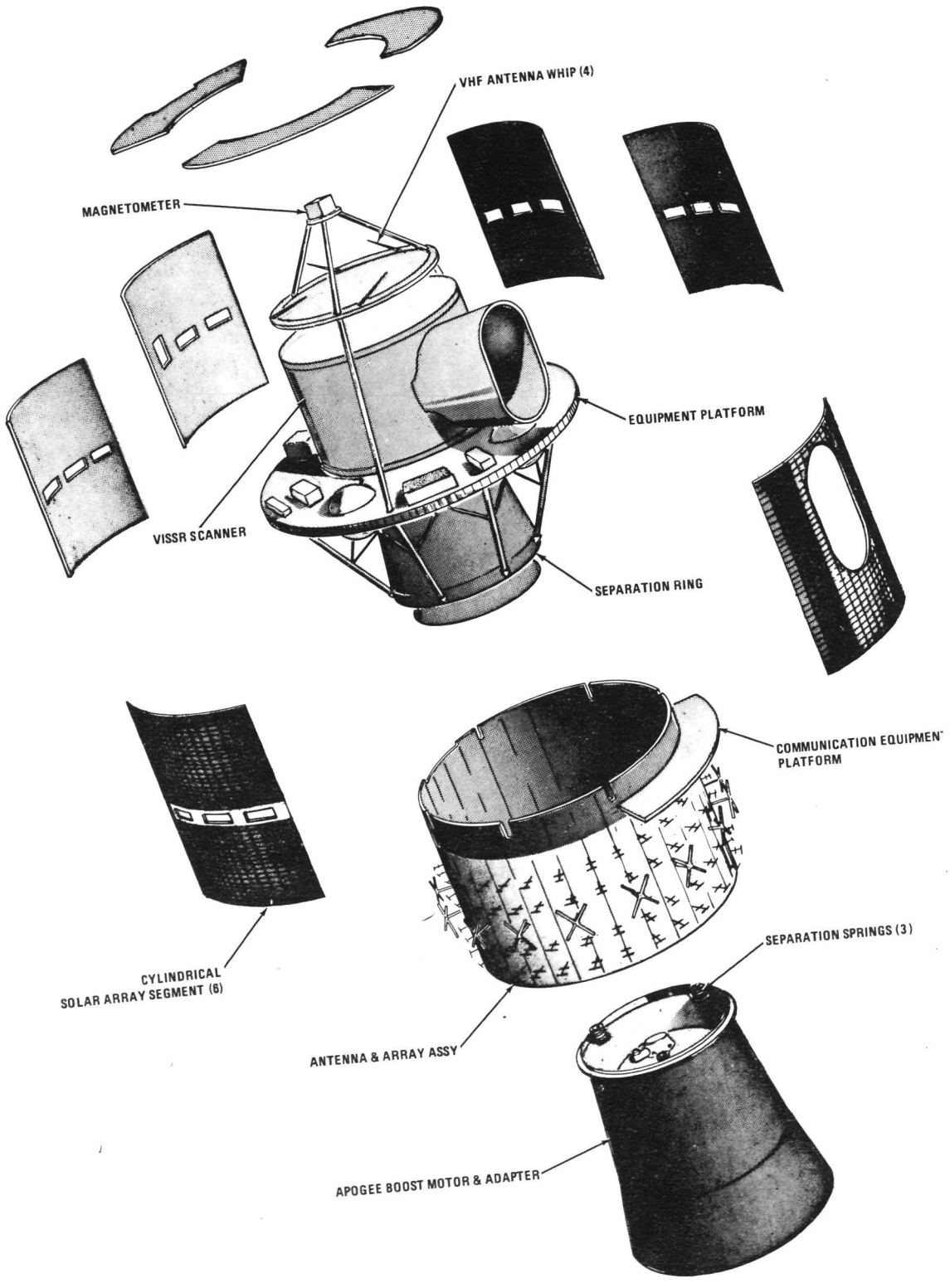

Figure 5-1. Exploded View of Spacecraft

5.1.2.1 Exterior Design of Spacecraft

The overall physical configuration of the spacecraft is shown in Figure 5-2 and is basically a cylinder with an outside diameter of 75 inches and a height of 71 inches not including the ABM adapter. The spacecraft has the following exterior features:

- Main cylindrical solar array - 75 inches in diameter and 49.5 inches long
- Communications antenna assembly - 50 inches in diameter and 20.4 inches long

The main cylindrical solar array is cut out to (1) accommodate the fields-of-view of the VISSR, components of the SEM, sun sensors, and earth sensors, and (2) accommodate the radial thrusters of the AP subsystem. To provide balance to the power system as well as limit the effective power drop in the area of the VISSR aperture, the majority of the array cutouts are positioned in a band around the spacecraft.

The hole provided in the array for the VISSR scanner results in momentary dip in the power available from the array when oriented with the sun. The spacecraft design allows for normal operation with this reduced power while making use of the added power available during the remainder of the spin revolution for battery charging and duty cycling of transient or intermittent loads such as are caused by the VISSR multiplexer. The solar array is constructed of 3/8-inch aluminum honeycomb core with 0.004-inch Fiberglas epoxy face sheets to which the solar cells and wiring are attached. The array is divided into six segments to facilitate fabrication and assembly. At present, there are three different types of array segment configurations with respect to cutouts.

The S-band and UHF antenna array assembly (see Figure 5-3) is basically a cylinder 50 inches in diameter with an exposed length of 20.4 inches below the main solar array cylinder. The exterior surface of the assembly consists of 128 self-supported yagi S-band elements and 16 crossed-dipole UHF elements.

The antenna assembly is configured as one assembly where the basic cylinder is a one-piece honeycomb substrate with an outside diameter of 50 inches and a total length of 27.0 inches. The exterior surface of the cylinder has a 0.001-inch aluminum skin which provides the RF ground plane for the antenna system. The honeycomb area above the antenna elements is utilized for mounting the antenna-related equipment. The S-band and UHF power amplifiers are located on a thermal radiator platform attached to this upper portion of the antenna structure.

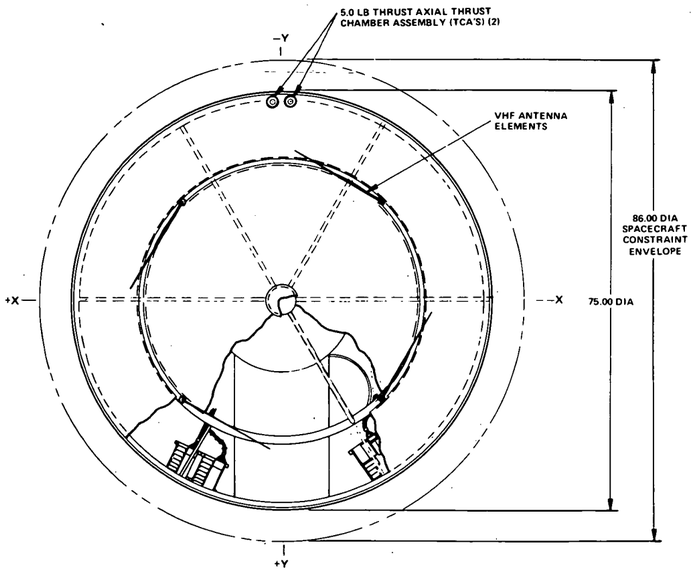

NOTE: ALL DIMENSIONS ARE IN INCHES

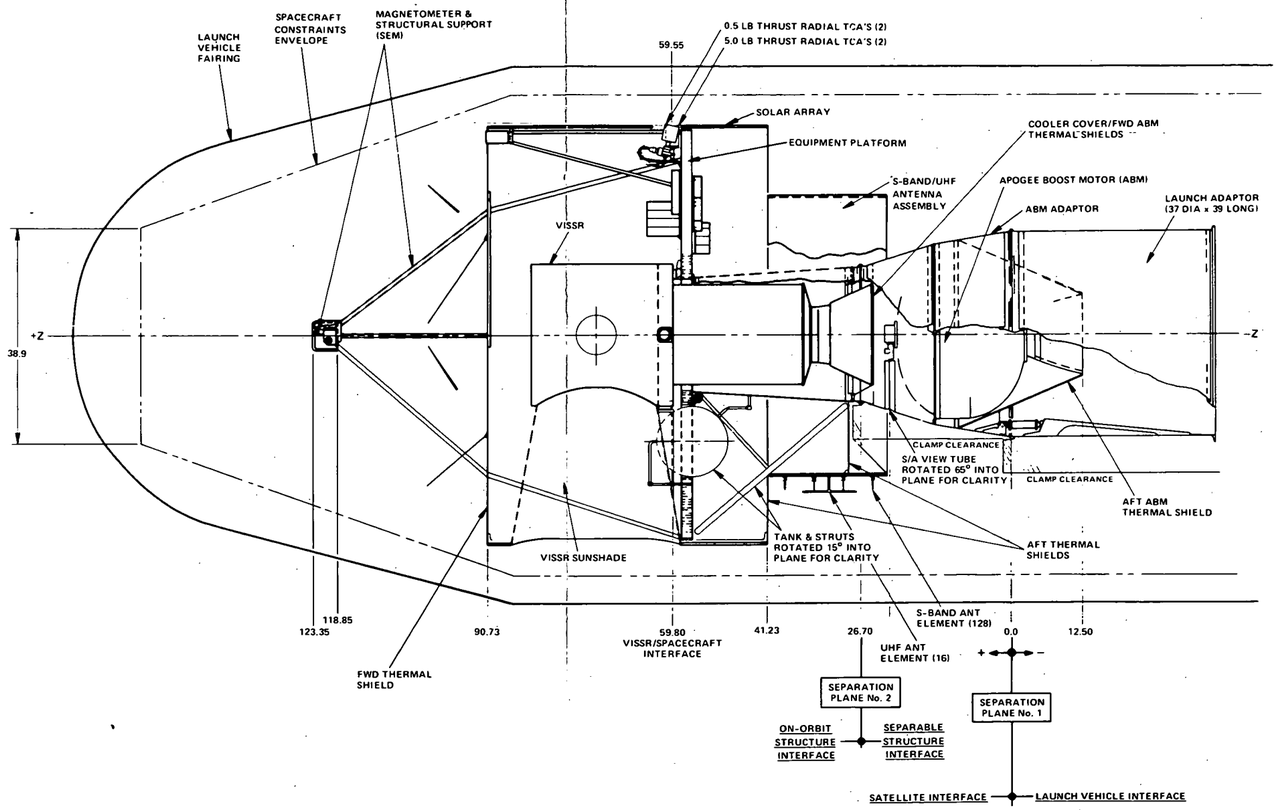

Figure 5-2. Spacecraft Configuration

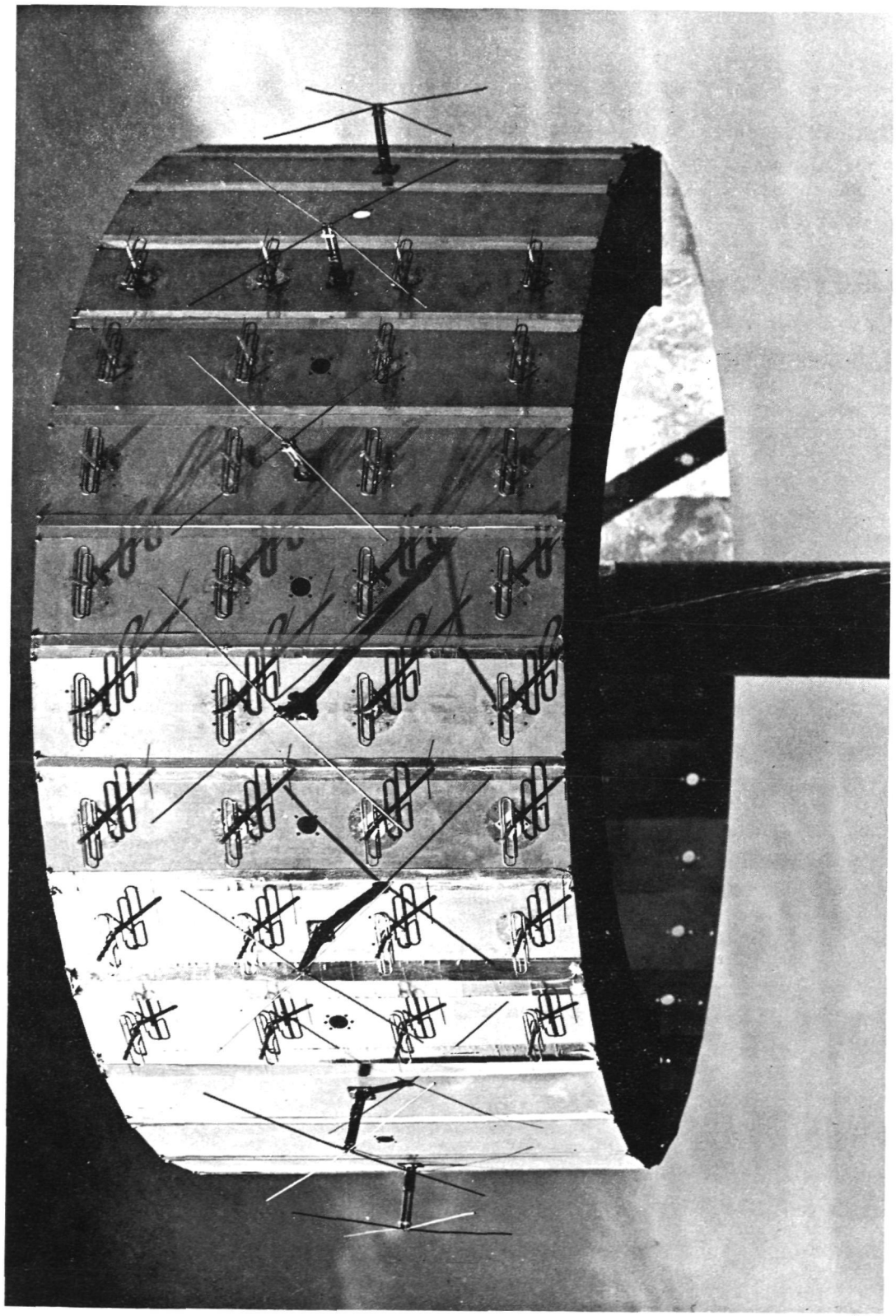

Figure 5-3. (Development Model) of the S-band and UHF Antenna Array

The antenna assembly is tested as a unit for pattern gain and power amplifier performance at the subsystem level prior to spacecraft integration.

With the subsystem requirements for minimizing coaxial line lengths, the layout reflects design symmetry as well as close coupling of components as a basis for achieving these requirements.

5.1.2.2 Interior Design of Spacecraft

Subsystem components are located on both sides of the equipment platform and positioned as illustrated in Figure 5-4. Tradeoffs concerning thermal and subsystem requirements, along with balance weight reduction requirements, are continually exercised to optimize final locations of each component/equipment within the satellite.

The three spherical propellant tanks of the AP subsystem are located and mounted directly on the equipment platform. Assembly of the AP subsystem to the platform occurs in the early stages of satellite assembly. Welded joints are incorporated in the wet-lines in order to facilitate assembly on the equipment panel. Two 5.0-pound and two 0.5-pound thrust radial thrusters are located 180 degrees away from the VISSR aperture and along the -Y axis plane of the spacecraft.

5.1.2.2.1 View Angles. The following components are located within the satellite with consideration to their respective fields-of-view:

(a) VISSR scanner

(b) VISSR scanner radiation cooler

(c) Sun angle sensors and earth sensors

(d) Scientific experimental monitors

1. Magnetometer

2. Particle counter

3. X-ray counter

5.1.2.2.2 Access. The following items aboard the satellite are in a position such that access to the above components can be accomplished:

(a) Battery charge/monitor connector (through the two umbilical connections)

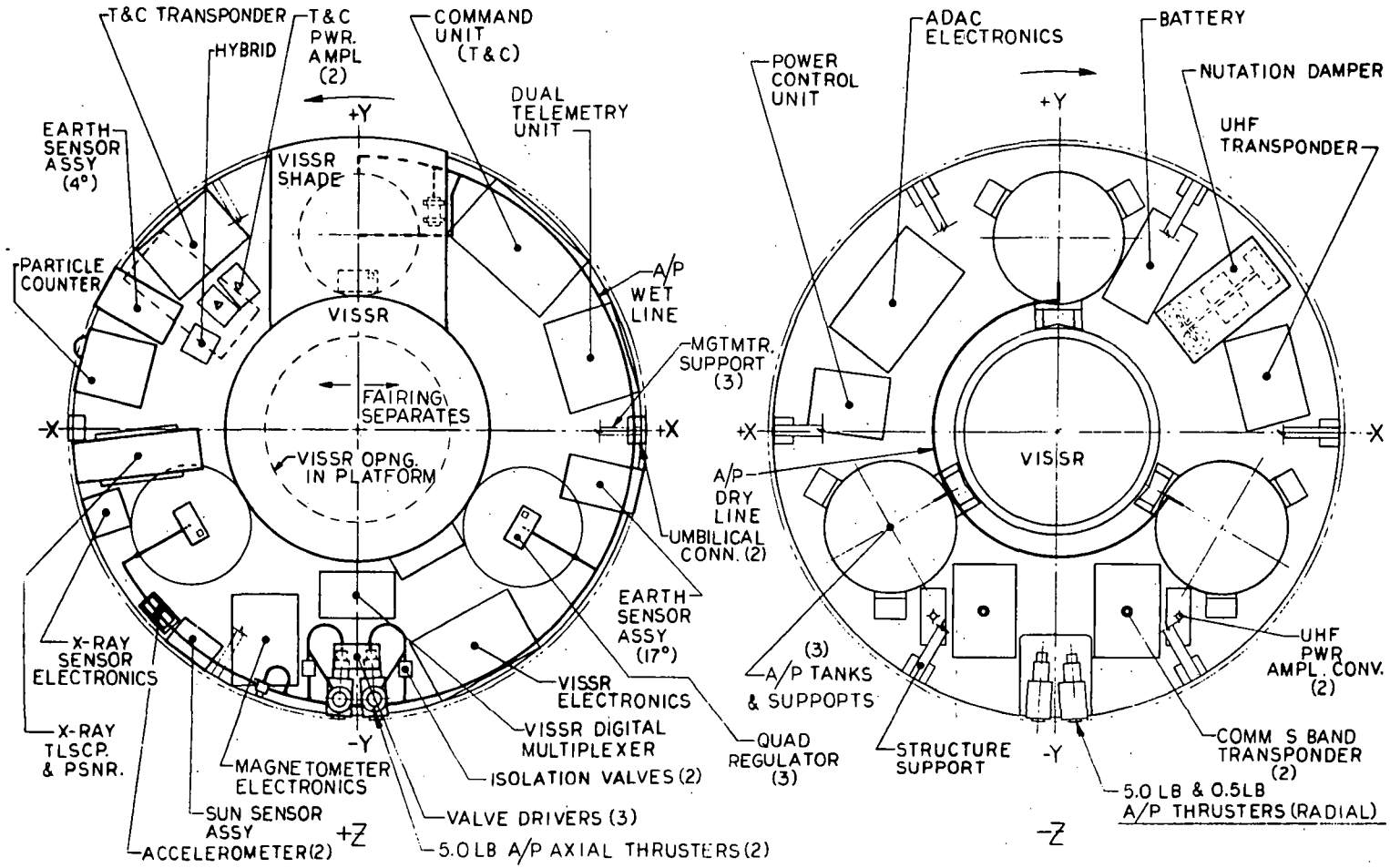

Figure 5-4. Satellite Equipment Layout

(b) Aerospace ground equipment (AGE) power and fusistor test connector (through a solar panel cutout)

(c) Separation initiation igniters

(d) Inflight-jumper connector (through a solar panel cutout)

The fill and drain valve of the AP subsystem is located on the +Z side of the equipment platform and slightly off center of the -Y axis of the satellite. Access is achieved through a solar panel cutout.

5.1.2.3 Mass Properties

Table 5-1 shows the results of the mass properties analysis as of November 1971.

5.1.2.4 Alignments and Balancing

The spacecraft alignment requirements impose restrictions in two distinct categories: (a) static alignments, and (b) mass balance. These requirements are shown in Figure 5-5. Note that all requirements for both static alignment and mass balance are referenced to either of two surfaces: (a) the separation plane and mounting diameter to the launch vehicle adapter, or (b) the separation plane and mounting diameter of the orbiting spacecraft to the ABM adapter. The basis for the choice between the two references depends on whether the particular requirement stems from launch or orbit conditions.

5.1.2.4.1 Static Alignment. The static alignments of the various equipments on the spacecraft are accomplished in several ways. Some equipment is restrained by the mounting method so that no adjustment is required to maintain the alignment tolerances. These equipments only require an inspection (visual and dimensional) to check their alignment to the spacecraft. Some equipment is mounted in a manner which permits complete adjustment of the position with respect to the spacecraft. These units are optically measured and aligned until they meet the requirements of Figure 5-5. Other units mounted to surfaces of the spacecraft which restrain the item in one or more directions permit adjustments in other directions. These items are also optically checked and aligned until they meet the requirements.

The following equipments are restrained by mounting surfaces, and the alignments are checked:

(a) Apogee boost motor

(b) Auxiliary propulsion tanks

Table 5-1
SMS Sequenced Mass Properties Data

SEQUENCE NUMBER	DESCRIPTION	WEIGHT LB	CENTER OF GRAVITY (IN)			MOMENT OF INERTIA (SLUG-FT^2)			PRODUCT OF INERTIA (SLUG-FT^2)			INERTIA RATIO
			X	Y	Z	Ixx	Iyy	Izz	Ixy	Iyz	Ixz	
	Total Spacecraft (Dry) (1)	520.88	0.00	0.00	56.61	59.432	58.584	63.800	-0.789	0.000	0.000	1.080
	Fuel and Pressurant	34.81	0.00	0.00	56.02	1.852	1.852	3.604	0.000	0.000	0.000	
	ABM Adapter (1)	41.31	0.00	0.00	13.99	1.992	2.000	1.995	0.017	0.000	0.000	
	ABM (Full) (1)	678.00	0.00	0.00	9.86	11.932	11.932	15.225	0.000	0.000	0.000	
1	Launch	1275.00	0.00	0.00	30.35	221.505	220.665	84.624	-0.772	0.000	0.000	0.383
	Less: Fuel	- 4.36	0.00	0.00	56.02	.232	.232	.451	0.000	0.000	0.000	
2	Post Attitude Correction	1270.64	0.00	0.00	30.26	220.651	219.811	84.173	-0.772	0.000	0.000	0.382
	Less: ABM Expendable (1)	623.09	0.00	0.00	9.96	10.180	10.180	13.992	0.000	0.000	0.000	
3	Final Transfer Orbit	647.55	0.00	0.00	49.80	101.675	100.835	70.181	-0.772	0.000	0.000	0.693
	Less: ABM Inerts (1) (2)	-54.91	0.00	0.00	8.71	1.735	1.735	1.233	0.000	0.000	0.000	
	ABM Adapter (1) (2)	-41.31	0.00	0.00	13.99	1.992	2.000	1.995	0.017	0.000	0.000	
4	Post ABM Separation	551.33	0.00	0.00	56.58	61.037	60.189	66.953	-0.789	0.000	0.000	1.104
	Less: Fuel	-18.06	0.00	0.00	56.02	.961	.961	1.870	0.000	0.000	0.000	
5	Initial Orbit	553.27	0.00	0.00	56.60	60.075	59.227	65.083	-0.789	0.000	0.000	1.090
	Less: Cooler Cover	- 0.77	0.00	0.00	25.04	.004	.004	.009	0.000	0.000	0.000	
6	Orbit	532.50	0.00	0.00	56.64	59.905	59.057	65.074	-0.789	0.000	0.000	1.093
	Less: Fuel & Press	-12.39	0.00	0.00	56.02	.659	.659	1.283	0.000	0.000	0.000	
7	Final Orbit (End of Life)	520.11	0.00	0.00	56.66	59.245	58.397	63.791	-0.789	0.000	0.000	1.083

(1) Includes applicable margin

(2) The transverse (average) and roll moment of inertia of the ejected assembly (adapter/inert ABM) are 3.873 and 3.228, respectively, with a resulting inertia ratio of 0.834.

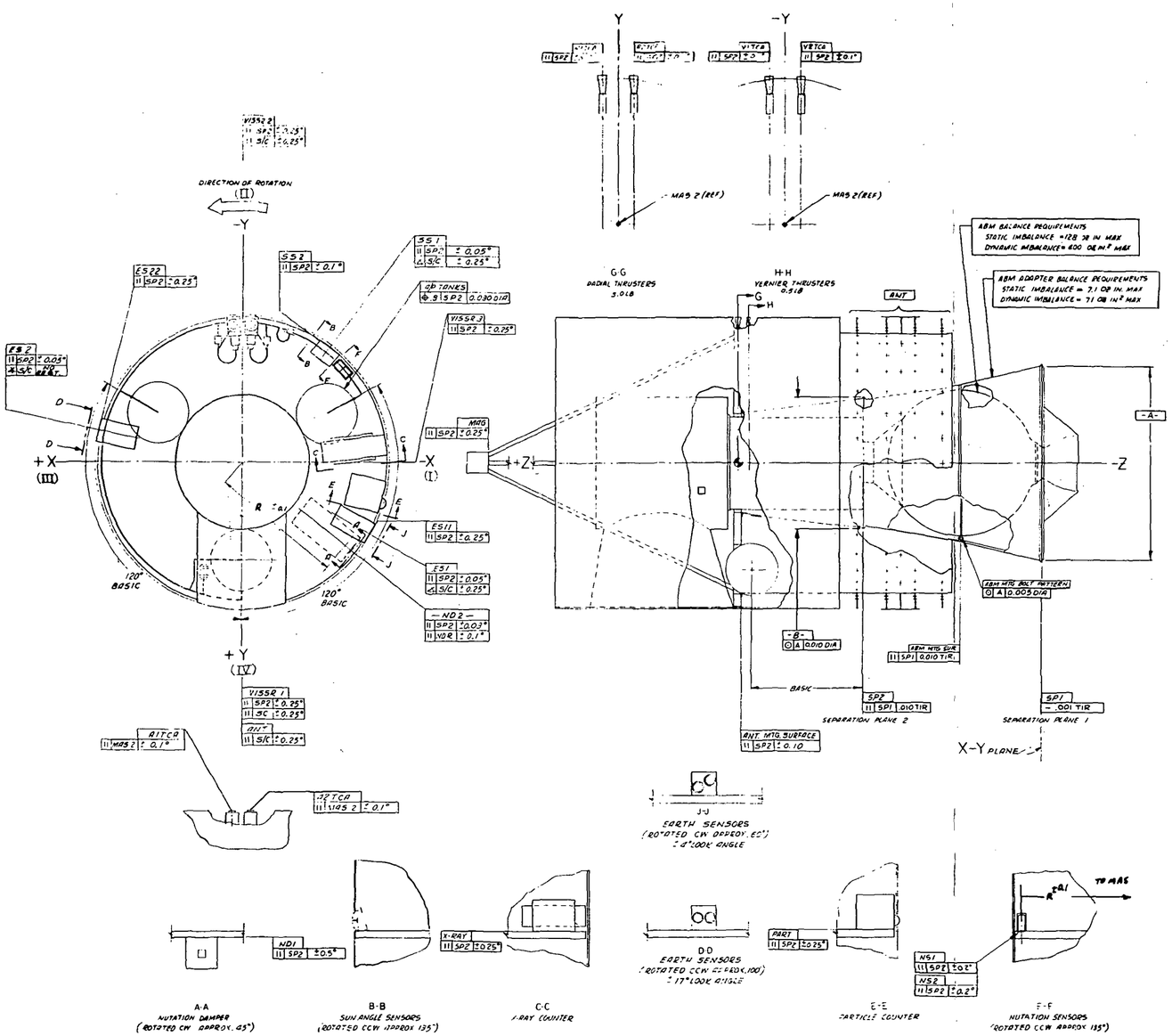

NOTES (UNLESS OTHERWISE SPECIFIED)

1. DEFINITIONS:
   - A = MATING DIA ABM ADAPTER/LAUNCH VEHICLE ATTACH FITTING
   - ANT = RADIAL LINE THRU MAS 2 & S-BAND ANTENNA REFERENCE MARK
   - B = MATING DIA SATELLITE / ABM ADAPTER
   - CG 1 = CENTER OF GRAVITY OF SATELLITE WITH HYDRAZINE, ABM ADAPTER, & ABM LOADED
   - CG 2 = CENTER OF GRAVITY OF SATELLITE WITHOUT HYDRAZINE, ABM ADAPTER, & ABM
   - d = OFFSET TO COMPENSATE FOR CHANGE OF INERTIA OF FUEL
   - ES1 = LINE PERPENDICULAR TO EARTH SENSOR ASSY ALIGNMENT MIRROR
   - ES11 = REF MARK ON EARTH SENSOR ASSY BRACKET

   - MAG = MOUNTING SURFACE OF MAGNETOMETER SENSOR
   - MAS 1 = MECHANICAL AXIS OF SATELLITE & ABM ADAPTER = LINE PERPENDICULAR TO SP1 THRU CENTER OF A.
   - MAS 2 = MECHANICAL AXIS OF SATELLITE = LINE PERPENDICULAR TO SP2 THRU CENTER OF B.
   - MPA 1 = MAJOR PRINCIPAL AXIS OF SATELLITE WITH HYDRAZINE, ABM ADAPTER & LOADED ABM = AXIS THRU CG1 ABOUT WHICH THE MOMENT OF INERTIA IS MAXIMUM & THE INERTIA PRODUCTS ARE ZERO
   - MPA 2 = MAJOR PRINCIPAL AXIS OF SATELLITE WITHOUT HYDRAZINE, ABM ADAPTER OR ABM = AXIS THRU CG2 ABOUT WHICH THE MOMENT OF INERTIA IS MAXIMUM & THE INERTIA PRODUCTS ARE ZERO.
   - ND1 = MOUNTING SURFACE OF NUTATION DAMPER ASSY
   - ND2 = NUTATION DAMPER ASSY. MIRROR NORMAL
   - NDR = RADIAL LINE THRU MAS 2 & NUTATION DAMPER REF MARK
   - NS1 = MOUNTING SURFACE OF NUTATION SENSOR #1
   - NS2 = MOUNTING SURFACE OF NUTATION SENSOR #2
   - RET = MOUNTING SURFACE OF PARTICLE COUNTER
   - SR = RADIAL LINE THRU MAS 2 & REF MARK ON SATELLITE
   - SP1 = SEPERATION PLANE #1 (ABM ADAPTER/LAUNCH VEHICLE ATTACH FITTING)
   - SP2 = SEPARATION PLANE #2 (SATELLITE / ABM ADAPTER)
   - SS1 = LINE PERPENDICULAR TO SUN SENSOR ASSY ALIGNMENT MIRROR
   - SS2 = REF MARK ON SUN SENSOR ASSY BRACKET
   - SS2 = RADIAL LINE THRU MAS 2 & SUN SENSOR ASSY REF MARK ON ALIGNMENT MIRROR
   - AITCA = CENTER LINE OF THRUST OF AXIAL TCA #1 (LINE THRU CENTERS OF EXIT DIA & THROAT DIA)
   - A2TCA = CENTER LINE OF THRUST OF AXIAL TCA #2
   - R1TCA = CENTER LINE OF THRUST OF RADIAL 0.6 LB TCA #1
   - R2TCA = CENTER LINE OF THRUST OF RADIAL 0.6LB TCA #2
   - VITCA = CENTER LINE OF THRUST OF RADIAL 0.5LB TCA #1
   - V2TCA = CENTER LINE OF THRUST OF RADIAL 0.5 LB TCA # 2
   - VISSR 1 = LINE PERPENDICULAR TO ALIGNMENT MIRROR #1 ON VISSR
   - VISSR 2 = LINE PERPENDICULAR TO ALIGNMENT MIRROR #2 ON VISSR
   - X-RAY = MOUNTING SURFACE OF X-RAY COUNTER
2. MPA1 PARALLEL TO MAS1 WITHIN 0.008 RADIAN
3. CG 1 LOCATED ON MAS 1 WITHIN 0.048 IN.
4. MPA2 PARALLEL TO MAS 2 WITHIN 0.003 RADIAN
5. CG 2 LOCATED ON MAS 2 WITHIN 0.020 IN.
6. SPACECRAFT LOCATION COORDINATES ORIGINATE AT INTERSECTION OF Z AXIS WITH X-Y PLANE (CENTER OF DIAMETER A AT SP1.)

NOT TO SCALE

Figure 5-5. Spacecraft Alignment

(c) Auxiliary propulsion thrusters

(d) Magnetometer sensor

(e) Communications antenna

(f) X-ray counter

(g) Particle counter

(h) VISSR

The following equipments are either partially or fully adjusted and optically aligned after installation into the spacecraft:

(a) Nutation damper

(b) Sun-sensor assembly

(c) Earth-sensor assembly

(d) Nutation sensor

The following is a brief description of the SMS spacecraft static alignment procedure.

A rotary table capable of angular accuracy of ±30 sec is permanently installed in the alignment station and leveled to ±5 sec. A theodolite capable of autocollimation and angular accuracy of ±1 sec is mounted on a vertical tooling bar approximately 15 ft from the center of the rotary table. Optical targets are permanently located to sufficiently define a plane passing through the center of the rotary table. Figure 5-6 shows a plan view of the alignments station. The spacecraft is mounted on the rotary table, as shown in Figure 5-7.

The spacecraft is rotated to view the VISSR from the theodolite. With the theodolite in the plane of the centerline of the rotary table and leveled to within 2 sec, the spacecraft on the rotary table is adjusted to obtain a collimated image in the theodolite from the VISSR alignment mirror. The position of the rotary table in combination with the azimuth and elevation angles of the theodolite defines the VISSR angular position.

The rotary table is then adjusted to view and collimate to an alignment mirror on the sun-sensor assembly with the theodolite. The angle reading of the rotary

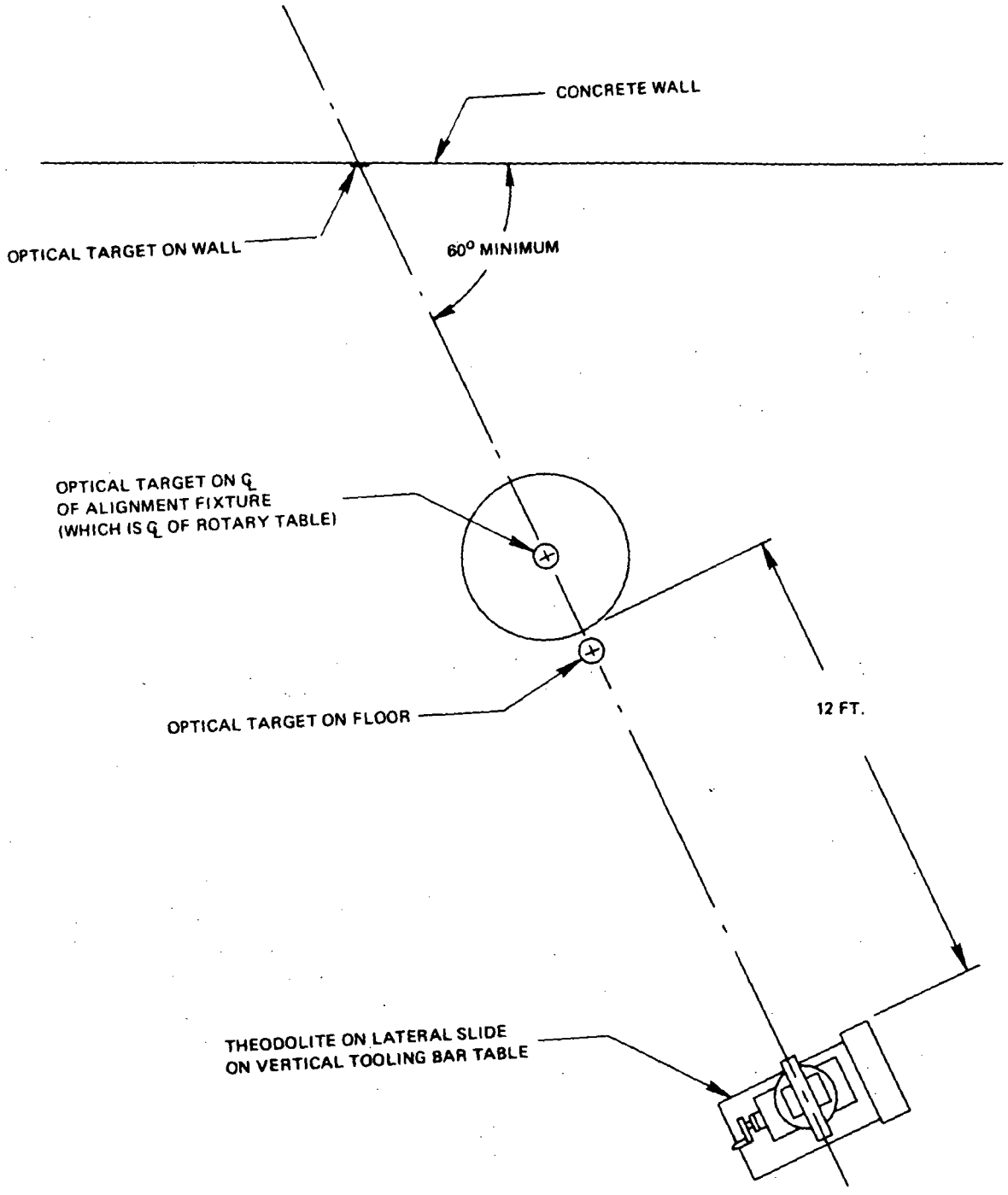

Figure 5-6. Static Alignment Equipment Setup

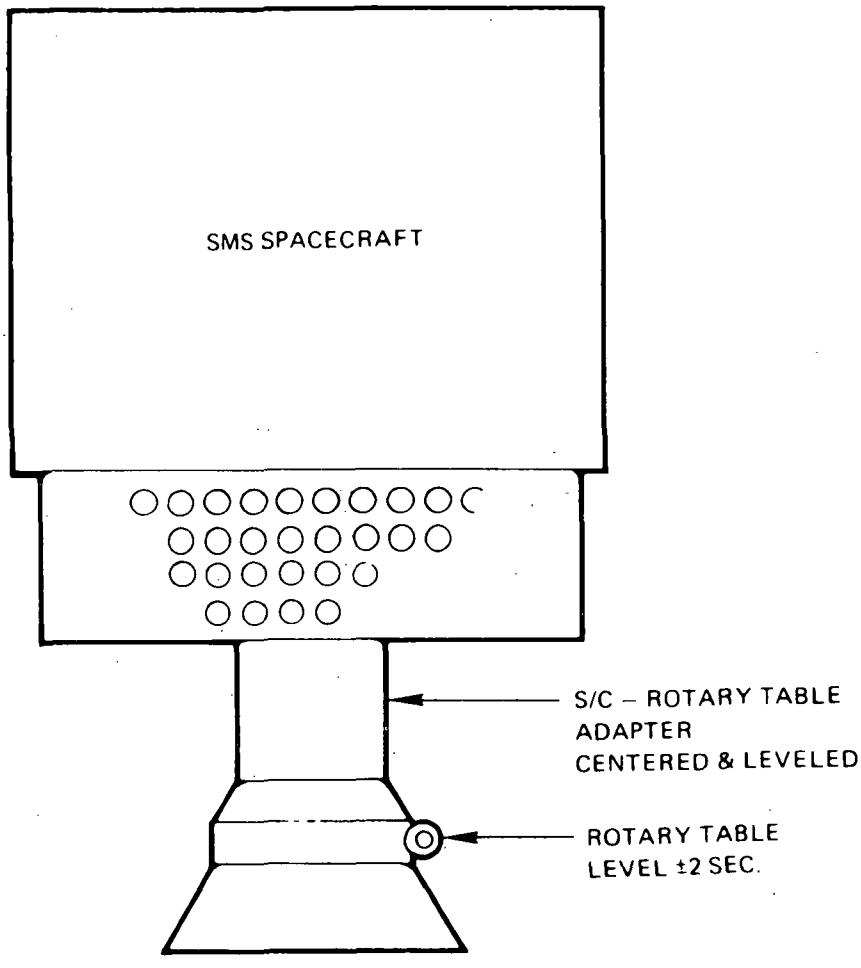

Figure 5-7. Spacecraft Mounted on a Rotary Table

table, plus the azimuth and elevation angles of the theodolite, represents the position of the sun-sensor assembly in the spacecraft. The azimuth and elevation position of the sun-sensor assembly will be adjusted to obtain the desired angle between sun-sensor assembly and VISSR. Alignment of other assemblies is accomplished in a similar manner.

5.1.2.4.2 Mass Balance. The following paragraphs describe the balance procedures required to meet the launch and orbital requirements.

(a) Balance of Apogee Boost Motor. The apogee boost motor is balanced separately in the following manner. Each empty flight ABM assembly, including the nozzle, is statically and dynamically balanced with respect to the ABM/adapter mounting interface. Each ABM is then loaded with propellant, reassembled and remounted on the balance machine. The

static and dynamic balance of each complete ABM is then checked for compliance to the required limits.

(b) Balance of ABM Adapter. Each flight or protoflight ABM adapter is balanced on the trebel balance machine located in the Philco-Ford satellite assembly and test area. A fixture is utilized that is designed to accurately place the separation ring (ABM adapter/launch vehicle attach fitting) of the ABM adapter on the centerline of the balance machine. This balance fixture is also accurately balanced prior to mounting the ABM adapter. Another fixture simulates the separation ring of the spacecraft so that it can be mounted on the ABM adapter, and the separation clamp installed simulating the launch condition as shown in Figure 5-8. The ABM adapter is then statically and dynamically balanced within the required limits.

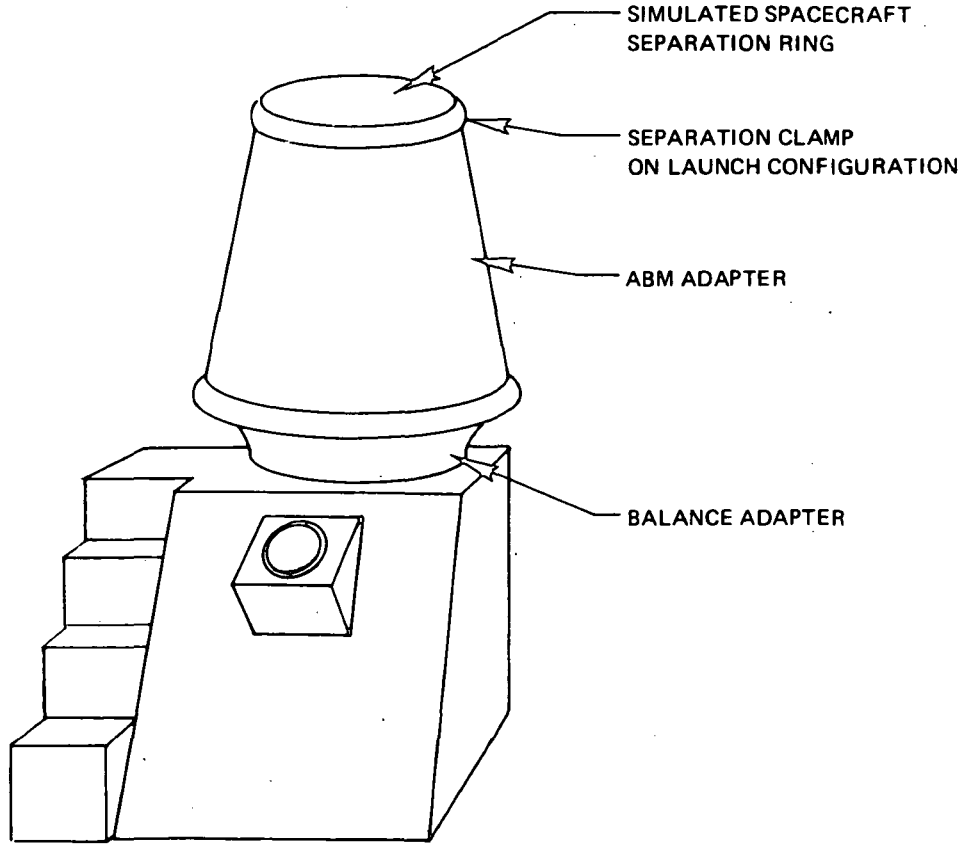

Figure 5-8. ABM Adapter and Separation Clamp Installed on the Balance Machine

(c) Balance of Spacecraft. Each spacecraft in flight configuration, without hydrazine, is mounted onto a previously balanced fixture with a balanced

clamp fastened to the separation ring of the spacecraft (Figure 5-9). This entire assembly is mounted on the balance machine and statically and dynamically balanced within the required limits.

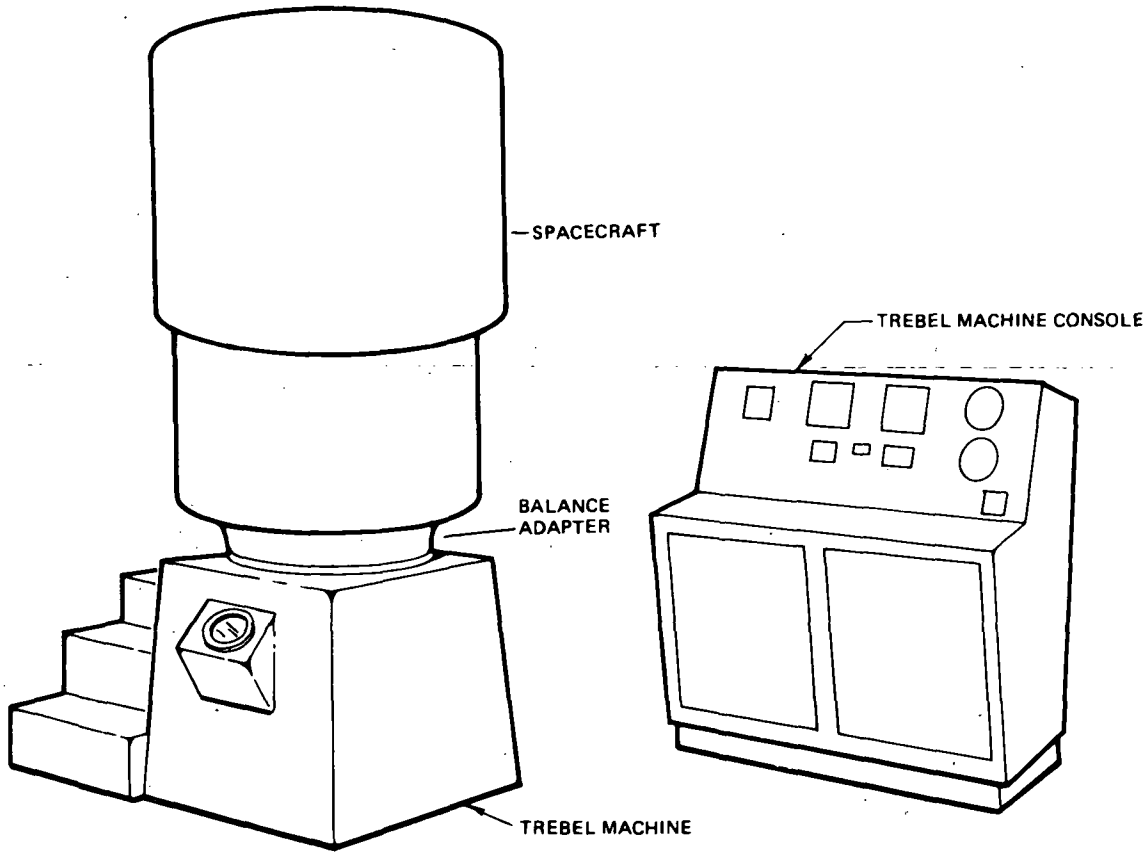

Figure 5-9. Spacecraft on Balance Machine

(d) Balance Analysis. The results of the present balance analysis are summarized in Table 5-2.

Table 5-2

Balance Analysis Results

Imbalance	Balance Errors		Specification	
	Static (in.)	Dynamic (rad)	Static (in.)	Dynamic (rad)
Launch	0.0097	0.0004	0.043	0.008
At station acquisition	0.013	0.00178	None	None
End-of-life	0.011	0.00185*	0.020	0.002

The dynamic imbalance shown by the asterisk reflects the VISSR scan-mirror assembly imbalance as specified to date, assuming a scan-mirror assembly static imbalance less than 0.1 inch between the center of gravity and the axis. This also reflects the movement of the X-ray telescope in its configuration as reported at the time of this writing.

5.1.3 STRUCTURAL DESIGN

5.1.3.1 Structural Requirements

The SMS spacecraft structure must survive the loads environment experienced during launch, ascent, and orbit without failure, excessive deformation, or degradation of mission performance. Excessive deformation is that amount of elastic or permanent deformation causing interference between parts of the spacecraft, interference between the spacecraft and the booster fairing, or unsuccessful spacecraft operation. The following describes the development of strength and stiffness criteria to satisfy these requirements.

5.1.3.1.1 Structural Loads Criteria. The loads experienced by the spacecraft structure are generated by the following environmental conditions:

(a) Ground handling environment during fabrication and transportation.

(b) Launch and ascent acceleration environment from launch vehicle and ABM consisting of steady state, vibration, acoustic, and shock loads.

(c) Forces associated with spinup of the spacecraft-booster third stage including attendant vibrations.

(d) Centrifugal forces due to spacecraft spin and forces associated with operation of the attitude control system.

(e) Thermal loads during all phases of the mission.

It is a program philosophy that the ground handling environment has minimum effect on the sizing of any structural components. Thus, ground handling equipment is carefully designed to protect the spacecraft from all potentially harmful ground environments.

Loads produced by the launch and ascent environment represent the critical criteria for structural design. These loads consist of steady-state "static" accelerations due to engine thrust; transient vibrations due to wind loads, staging, engine ignition, and engine cutoff; random and acoustic vibrations due to engine

burn and aerodynamic buffeting; and high frequency shock loads due to fairing, spacecraft, and ABM separation. For structural design and analysis, these loads are separated into two groups based on frequency, namely, low-frequency excitations and high-frequency excitations.

The low-frequency excitations consist of the steady-state "static" accelerations and the transient excitations of the combined booster/spacecraft vibration modes below approximately 50 Hz. These low-frequency excitations are accounted for in the "quasistatic" ultimate load factors summarized in Table 5-3.

Table 5-3

Quasistatic Ultimate Load Factors

Event	Total Load Factors		
	Longitudinal	Lateral	Radial (1)
Liftoff	4.5g Fwd	3.0g	—
First stage "POGO"	18.0g Aft	3.0g	—
Third stage thrust	16.8g Aft	—	0.516rg
ABM thrust	13.5g Aft	—	0.516rg

(1) Based on 110 rpm/min spin rate with r as the distance in inches from the spin axis.

Table 5-3 presents the current design criteria. First stage POGO leads consist of a 5.2-g limit aft steady state load combined with a ±6.8-g limit oscillatory load. The maximum aft load is then 12.0-g limit, which yields the 18.0-g ultimate aft load factor given in the table. Maximum forward loads during the POGO event are less severe then liftoff loads and are not considered in the table. The ABM thrust load factor is based on the anticipated ABM thrust-time curve and considers propellant consumption during burn. All load factor values are subject to modification in accordance with any changes in projected ABM performance and results of combined spacecraft/launch vehicle dynamic analyses performed by the launch vehicle contractor.

High frequency loads consist of acoustic, shock and high frequency vibration excitations. These loads typically excite local resonances in the spacecraft and govern the design of certain local hardware, bracketing, and panels. The high

frequency loads are defined by frequency spectra given in the applicable environmental specifications. Structural design for high frequency excitations is based on utilization of techniques and materials known to perform well under vibration, acoustic, and shock loadings. Detailed dynamic stress analysis are employed in appropriate instances. Structural adequacy is demonstrated by vibration, acoustic, and shock testing on development and flight quality hardware.

Forces associated with spinup of the spacecraft-booster third stage and operation of the attitude control subsystem are small.

Centrifugal acceleration due to spin at the maximum spin rate of 110 rpm/min produces radial loads within the spacecraft of 0.344 rg where r is distance from the spin axis in inches. At the periphery of the spacecraft (r = 37.5 inches) the radial load is 12.9. Hardware within the spacecraft is designed to carry the sustained centrifugal acceleration loads for the total duration of the mission. The spacecraft is also designed to withstand centrifugal acceleration forces created by test spin rates of 137.5 rpm/min as required by sections 2.1.6 and 2.1.16 of GSFC document S-320-G-1. This spin rate creates radial loads within the spacecraft of 0.537-rg limit in combination with a 1.0-g limit gravity load.

Extreme temperature environments are experienced during ascent following fairing removal and on-orbit during eclipse operation. These extreme temperature conditions are determined by detailed thermal analyses.

5.1.3.1.2 Structural Stiffness Criteria. Structural stiffness criteria dictate that the lowest fundamental frequencies of the spacecraft in both the longitudinal and lateral axes are greater than the corresponding fundamental booster frequencies. Thus, response of spacecraft components are not unduly amplified by coupling of spacecraft modes with booster modes in the same frequency range. To ensure that such coupling between booster and spacecraft modes does not occur, the spacecraft is designed to exhibit fixed base frequencies above 30 Hz in the longitudinal axis and above 20 Hz in any lateral axis as specified in reference 1. An additional design goal is to maintain minimum frequencies of 25-Hz longitudinal and 15-Hz lateral with the spacecraft attached to the cantilevered launch vehicle attach fitting. A detailed dynamic analysis is performed in order to accurately define the spacecraft mode shapes and frequencies. This detailed mathematical model is modified as appropriate to reflect all significant structural changes that evolve during the progress of the program.

A second stiffness requirement is that coupling of the spacecraft structural vibrations with the spacecraft attitude and position control subsystems does not produce deleterious performance of the spacecraft structure of the control subsystem. This requirement is addressed by providing a large margin between

the lowest spacecraft structural resonance and the highest significant frequency in the spacecraft attitude control subsystem. The controls subsystem design has identified 1.83 Hz as the highest significant frequency in the control subsystem. This frequency is associated with the maximum rotation rate of 110 rpm/min and the pulse rate of the position jets.

In consideration of this requirement, the critical vibration mode is bending of the complete spacecraft assembly as a free-free beam prior to ABM burn and separation.

A frequency separation of 2.0 Hz was selected as representing an adequate separation between the highest significant frequency in the control subsystem and the minimum allowable structural resonant frequency. That is, the free-free beam frequency described above is greater than 3.83 Hz. It is noted that this minimum free-free modal frequency of the spacecraft is critical for a second reason. It is required that the spacecraft respond as a rigid body when excited due to spacecraft nutation. Since this nutation rate is approximately 1.83 Hz, the minimum free-free spacecraft modal frequency of 3.83 Hz is considered adequate to prevent any significant dynamic response.

A detailed analysis is performed of the spacecraft control subsystem coupled with the spacecraft structural vibration characteristics. A computer program, capable of coupling the effect of spacecraft rigid-body dynamics with structural elastic deformation is available for this purpose. The present structural requirement of 3.67-Hz minimum resonant frequencies is based upon judgement. The analysis shows that lower structural frequencies are acceptable. The structural stiffness performance of the spacecraft is demonstrated by test. Vibration modal surveys are performed on development and flight quality hardware. Static load tests are performed to verify influence coefficients and stiffness parameters.

5.1.3.1.3 Design Factors. Table 5-4 lists the minimum factors of safety that are employed in the structural analyses. These factors of safety are applied to all load factors given in Table 5-3 including any changes to the load factors evolving from possible modifications in the flight environment or the qualification test requirements.

5.1.3.1.4 Material Properties. Material strengths and other mechanical and physical properties are selected from the minimum guaranteed values of MIL-HDBK-5, or other authorized sources of reference. The allowable material strengths used in design reflect the effects of temperature and fatigue associated with the design environment. For single load path structures the minimum guaranteed values and minimum material thicknesses are used. For multiple load path structures, the 90 percent probability values and nominal material thicknesses are used.

Table 5-4

Factors of Safety

Flight Loads	Limit	Proof	Ultimate	Burst
Spacecraft	1.00		1.50	
Non-flight loads (other than pressure)				
Dangerous to personnel	1.25		2.00	
Remote to personnel	1.00		1.50	
Pressure loads				
Main propellant tanks	1.00	1.50		2.00
Vessels, accumulators and pressurization bottles	1.00	1.50		2.50
Hydraulic and pneumatic lines, fittings and hoses	1.00	2.50		4.00
Propellant supply and vent components	1.00	1.50	2.00	

5.1.3.1.5 Physical Envelope and Interface Requirements. The overall physical envelope of the spacecraft is constrained by the launch vehicle fairing dynamic envelope. The spacecraft structure, therefore, supports the spacecraft throughout the launch sequence such that dynamic excursions because of accelerations and vibration do not permit any portion of the spacecraft to exceed this envelope.

In addition, the spacecraft structure interfaces with the booster at the forward end of the 37.0-inch diameter attach fitting and is secured with the V-band clamp provided.

In addition, interfaces between the subsystem components and the structure are defined and controlled to achieve an integrated spacecraft design. These interfaces include the requirement for thermal control and electrical interconnection where appropriate. Field-of-view for environmental experiments, sun sensors, earth sensors, and VISSR are maintained.

Spacecraft maximum deflections are predicted by analysis and verified by static tests. In addition, analyses are performed to verify the adequacy of the clearances provided for separation of the spacecraft from the third stage and for separation of the ABM from the remainder of the spacecraft, including the condition of a "flat spin," that is, spinning about any lateral axis prior to ABM burn.

5.1.3.2 Structural Description

The structural concept employed in the design is a simple central conical shell which is used to support the ABM, a single horizontal platform and the VISSR. Radial truss members support the outer edge of the equipment platform. The majority of the equipment carried on the platform is situated as far from the spin axis as possible in order to maximize the spin axis moment of inertia. Separation of the lower portion of the central cone with the spent ABM (ABM adapter) occurs at a plane 29.35 inches below the equipment platform.

Separation is achieved by means of a squib actuated v-band clamp and three separation springs. The secondary structures support the segments of the cylindrical solar array, the S-band/UHF antenna assembly, the three hydrazine fuel tanks, and the axial auxiliary propulsion subsystem thrusters. Detail descriptions of the spacecraft structure, the ABM adapter and the separation system follow.

5.1.3.2.1 Spacecraft. Figure 5-10 shows a design layout of the spacecraft structure. The primary structure consists of a horizontal honeycomb equipment platform which is supported by the upper portion of the central cone and six radial truss members.

The horizontal equipment platform is an annulus 73.75-inch outer diameter and 20-inch inner diameter of aluminum honeycomb sandwich construction. The 2.0-inch deep core is 3.1 lb ft^3 and is adhesively bonded to 0.012-inch aluminum face sheets on both sides. The 20-inch diameter hole at its center accommodates the VISSR, while three 12.50-inch diameter holes equally spaced in the platform accommodate the three hydrazine fuel tanks. The cylindrical solar array panels are supported at the periphery of the platform. Components of the various subsystems are mounted on both sides of the platform as close as is practical to the outer periphery. Through inserts are provided in the platform at all primary structural attachments.

The platform is attached to the central cone at its inner diameter, and the cone extends below the platform 29.35 inches. The cone is tapered from 20-inch diameter at its upper attachment to the platform to approximately 25-inch diameter at its lower end. It is a pure monocoque having 0.057-inch aluminum sheet

"Page missing from available version"

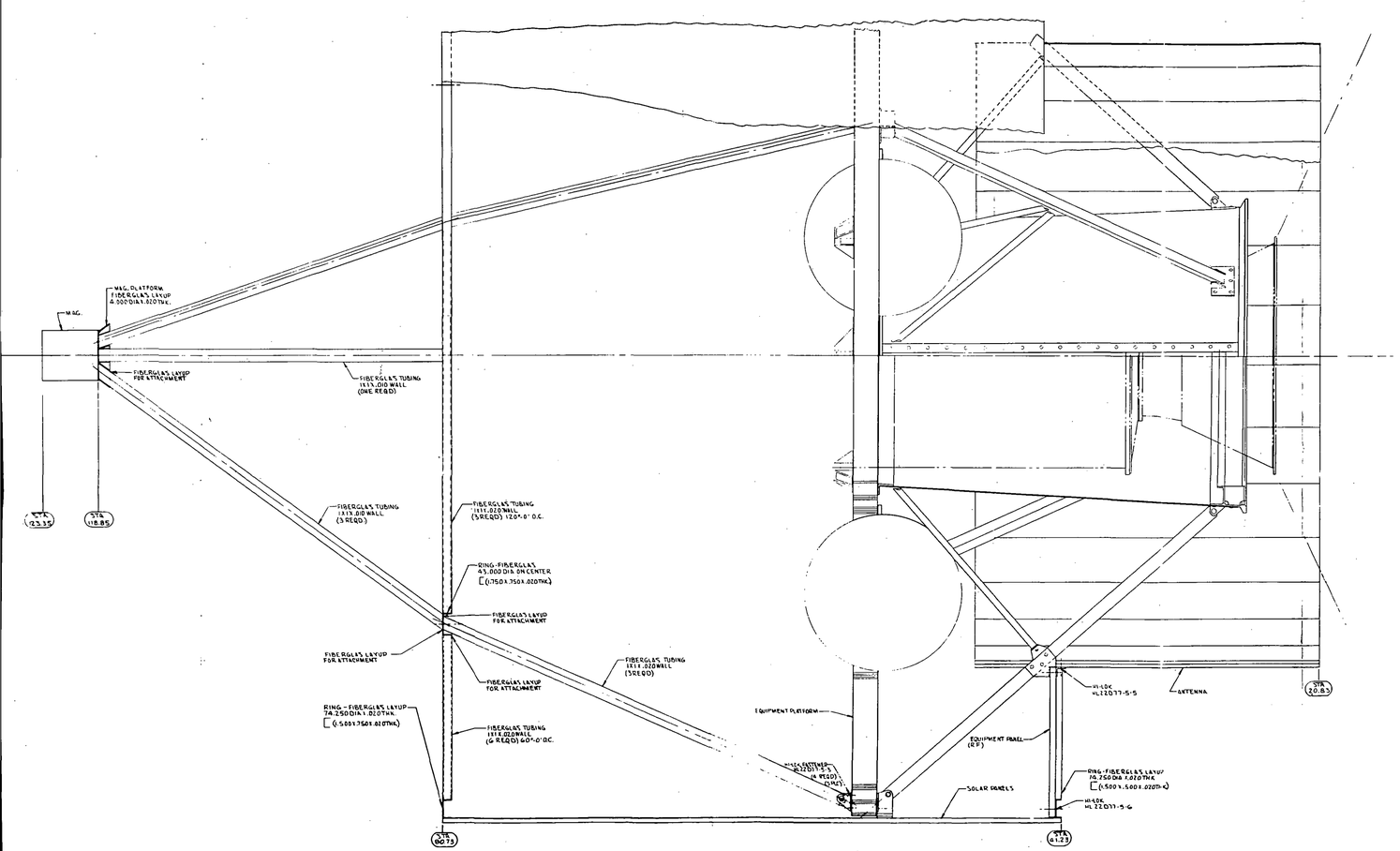

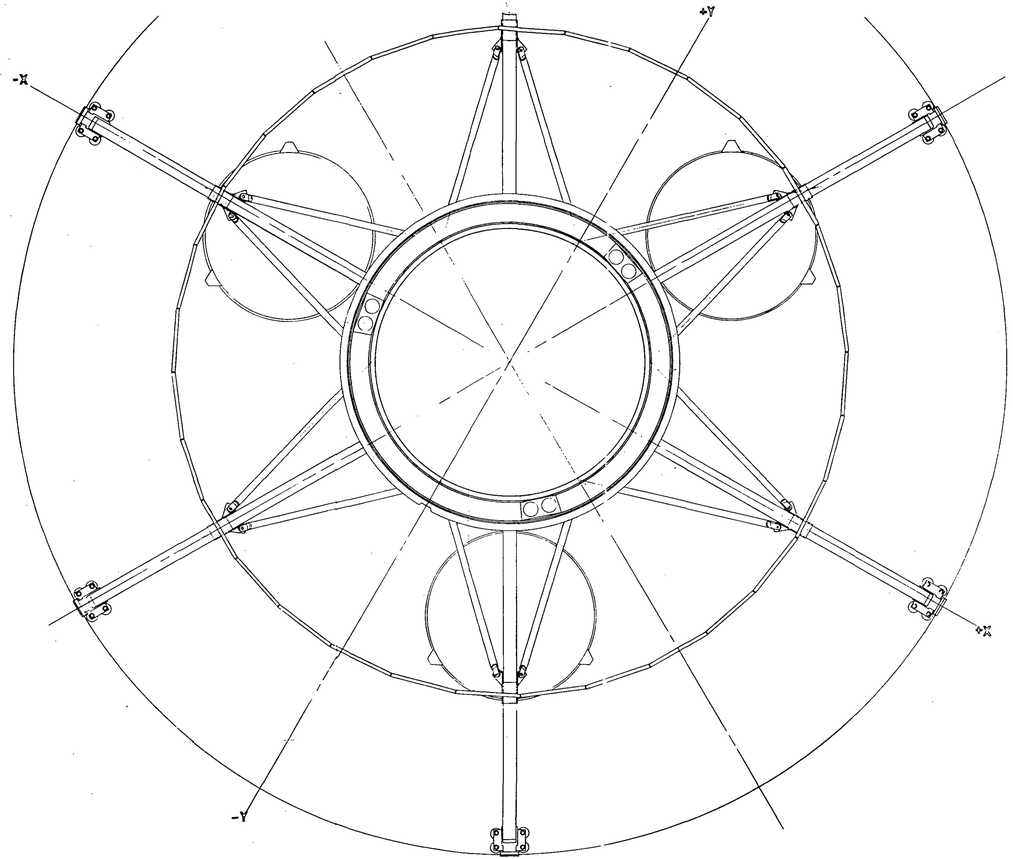

Figure 5-10. Spacecraft Structure (sheet 1 of 2)

"Page missing from available version"

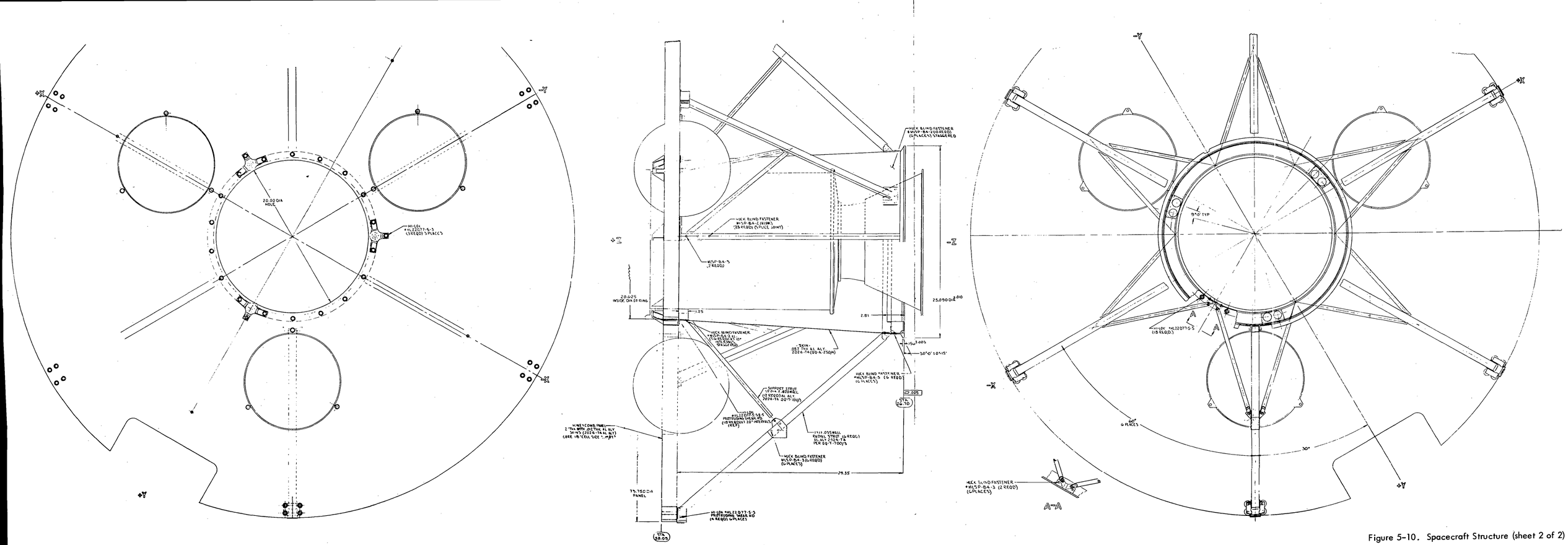

Figure 5-10. Spacecraft Structure (sheet 2 of 2)

"Page missing from available version"

metal shell which is riveted to an aluminum ring at both ends. The upper ring is a simple L-shaped machining, while the lower ring is dimensionally compatible with the upper mating ring of the ABM adapter and V-band separation clamp. In addition, the lower ring is provided with radial stiffness by means of an integral channel to which six radial truss members are attached. These extend from the lower ring to the outer edge of the equipment platform providing it with longitudinal support. The truss members are 1.0-inch square drawn tubes of 0.035-inch aluminum, and are attached to the platform and the lower ring by means of special aluminum machined fittings to which they are riveted. The machined fittings at the equipment platform have provisions for the attachment of the spacecraft handling ring which is used to support the spacecraft through all stages of handling and shipping. Access to the fittings for this purpose is through 1.0-inch diameter holes provided in the solar array. The fittings are permanently attached to the lower ring by means of Huck-type lock bolts. Six fittings are provided at the inside of the lower ring, three of which react the compression loads of the three springs required for ABM adapter separation and the other three support electrical connectors required to initiate ABM ignition and separation across the interface.

Each of the six radial truss members is stabilized by means of two additional members which are attached at its center span and are connected to the upper ring of the central cone. The resulting truss structure then consists of the six radial members and twelve stabilizing members and provides six "hard points" at 50-inch diameter at approximately the center span of the radial members. These hard points are utilized for the support of the communications antenna assembly. The communications antenna structure consists of a 50-inch diameter cylinder having 32 facets on which the 128 elements of the S-band and the 16 elements of the VHF subsystems are mounted. The antenna components are supported on an extension of the 50-inch diameter cylinder and on a horizontal platform which extends from the antenna cylinder to the lower solar array ring. The horizontal platform is a 60-degree annular segment which also provides a thermal radiator for the high-power dissipating components of the communications subsystem. The platform consists of 0.5-inch deep aluminum honeycomb core with 0.025-inch face sheet adhesively bonded on each side; it is supported at its inner radius on the outer surface of the antenna cylinder, and at its outer edge at the lower solar array ring.

The VISSR is mounted, by means of the three mounting pads provided, to the upper side of the equipment platform. Three special fittings are provided which are attached to the platform at a radius of 10.875 inches from the spin axis. The three fittings are positioned with respect to the spacecraft mechanical axis by means of special assembly tooling and with respect to each other by means of a master template representing the VISSR mechanical interface.

The fittings are of aluminum and are provided with studs to match the VISSR mounting holes. Adequate thermal isolation between the VISSR and the structure are provided by means of 0.25-inch thick Fiberglas washers at these interfaces.

The three fuel tanks of the auxiliary propulsion subsystem are provided with three mounting lugs which are oriented parallel to the equipment platform. Each tank is supported directly to the underside of the equipment platform by three inserts provided. These inserts are positioned with respect to the spacecraft's mechanical axis by means of special assembly tooling, to maintain accurate positioning of the fuel tanks.

The axial thrusters are situated at the upper edge of the solar array and are mounted together on a machined platform, which is supported to the appropriate height above the equipment platform by means of a tripod structure secured at its base to the upper side of the equipment platform.

The remaining secondary structures are provided to support the segments of the solar array and the magnetometer sensor. These structures are very lightweight and for the most part fabricated of Fiberglas/epoxy.

The solar array is a cylinder divided into six segments. The six segments are supported at the equipment platform and are attached to each other along the four longitudinal interfaces by means of Fiberglas/epoxy channel members. The cylinder is also supported by means of a Fiberglas/epoxy ring employed at the upper and lower edge of the assembly to provide stiffness and to support the thermal shields. The magnetometer sensor is mounted on a tripod structure supported at the equipment platform. The tripod is fabricated of Fiberglas/epoxy tubes. Fiberglas/epoxy is used for extreme light weight since these items are situated far from the spacecraft center of gravity and therefore their contribution to the transverse moment of inertia is minimized to maintain a stable inertia ratio for the spacecraft.

5.1.3.2.2 Adapter. Figure 5-11 shows a design layout of the ABM adapter. It forms the lower, separable portion of the spacecraft central cone structure interfacing with the launch vehicle attach fitting at its lower end and the spacecraft at the upper. The ABM is supported approximately midway along its length.

The adapter is an all-aluminum pure monocoque structure consisting of three machined rings joined together by two sections of sheet metal shell. The lower machined ring is dimensionally compliant with the requirements set forth in the "Delta Spacecraft Design Restraints" for compatibility with the mating V-band flange of the 37-inch diameter standard delta attach fitting (launch vehicle adapter). The 0.057-inch thick lower portion of the sheet metal shell tapers from the 37-inch diameter ring to 32.0-inch diameter at the central machined ring. The central ring serves two functions: to join the upper and lower sheet metal sheets together and to provide attachment for the ABM. The ABM is attached to the ring by means of 24 bolts in shear which support the motor at its attachment

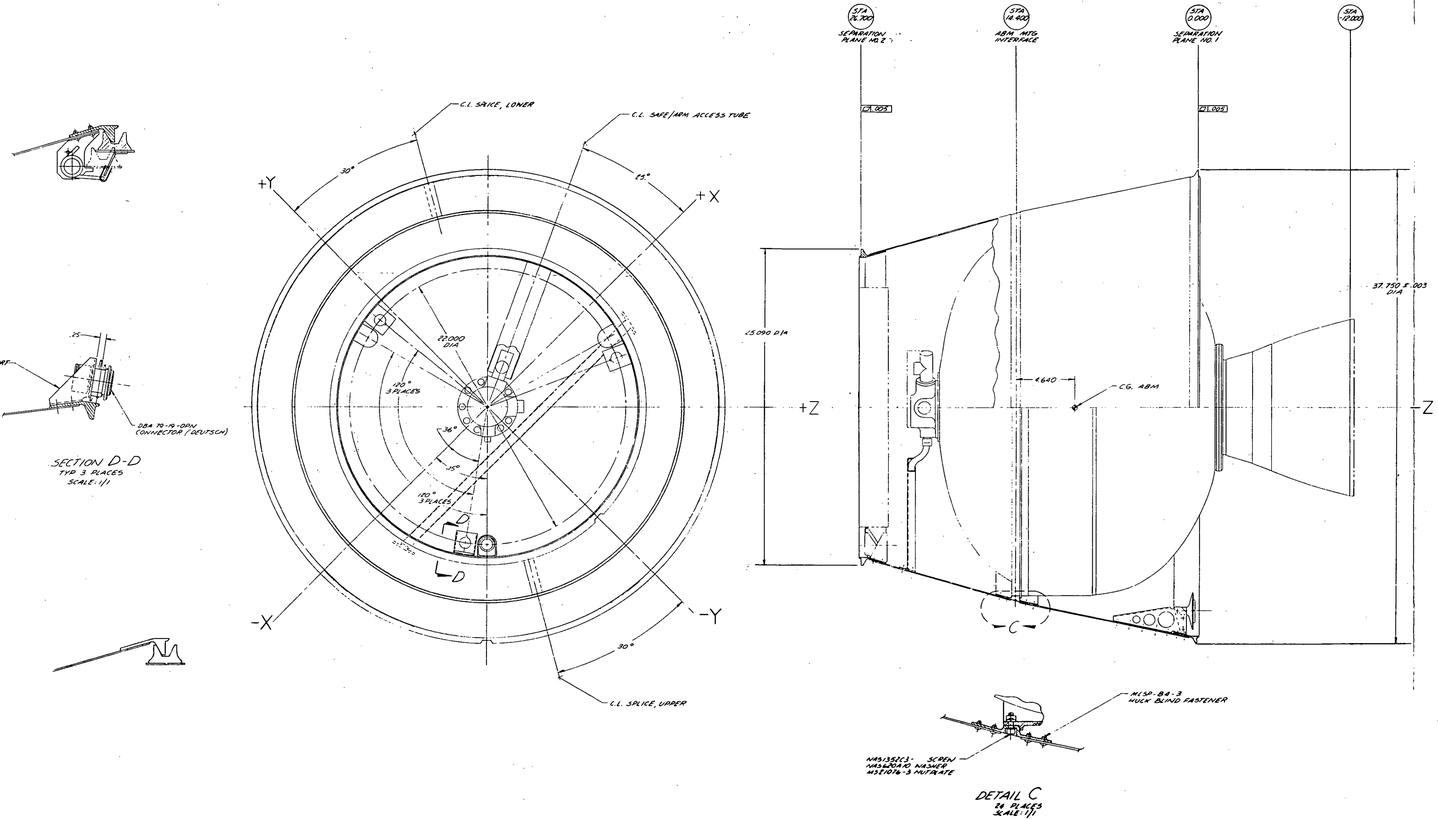

Figure 5-11. ABM Adapter

ring. Anchor nuts are provided in the ABM ring so that bolt installation can be effected from the outside of the adapter through the central ring.

The 0.057-inch thick upper portion of the adapter shell is also tapered from the central ABM attachment ring to the upper interface with the spacecraft. The upper interface ring is dimensionally similar to the spacecraft interface ring of the 25 x 12-inch diameter conical attach fitting described in the "Delta Spacecraft Design Restraints." This feature permits the utilization of the flight proven separation system employed on this standard delta adapter for the separation of the spent ABM and adapter structure from the spacecraft. The V-band clamp and retention devices already existing for the 25-inch standard adapter are secured to the ABM adapter structure.

Three brackets supporting separation springs are provided at the inside of the upper interface ring. Four brackets reacting the separation forces from the launch vehicle/spacecraft separation springs are provided at the inside of the lower interface ring. Three brackets supporting electrical connectors are also provided at the inside of the upper interface ring.

Riveted construction is employed throughout, the three rings being accurately positioned with respect to each other by special assembly tooling. The attachment holes for the ABM are located by means of a master template supplied by the ABM contractor in order to ensure the correct location of the ABM.

The length of the adapter structure is 26.70 inches and the ABM is supported by the central ring a distance of 14.40 inches from the lower separation plane. This configuration is possible if the nozzle of the ABM protrudes 12.0 inches into the launch vehicle attach fitting.

Redundant separation switches located on the spacecraft side of the separation interface are required to indicate spacecraft from the launch vehicle third stage.

5.1.3.2.3 Separation System. Separation of the ABM and its structural adapter from the spacecraft, in orbit, occurs on command after ABM burnout. After the appropriate delay the V-band clamp is released by ground command and the adapter and spent ABM are ejected from the spacecraft by means of three compression springs. Nominal separation velocity of the spacecraft with respect to the adapter is 5 ft/s, sufficient to ensure adequate clearance between the two separating bodies under large-nutation or flat-spin conditions.

The V-band clamp utilized for the SMS spacecraft is identical to that which has been developed and flight proven for the 25 x 12-inch conical attach fitting described in the "Delta Spacecraft Design Restraints" document. The attach fitting was developed for the Intelsat III spacecraft and its clamp assembly is used without modification. The clamp assembly is Government furnished equipment (GFE) and is secured to the ABM adapters in precisely the same manner as it is on the 25-inch delta attach fitting utilizing the same retention devices. Installation and

separation envelopes specified for the clamp in the "Delta Spacecraft Design Restraints" have been maintained within the SMS spacecraft assuring adequate clearance for successful release of the clamp and the separation of the ABM adapter from the spacecraft. See document SMS-PCC-1227, "SMS Separation System Study," for discussion of separation system and analysis.

5.1.4 STATIC LOAD TEST

The sequence of events of the spacecraft structural development tests is shown in Figure 5-12.

5.1.4.1 Test Configuration

The primary purpose of the spacecraft load test is to verify structural integrity and stiffness requirements of the spacecraft under all critical loads events. A second purpose of the test is to establish final notching criteria for the sinusoidal and random vibration tests to be conducted during the spacecraft qualification test program. Preliminary notching criteria determined in the structural components static load tests phase of this test program are re-evaluated and modified to reflect results of this static load test of the entire spacecraft.

The steady state accelerations load test of the spacecraft structure is conducted by subjecting the development model to a static loads test and by subjecting appropriate subsystems to an acceleration test. This is judged a better approach than subjecting the complete spacecraft to an acceleration test for the following reasons:

(a) Configuration of the spacecraft is relatively simple in that major components are reasonably compact and thus lend themselves to accurate application of static loads which closely approximate actual flight loads. The large size of the spacecraft makes it difficult to apply a reasonably uniform load level to all portions of spacecraft on a centrifuge facility, particularly if a combined spin condition is required.

(b) The static load test is conducted in the Philco-Ford environmental test laboratory whereas an acceleration test has to be conducted at an outside facility. Conducting the test in-house reduces the time and the cost of the test and eliminates the potential hazards of transporting the test unit to and from the outside facility.

(c) Conducting the test in-house affords the advantage of closer control over conduct of the test and permits efficient redesign and retest if structural deficiencies are disclosed.

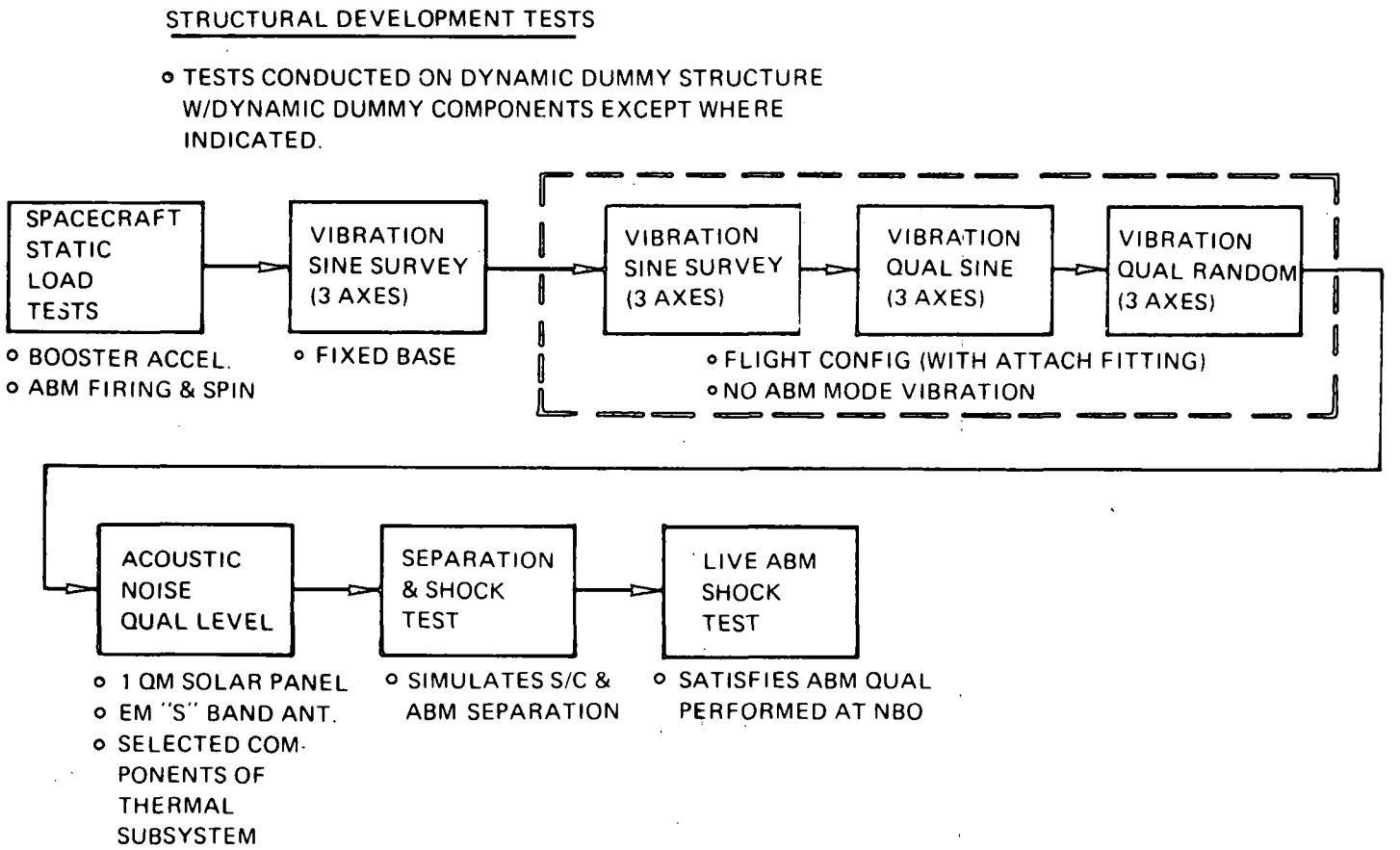

Figure 5-12. SMS Structural Development Test Flow Diagram

(d) The large size of the spacecraft severely limits the selection of centrifuge facilities which handle the job. This imposes severe scheduling problems on the test program.

Static load tests are also conducted to simulate inertia loads acting on the sun sensors, thrust chamber assemblies, and other components requiring critical alignment. The purpose of these tests is to ensure adequate local stiffness of the spacecraft structure to maintain acceptable alignment of these components.

It is not necessary to conduct a static load test simulating the ABM thrust event because the loads produced by this event are significantly lower than launch loads and are in the same direction and are transmitted by the same structure as the launch loads.

5.1.4.2 Test Description

The test unit for these tests consists of the development model with the attach fitting attached. The unit is placed in a load frame which is used to react all loads applied to the spacecraft. Limit and ultimate loads simulating critical acceleration loads developed during flight are imposed at all primary load points within the spacecraft using a typical whiffletree arrangement. Electronic components and other subsystems are removed as required and replaced with fittings designed to accept the application of a concentrated static load.

Instrumentation consists of strain gages and displacement gages. The strain gages are installed on structural members whose performance is critical to successful completion of the test and on any other structural members whose monitoring is dictated by stress analysis calculations. Care is taken to insure that sufficient strain gage information is obtained to accurately establish the vibration notching criteria.

Strain gage data recorded on magnetic tape and computer programs are utilized to convert the data to stress values. The stress values are then correlated with appropriate sections of the stress analyses. Dial displacement gages are installed where appropriate to measure displacements of critical components. These displacements are used to verify displacement requirements of the spacecraft and to confirm stiffness characteristics of the spacecraft as used in the dynamic analyses.

Any structural deficiencies detected during the static load test are corrected by redesign.

5.1.5 FIXED BASE SINUSOIDAL VIBRATION SURVEY

5.1.5.1 Test Configuration

The fixed base sinusoidal vibration survey is conducted to verify calculated dynamic characteristics of the spacecraft and to establish that minimum frequency requirements have been met. If required, modifications are made in the dynamic analyses so that those analyses would more accurately depict actual dynamic characteristics of the spacecraft. The development model spacecraft used in the test has structural components that are identical with flight hardware. Certain non-structural components are replaced with units which exhibit the same weight and inertia properties as the actual components.

5.1.5.2 Test Description

The spacecraft separation flange, located at the spacecraft interface with the launch vehicle attach fitting, is rigidly clamped to a test fixture which in turn is bolted to the table of the vibration test machine. Inputs of 1/2g are applied along the thrust axis and two orthogonal lateral axes of the spacecraft over the 5- to 200-Hz frequency range.

Accelerometers are installed on components whose responses accurately define the dynamic characteristics of the spacecraft. Exact locations of accelerometers are selected after the detailed dynamic analysis has been completed so that responses reflect areas of interest as determined by the analyses. All accelerometer data are recorded on magnetic tape and data reduction includes plotting of transmissibility graphs.

For this test and subsequent structural development tests, the VISSR thermal/structural development model is installed.

5.1.6 FLIGHT CONFIGURATION SINUSOIDAL VIBRATION SURVEY

5.1.6.1 Test Configuration

The primary purpose of this test is to determine preliminary information for proper conduct of the follow-on flight configuration sinusoidal vibration test. Results of this survey test are used to establish accelerometer calibration levels and to give additional insight into anticipated notching requirements for the vibration test. The test specimen is the same development model unit used in the fixed base survey test except that the launch vehicle attach fitting is mated to the spacecraft separation flange using a flight quality attach clamp.

5.1.6.2 Test Description

The base of the attach fitting is rigidly attached to a mounting fixture which is then bolted to the table of the test machine. Inputs of approximately 1.2g are applied along the thrust and two orthogonal lateral axes over the frequency range from 5 to 200Hz.

Since it is anticipated that notching is necessary for the sinusoidal vibration tests, it may be advisable to run additional survey tests at increased load levels before subjecting the test unit to the full qualification levels specified for the vibration test. This procedure has the advantage of exercising the structure to higher response levels, thus allowing a more accurate determination of final notching requirements. The need for these additional survey tests is evaluated as the program progresses.

It is planned that accelerometer locations for this test remain the same as in the fixed base survey test. However, if results of the fixed base survey test indicate that additional accelerometers or relocation of accelerometers are desirable, the necessary instrumentation changes are implemented. Strain gages are also installed on critical structural members so that the relationship between dynamic inputs and resulting structural loads can be determined. This information is then used to verify input notching requirements for the follow-on vibration test.

Accelerometer data are recorded on magnetic tape and data reduction includes plotting of transmissibility graphs. Strain gage data are also recorded on magnetic tape which can be input to computer programs for computation of stresses.

5.1.7 FLIGHT CONFIGURATION SINUSOIDAL VIBRATION TEST

5.1.7.1 Test Configuration

The flight configuration sinusoidal vibration test is conducted to verify spacecraft structural adequacy under the qualification level sinusoidal vibration environment. It is anticipated that the vibration input is notched (reduced over certain frequency ranges) in order not to impose unrealistic loads on the spacecraft structure. The proposed notching procedure is that described in Philco-Ford SH-212002, Environmental Requirements Specification. This procedure allows the limiting of spacecraft response at response at resonant frequencies so that the design strength of the structure is not exceeded. Results of the structural component static loads test are used to establish the maximum member stresses to be permitted during conduct of this sinusoidal vibration test. All proposed notching procedures are coordinated with NASA/GSFC.

Any structural deficiencies disclosed during the sinusoidal vibration test are corrected by appropriate design modifications and, where applicable, test results are correlated with the dynamic analyses. If modifications are made, portions of the test are repeated as deemed necessary.

5.1.7.2 Test Description

The test unit consists of the development model with the booster attach fitting attached. Vibration input is applied to the base of the attach fitting along the longitudinal axis and two orthogonal lateral axes according to the test schedule given in Philco-Ford SH-212002, Environmental Requirements Specification.

Accelerometer and strain gage instrumentation is identical with that used in the previous survey test unless results of the survey test indicate the desirability of different locations. All data are recorded on magnetic tape and appropriate transmissibility graphs and stress calculations are made.

5.1.8 FLIGHT CONFIGURATION RANDOM VIBRATION TEST

5.1.8.1 Test Configuration

Philco-Ford has selected the option of conducting random vibration tests rather than acoustic tests for qualification of the SMS spacecraft. It is judged that a random vibration test more adequately tests the ability of the majority of components to survive the launch and ascent environments. Exceptions to this philosophy are the solar panels and antennas which, because of their large surface areas, are more adequately tested under the acoustic environment.

Thus, this test is conducted to give preliminary confirmation of spacecraft structural adequacy under the qualification level random vibration environment. The test unit consists of the development model spacecraft and attach fitting. Since the solar array and communications antenna are more realistically tested in the acoustic test, substrate structures similar to the flight items with element/cell weight simulation is used.

As in the previous sinusoidal vibration test, it is necessary to notch the test input over selected input frequencies in order to eliminate the application of unrealistic loads to the spacecraft structure. Depending on the notching criteria established in the structural component static loads test and the sinusoidal vibration test, it is advisable to conduct preliminary reduced level tests to establish notching requirements for the full-level random inputs. All notching procedures are coordinated with NASA.

Any structural deficiencies disclosed during the random vibration test are corrected by appropriate design modifications, and the test repeated as deemed necessary.

5.1.8.2 Test Description

Random vibration input is applied to the base of the attach fitting along the longitudinal and two orthogonal lateral axes according to the test schedule given in Philco-Ford SH-212002, Environmental Requirements Specification.

Accelerometer and strain-gage instrumentation is identical with that used in the previous sinusoidal vibration test. All data are recorded on magnetic tape, and appropriate power spectral density graphs are made.

5.1.9 SPACECRAFT ACOUSTIC TEST

5.1.9.1 Test Configuration

The purpose of the acoustic test is to realistically excite those components which are not realistically tested during the random vibration tests. Components which especially fall into this category are the solar panels and the communications antenna. Because of their large surface area these components are more likely to be excited by an acoustic environment than by a random input applied to the somewhat distant attach fitting.

Experience has shown that minor modifications in spacecraft structure do not affect performance of large panels under an acoustic environment. Thus, it is proposed that this test be performed with one qualification model solar panel and the development model antenna. This test serves as the structural qualification test for this category of components. The remaining panel positions are filled with representative panels consisting of the panel substrate either without solar cells and antenna components or with representative units in their place.

Additional acoustic sensitive components, such as heat shields, are installed in representative locations.

The basic spacecraft used for the acoustic test is the development model with the attach fitting attached. As previously discussed, structural configuration of the spacecraft is essentially identical to the flight configuration. Representative components simulating the mass properties of the flight units are utilized if the actual components are not available.

5.1.9.2 Test Description

The test unit is placed in an acoustic chamber and subjected to the qualification level acoustic excitation as described in Philco-Ford SH-212002. The qualification model solar panel is examined and functionally tested before and after the acoustic test to check performance.

Accelerometer data are recorded at critical locations on sensitive components. Any structural deficiencies are corrected by appropriate redesign.

5.1.10 SEPARATION/SHOCK TEST

The separation/shock test consists of a series of tests during which a simulated spacecraft is separated from the ABM and its adapter, and the simulated spacecraft and adapter (with ABM) are separated from a simulated third stage launch vehicle. The objectives of this series of tests are:

(a) Determination of the separation event which produces the largest shock for later qualifications of the spacecraft and ABM.

(b) Validation of separation dynamics analysis techniques.

(c) Verification of separation clearances.

(d) Determination of component response levels to be used in updating component shock tests requirements.

5.1.11 TEST CONFIGURATION

All items in the area of the separation planes are the equivalent of flight hardware. Included in this category of flight type equipment are:

(a) 37 x 39-in attach fitting assembly (GFE)

(b) 37-in V-band clamp (GFE)

(c) ABM adapter with simulated ABM

(d) 25-in V-band clamp (GFE)

(e) Development model spacecraft appropriately modified for attachment to the test fixtures.

The third stage vehicle is simulated by attachment of appropriate weights to the GFE attach fitting assembly.

5.1.12 TEST DESCRIPTION - SPACECRAFT SEPARATION AND SHOCK TEST

In this test, the spacecraft and the simulated third stage are supported from the spacecraft handling ring with the simulated third stage free to fall. Upon initiation of the GFE bolt cutter pyrotechnic devices the third stage is released from the remainder of the spacecraft. Accelerometers are placed on the ABM flange and in representative locations throughout the spacecraft. All accelerometer data are recorded on magnetic tape and appropriate shock spectrum graphics are constructed.

5.1.12.1 Spacecraft/ABM Separation Shock Tests

This test has, as one of its objectives, the verification of the spacecraft dynamic analysis.

Instrumentation requirements for analysis verification are determined when the analysis and design are more mature.

High speed motion picture cameras are located at strategic spots so that visual observation for clearance determinations is made. Accelerometers are positioned on selected components and in selected locations throughout the spacecraft. These data are plotted as in the previous test and comparisons made for selection of shock loads to be later used in qualification of components as well as the spacecraft. It is anticipated that examination of response data from the two series of tests disclose that response is significantly greater in one of the two test configurations. Only the critical test configuration are then used for the separation shock test to be conducted during the qualification test program.

5.1.12.2 Live ABM Shock Tests

Because of the safety requirements involved with handling and testing a live ABM, the live ABM shock test is conducted at the Philco-Ford remote test facility located at Newport Beach, Calif. These tests are conducted upon suitable fixtures and are subjected to the shock loads associated with separation of the spacecraft and the launch vehicle third stage, and serve to complete the qualification of the ABM.

5.2 AUXILIARY PROPULSION SUBSYSTEM

The auxiliary propulsion subsystem (APS)[1] employs hydrazine as a monopropellant and provides all the propulsion for the satellite after separation from the third stage of the launch vehicle as shown in Table 5-5. A separate ABM provides the synchronous altitude orbit insertion energy. Specifically, the APS is functional during the following satellite operations:

(a) Active nutation control

(b) Attitude (spin-axis) orientation

(c) Attitude correction and maintenance

(d) Station acquisition

(e) Station change

(f) Longitudinal (E-W) stationkeeping

(g) Inclination control

(h) Spin-rate change and maintenance

Table 5-5

Summary of APS Design

Propellant	Hydrazine, MIL-P-26536C
Propellant storage tanks	Three spherical tanks, 3069 cubic inches combined volume (12.5 in ID)
Feed system	Unregulated inert-gas pressurized, spin oriented
Pressurant	GN_2 and/or helium
Maximum pressure range	300-psia initial; 70-psia blow-down
Propellant capacity	80 pounds maximum at maximum pressure blow-down ratio

Table 5-5 (continued)

Propellant	Hydrazine, MIL-P-26536C
Current estimated weight of on-loaded propellant (for first flight)	35 pounds
Blow-down ratio for 45 pounds on-loaded propellant	260/155
Propellant temperature	4 to 50°C
Nominal initial pressure	260 psia
Maximum operating (limit) pressure	350 psia
Proof pressure	525 psia
Burst pressure	700 psia (tank); 1400 psia (other components)
Thruster assemblies	Six; 4 rated at 5-lb thrust and 2 rated at 0.5-lb thrust at 260-psia system pressure
Thrust turndown ratio	Shall not exceed 2/1 for 260/100 blow-down
Thrust operating modes	Steady state and pulsed at rate of 1 pulse per revolution of satellite
Pulse mode duty cycles	3 to 12 percent for 0.5-lb TCA; 12 percent to 15 percent for 5-lb TCA
Steady state duration for single burns	0.50 to 180 seconds

The APS contains six electrically operated thrust chamber assemblies (TCA's). The TCA's are arranged in redundant pairs of functional groups, each of which is able to produce axial, radial, and spin velocity changes. Each functional group has one valve upstream which is latched open or closed by command in order to compensate for any thruster valve leakage.

The liquid propellant storage system uses a nonregulated (blow down) inert gas (nitrogen, helium) pressurized feed and consists of three tanks that serve all TCA's through an arrangement of manifolds and branch feed lines. There are two thruster manifolds each containing one 5 lb_f radial TCA, one 5 lb_f axial TCA and one 0.5 lb_f radial vernier TCA. Between the propellant storage supply (the tanks) and the thruster manifolds are isolation valves, one per manifold, which are normally closed and opened on command when thruster operation is imminent. These isolation valves provide a secondary seal mechanism to protect the fuel supply against any leaky thruster valve. A pressure transducer is connected to the liquid feed line to indicate storage tank pressure. Components are interconnected by rigid tubing (1/4-inch O.D. stainless steel) with welded or brazed joints. Propellant flow is initiated by ground command, which electrically activates the desired TCA's through the valve-driver units which are part of the APS. The TCA's are operated in both pulsed mode and steady state.

A fill-and-drain valve is connected to the liquid manifold; this allows two-directional transfer of propellant and pressurant and permits complete drainage when the APS is oriented by the launch support handling dolly.

5.2.1 REQUIREMENTS

The storage system accommodates all anticipated propellant requirements including contingency allowances for non-usable fractions and reserve for growth potential. Summaries of maneuvers and corresponding allocations of propellant are contained in the fuel budget schedules.

The three tanks used for hydrazine storage have a combined volume capacity for 80-pounds hydrazine at an initial pressure of 260 psia with blow-down to 74 psia at propellant exhaustion. The design requirement is 80 pounds capacity within a pressure blowdown range of 300 to 70 psia. When the APS is on-loaded with 45 pounds of propellant, blow-down is from 260 to 155 psia.

Feed system plumbing serves several functions, including filling, draining, pressurization and venting of propellant and inert gas pressurant for prelaunch and other ground servicing operations. The feed system also ensures liquid propellant delivery to the thruster assemblies for ground test and flight operational periods.

Connecting lines in the feed system are completely sealed and contain welded and brazed joints to minimize leakage and also provide the required degree of flexibility for cleaning and assembly of APS components. All materials must be rated class 1 for hydrazine service within the operating temperature range of 4.4 to 60°C.

Prevention of propellant freezing is included among thermal management requirements which are part of the basic satellite design, and consequently is not imposed directly as an APS requirement. Protection of adjacent components or structure from elevated temperature environments generated by the hydrazine reactors is afforded by satellite subsystem design with partial protection included as an optimal requirement for the APS.

Thruster assemblies are the primary operational components in the APS. Maneuver requirements prescribe corrections for active nutation control, position and attitude changes and spin-rate adjustments.

Each propulsive maneuver can be accomplished by at least two different thruster assemblies. This affords complete redundancy for fail-closed contingencies. Each thruster contains either a dual-seat control valve or two single-seat valves in series; these valves and the isolation valve in each branch of the feed system afford complete redundancy for fail-open contingencies. Thruster control valves are normally closed and are electrically actuated to open, providing further protection against fail-open events.

Thruster performance requirements, as specified by Philco-Ford, are summarized in the following paragraphs.

The specification requirements for the 0.5-lb. TCA are as follows:

Total impulse	4,000 lb_f-s
Nominal thrust rating (P_F = 250 psia, T_P = 20°C)	0.4-0.5 lb_f
Minimum thrust range	2:1
Maximum thrust overshoot:	
First pulse	400%
Subsequent pulses	40%
Feed system:	
Nominal initial pressure	260 psia
Nominal propellant temperature	20°C
Maximum propellant temp.	50°C
Minimum propellant temp.	4.4°C
Minimum pressure	< 100 psia

Duty cycle:

Pulsewidth range	30 - 125 ms
Period range	0.55 - 1.20 s
Nominal duty cycle	0.05 sec ON/0.55 OFF

Minimum pulse-mode average specific impulse:
(for 5-20 pulses including 3σ error)

For $T_P \geq 20°C$	100 lb_f/lb
For $4°C \leq T_P < 20°C$	90 lb_f/lb

Rotational impulse prediction accuracy: ±10%

Absolute rotational centroid: (excluding first pulse) < 120% on-time

Life: 30,000 pulses and 6 minutes steady-state

The specification requirements for the 5-lbft TCA are as follows:

(a) Total impulse 24,000 lb_f/s

(b) Nominal thrust rating (P_F = 250 psia, T_P = 20°C) 4.75 - 5.25 lb_f/

(c) Minimum thrust ratio range 2:1

(d) Maximum thrust overshoot

First pulse	400%
Subsequent pulses	40%

(e) Maximum chamber pressure oscillations:

Steady-state acceptance test (excluding initial 0.5 sec)	±6 psia
Steady-state life (excluding initial 0.5 sec)	±12 psia
Pulse-mode acceptance test (last 50% of commanded pulsewidths)	±3 psia

Pulse-mode life (last 50% of commanded pulsewidth)	±6 psia

(f) Feed system:

Nominal maximum pressure	250 psia
Nominal propellant temp.	20°C
Maximum propellant temp.	50°C
Minimum propellant temp.	4°C
Minimum pressure	< 100 psia

(g) Duty cycle:

Pulsewidth range	50 - 125 ms
Period range	0.55 - 1.2 s
Nominal duty cycle	0.078 sec on/0.522 off

(h) Minimum steady-state specific impulse: (including 3σ error)

Feed pressure = 250 psia	220 lb_f-s/lb_m
Feed pressure - 180 psia	215 lb_f-s/lb_m
Feed pressure - 120 psia	210 lb_f-s/lb_m

(i) Minimum average pulse mode I_{sp} : (including 3σ error)

Feed pressure = 250 psia

For train of 100 pulses	205 lb-s/lbm
For train of 200 pulses	212 lb-s/lbm
For trains greater than 500 pulses	215 lb-s/lbm

Feed pressure = 180 psia

For train of 100 pulses	200 lb-s/lbm
For train of 200 pulses	210 lb-s/lbm
For trains greater than 500 pulses	214 lb-s/lbm

(j) Rotational averaged centroid repeatability:

Pulse train length:

3-10	±40 ms
11-100	±30 ms
>100	±10 ms

(k) Absolute rotational centroid: (excluding first pulse)	100% on-time

(l) Rotational centroid variability:
(for 50 pulses starting with pulse 51) ±5 ms

(m) Rotational impulse prediction accuracy:

Less than 10,000 pulses and 4 minutes steady-state	±5%

(n) Minimum rotational impulse efficiency: (for trains >100 pulses)

Pulse train efficiency:

Feed pressure = 250 psia	95%
Feed pressure = 180 psia	94%
Feed pressure = 120 psia	92%

Individual pulse efficiency:

Feed pressure = 250 psia	92%
Feed pressure = 180 psia	90%
Feed pressure = 120 psia	88%

(o) Life:

Minimum cycles	23,000
Minimum accumulated steady-state	55 minutes

Functional Characteristics

Propellant is stored in equal portions in three spherical tanks and at identical pressure heads by virtue of interconnected plumbing on the gas and liquid ends of each tank and controlled positioning of each tank at the same distance from the spin axis. Close tolerances imposed on tank dimensions and volume assure sphericity. Consequently, the center of propellant mass does not shift as propellant is consumed during flight.

Feed lines are sized to prevent bubble lock-up even at one "g". Extra margin exists to assure proper bubble migration at the higher sustained accelerations experienced in flight, when spinning.

Mass stabilization occurs soon after initial spinup. The distribution of total propellant among multiple tanks enhances the full capture of propellant thereby minimizes energy dissipation through slosh.

Feed and storage components are not susceptible to leakage. The APS is a completely sealed unit, using no mechanical joints. Isolation valves, one in each thruster manifold, protect the feed and storage system from depletion due to a leaky thruster valve. Field welding techniques are employed during final assembly of the APS in the spacecraft.

A fill/drain/vent valve is located at an accessible region to permit two-way pressurized and propellant transfer.

The APS is received at the launch site in a dry state, with the storage system under a slightly positive head of gaseous nitrogen. Thruster nozzles are kept covered with protective caps. The subsystem is filled, pressurized and leak tested prior to launch. A ground service cart and leak detection equipment are used for pre-launch servicing and checkout.

Propellant on-loading is initiated after the APS is evacuated. Propellant is admitted through the fill/drain valve in the liquid line. Direct-weighing is used to determine quantity transferred. Pressurization is accomplished in two stages. Initial pressurization is to a low level at reduced risk to personnel. Final pressurization to the final valve is scheduled among the later launch preparation events. While the APS is attached to the service cart, system pressure is monitored by cart instrumentation. The APS flight transducer is used for ground monitoring if terminals are made available for this input during checkout. Protective caps are removed from the thruster after propellant is on-loaded.

In the boost phase, the APS is non-operating. Each command sequence for a thruster operation is preceded by a single pulse command to the appropriate isolation valve. The branch feed line to the thruster remains open during the thruster operating period. After this period the isolation valve is actuated to the closed position by another single pulse command. The first operation occurs during the transfer orbit. Active nutation control (ANC) is achieved by executing ground commands to one of the 5-lb_f thrust axial thrusters or by a back-up, automatic mode, which has less flexibility in its design. On-time is selected to coincide with even multiples of spin periods, such that each correction covers a full 360-degree rotation, properly phased with the nutation peak. As many as 84 ACN corrections, each of 600 to 1000 milliseconds duration (depending on spin-rate), are made. Consistent with the accepted terminology, which references duty cycle to the period of rotation, each ACN burn is identified as a steady-state operation instead of as a single pulse. The ground control input signal causes the control valve of the selected axial thruster to be energized open. Removal of input signal restores the valve to the normally-closed position. The thruster control valve is equipped with series-redundant seats; both seats open simultaneously.

The second maneuver is a course spin axis precession correction, involving an approximately 132-degree change in axis position. The correction is achieved by an axial thruster (either may be selected). The correction may be made in one or two large increments in pulsed mode, using an approximately 13-percent duty cycle, which is near optimum for maximum effective specific impulse with a quasi-limited time window. Each pulse is ground commanded and is timed to start at a preselected interval with respect to a sun-sensor or earth-sensor signal, so that the centroid of the resulting group of impulse bits occurs in the aiming direction.

The number of pulses commanded is determined from a look-up table (computerized), inputted with system pressure, temperature, duty-cycle, spin-rate and spacecraft mass properties. Each of the thruster performance characteristics is documented individually. In the absence of system pressure data, inflight calibration techniques are employed. Actual spacecraft response to a known command is fed back to the look-up tables and is assigned to a pressure level for the operating TCA. Pressure decay is calculated routinely, using predicted specific impulse data. The calculated value is available as a supplemental guide to inflight calibrations.

Final attitude correction for aiming the ABM is achieved in one or two shorter pulse-train commands, preferably given to the same thruster. If desired, the final vernier corrections are made with the vernier engines. This option is available, but is not considered necessary to be exercised in view of the existing resolution capabilities of the 5-lb_f TCA.

During the final orbit phase, another spin-axis adjustment is made to orient the spin axis normal to the orbit plane. This maneuver is also performed as multiple corrections, similar to the ABM aiming maneuver described in the preceding paragraph.

Station acquisition is achieved by pulse-mode firings of the large radial engines. Because of the spin-torque generated during radial engine firings, it becomes necessary to limit the spin-rate excursion to the prescribed limits by alternately commanding opposing radial thrusters. Since camera operation is not scheduled until the spacecraft is on station, it is currently planned to execute large commands on a thruster before switching to the other TCA. During this sequence, spin rate may be trimmed to the assigned target level at no additional propellant expenditure.

After the spacecraft is on station, the annual requirement for drift adjustment is within range of the spin-rate tolerance, even if the command is executed with one thruster. In practice, it is expected that the E-W station-keeping adjustments are made at more frequent intervals, which are further within the spin-rate

control tolerance band. However, if finer control of spin rate is desired, it is possible to command either the 5-lb_f or the 0.5-lb_f TCA to neutralize the slight spin error initially introduced.

Fine spin-axis precession adjustments require use of the vernier engines. These are expected to be operated daily if required. The average daily requirement is approximately 13 arc seconds.

Large adjustments of spin rate are obtained from steady state firing of the 5-lb_f radial thrust engine that is in the correct position for the direction intended (spin-up or spin-down). In the event of failure of that particular engine, the corresponding 0.5-lb_f thruster is employed.

The inclination adjustments (N-S stationkeeping) are made by steady-state burns of either of the axial thrusters.

The operation of the vernier thrusters differs slightly from that of the larger engines because of the valving arrangement. The small engine contains two separate valves, in tandem, each with separate coils and independent circuitry. The upstream valve is used as a pre-fire valve. It is energized to the open position prior to commanding pulses (or steady-state) to the downstream valve. The upstream valve is closed after completion of the burn sequence. Thus, only one valve serves the on-off control function during commands. This feature sharpens the crispness of pulse characteristics, principally during tail-off, and still retains the redundant sealing characteristic which is considered mandatory for realization of reliable system performance during the entire 5-year service life.

5.2.2 PHYSICAL DESCRIPTION

5.2.2.1 Propellant Storage

Propellant is stored in 3 spherical tanks, 12.5 inches in diameter, which are made of stainless steel. Volume capacity of each tank is 1023 cubic inches, resulting in a total propellant volume capacity of 3069 cubic inches.

The tanks are installed with centers equidistant from the spin axis in a plane offset slightly from the spacecraft center of mass (at final orbit phase). Pressurant and liquid are both contained within the tanks. No bladder or expulsion device is necessary.

The plumbing arrangement and outlets of the tanks are positioned so that positive and complete fluid expulsion takes place during both ground test and flight conditions. Locations of ports is shown in Figure 5-13. Maximum specified weight

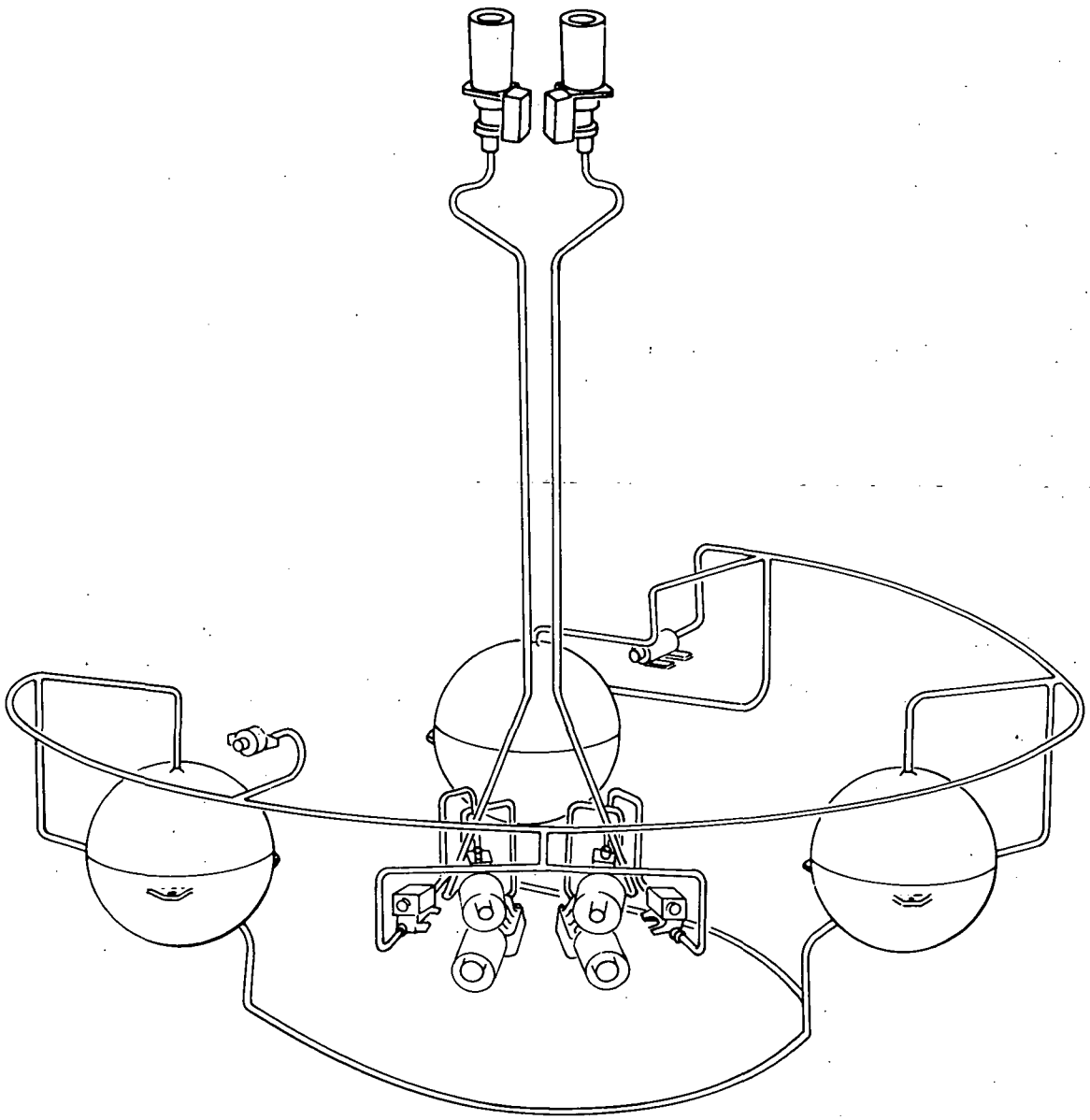

Figure 5-13. Auxiliary Propulsion System

is 2.5 pounds/tank. Minimum burst pressure specified is 700 psia. The tank is delivered with stainless steel tube stubs on the gas port and liquid ports.

5.2.2.2 Propellant Feed

The feed subsystem interconnects components as shown in Figure 5-13. It is comprised of adapters, fittings and tubing in the gas and liquid branches.

To accommodate system integration requirements, final joining of gas manifold to the tanks is performed when the APS is assembled in the spacecraft. A welding technique is used.

Tube size for manifolds is 1/4-inch diameter x 0.020-inch thick wall; material is 304L stainless steel.

Orbital welding under inert gas is used for the APS welds. All fittings and tubing are chemically and ultrasonically cleaned following forming and end-preparation operations. Welding operations are performed in a class 100 Laminar flow booth. Ends are protected and bagged during all fabrication and assembling operations which do not require exposure or access.

Welded fittings are machined from 304L material to afford minimum weight, matched interfaces at all welded joints, resulting in a uniform bore diameter. Brazed joint fittings do not permit butt-joining. A short expansion (wall thickness height) exists between tube ends within the joint but contours are relatively smooth as fillets form during the liquidus state, and flow of working fluid is not impaired. The liquid branches of the feed subsystem link the thruster assemblies, pressure transducer, and fill/drain valve to the propellant tank outflow lines. Each tank is equipped with a tube assembly which combines lines from the side and vertical outflow ports to a common effluent line. The junction of the outflow lines from each tank is located outboard from a plane normal to the side outflow port and is full bore, to preclude pressurant ingestion from the vertical port which is open to pressurant during most of the flight.

Maximum line velocity for single thruster operation is only 1.8 feet per second, at a bore diameter of 0.20 inch. At this flow rate, the dynamic head is 0.05 foot or 0.6 inch. Consequently, a positive flow of liquid is assured even at the maximum possible pressure differential across the outflow feed line configuration.

Safety margins are adequate for prevention of gas ingestion at all operational conditions including full depletion of usable propellant with the storage tank envelope.

The vertical outflow port is used for propellant off-loading or delivery during ground test and ground service operations. The APS orientation in launch position places the vertical outflow port at the "top." Liquid feed is prohibited in this orientation when the spacecraft is not spinning. The arrangement permits positive feed to thrusters during both normal and abnormal post-launch operations when the spacecraft is spinning about either the major or minor axis. This feature affords means to recover from an adverse decay to a tumbling spin in the event of loss of rotation control.

The fill/drain/vent valves are supplied by Pyronetics, Inc., and are of an in-line, dual-seal configuration, qualified for hydrazine service to the environmental conditions of SMS.

The pressure transducer is installed in the liquid branch of the feed subsystem. The downstream ends of the feed subsystem interface with the thruster assemblies. Brazed joints are employed at locations which are accessible for "insitu" brazing to facilitate replacements of thrusters and the pressure transducer without necessitating complete disassembly of the APS.

5.2.2.3 Thruster Assemblies

Two different size (thrust-ratings) are used in the APS. Thruster assemblies contain propellant control valve(s), a thrust chamber and nozzle assembly and support structure. A heat shield is included as part of the assembly. The inlet line interfaces with the APS feed system. The inlet side of the valve (or valve pair) contains a filter. The downstream side of the valve (or valve pair) is coupled directly to the injector portion of the thrust chamber. The thrust chamber and nozzle assembly accommodates the injector and houses Shell 405 spontaneous catalyst. Exhaust products from the decomposition of hydrazine are expanded through either a contoured or conical nozzle with an expansion ratio of 40:1 to 100:1.

5.2.2.3.1 5-lb_f Thrust Chamber Assembly (TCA). This thruster is supplied by Rocket Research Corporation (RRC) and is flight qualified from the reaction engine module (REM) program. Design features are summarized in Table 5-6. The TCA configuration is shown in Figure 5-14. Estimated unit weight is 1.3 pounds, including a heat shield assembly and a slightly heavier version of the hard-seat hydraulic research valve. The modified valve is rated at 18 watts providing greater force margin than the existing 14-w valve.

The reactor of the 5-lb_f engine in combination with a single-seated Parker valve has been tested at the conditions listed in Table 5-7. Qualification requirements for the REM engine are summarized in Table 5-8.

The thrust chamber design consists of the following components:

(a) Injector assembly

(b) Thrust chamber and nozzle

(c) Lower bed plate assembly

(d) Shell 14- to 18-mesh and 25- to 30-mesh ABSG granular catalysts

Table 5-6

Design Summary 5 lb_f Thrust Chamber Assembly

Catalyst	Shell 405
Upper bed	25- to 30-mesh granules
Lower bed	14- to 18-mesh granules
Bed diameter, inches	1.179
Bed length	
Upper bed, inches	0.25
Lower bed, inches	0.65
Total bed length, inches	0.90
Nozzle	80 percent bell contour
Expansion ratio	40:1
Throat diameter, inches	0.197
Exit diameter, inches	1.246
Material selection	
Thrust chamber	Haynes 25 (L605)
Injectors	Inconel 600
Capillary feed tubes	Inconel 600
Weight, lb_m	
Thrust chamber	0.39
Heat shield and support	0.36
Propellant valve	0.55
	1.30

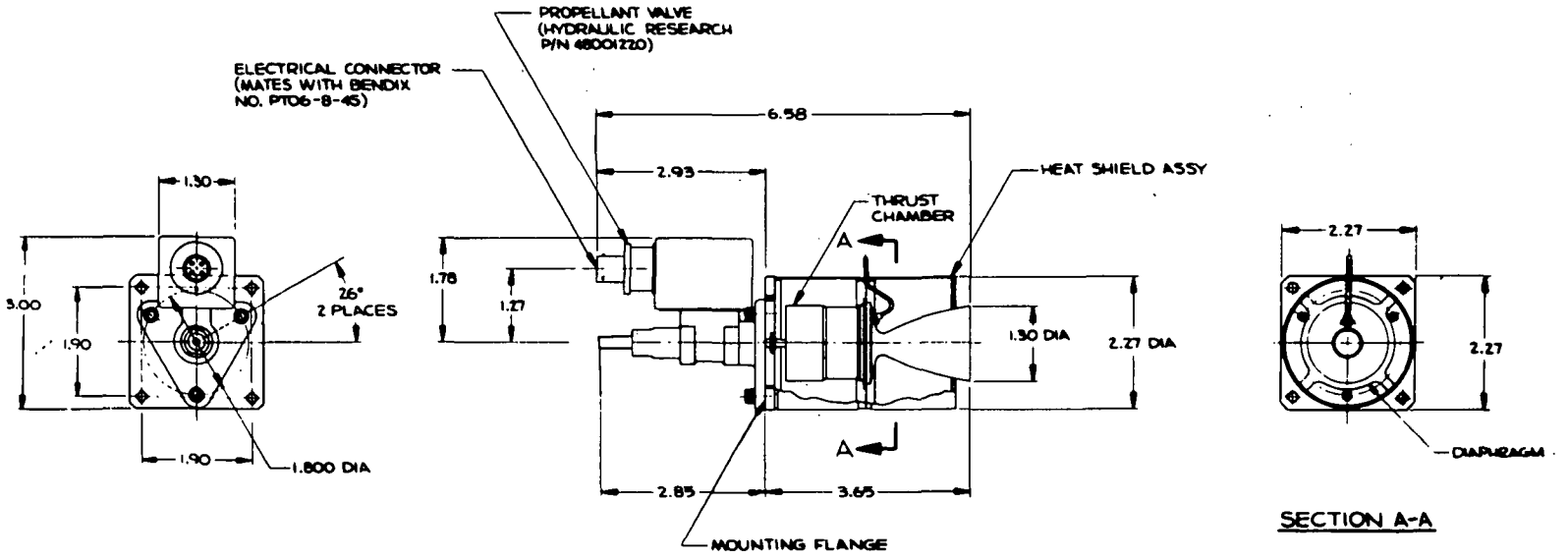

Figure 5-14. 5-lb_f Reaction Engine Assembly

Table 5-7

Development/Prequalification Tests Completed
5-lb_f Rocket Engine Assembly (REA) Used in REM

Test	Number of Units	Test Level(s)	Remarks
Life cycle	5 (D2, D2A, D2B, D3, and D4A)	Duty cycles from 0.01 cps to steady state; accumulated pulse life and total impulse per: D2 = 305,000 pulses; 40,000 lbf-sec D2A = 154,000 pulses; 23,000 lbf-sec D2B = 310,000 pulses; 40,000 lbf-sec D3 = 185,000 pulses; 22,000 lbf-sec D4A = 200,000 pulses; 19,000 lbf-sec	Early prototype REA life testing over duty cycle extremes; engine life characteristics established as a function of pulse life and total impulse.
Elevated propellant temperature	1 (D2)	Propellant feed temperatures up to 160°F with valve electrically heated to 250°F (i.e., propellant temperatures entering injector approximately 250°F	No indications of adverse or boiling operation under elevated propellant and valve temperature conditions over pulse mode and steady state duty cycle extremes.
Performance map with thrust measurement	1 (D3)	Duty cycles from 0.01 cps to steady state; pulse widths of 11, 22, and 44 ms	Thrust coefficient, impulse bit, and I_{sp} map test versus bed temperature.

Table 5-7 (continued)

Test	Number of Units	Test Level(s)	Remarks
REA vibration margin	1 (D4B)	Random vibration at 54 g's rms	Successful, not structural and/or catalyst problems noted.
30-day vacuum thermal life tests (prequalification REM S/N 0001)	2 (active REA's)	Duty cycles from 0.004 cps (22 ms pulse width) to steady state; propellant temperatures from +40°F to +140°F; environmental temperatures from 0°F to +140°F; nozzle target, temperatures of -300°F to +140°F propellant inlet pressures of 264 psia to 110 psia; 175,000 life cycles and 18,000 lbf-sec total impulse per REA	Demonstration of REA performance and life capability over 30-day continuous test period when subjected to specification temperature, duty cycle, and pressure extremes (conditions varied throughout 30-day test).
REM qualification level vibration (REMS S/N 0002)	4 (standby REA's)	Three (3) axes sine (5-50 cps, 2.0 g; 50-2000 cps, 4.0 g) Three (3) axes random (180 seconds per axis, 37.8 g's rms)	Successful; no structural and/or catalyst problems noted; units subsequently subjected to overstress and performance firing tests noted below.
REM qualification level mechanical shock (REM S/N 0002)	4 (active and standby REA's)	Six shocks, ±each of three axes; 1/2 sine wave, 30 g's, 8 ms.	Successful; no structural and/or catalyst problems noted; units subsequently subjected to overstress and performance firing tests noted below.

Table 5-7 (continued)

Test	Number of Units	Test Level(s)	Remarks
REM qualification level pyrotechnic shock (REM S/N 0002)	4 (active and standby REA's)	Two shocks, vehicle simulated structure with explosive separation; 5,800 g's peak.	Successful; no structural and/or catalyst problems noted; units subsequently subjected to overstress and performance firing tests noted below
Performance map (REM S/N 0002)	4 (active and standby REA's)	Duty cycles from 0.1 cps to SS (ambient temperature) maximum. MIB condition at +140°F propellant and environmental temperature following SS operation at 10 cps duty cycle (22 ms pulse width).	Performance map over duty cycle range; determination of maximum MIB values; determination of MIB versus duty cycle influence coefficient.
Overstress tests	2 (active REA's)	Overstress testing in areas of: Pressure (315 psia to 85 psia feed pressure). Temperature (160°F propellant and environment). Voltage (20 vdc to 37 vdc). Heat rejection (4 REA's simultaneous firing).	Demonstration of REA overstress performance and capabilities following qualification level environment; total accumulated life on REA's (including above performance map tests): Active yaw = 141,000 pulses; 29,000 lbf-sec Active pitch = 135,000 pulses; 22,000 lbf-sec

Table 5-7 (continued)

Test	Number of Units	Test Level(s)	Remarks
Overstress tests (continued)	2 (active REA's) (continued)	Propellant (fully saturated and unsaturated; two 1-inch^3 bubbles through each REA).	Standby yaw = 68,000 pulses; 13,000 lbf-sec Standby pitch = 12,000 pulses; 12,000 lbf-sec

Table 5-8

5-lb_f REM Engine Qualification Requirements

Vibration	Random vibration: 3 axis, 180 seconds/axis, 37.9 grms, increasing at 6 db/octave from 20 to 100 cps, flat a $1 g^2$/cps from 100 to 1,000 cps, decreasing at 6 db/octave from 1,000 to 2,000 cps. Sinusoidal sweep: 3 axis, 10 to 50 cps at 2 g (0.5 DA), 50 to 2,000 cps at 4 g, 2 minutes per octave. Procedure 1, method 516 in MIL-STD-810
Acoustic	Method 515 of MIL-STD-810 with sound pressure level varying from 131.8 db to 138 db over 63 to 8,000 cps.
Mechanical shock	3 axes, 3 g peak, half sine wave, 0.008 second duration. Procedure 1 of Method 516 in MIL-STD-810.
Pyrotechnic shock	5,800 g's LMSC test procedures 73382, 73383, and 73384.
Acceleration	8 g's for 5 minutes on Y axis (flight axis) 3 g's for 5 minutes on ±Z axis 3 g's for 5 minutes on -Z axis 3 g's for 5 minutes on +X axis 3 g's for 5 minutes on -X axis
Electromagnetic Interference (EMI)	MIL-STD-826 class Au, Type-C equipment
Humidity	95-percent relative humidity. Method 507 of MIL-STD-810
Operating temperature	+40 to +140°F. Demonstrate +160°F
Engine life	175,000 pulses and 18,000 lbf-secs of total impulse
Pulse widths	Capable of pulse widths varying from 0.021 seconds to steady-state continuous firings of 20 minutes.
Duty cycle	0.01 pulses per second to 10 pulses per second

The injector design on the proposed engine uses a Rigimesh injector element which provides for propellant distribution across the surface of the catalyst bed and low stream momentum. Rocket Research Corporation has conclusively demonstrated on a number of contracted programs that high orifice stream momentum does result in increased catalyst loss when compared with the use of low stream momentum type injectors.

The injector body is made of Inconel 600 and was selected for its high temperature compatibility with hydrazine. The Rigimesh element is made of Haynes Alloy No. 25. The Rigimesh element is welded into the injector body by the Heliarc welding process.

The chamber and nozzle assembly consists of the catalyst chamber, nozzle, and chamber pressure-tap fitting. The pressure tap fitting is used for acceptance firing and is sealed after acceptance testing of the APS.

Control Valve (for 5-lb_f Thruster)

The propellant control valve is a redundant hard-seat, torque-motor-actuated configuration supplied by Hydraulic Research & Manufacturing Company (HR&M) and is flight qualified.

A schematic of the basic HR P/N 48000680 is shown in Figure 5-15. The valve is modified by incorporation of a trim orifice in the inlet fitting and provision of mounting points compatible with the thruster design.

The Hydraulic Research valve is a normally-closed, torque-motor-actuated, single-flapper, dual-seat shutoff valve. The design incorporates two metal-to-metal flat-lapped poppets and seats in series to provide redundancy in the critical fail-open mode. The downstream poppet is actuated directly by the flapper which is an integral part of the armature. The upstream poppet is mechanically opened by a pin connected to the flapper. The poppet and seat material is extremely hard (1800 to 2000 Knoop) and thus resists damage by any particles in the fluid. The metal-to-metal poppets and seats ensure long storage life, compatibility with the propellant, resistance to adverse thermal and vibration inputs, and inherent repeatability due to fixed stroke geometry. Poppet-to-seat alignment is provided by the "Metflex" configuration. ("Metflex", a Hydraulic Research-registered trademark, is a metal-to-metal seat which has a unique flexible poppet design permitting self-alignment with the seat contact area.) An important consideration in establishing this concept is the avoidance of any single failure which keeps both poppets open. There is a 0.002-inch gap between the pin in the downstream flapper arm and the upstream poppet. Thus a particle of greater than 0.002-inch has to be trapped under the downstream seat to cause

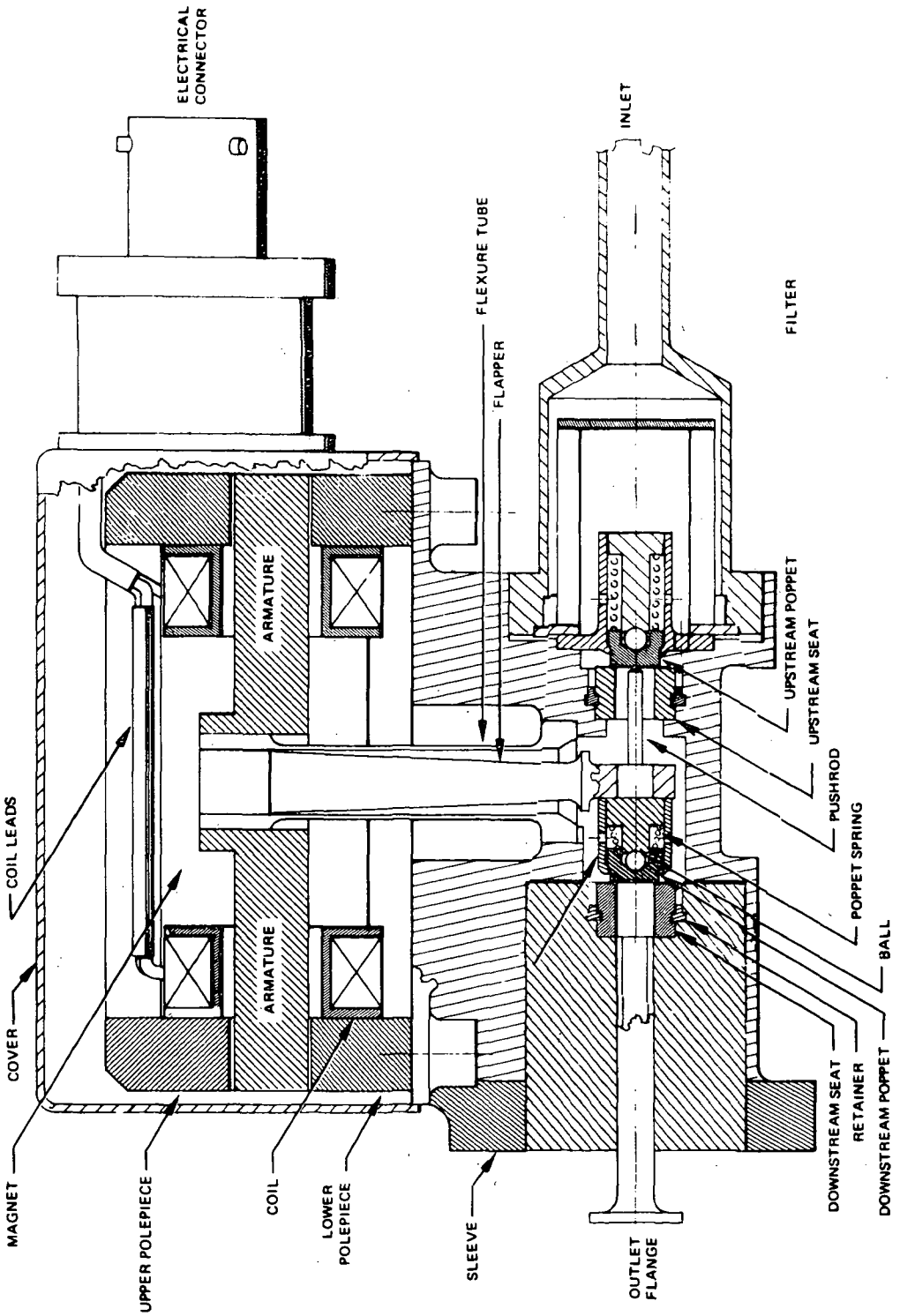

Figure 5-15. Hydraulic Research Valve Schematic

this double failure. This size is an order of magnitude greater than the nominal filtration level of the built-in valve filter. In addition, the probability of a particle being trapped between the hard poppet and seat is extremely remote.

All materials in the fluid flow path have been selected for compatibility with hydrazine. The unexposed materials have been selected to produce an efficient lightweight valve. All joints in the hydrazine flow paths are accomplished by electron beam welding to provide maximum joint integrity, long-term storage capability and high thermal compatibility.

Hydraulic Research has subjected all exposed materials to boiling hydrazine with no deterioration. Furthermore, a seat/poppet assembly was subjected to a 24-hour boiling hydrazine test and then checked for leakage. The leakage rate of the valve did not change. The weld joint between the flapper, flexure, and armature was subjected to a 48-hour water exposure test with no degradation of the weld joint.

The metal-to-metal seats and poppets plus all other materials in the valve, including the electrical coils, are capable of operation at a temperature of 430°F. This temperature capability provides a substantial margin of safety over the specified maximum valve temperature of 250°F. Demonstrated valve performance is shown in Table 5-9.

5.2.2.3.2 The 0.5-lb_f Thrust Chamber Assembly. The TCA selected for the vernier engine function is a nominal 0.5-lb_f thruster qualified by RRC on the hydrazine propulsion module (HPM) program. The engine is designed and has been operated over a range of 1 to 0.1 lb_f. The engine has been qualified for a burn time of 21,500 seconds, which exceeds the primary mode SMS requirement by a factor of ten.

A cross-sectional view of the reactor is shown in Figure 5-16. A summary of the engine design is given in Table 5-10. The engine is of all-brazed and welded construction and consists of an injector, an orifice, thrust chamber assembly, catalyst, catalyst bed retaining plate, catalyst bed retaining screens, and a heat shield assembly. It includes the reactor, heat shield, propellant valve, heaters, and temperature transducer.

The 0.5-lb_f TCA for the SMS APS does not use the heater or temperature transducer. The TCA includes provisions for chamber pressure measurement and is designed to allow installation of the thermocouple on the aft end of the chamber. The chamber pressure line is removed and sealed with the remaining stub at a distance of less than 0.3 inch from the outer surface of the unit at the attach point. The thermocouple is installed on the aft end of the chamber and there is sufficient space between the nozzle and heat shield to allow installation of the

Table 5-9

Control Valve Performance

Parameter	HR & M Performance (demonstrated)
Inlet pressure, nominal	300 psia
Pressure drop	< 20 psia at 0.0224 pps
Open response	14 ms (max); 8 ms (nominal)
Close response	5 ms (max); 4 ms (nominal)
Open response range	5-14 ms
Close response range	3-5 ms
Response Repeatability	±1 ms (at fixed conditions)
Internal leakage	0.5 SCC N_2/hr (max)
External leakage	1 x 10^{-6} SCC He/sec
Maximum power	14 watts
Maximum weight	0.47 pound
Cycle life	2 z 10^6 cycles
Voltage range	24-36 Vdc (all requirements) 18-36 Vdc (degraded response at 24 vdc)
Maximum operating temperature	200°F (non/degraded); 250°F (degraded)
Size	1.33 W x 2.17 H x 2.84 L
Number of seats	2 (series)
Number of coils	2 (parallel)

Note: Response values given are at extreme conditions with 12.5 volts transient suppression, at all operating conditions, from 50 to 300-psi inlet pressure; voltage from 24 to 36 vdc; 40 to 200°F.

thermocouple after assembly of the heat shield to the TCA. The 0.5-lb_f TCA weight is 0.9 pound, including the propellant valve and heat shield assembly.

An extensive development program was carried out on the engine at RRC. Development tests were conducted on the reactor to optimize the catalyst bed and injector, verify its life-time requirements, demonstrate vacuum-restart requirements, measure vacuum performance, and conduct low-temperature ignition

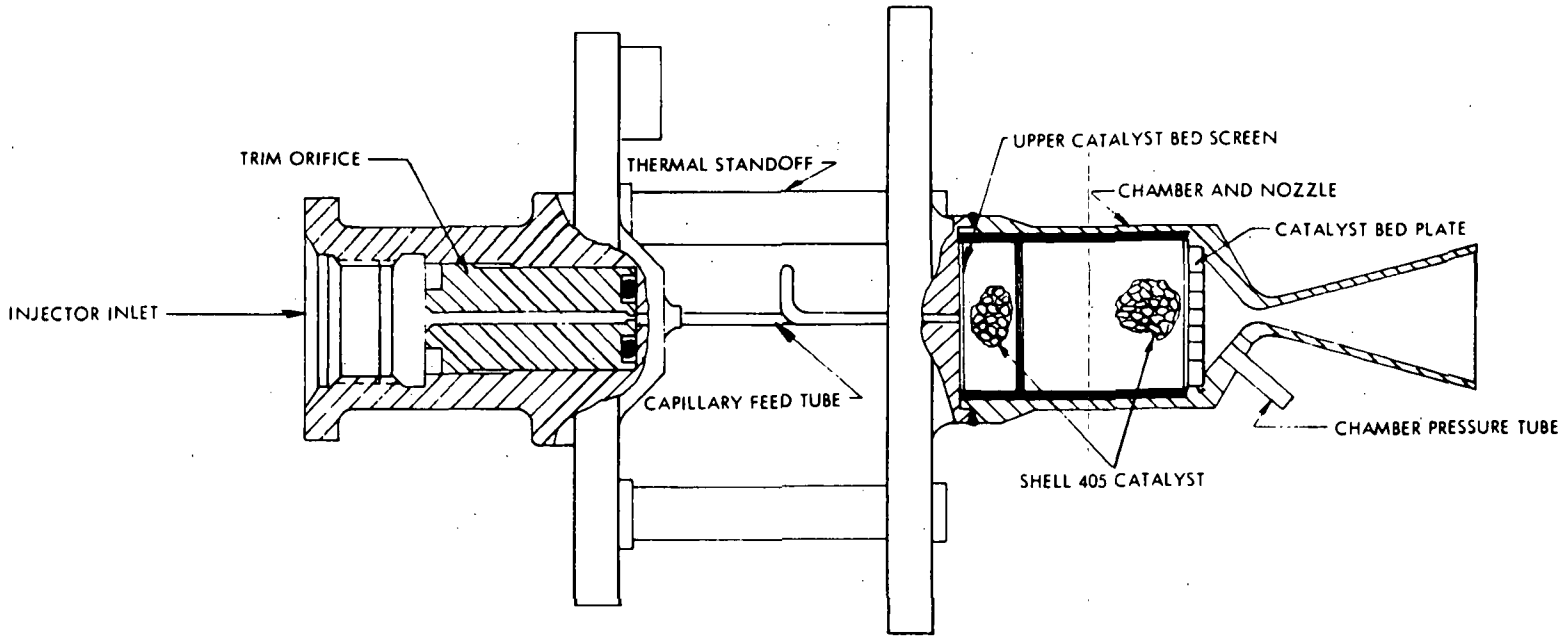

Figure 5-16. Cross Section of 0.5-lbf Reactor Assembly

Table 5-10

0.5-lb_f Thruster Design Summary

Catalyst	Shell 405, 25-30 mesh granules
Bed diameter	0.498 inch
Bed length	0.785 inch
Nozzle	15 degree conical
Expansion ratio	100:1
Throat diameter	0.043 inch
Exit diameter	0.430 inch
Material selection:	
Thrust chamber	347 stainless steel
Injector	347 stainless steel
Capillary feed tube	Inconel 600
Thermal standoffs	AM 355
Weight, lb_m:	
Thrust chamber	0.37
Propellant valve	0.53
Total	0.90

tests. A summary of development testing is shown in Table 5-11. Two problems were encountered in reactor development. These problems were:

(a) Chamber pressure oscillations caused by catalyst loss.

(b) Drop-off in chamber pressure during pulse-mode operation.

Table 5-11

Hydrazine Propulsion Module Engine Development Program Summary

Type Test	Engine Burn Time (Sec)	Test Results
Catalyst bed and injector optimization	392,400 total	1. Catalyst bed and injector configuration finalized to provide smooth operation and meet engine life requirements
Final steady-state life demonstration	21,410 seconds and each of two TCAs	2. Engine meets all requirements
Final pulse-mode life demonstration	21,300 seconds/19,870 pulses	3. Engine meets all requirements
Life restart	21,540 seconds	4. Forty starts with ambient temperature bed. Engine meets all requirements
Vacuum ignition	150 seconds (15 tests)	5. Successful ignition with propellant from 40 to 120°F and catalyst from 20 to 70°F
Vacuum performance	21,500	6. Vacuum specific impulse 223 to 220lb -sec/lbm over thrust range 0.5 to 0.25lb

The chamber pressure decay problem was caused by two-phase flow in the injector which resulted from heat soak-back from the thrust chamber to the injector under certain duty cycles of pulse-mode operation. This problem was resolved by injector redesign, and the engine now has demonstrated thermal capability to operate at all duty-cycle conditions.

The chamber pressure oscillation problem was solved through the use of Rockide "Z" insulation on the thrust chamber walls to minimize heat losses; optimization of the catalyst bed composition; and specially processed Shell 405 catalyst.

Low temperature ignition tests were conducted with varying propellant and catalyst-bed temperatures. Propellant temperature varied from +40 to +120°F and catalyst bed temperature from +20 to +70°F. Satisfactory ignition was achieved over the full range of temperatures.

Life cycle capabilities of the 0.5-lb_f engine far exceed the primary requirements for the SMS application. In addition to the 19870 pulses shown in Table 5-11, which were at duty cycles of 0.500 and 0.150 seconds on-times and 0.100 seconds off-time, other engines were tested successfully for 54,000 cycles (0.400 sec/on/0.100 sec off) and 1,011,383 cycles, covering a wide range of duty cycles with pulsewidths from 10 to 500 milliseconds and off-times ranging from 0.010 to 60 seconds (most less than 0.200 second). This past history of cycle-life capability, although not required for the HPM application, provides a firm base for expecting full protection against a large thruster failure by using the 0.5-lb_f engine as its back-up for the SMS APS.

A formal qualification program was conducted by RRC on the rocket engine assembly. This testing consisted of acceptance, mechanical shock, sinusoidal and random vibration, and altitude-performance testing. A summary of this testing is shown in Table 5-12.

Table 5-12

Hydrazine Propulsion Module Engine Qualification Program Summary

Type Test	Engine Burn Time (Sec)	Test Results
Acceptance	480	1. Reactor successfully passed proof, leakage, acceptance-firing and catalyst bed X-ray tests.
Shock		2. No damage from 18 shocks in 6 axes at 30-g's peak 8-ms duration.
Sinusoidal vibration		3. No damage at 7.5-g's peak 14-2000 cps in each of three axes for 25 minutes per axis.
Random vibration		4. No damage at 19-g's rms for 3 minutes in each axis and 6.1-g's for 4 minutes in each of three axes.
Vacuum performance	23,690	5. Seven ambient temperature starts with engine performance meeting specification.

In addition to the qualification tests conducted on the rocket engine as a component, six engines were used in the system qualification program at RRC. A summary of the HPM system qualification testing is shown in Table 5-13.

Table 5-13

Hydrazine Propulsion Module System Qualification Test Program Summary

Type Test	Engine Burn Time (Sec)	Test Results
Electromagnetic interference	—	1. System passed test except of temperature transducer out of specification broadband conducted interference at 0.8 MHz. Waiver granted.
Humidity and post-test electrical checks	—	2. System passed test except for low insulation resistance on one temperature sensor. Waiver granted.
Acoustic test	—	3. System subjected to overall level of 144 db.
Leakage test - system joints and propellant valves	—	4. No measurable leakage
Vacuum performance - ambient temperature	20,794 TCA #1 16,448 TCA #2	5. Seven ambient temperature starts on each TCA. Delivered impulse within required accuracy.
Vacuum performance - low temperature (40°F)	15,203 TCA #3 12,262 TCA #4	6. Seven ambient temperature starts on each TCA. Delivered impulse within required accuracy.
Vacuum performance - high temperature (120°F)	17,453 TCA #5	7. Seven ambient temperature starts on each TCA. Delivered impulse within required accuracy.
Leakage test - system joints and propellant valves	—	8. No measurable leakage

Propellant Valves (for 0.5-lb_f Thruster)

RRC's evaluation and selection of propellant valves for the 0.5-lb_f thrusters are based primarily on the use of proven and qualified hardware. The valves selected for both thruster sizes are fully flight-qualified, production valves.

The valve used on RRC's flight-qualified 0.5-lb_f HPM thruster uses Teflon soft seats which provide excellent contamination resistance and low leakage, and has no sliding fits. Its complete series-redundancy provides the desired capability of using the upstream seat as an isolation valve which can be opened and held open in advance of downstream seat pulse operation.

The sole changes necessary to the functional portions of this valve for the SMS application is a reduction in the outlet bore diameter to minimize downstream dribble volume. This change is accomplished simply by drilling a smaller hole during machining of the end cap of the valve. The other change involves simplification of the sheet metal box on HPM to house signal-conditioning and suppression-circuit elements. This box is required to serve only as a mounting bracket for the electrical connector for the SMS application, and the signal-conditioning/clipping circuitry is omitted. Separate leads are used for each coil, permitting independent actuation of each valve.

The propellant valve employed for the 0.5-lb_f thrusters of the MRS-6A system is the P/N 5680048 series-redundant, normally-closed, solenoid-actuated valve manufactured by the Parker-Hannifin Corporation, Systems Division. A cross-sectional view of the valve is shown in Figure 5-17. The principles of operation of the valve are described below. This valve was qualified by RRC as a part of the hydrazine propulsion module program.

The HPM valve has the following performance characteristics:

Maximum operating pressure	660 psia
Proof pressure	990 psia
Minimum burst pressure	1320 psia
Internal leakage (each seat)	5 std cc/hour GN_2 max
External leakage	1×10^{-6} std cc/sec He max
Flow characteristics	5 psia max at 0.00218 lb_m/s
Opening time	12 ms max
Closing time	10 ms max 30 volt clipping
	34 ms max 10 volt clipping
Cycle life	20,000 actuations
Qualification requirements	700,000 actuations
Development testing	19 - 31 vdc

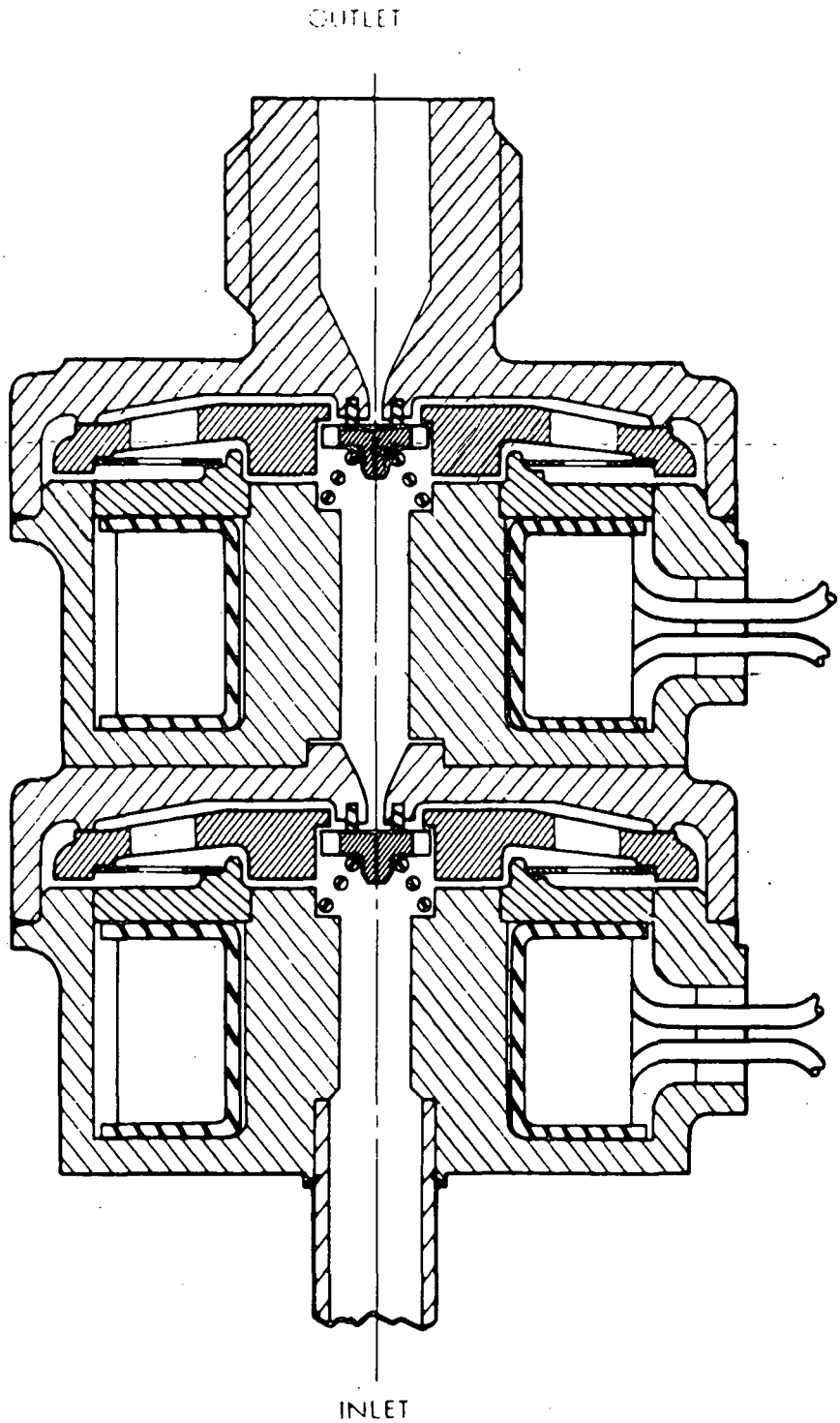

Figure 5-17. Cross-Sectional View of HPM Propellant Valve

Operating voltage	$\leq$10 watts at 31 vdc, 40°F
Power (both coils)	1 Vdc minimum
Dropout voltage	

The HPM propellant valve was subjected to a complete qualification program at the component level. Before starting the qualification test program, the valve was subjected to acceptance testing, which consisted of the following tests:

(a) Electrical characteristics

1. Operating voltage
2. Power drain
3. Dropout voltage
4. Insulation resistance
5. Dielectric strength
6. Clipping voltage
7. Signal conditioning output voltage

(b) Internal leakage

(c) Flow characteristics

(d) Vibration

(e) Contamination test

(f) Proof pressure

(g) External leakage

(h) Response

(i) Internal leakage

Following successful completion of acceptance testing, the valve was submitted to qualification testing. The valve was subjected to the following environmental tests:

(a) Shock test at 30-g's peak, 1/2 sine wave for 8 milliseconds duration three times in each direction of three orthogonal axes.

(b) Sinusoidal vibration for 25 minutes in each of three axes at the following levels:

5-14 cps	0.5 in D.A.
14-400 cps	5 g peak
400-200 cps	7.5 g peak

(c) Random vibration at 18.2 g's rms

(d) Random vibration at 6.2 g's rms

(e) Acceleration at the following levels:

1. Flight axis +11 and -3 g's
2. Two orthogonal axes, 3.5 g's in each of four directions

After each of the above environmental tests, the valve was subjected to a functional check. The functional test consisted of the following:

(a) Contamination test

(b) Internal leakage (each seat at 50 and 350 psig)

(c) 100 operational cycles

(d) Internal leakage (each seat at 50 psig)

(e) Flow characteristics

(f) Response

Following the environmental tests, the valve was subjected to 20,000 cycles of operation with a functional test being made after each 5,000 cycles. After completion of the cycling tests, the valve was subjected to response testing at a matrix of inlet pressure, valve temperature, and valve voltage. Inlet pressure was varied from 50 to 350 psig, temperature from 40 to 150°F and voltage from 19 to 31 vdc. After completion of the response test matrix, an additional 20,000 cycles was accrued on the valve with a functional test conducted each 10,000 cycles.

The valve met all specification requirements except for excessive leakage of the upstream seat after sinusoidal vibration. Failure analysis conducted revealed

that an "O"-ring in a test fixture, used to hold the valve during functional testing, had been cut and had lodged in the valve seat area. The valve was flushed to clear the material, and the leakage returned to within specification requirements.

In addition to the qualification tests conducted on the valve as a component, one valve was subjected to development testing with 700,000 cycles accrued on it. The development program was a duplication of the qualification program except for the larger number of cycles. A total of 16 valves were also used during prequalification and qualification testing at the system level.

5.2.2.4 Pressure Transducer

Fairchild Controls Model TF 125-4-0062, 0-500 psia transducer was used on Skynet in the auxiliary propulsion subsystem. The same basic transducer is used for SMS, with full scale output voltage increased to 5 volts.

5.2.2.5 Isolation Valve

Two isolation valves, one for each thruster manifold, are used in the APS. The isolation valves individually change valve position (open or closed) with each emergizing electrical command signal and remain stable in that position.

5.3 RELIABILITY SYSTEM DESCRIPTION

The basic purpose of the reliability program[1] is to contribute to the project, in a supporting role, the planning of necessary actions to ensure design reliability into the SMS spacecraft hardware and to prevent degradation of the reliability of the design through the succeeding steps, from fabrication to end use (mission accomplishment). It provides confidence that the SMS spacecraft and all systems will perform reliably during actual flight environments.

Philco-Ford's reliability program, as spelled out in the SMS reliability program plan, is responsive to the requirements of NPC 250-1 "Reliability Program Provisions for Space Systems Contractors," and NPC 400 (ref. 2) "NASA Procurement Regulation." The program is implemented by the SMS Contractor(s) and is monitored by NASA/GSFC/SMS project.

The SMS reliability program plan, along with the SMS quality program plans, must be officially approved by the GSFC/SMS project office and are designed to manage the reliability assurance functions at all the facilities performing work on the SMS program.

Monitoring is particularly important to the effective management of the program. Continuous surveillance and assessment is necessary to assure the effectiveness of the plan as work progresses. Therefore, a letter of delegation has been forwarded to the Defense Contracts Administration Services office at Philco-Ford, Palo Alto, Calif. This delegation letter spells out the quality assurance functions and areas where the GSFC/SMS project office desires Defense Contract Administration Service Office (DCASO) assistance. Specific inspection points are also delineated in the letter. The DCAS Regional Office at Burlingame, Calif., has accepted the full workload of delegated functions and has assured the SMS reliability and quality assurance (R&QA) manager that adequate manpower would be provided, as required.

The GSFC/SMS resources for evaluating the SMS program consist of: individual systems technical officers, assistance from DCAS resident-in-plant members, and periodic visits of project personnel during critical areas of design or production or testing.

The GSFC/SMS R&QA manager performs the overall supervision of the contractor's reliability program by following the reliability program plan's progress and milestones. Evaluation of the program is judged from results of contractor's reliability & quality status reports, monthly quality status reports from DCAS representatives, malfunction reports and other contract required documentation, the SMS parts program, visits to the contractor's (Philco-Ford) and subcontractor's facilities and many other related areas of information.

Some of the reliability program elements covered by the SMS reliability program plan are:

1. Reliability program management
   - (a) Contractor's organization
   - (b) Program plan
   - (c) Reliability program control
   - (d) Progress reporting
   - (e) Reliability training
   - (f) Supplier control
2. Reliability engineering
   - (a) Design specifications
   - (b) Reliability predictions

(c) Failure mode effect and criticality analyses

(d) Design review program

(e) Failure reporting and correction

(f) SMS parts program (tailored for the SMS project)

3. Testing and reliability evaluation

(a) Reliability evaluation plan

(b) Testing (qualification of hardware)

1. Parts, components, subsystems and systems

2. Test specifications, procedures and reports

(c) Life testing and reliability demonstration

(d) Reliability assessment

(e) Readiness reviews

(f) Reliability evaluation program reviews

Since the reliability program is designed to support the SMS project, it is essential that the reliability tasks be conducted integrally with the other project tasks and provide usable inputs at project decision points. This is presently being done by early definition of an SMS parts program, recognizing areas of new processes and developments (i.e., hybrid microcircuit, thick/thin film processes).

5.3.1 RELIABILITY SYSTEM DESCRIPTION

The reliability of the Philco-Ford portion of the SMS spacecraft design is based on mathematical concept's reliability assessment and utilizing MILCOMSAT demonstrated failure rates. The spacecraft operational reliability, on the order of 11 years mean time to failure (MTTF), is expected (according to Philco's assessment) even when considering the VISSR reliability parameters. The MILCOMSAT reliability has been demonstrated, at 50 percent confidence, to be in excess of 12.2 years MTTF.

The SMS spacecraft reliability was assessed as shown in Table 5-14. The indicated MTTFs based on these sets of data are:

Part Failure Rates	MTTF (years)
SRS division std	4
Orbit demonstrated (DEMO)*	11
MIL-HDBK 217A	0.6

*Based on DEMO reliability of 26 MILCOMSAT spacecraft with 605,000 hours of operation

Table 5-14

Dual Frequency Configuration Subsystem Reliability Assessments

Nomenclature	Philco-Ford Analysis	In-Orbit Demonstration
	P_s (5 yr)	
Overall satellite	0.3236	0.6975
Structure	0.9901	(**)
ABM separation	0.9992	(**)
Harness	0.9880	0.9942
Attitude control	0.8451	0.9783
Thermal control	N/A	N/A
Electrical power	0.8204	0.9398
Telemetry unit	0.8867	0.9850
Command unit	0.9633	0.9926
T & C transponder	0.9738	0.9929
S-band comm transponder	0.9234	0.9910
S-band comm antenna	0.7869	0.9368
UHF comm transponder and antenna	0.9643	0.9930
UHF comm antenna	0.9426	0.9822
Auxiliary propulsion	0.9683	0.9683
Apogee boost motor	0.9968	0.9968
Space environmental monitor	0.9979	0.9992
VISSR digital multiplexer	0.9893	0.9974

**No equivalent orbit demonstration data available

5.3.2 ASSUMPTIONS COMMON TO ALL THREE SETS OF DATA

1. Parts will be high quality and 100 percent screened and burned in.

2. Part application, on the average is 30 percent of the manufacturer's rating and at 25 ±10°C.

3. Failure rates are considered at the 60 percent confidence level.

5.4 APOGEE BOOST MOTOR (ABM)

The proposed high-performance ABM[1] shown in Figure 5-18 meets or exceeds all specification requirements. The motor is optimized for minimum weight within the length constraints imposed by the SMS vehicle. To impart the required velocity increment of 5975 ft/sec to a total spacecraft separation weight of 1325 lb at SMS motor ignition, the motor is designed to deliver a total impulse of 179,070 lb_f/sec with an average thrust of 4980 lb_f over a duration of 36.2 sec. This performance is provided at +55° F and vacuum conditions. The 3-sigma maximum thrust of 7738 lb_f imparts a maximum acceleration of 9.0 g to the spacecraft and is below the specified vacuum thrust limit of 8000 lb_f. A tabulation of the principal motor characteristics is given in Table 5-15.

The performance of an off-loaded motor design necessary to impart a velocity increment of 5975/ft/sec to a spacecraft weight of 1275 lbm was also determined. The off-loaded motor configuration is easily accomplished by trimming 24.1 lb of propellant from motors cast to the on-loaded design and results in less severe internal operating conditions. The amount of propellant removed can be easily varied to provide spacecraft design flexibility. Performance of the off-loaded motor is also shown in Table 5-15.

The same propellant-insulation-liner system used successfully in the space vehicle motor (SVM)-1, -2, and -4 motors was selected for the SMS motor because it best meets the specified performance and reliability requirements. This is the same system used in the Minuteman programs and has a real-time experience base of more than seven years. The propellant member of this system is ANB-3066, a production carboxy-terminated polybutadiene (CTPB) propellant that has been fully characterized in the Minuteman programs. The propellant has a production history of more than eleven million pounds mixed in over 2200 batches that have provided extensive variability and aging data and proven process control techniques.

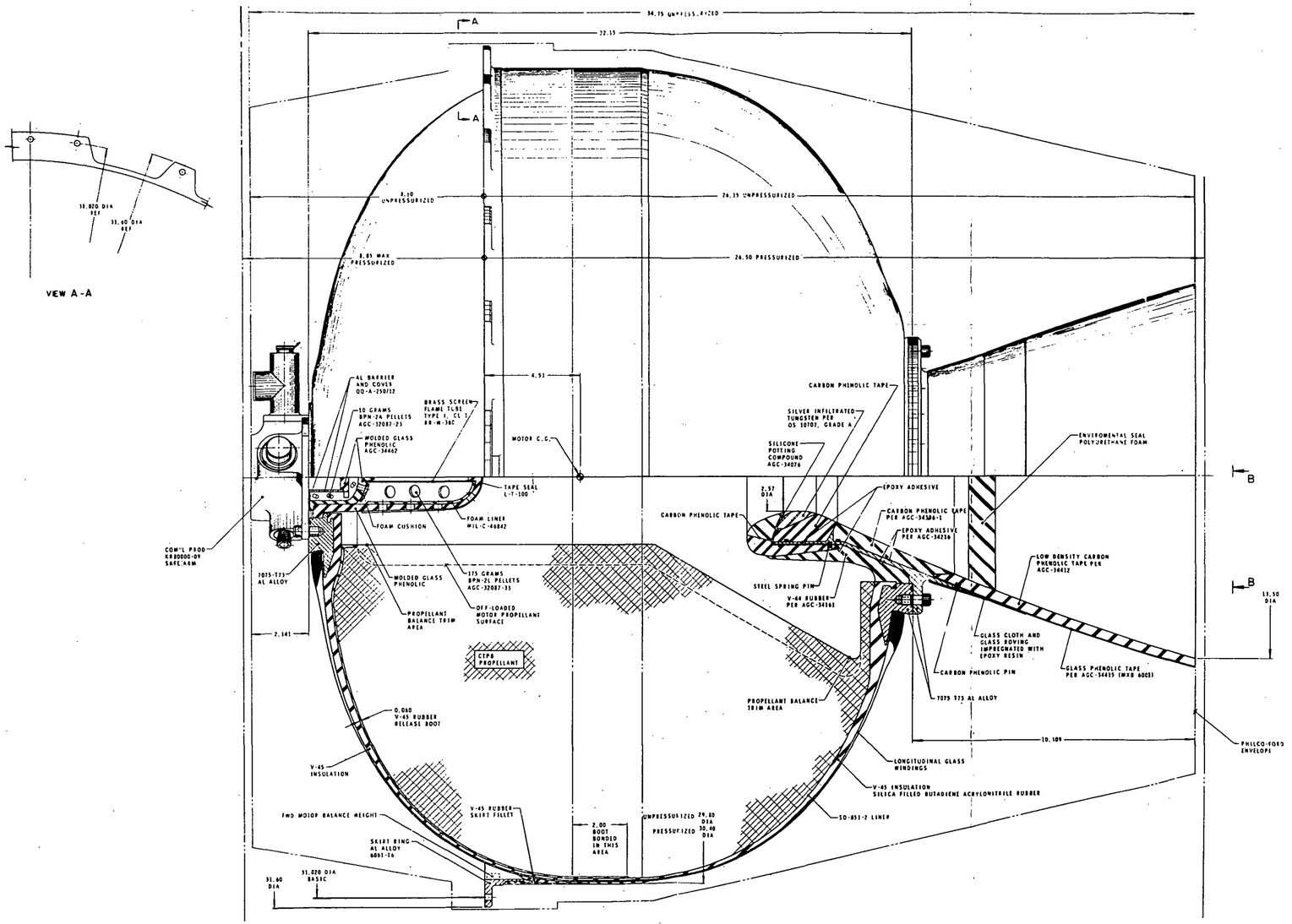

Figure 5-18. Apogee Boost Motor Design

Table 5-15

SMS Motor Performance Summary

Parameter	On-Loaded Configuration	Off-Loaded Configuration
Payload wt, lbm	1325	1275
Velocity increment, ft/s	5975	5975
Total vacuum impulse, lb_f/s	179,070	172,280
Total duration, sec	36.2	34.3
Average thrust, lb_f	4980	5090
Max thrust at +110°F, lb_f	7738	7738
Average pressure, psia	543	555
MEOP at +110°F, psia	865	865
Delivered motor specific impulse, $lb_f/s/lbm$	283.2	283.2
Delivered propellant specific impulse, $lb_f/s/lbm$	282.4	282.4
Total motor wt, lbm	677.7	653.6
Propellant wt, lbm	610.8	586.7
Burnout wt, lbm	57.4	57.4
Mass fraction	0.915	0.912
Maximum acceleration at +110°F, g	9.0	9.3

Note: Delivered motor specific impulse = $\frac{I_T}{W_P}$

The propellant has a demonstrated ±3-sigma total impulse variability of only 0.59 percent based on test results from 44 Minuteman motors cast from over 780 propellant batches. In the SVM motors, with a lower number of propellant

batches and motors, the 3-sigma impulse variability of 0.64 percent for the SVM-2 and 0.66 percent for the SVM-4. From the above, it is evident that the requirement for the demonstrated 3-sigma total impulse variability of 0.75 percent can be easily met by the proposed SMS motor.

The insulation member of the system is V-45, a silica-filled polybutadiene acrylonitrile rubber material. Thousands of pounds have been used in the Minuteman motor and, in a smaller quantity, in the SVM motors. This extensive usage has provided in-depth test data for fully characterizing its erosive and thermal properties under actual motor conditions of temperature, pressure, and flow rates, thereby allowing precise analytical determination of its behavior in the SMS motor. As shown in Figure 5-18, the insulation is designed to provide added thickness where the duration of exposure to gas flow is longest and most severe, and to taper to a minimum thickness at the case midsection where exposure duration is shortest. This design provides minimum weight in keeping with 100-percent flight reliability. A thermal analysis shows that the proposed insulation design maintains case integrity as well as external case wall temperatures at or below the specified 700°F.

The liner member of this system is DS-851-2, an imine-cured carboxy-terminated polybutadiene binder with 5-wt percent inert filler, and is fully compatible with propellant and insulation. The liner has bonding properties in a storage life environment that well exceeds SMS motor requirements.

The selected ANB-3066 propellant is cast in a simple surface-of-revolution grain configuration that is compresed of a cylindrical bore with a conical shaped plenum in the aft end. A full diameter boot, released to the tangent point, is used in the forward head to provide substantial grain structural margins during motor pressurization and temperature cycling over the required temperature range of +10 to +110°F. Provisions are made for trimming the grain for weight control and balance as shown in Figure 5-18.

Analysis of the SMS motor grain design, using this propellant-insulation-liner system and the simple surface-of-revolution grain configuration with a forward release boot, has resulted in positive safety margins for all operating and storage conditions. Because of the wealth of aging data available with ANB-3066, a five-year shelf life at 80 ±10°F can be offered, in lieu of the three-year shelf life at +10 to +110°F, if preferred.

The motor case is fabricated with S-901 glass filament having a minimum ultimate filament tensile strength of 440,000 psi. The shape of the chamber has been optimized to produce equal stress in all fibers and results in maximum load-carrying capability. The case is fabricated by installing the internal

insulation on a mandrel and overwrapping with glass filament. The aft and forward polar bosses and attachment ring are incorporated during the operation. The skirt design is similar to that used on the SVM-2 and -4 motors, and has successfully withstood longitudinal loads in excess of 32 g during vibration testing.

The nozzle design is identical to that used successfully in the SVM-2 motor except for use of low-density MXC-113 carbon phenolic material for the exit cone. This material is used on third-stage Minuteman motors and for the exit cone on the SVM-4 motor. Silver-infiltrated tungsten for the nozzle throat insert provides accurate thrust alignment as demonstrated in the SVM motors.

The SMS igniter is the same as the igniter used in previous SVM motors, except for a reduced pyrotechnic charge to accommodate the free volume of the SMS motor. It consists of a fiberglass chamber with boron-potassium nitrate (BPN) as the pyrotechnic material. An analysis of the igniter transient shows that the igniter for the on-loaded motor is also adequate for igniting the off-loaded motors. The KR-80000 safe-and-arm device has been used in the SVM-2 and -4 motors and all three stages of the Minuteman. It has been approved for use at Air Force Eastern Test Range (AFETR). The safe-and-arm device includes a completely redundant initiator system with a separate ground for each initiator.

Salient program events are one chamber hydroburst test, four igniter verification tests, three motor development tests, and four motor qualification tests followed by delivery of three flight motors to conclude the program.

5.5 HARNESS

The harness subsystem[1] consists of a main harness and separate ancillary cables as required for electrical interconnection of all spacecraft subsystems, components and sensors. The main harness is routed in a semicircle around the equipment platform with branch breakouts routed to the electronic equipment as required. Ancillary cables include a primary power harness connecting the solar array and batteries with the power-control unit, a separate thruster valve harness and others that can be separated from the main harness bundle.

Electrical connectors are the crimp contact type with wire-strain relief provided at the back in the form of strain relief clamps or potting boots. Connector savers are employed where frequent mating and unmating with the equipment is required. A record is kept of the number of times each connector is mated and unmated.

The wire used in fabricating the harnesses is light-weight, space-qualified wire. This wire has a radiation resistant insulation of crosslinked polyalkene combined

with crosslinked polyvinylidene flouride. This combination provides excellent electrical insulation properties as well as abrasion resistance and minimum weight and size. Where shields are used, the grounding wires are brought through connector contacts and grounded inside the component.

The system employs single-point grounding to the spacecraft structure at a point near the power-control unit. The structure is not used as a current return path. The communications antenna including the S-band power amplifiers are electrically isolated from the spacecraft primary structure. Dc/dc converters are provided for the remaining electronic components so that isolation from the primary power bus is obtained.

The harness includes a spacecraft system/AGE interface connector used for in-plant system checkout and test. A separate connector is provided for battery on-board charging and monitoring and is accessible on-pad for prelaunch battery charging and monitoring.

Harness in-process tests and acceptance tests consist of continuity and high-potential leakage resistance tests. The continuity test verifies correct wiring by measuring conductance of each circuit, pin-to-pin. The leakage resistance test consists of impressing a high voltage from conductor to conductor and from conductor to shield and measuring the leakage current.

5.6 SPACECRAFT ELECTRICAL GROUNDING CRITERIA

5.6.1 GENERAL

The following SMS spacecraft grounding criteria are used to attain an integrated grounding system commensurate with accepted interference control practices. As a general design guide, the spacecraft electrical grounding system employs a single structure ground point (SGP). The SGP is bonded to the primary and secondary structures with an impedance of less than 80×10^{-3} ohms in the frequency range of 0 to 20 MHz. The SGP is located near the PCU. Also, the provisions of MIL-B-5087B with respect to characteristics, application and testing of electrical bonding is observed.

5.6.1.1 Grounding of Return Lines

Primary power and secondary power return lines are connected to structure ground. Figure 5-19 shows typical return-line grounding requirements.

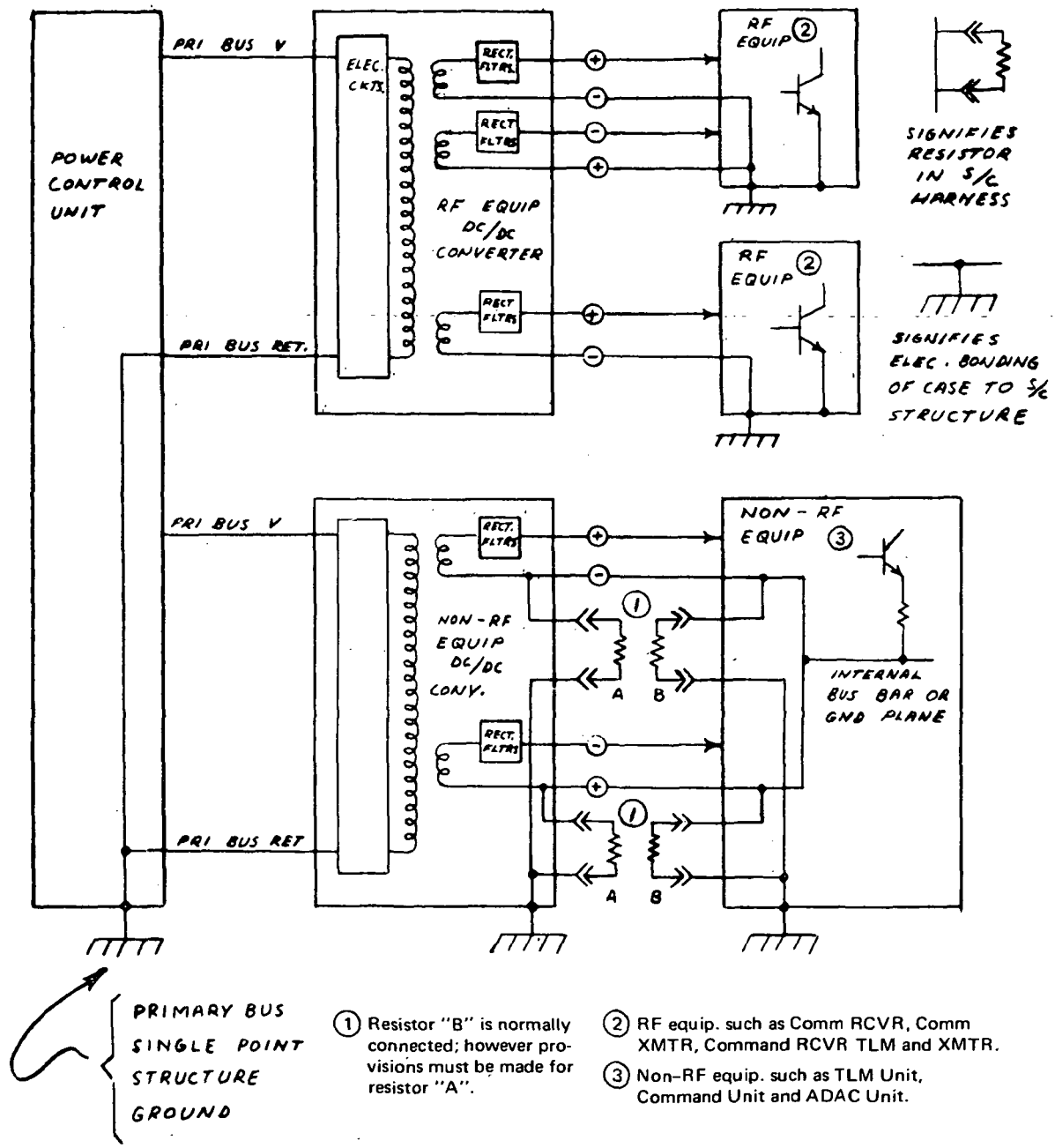

① Resistor "B" is normally connected; however provisions must be made for resistor "A".

② RF equip. such as Comm RCVR, Comm XMTR, Command RCVR TLM and XMTR.

③ Non-RF equip. such as TLM Unit, Command Unit and ADAC Unit.

Figure 5-19. Typical-Line Grounding Requirements

(a) The primary power return lines are connected to the SGP located near the power control unit (PCU). An exception is the primary power return line which is connected to the spacecraft structure ground plane at the S-band power amplifier.

(b) Secondary power return lines at the outputs of subsystem dc-dc converters for non-RF equipment are connected to the converter and/or equipment case by external harness jumpers (resistors) located in the mating connector contacts; the chassis in turn is bonded to the spacecraft structure.

(c) Secondary power return lines at the outputs of subsystem dc-dc converters for RF equipment are floated at the converter and connected to the equipment case which in turn is bonded to the spacecraft structure.

5.6.1.2 Isolation

A minimum dc isolation of 1 Megohm resistive exists between primary bus leads and load equipment case (except the S-band power amplifier) and between primary bus leads and dc-dc converter secondary leads, with harness jumpers (resistors) disconnected.

5.6.1.3 Bonding

(a) The spacecraft primary structure and secondary structure, which supports electrical/electronic equipment, are electrically bonded together to provide a continuous, low-impedance path from the equipment to the basic structure, with a maximum dc bonding resistance of 2.5 Megohms.

(b) All electrical and electronic cases are bonded to the structure by means in accordance with MIL-B-5087B and provide a dc impedance of less than 2.5 Megohm.

5.7 COMMUNICATIONS SUBSYSTEM

5.7.1 SUBSYSTEM REQUIREMENTS

The communications subsystem[1] consists of the S-band transponder, UHF transponder, and the dual-frequency antenna assembly. Both the UHF and S-band transponders are redundant. Each transponder includes a receiver, a dc/dc converter, and a transmitter (except the final RF power amplifiers). The RF amplifiers are part of the antenna assembly rather than part of the transponder

because they are physically mounted as an integral part of the antenna assembly. The communications antenna assembly is composed of an antenna array, phase shifters, switches, diplexers, and solid-state power amplifiers. The S-band array includes 128 yagi elements mounted in 32 rows of 4 each, spaced equally around the circumference of the spacecraft. The UHF array includes 16 crossed dipoles, 8 of which are used for transmitting and 8 for receiving. Figure 5-20 is a preliminary functional block diagram of the subsystem.

5.7.1.1 Functions

The functions to be performed by the communications subsystem are listed below:

(a) VISSR data transmission. Accept two 14-Mb/sec inputs from the VISSR multiplexer, and quadriphase modulate an 81.6-MHz carrier signal with these data. The carrier signal is such that the transmit spectrum is centered at 1681.6 MHz.

(b) Telemetry data transmission. Accept a telemetry baseband signal consisting of 194-b/sec PCM and IRIG channel B or a 70-kHz gated oscillator signal, and phase modulate a carrier signal. The signal is then converted to a nominal transmit frequency of 1694.0 MHz, amplified and radiated via the despun antenna. This function is performed continuously. Modulation index is nominally 1.8 radians.

(c) Command reception. Receive AM/FSK/PM S-band command signal via a separate 80-kHz bandwidth IF channel, and provide an FSK/AM baseband signal to the command detector of the T&C subsystem.

(d) Stretched VISSR transmission. These data are received at S-band, routed through an 8.2-MHz bandwidth limiting IF amplifier, and subsequently retransmitted at 1687.1 MHz via the S-band despun antenna. This signal occupies the wideband channel during VISSR operation.

(e) WEFAX relay. Receive a narrowband (50-kHz) WEFAX signal at S-band and amplify and up-convert this signal for subsequent retransmission via the S-band transmitter and despun antenna. This function is performed when the VISSR is not operating and the ranging function is not being used.

(f) DCP data. Reception of DCP data falling within a 400-kHz bandwidth at a nominal center frequency of 401.9 MHz. These data are frequency-converted, amplified, and provided to the S-band transponder at a designated level and frequency for retransmission at 1694.5 MHz.

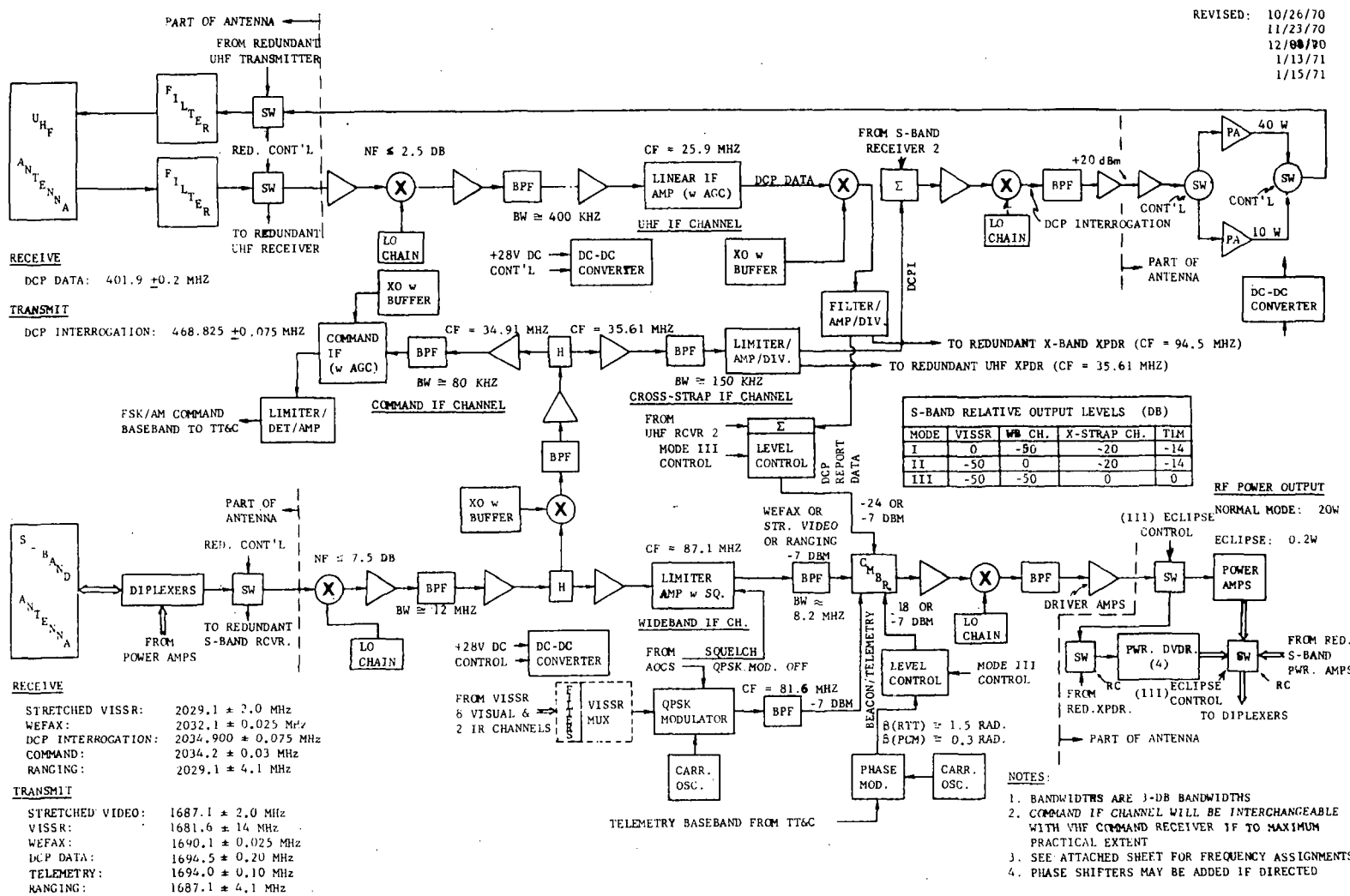

Figure 5-20. SMS Communication Transponder, Preliminary Block Diagram

(g) DCP interrogation. Receive narrowband (within 150-kHz band) DCP interrogation signals at 2034.9 MHz and process the subject signals for retransmission at a frequency of 468.825 MHz

(h) Ranging. Receive S-band ranging signals within an 8.2-MHz band and retransmit these signals at specified levels in an 8.2-MHz band centered at 1687.1 MHz. This function is performed when the VISSR is not operating and when WEFAX data are not being transmitted.

5.7.1.2 Operating Modes

The operating modes of the subsystem are shown in Table 5-16 along with the relative output levels for each mode. There are three basic operating modes: normal, UHF high power and S-band low power. During the normal mode, VISSR data is transmitted during approximately 1/16 of the satellite spin cycle (when the VISSR camera is pointed toward the earth) with the remainder of the spin cycle devoted to transmission of the signals present in the wideband channel (stretched VISSR or ranging or WEFAX). When the VISSR is not operating, these data are transmitted continuously. Telemetry and DCP reports are transmitted continuously during the normal mode. The UHF high power mode is used to interrogate data collection platforms that have low values of gain/temperature (G/T) (DCP buoys located at earth's edge), that is, that require a 6-db increase in satellite effective radiated power (ERP) to satisfy link margin requirements. During this mode, the S-band power amplifiers are by-passed and only telemetry and DCP reports are transmitted via the S-band channel. During eclipse, the subsystem can be operated from battery power, and only DCP interrogation signals, telemetry and DCP report signals are transmitted. Capability for command reception (S-band) and DCP report reception is continuous in all three modes.

A detailed discussion of operating modes is given in volume 1, paragraph 2.1.10.3.

5.7.1.3 Performance Summary

Table 5-17 presents a summary of subsystem performance requirements. These parameters satisfy requirements for the various communications links as well as the constraints on form factor, size and weight imposed by satellite design requirements.

Exact operating frequencies and signal bandwidth allocations are listed in Table 5-18.

Table 5-16

SMS Communications Subsystem Operation

Signal Functions	Frequency Band		(1) Relative Levels of Transmitted Signals (db)					
			Normal Mode				UHF Hi-Power Mode (2)	S-Band Low-Power Mode (2)
	Xmit	Rcve	VISSR	Stretched Video	Ranging	WEFAX S-Band		
VISSR data	S	-	0	OFF	OFF	OFF	OFF	OFF
Stretched video	S	S	OFF	0	OFF	OFF	OFF	OFF
Ranging	S	S	OFF	OFF	0	OFF	OFF	OFF
WEFAX	S	S	OFF	OFF	OFF	0	OFF	OFF
DCP interrogation (4)	U	S	0	0	0	0	+6	0
DCP data	S	U	-20	-20	-20	-20	-20	-20
Telemetry	S	-	-14	-14	-14	-14	-20	-20
Command (5)	-	S	-	-	-	-	-	-

NOTES:

1. Relative levels are referenced to the strong signal output level for the respective S-band (S) and UHF (U) transmit channels.
2. In the UHF hi-power and eclipse modes, the S-band 20 watt amplifier is by-passed.
3. "OFF" signifies the designated signal is at least 50db below the strong signal.
4. The UHF power amplifiers are operative only when the data collection platform interrogation (DCPI) is present.
5. Command reception capability is continuous, i.e., whenever the S-band transponder is activated.

Table 5-17

Performance Summary

Receive Frequencies	Center Frequency	Bandwidth Allocation
UHF		
• DCP data	401.900 MHz	400.0 kHz
S-band		
• Stretched VISSR	2029.100 MHz	6.2 MHz
• WEFAX	2032.100 MHz	50.0 kHz
• DCP interrogation	2034.900 MHz	150.0 kHz
• S/C command	2034.200 MHz	60.0 kHz
• Ranging	2029.100 MHz	8.2 MHz
Transmit frequencies		
UHF		
• DCP interrogation	468.825 MHz	150.0 kHz
S-band		
• VISSR data: normal mode	1681.600 MHz	23.2 MHz
• Stretched VISSR	1687.100 MHz	6.2 MHz
• WEFAX	1690.100 MHz	50.0 kHz
• DCP data	1694.500 MHz	400.0 kHz
• Telemetry	1694.000 MHz	200.0 kHz
• Ranging	1687.100 MHz	8.2 MHz

Table 5-18

Communications Subsystem Frequency Assignments

Parameter	UHF	S-band
G/T(1)	≥ -23.4 db/K	≥ -24.7 db K
ERP***(1)	≥ +43.9 dbm	≥ +57.9 dbm
Polarization	RHC	Co-Linear
Bandpass characteristics		
Image rejection	≥ 60 db	≥ 60 db
BW: Wideband IF	—	8.2 kHz
Command IF	—	60 kHz
Cross-strap IF	—	150 kHz
UHF IF	400 kHz	—
Dynamic range	-100 dbmW to -135 dbm	-70 dbm to Th No.
Amplitude response****	±1.0 db	±1.0 db
Variation in time delay	—	<10 ns*
Frequency stability**:		
1 yr	0, +1 part per 10^6	0, 1 part per 10^6
0.25 s	1 part per 10^9	1 part per 10^9
VISSR modulation	—	QPSK, Data rate = 28 Mb/sec
Telemetry	—	PM, $\beta \approx 1.8$ rad, BW ≈ 200 kHz PCM & Analog
Command output	—	FSK/am to T&C

(1) G/T & ERP values apply anywhere within 9.1 degrees and anywhere within 31.7 degrees of beam center for S-band and UHF, respectively.

*If directed, calibration curves are used to reduce uncertainty in time delay.
**Cross-strap IF oscillators are 1 part per 10^5/yr and 1 part per 10^9/0.25 sec.
***Total ERP for normal mode only; see Table 5-17 for changes in ERP for UHF high-power and S-band low-power eclipse modes.
****Amplitude response requirement applies from -115 dbm to -135 dbm.

5.7.2 SUBSYSTEM DESIGN

5.7.2.1 Design Approach

Performance requirements for the SMS communications subsystem dictated development of state-of-the-art low-loss microwave switches, development of a switched despun antenna array capable of operation at both UHF and S-band frequencies, development of efficient solid state RF power amplifiers, and development of UHF and S-band transponders using parts, designs and techniques consonant with high-reliability space-borne equipment. The proposed design is based upon circuits, components and assemblies developed for other space programs or developed as a part of the preproposal and postproposal program support activity. Specific design features include:

(a) Microwave switch. A wideband positive intrinsic negative type sandwich (PIN) diode microwave switch with low-insertion loss. This switch is based on a similar narrowband switch developed by Philco-Ford for the ATS-F/G satellites. It is used to despin the antenna array.

(b) Antenna array. A despun antenna array has been developed especially for SMS. It provides about 19-db gain with linear polarization at the S-band frequencies using yagi radiating elements to obtain this performance with high efficiency and minimum weight. Crossed dipoles are used at UHF to provide about 5.5-db gain with circular polarization. The array requires no deployment after launch.

(c) Transmitter power amplifier. A solid-state power amplifier delivering 5 watts at 1700 MHz with 50-percent overall efficiency was developed for SMS. The UHF power amplifier design features 60-percent collector efficiency with high reliability. A dual-power output is provided with the high power available for increased link margin when the VISSR and S-band transmitter are turned off.

(d) Quadriphase modulator. This modem operates at a maximum data rate of 40 Mb/sec which is greater than the 28-Mb/sec rate proposed for SMS. The quadriphase shift-keyed (QPSK) modulator design for the SMS transponder is based upon the design of the aforementioned modulator.

(e) DC-DC converters. Efficient and lightweight dc/dc converters are used to power each of the four transponders and the two UHF power amplifiers. Reliability and performance of these pieces of equipment have been demonstrated on prior and current space programs.

(f) Receivers. A mixer-preamplifier with a 7.5-db noise figure is used as the S-band receiver front end. The S-band uplink power level is not limited; as a consequence, a higher receiver noise temperature is utilized without affecting the link performance. DCP performance limits the UHF uplink levels; hence, a transistor preamplifier is used in the UHF receiver to achieve a 2.5-db noise figure.

(g) Receive channel bandwidths. Link margins and RFI considerations dictate that the noise bandwidths of the various receiver channels (IF's) be reduced to minimum practicable values. Hence, double conversion is used to allow use of crystal filters in IF channels, except the wideband channel of the S-band receiver. The frequency of the wideband IF was chosen as 87 MHz to allow use of wideband hard limiting amplifiers developed for other Philco-Ford programs.

(h) Reliability. In addition to the use of conservatively rated power components and circuits, the S-band communications subsystem contains redundant transponders, multiplexers, and power amplifiers. Failure of a switch or phase shifter in the antenna array is non-catastrophic and the system continues to operate with reduced link margin.

5.7.2.2 Antenna Assembly

5.7.2.2.1 Functional Description. Figure 5-21 is a block diagram of the antenna assembly. The S-band communications antenna assembly consists of an electronically-switched, despun, linearly-polarized antenna with 20-db gain and a redundant solid-state power amplifier with 20-watt output. The antenna array consists of 32 rows of wideband S-band radiating elements mounted around the circumference of the spacecraft. Each of the 32 rows contains four radiating elements, while the beam is formed by energizing only four adjacent rows to form a 16-element phased array.

The design of the spacecraft, utilizing both UHF and S-band transponders, has the two antenna systems sharing a common ground plane. The greater than four-to-one ratio of operating frequencies results in little or no interaction.

The antenna array is driven by four 5-watt transistor amplifiers operating at 1670 MHz with better than 50-percent efficiency. Each amplifier is connected to a row of four yagis, as determined by the switching matrix.

Four varactor phase shifters are provided in both the transmit and receive paths. These phase shifters reduce the antenna gain ripple introduced by the switching arrangement, thereby maximizing gains, particularly toward the edge of the earth.

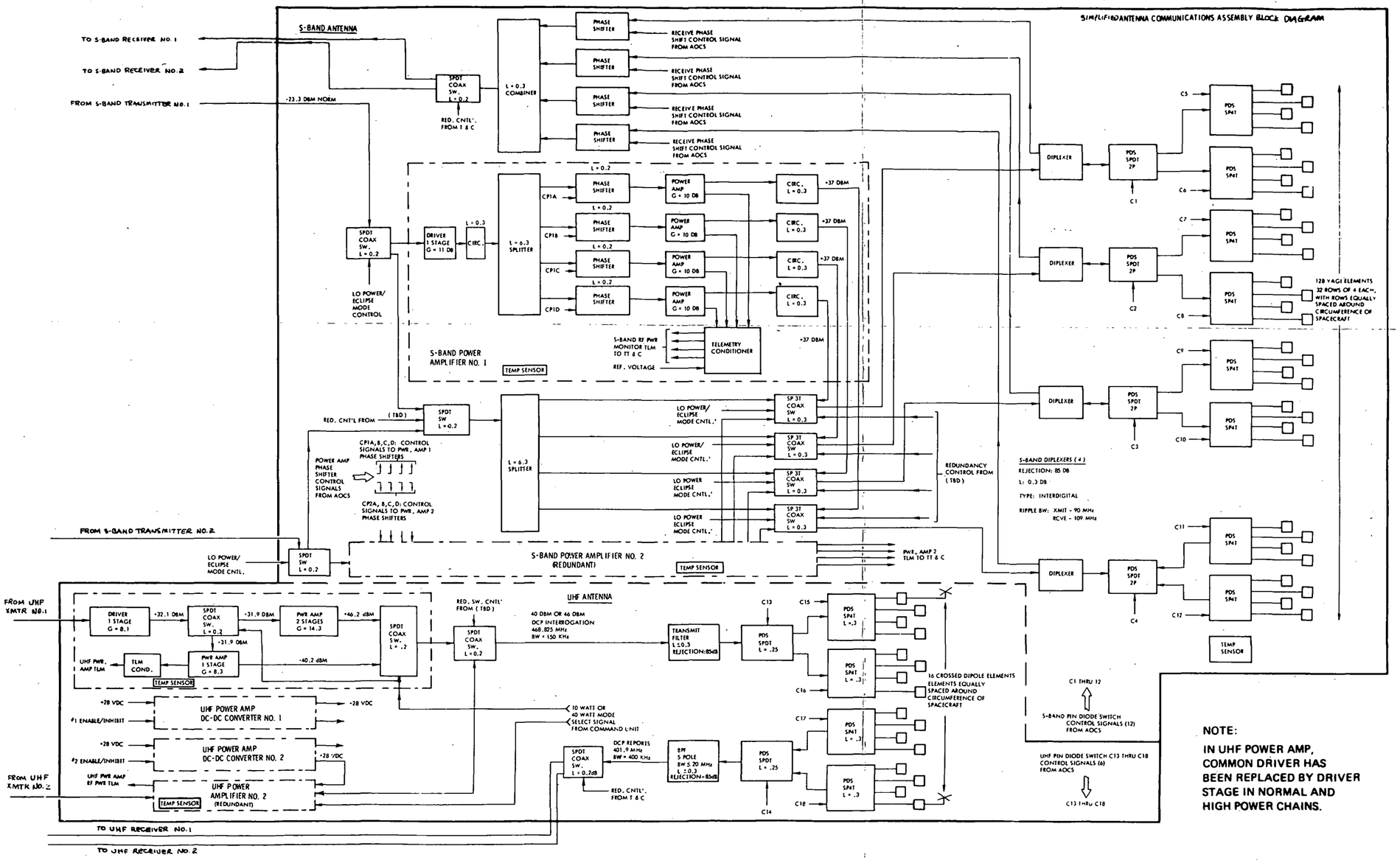

Figure 5-21. Antenna Block Diagram

The UHF antenna assembly is an electronically-switched array controlled by a switching matrix using PIN diodes. The transmitting array is composed of eight circularly-polarized crossed-dipole elements mounted around the circumference of the spacecraft. The receiving array consists of eight additional crossed-dipole elements, with each element mounted in between two elements of the transmitting array. All sixteen crossed-dipole elements are mounted in between elements of the S-band array.

The transmitting and receiving antenna elements are switched in 45-degree increments as the satellite spins so the beams continuously point toward earth. Only one element at a time is energized in each array.

5.7.2.2.2 Signal Levels. Tables 5-19 and 5-20 list the gains and losses of the transmit and receive channels to show how the ERP and receive gain numbers were derived for the S-band antenna. The gains and losses of individual contributors are subject to change, but values of ERP and G/T within 9.1 degrees are considered firm.

Table 5-19

Satellite S-Band ERP Budget (1700 MHz)

Parameter	Output Power (20 watts)
Transmitter power	43.0 dbm
Coupler loss	-0.1 db
Line loss	-1.0 db
PIN diode switch (SP4T)	-0.3 db
PIN diode switch (SPDT)	-0.3 db
Diplexer loss	-0.3 db
Coax switch loss	-0.3 db
Antenna gain (9.1 degrees)	+17.2 db
Effective radiated power (9.1 degrees)	57.9 dbm

Table 5-20

Satellite S-Band Receive Budget (2000 MHz)

Parameter	Decibels
Coupler loss	- 0.1
Coax cable loss	- 1.5
PIN diode switch loss (SP4T)	- 0.3
PIN diode switch loss (SPDT)	- 0.3
Diplexer loss	- 0.3
Phase shifter loss	- 0.03
Hybrid combiner loss	- 0.3
Coax switch loss	- 0.2
Total losses	- 3.3
Antenna gain (9.1 degrees)	+10.7 (min. for spec. G/T)
Net antenna gain (G/T = -24.7 db/deg K)	+ 7.4

Tables 5-21 and 5-22 list the gains and losses of the UHF transmit and receive channels. The gains and losses of the individual contributors are subject to change, but the values of receive gain and ERP within 31.7 degrees are considered firm.

Note: The losses listed in the subject table are as of 3/15/71 estimates for the 75-inch diameter satellite.

5.7.2.2.3 Array Scanning. As the satellite rotates, beam switching occurs every 11.25 degrees with a unique signal path for each of the 32 antenna elements provided to the single transmitter and receive junction points (Figure 5-22). Continuous phase shifting keeps the beam continuously centered on the earth during each switching interval of ±5.625-degree rotation. The switching sequence is continuous and connects four adjacent rows of antenna elements in the following typical sequence: 1, 2, 3, 4; then 2, 3, 4, 5; then 3, 4, 5, 6, etc. The phasing controls only the first and last row each time.

Table 5-21

UHF/ERP Budget

Components	10-Watt Mode	40-Watt Mode
Transmitter power	+40 dbm	+46 dbm
PIN diode switch (SP4T)	-0.3	
PIN diode switch (SPDT)	-0.2	
Line loss	-1.1 db	
Band reject filter	-0.3 db	
Coax switch	-0.2 db	
Antenna gain (31.7 degrees)*	+6.0 db**	
ERP (31.7 degrees)*	+43.9 dbm	+49.9 dbm

*31.7 degrees includes 8.7-degrees earth coverage, 22.5-degrees switching angle; and 0.5-degree pointing error.

**Increase in losses due to change to 75-inch diameter satellite requires higher element gain than listed in proposal. Weight and size of low-loss filter is prohibitive and require use of smaller filter with losses up to 0.8 db.

The ground plane of the antenna is curved since it is mounted on the cylindrical (faceted) surface of the satellite. This means that phase errors are introduced between signal paths as a result of the mechanical construction of the antenna. Compensation uses phase shifting in the outboard elements, resulting in the proper far-field pattern of a flat-phase front. The proper phase-shift angle is dependent on frequency of operation, where separate phase shifters are provided for the transmit and receive legs and on the difference between the mechanical and electrical beam axis. The use of continuous phase shifters causes small phase front discontinuities which result in a loss in gain at the points of maximum scan (±5.625 degrees). This ripple is symmetrical about the broadside angle of each beam and slowly increases to 0.3 db at the limit of the scan.

5.7.2.2.4 Power Amplifiers. The S-band and UHF power amplifiers are shown in Figures 5-23 and 5-24 respectively. The design is all solid-state, featuring high efficiency transistor power amplifiers. Figure 5-23 shows an input signal level of ±23 dbm watts from the transmitter assembly being amplified,

Table 5-22

Spacecraft UHF Receive Budget

Components	Losses/Gains
PIN diode switch (SP4T)	-0.3 db
PIN diode switch (SPDT)	-0.2 db
Line loss	-0.9 db
Bandpass filter**	-0.3 db
Coax switch	-0.2 db
Total losses	-1.9 db
Antenna gain (31.7 degrees)*	+5.1 db (Min. reqd. to meet G/T of -23.4)
Net antenna gain (31.7 degrees)*	+3.2 db

*31.7 degrees includes 8.7-degrees earth coverage, 22.5-degrees switching angle, and 0.5-degree pointing error.

**Weight and size of low-loss filter is prohibitive and requires use of miniature band-pass filter with insertion loss of up to 1.7 db.

split into four channels, phase-controlled, and then amplified to a 5-watt level. The input stage is class C, as are the 5-watt stages. A circulator is used on the input and the output of each 5-watt stage to prevent a load mismatch from destroying the amplifier by reflecting the power back into the stage for dissipation.

A four-way power divider is required to drive four transistor amplifiers from the driver stage. The divider consists of a tree of three two-way branchline dividers. To isolate the outputs from each other the branchlines are shunted by balancing resistors. The stripline layout of the four-way divider provides excellent terminal matching by adjustment of the junction capacitances. Continuous varactor diode phase shifters are presently being designed to provide the low loss, 0 to 120 degrees, phase shifting of the beams. Typically, a reverse voltage of up to 40 volts is required for the maximum phase variation. The use of continuous phase shifters causes small phase front discontinuities which result in a loss in gain at the points of maximum scan (±5.625 degrees). This

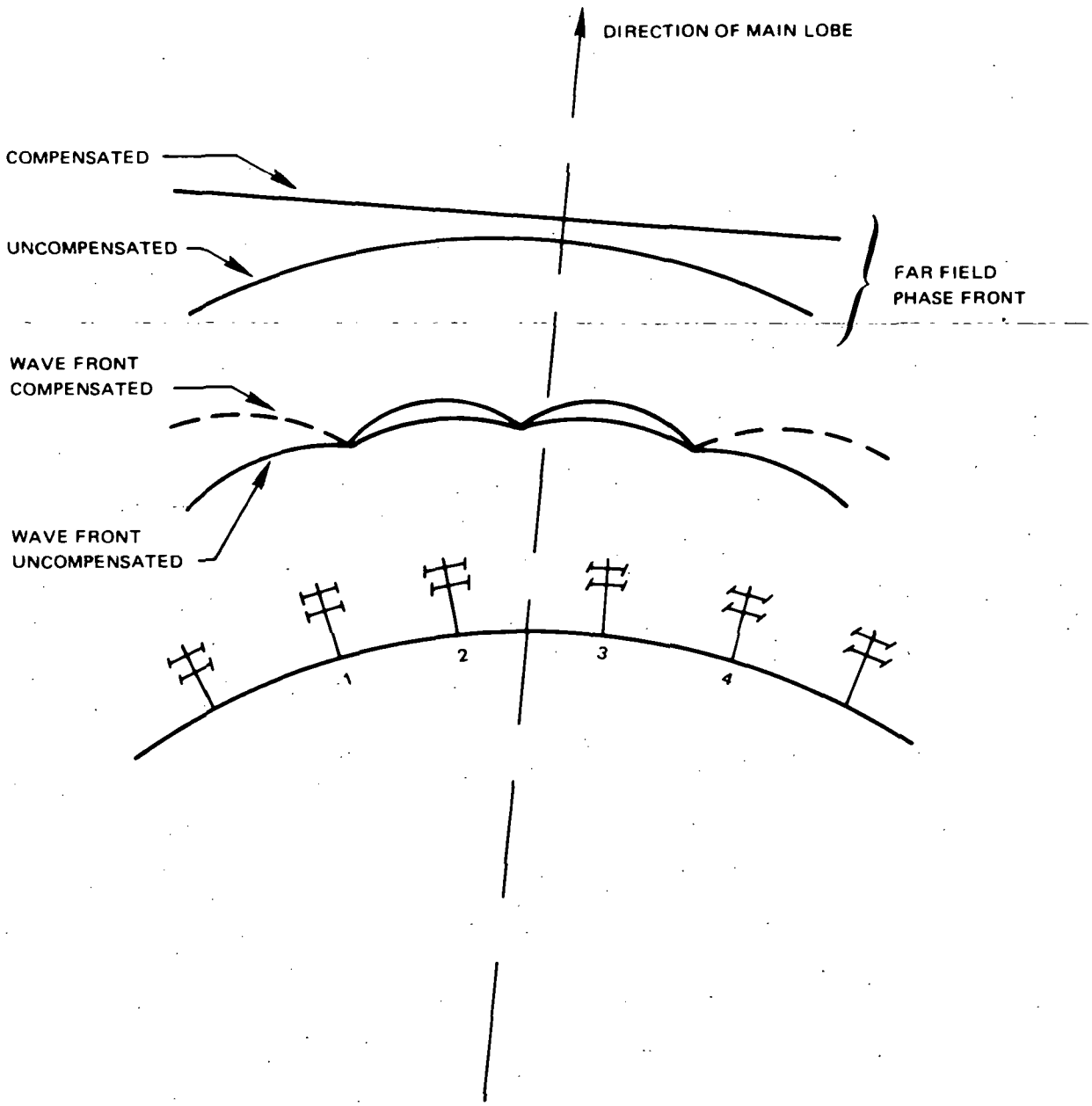

Figure 5-22. Phase Front of Four-Element Antenna

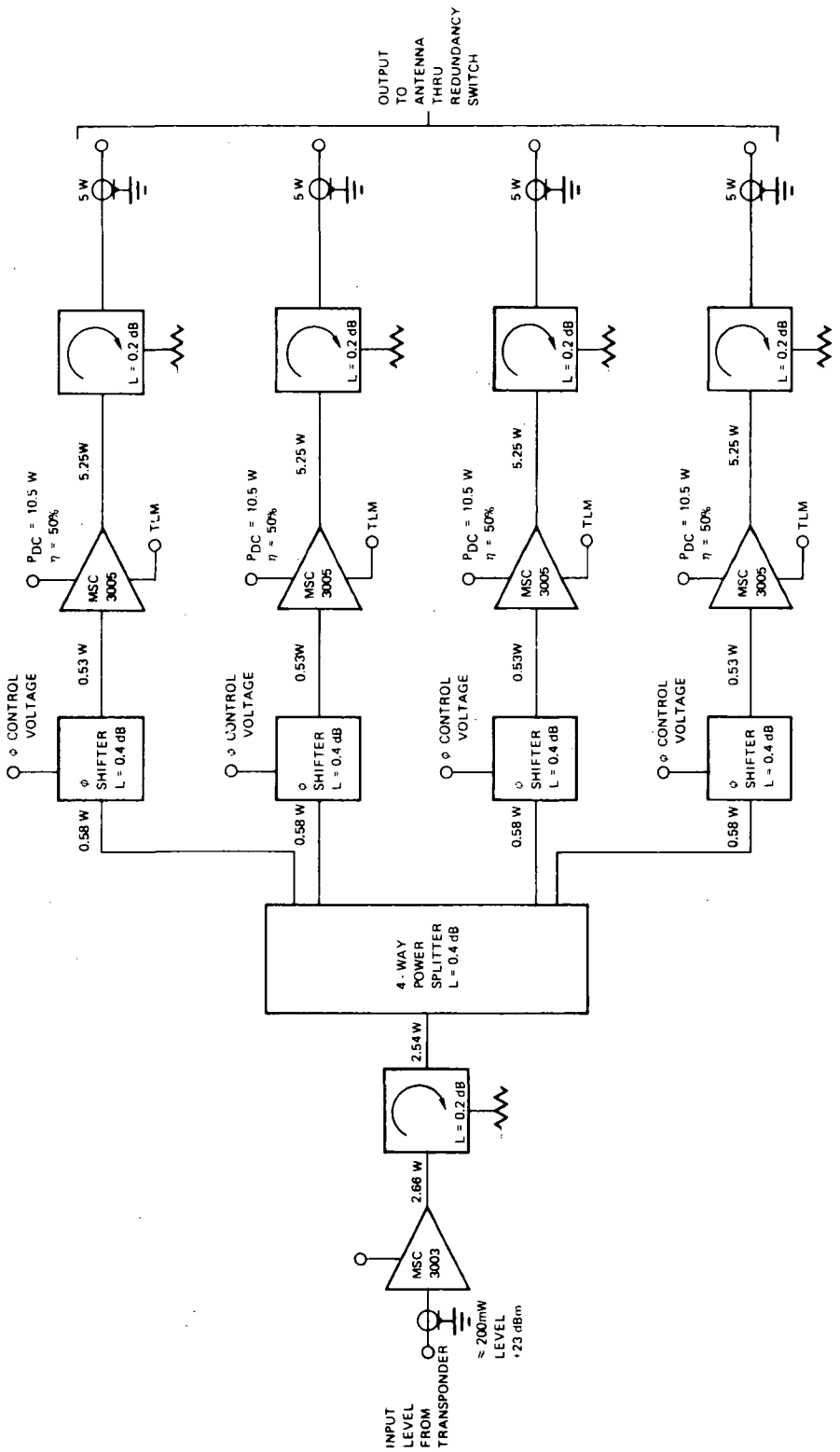

Figure 5-23. S-Band Power Amplifier Chain

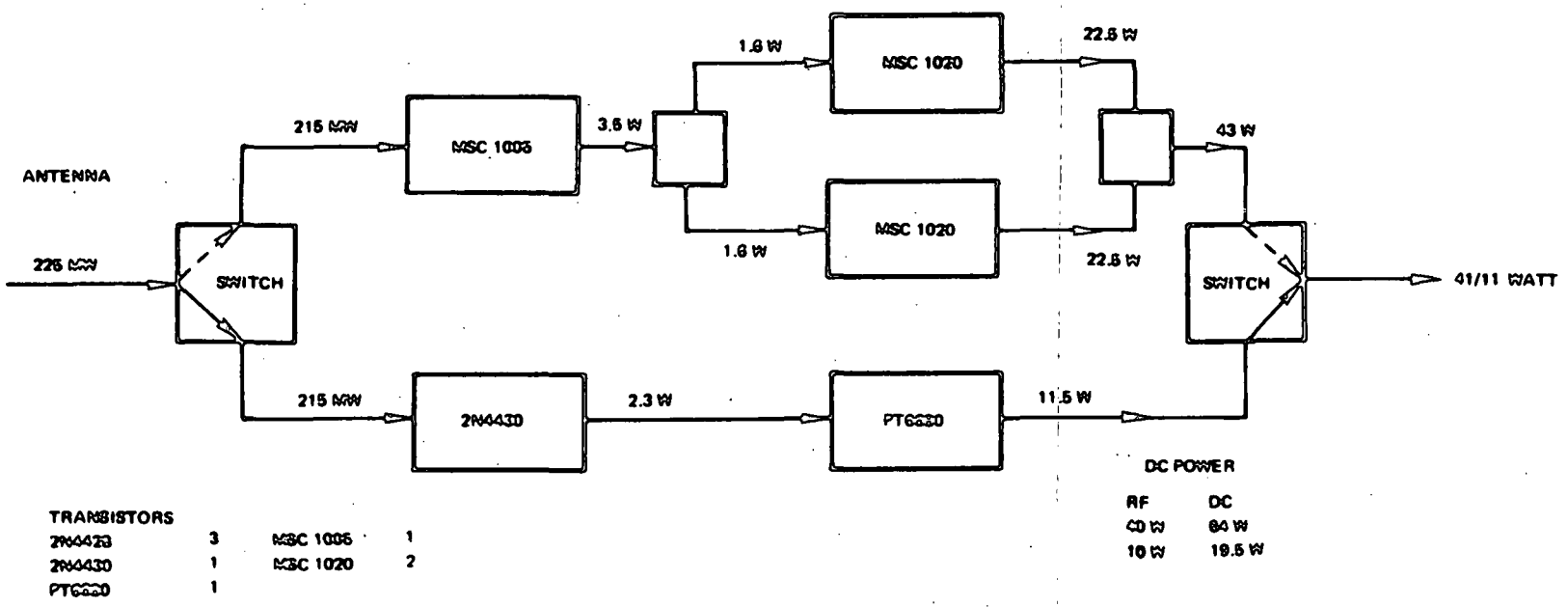

Figure 5-24. UHF Power Amplifier Chain

ripple is symmetrical about the broadside of each beam and slowly increases to 0.3 db at the limit of the scan.

The typical amplifier characteristics are summarized as follows:

Center frequency	1685 MHz
Output power	5.0 w
Power gain	10 db
Collector efficiency	50 percent
1 db bandwidth	90 MHz
Input VSWR	2:0:1
Collector voltage	28 v

The UHF power amplifier consists of two amplifier chains. The high power chain includes a parallel output stage capable of delivering 40 watts and its driver stage which can deliver 3.5 watts. The low power chain includes two stages which raise the power available from the UHF transmitter to 10 watts. The input and output of the amplifier assembly are switched remotely through an RF latching transfer switch to select the 40-watt chain for the high-power mode of operation of the 10-watt chain for the normal mode of operation.

The high power output stage consists of two parallel 20-watt stages whose inputs and outputs are combined using hybrids. The choice of two parallel 20-watt stages instead of a single 40-watt stage is dictated by thermal dissipation considerations as well as experimental data, indicating that high collector efficiency is obtained with the parallel configuration, as well as increased stability and reliability. Each individual amplifier is a class-C amplifier using the MSC 1020. Etched microstrip transmission lines are used for input and output matching. Each circuit requires a 2 x 5 inch circuit card which is mounted on an appropriate heat sink.

The 10-watt stage uses the PT 6680 which is tuned and biased to provide 10 watts of output power at a gain of 7 db.

5.7.2.2.5 PIN Diode Switches. Table 5-23 summarizes the performance characteristics and size and weight of the PIN diode switches used for despinning the antenna array.

Table 5-23

SMS Antenna PIN Diode Switch Performance Summary

Characteristic	UHF		S-Band	
	SPDT	SP4T	SPDT	SP4T (projected)
Insertion loss	0.15 - 0.19 db	0.19 - 0.23 db	0.27 db	0.30 db
Port isolation	22 - 25 db	21 - 24 db	24 - 25 db	25 db
Max holding power	200 mw	200 mw	150 mw	150 mw
Switching time	$<1\mu s$	$<1\mu s$	100 ns	100 ns
Min bandwidth	370 - 490 MHz (<1.2 input VSWR)	380 - 480 MHz (<1.2 input VSWR)	1683 ±15 MHz 2030 ±5 MHz (0.05 db roll off)	1683 ±15 MHz 2030 ±5 MHz (0.05 db roll off)
Power handling	>40 watts	>40 watts	>5 watts	>5 watts
VSWR	1.14	1.12	1.1	1.12
Weight	4 oz	5 oz	3 oz	4 oz
Size	2-1/2 x 4-1/2 x 1/2 inches	4-1/2 x 5-1/2 x 1/2 inches	2-1/2 x 2-1/2 x 1/2 inches	2-1/2 x 4 x 1/2 inches

The PIN diode switch was chosen over other types primarily because it offers ultra-low loss high-efficiency switching. In order to achieve this ultra-low loss high-efficiency switching, the PIN diodes have been placed in stub arms approximately $\lambda/2$ in electrical length, with the diodes being locates $\lambda/4$ from the arm to be switched. In this configuration the diodes are reverse biased to prevent signal passage out of one or more of the arms. The resultant diode capacitance is resonated with a shunt stub section in order to produce a voltage maximum at the diode location, which is then transformed to a short $\lambda/4$ away at the switch arm. The resulting high VSWR in that arm isolates the port. When forward biased in the range of 10 to 100 milliamperes forward current,

the location of the diode produces an approximate RF open at the stub junction and permits the RF signal to pass. One stub tuning permits the optimization (at one frequency) of port isolation when the diodes are reverse biased and another for switch insertion loss when forward biased. Such a stub arm diode configuration provides negligible switch holding current when off, a feature which becomes particularly beneficial in the required multithrow switch application. Further, because of the lower diode dissipation in the reverse bias configuration, switch insertion loss is minimized. In implementing of the transmission line switch, the diodes are mounted in shunt with a strip transmission line. This facilitates the heat removal rate for high power applications and has the further advantage of having lower insertion loss over a series diode configuration.

5.7.2.2.6 Filters. The characteristics of the antenna filters are summarized in Table 5-24. Four S-band diplexers are used, one in each of the four antenna feed lines. The diplexer is an interdigital filter to provide low-insertion loss at minimum size and weight.

A filter is located in the transmit/receive line of the UHF antenna. The UHF filter handles 40 watts of power and presents a potential multipacting problem. Therefore, a band-rejection type filter is used in this application to achieve the desired attenuation of any energy at the receive frequency which is present in the output spectrum. An interdigital bandpass filter is used in the UHF receive line to minimize RFI and to provide sufficient attenuation of transmitter energy to avoid saturation of the UHF low-noise preamplifier.

5.7.2.2.7 Elements. The S-band antenna uses wideband 8-db gain Yagi elements to cover from 1670 to 2040 MHz. The VSWR is optimized for these two bands, but is generally good over the entire band, with the VSWR rising sharply immediately after the 2030-MHz band. The ground plane serves as the reflector for the double folded dipole-driven elements, the upper frequency one being the shorter folded dipole and closest to the reflector. Two directors are used to obtain the necessary gain in the 1670-MHz band, but they are compromised to be slightly shorter and spaced differently in order to obtain an acceptable impedance match in the receive band. Figure 5-25 is a photograph of the prototype yagi element.

The UHF elements consist of thin crossed dipole radiators placed 3 inches (1/10 wavelength) above the same ground plane used for S-band. The tuning of the elements is accomplished by a shorting strap being placed around the two pairs of short dipole balum-type supports and the length of the radiators (typically 0.46 wavelength long).

Table 5-24

Filter Summary

S-Band Diplexer	Receive Section	Transmit Section
Center frequency (f_o)	2030 MHz	1682.5 MHz
Rejection	$\geq$ 85 db	$\geq$ 70 db
Insertion loss	$\leq$ 0.3 db	$\leq$ 0.3 db
Insertion loss bandwidth	$\geq$ 10 MHz	$\geq$ 25 MHz
Ripple bandwidth	$\leq$ 5 percent f_o	$\leq$ 5 percent f_o
RF power handling	—	5 watts cw
VSWR	$\leq$ 1.5:1	$\leq$ 1.5:1
Size	10 x 2 x 1 inches	
Weight	$\leq$ 0.55 lb	
Number	4	
UHF Filters	**Receive BPF**	**Transmit-BSF Filter**
Center frequency (f_o)	401.9 MHz	468.825 MHz
Rejection	$\geq$ 85 db at F_T	$\geq$ 90 db at F_R
Insertion loss	$\leq$ 0.3 db	$\leq$ 0.3 db
Insertion loss bandwidth	$\geq$ 1 MHz	$\geq$ 1 MHz
3-db bandwidth	$\leq$ 5 percent f_o	—
Rejection bandwidth	—	$\geq$ 1 MHz
VSWR	$\leq$ 1.3:1	$\leq$ 1.3:1
RF power handling	—	40 watts cw
Size	15 x 7.5 x 3.5 inches	8 x 4 x 2 inches
Weight	$\leq$ 2.5 lbs	$\leq$ 1.0 lbs
Number	1	1

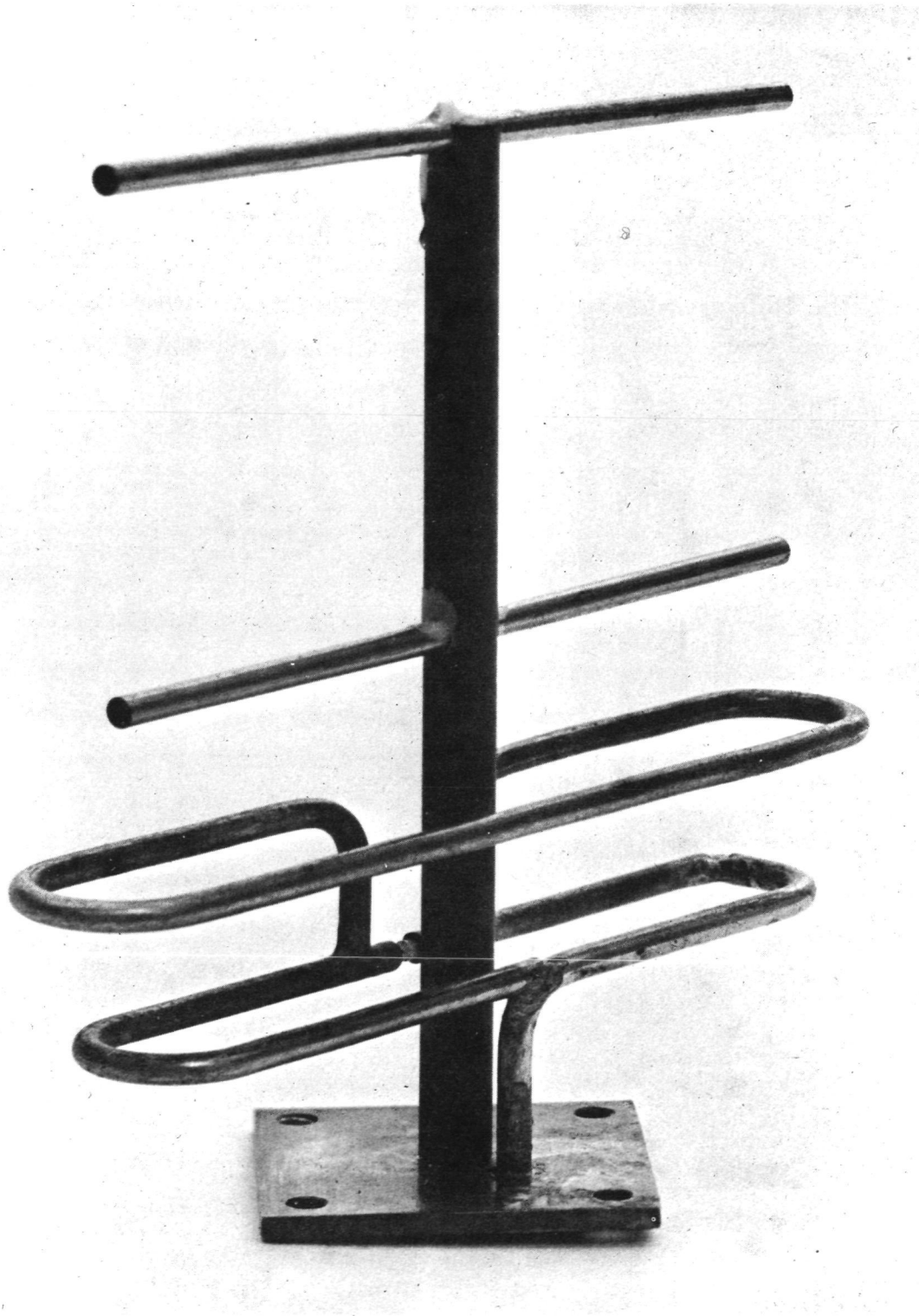

Figure 5-25. Yagi Antenna Element

5.7.2.2.8 Coax Relays. Coax relays are used for switching between redundant elements, for selection of the normal and high power operating modes of the UHF antenna and for selection of normal and eclipse modes of the S-band antenna. There are a total of four single pole double throw (SPDT) and four single pole triple throw (SP3T) switches in the S-band antenna and six SPDT switches in the UHF antenna. The relays are similar to those flown on other programs. Pulse-type switching is used to actuate the switches. The switches are controlled by separate command signals via relay drivers to minimize the power required for switching. Tentative specifications for the switches are:

Insertion loss	≤ 0.3 db
Frequency range	1.6 to 2.1 MHz and 400 to 470 MHz for UHF
Actuation	28 vdc pulse at $\approx$ 0.05 A for ≤ 100 ms
VSWR	1.5 to 1
Isolation	50 db
Power handling	40 watts for UHF, 5 watts for S-band

5.7.2.2.9 Antenna Assembly. The antenna design is configured to a single assembly which includes the basic structural cylinder, antenna elements, divider networks, and associated RF components to drive the antenna array. Figure 5-26 is a photograph of a partial array used for development testing.

The structural cylinder of this model, with the outer diameter faceted longitudinally in 32 equal spaces, is constructed of glass epoxy layup, sandwiching a 3/8-inch honeycomb core between a 0.004-inch epoxy face in the outer diameter and a 0.001 inch aluminum skin on the exterior diameter which provides the RF ground plane for the antenna system. In the preliminary design, the ground plane measures 56 inches in diameter with a length of 21.5 inches. The overall length of the structure measures 40 inches, thus allowing 18.5 inches of basically open surface area for mounting the antenna system RF components and coax cable.

The antenna assembly interfaces with the satellite at two mechanical junction planes. One interface occurs at the satellite equipment platform and the structural cylinder mounting points. The second interface occurs at the lower edge of the satellite solar panel substrates and a structural ring which circumvents the antenna assembly structure near mid-point of its total length.

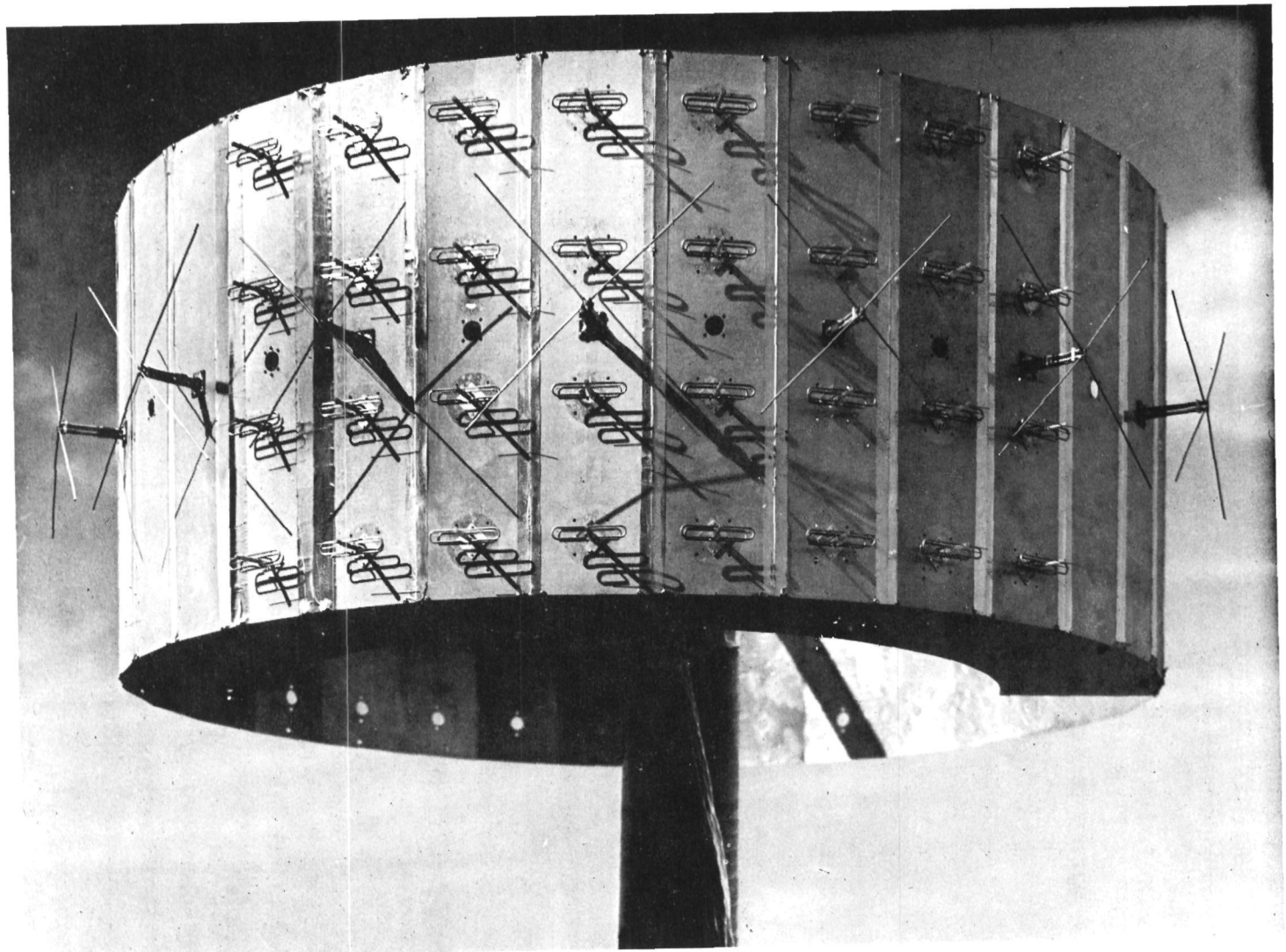

Figure 5-26. Partial Array

Upon this structural faceted cylinder are mounted the self-supported S-band yagi elements (128 each) with maximum dimensions 3.3 inches wide and 2.7 inches long. The elements are individually secured to the structure by mounting screws through the mounting flange.

Integrated with the S-band elements are 16 equally spaced UHF cross-dipole elements. These elements are also individually secured to the ground plane by mounting screws through the element mounting flange. Components are mounted to the structure by utilizing inserts and mechanical hardware. This extension of the structure also provides a thermal baseplate for the system power dissipating components.

The antenna assembly enhances the overall satellite design and assembly as well as the testing phase, where the assembly can be tested as a unit for pattern measurements, power amplifier measurements, etc. at the subsystem level prior to satellite integration. Since few RF connections are made or disconnected at the time of satellite integration, a high degree of confidence and reliability is gained from this design approach. Repair or replacement of RF components as well as changes in RF configuration, for example, are accommodated with little impact on the satellite interfaces.

5.7.2.3 Transponders

5.7.2.3.1 Functional Description. The transponder includes redundant S-band and UHF transponders, as shown in Figure 5-27. The following paragraphs briefly describe the functions of the transponders.

UHF transponder. The receiver uses a two-stage transistor preamplifier to obtain a noise figure (including the effects of the downconverter) of less than 2.5 db over the temperature range of 70 ±30° F. An ultra-stable crystal oscillator and multiplier chain provides the injection signal to the balanced mixer used for converting the received signal to an IF of nominally 25.9 MHz. The IF preamplifier is a low-noise linear amplifier stage. It is followed by a bandpass crystal filter which sets the receiver noise bandwidth at about 400 kHz. A five-stage linear IF amplifier has a gain in excess of 80 db and provides a constant level output of about -7 dbm at 94.5 MHz to each of the S-band transmitters via an upconverter/amplifier/filter unit.

A combiner/amplifier network is used to combine DCP interrogation signals received from either S-band receiver at a frequency of 35.61 MHz and a nominal level of -15 dbm. A balanced mixer upconverts the output of the combiner to 468.825 MHz. The mixer injection signal is derived from an ultra-stable crystal oscillator and multiplier chain. A bandpass filter then removes the lower

side band from the mixer output, and the filtered signal is amplified by a low-level driver assembly. The output of the driver assembly is in turn amplified to about 10 or 40 watts by UHF power amplifiers of the antenna assembly.

S-band transponder. The receiver assembly includes a conventional balanced mixer followed by a low-noise IF preamplifier. Injection frequency for down-conversion is provided by a solid-state multiplier chain. The noise figure of the downconverter assembly is nominally 7.5 db. A three-pole filter follows the preamplifier and sets the noise bandwidth at about 12 MHz. A hybrid then splits the signal into the wideband and command/cross-strap paths. The command and cross-strap signals are then downconverted to 34.91 and 35.61 MHz, respectively. The command channel includes limiting amplifier stages, a down-converter, a phase demodulator which detects the FSK/AM command baseband and a buffer amplifier stage to provide the baseband to the command detector of the T&C subsystem. The 3-db bandwidth of this channel is 80 kHz. The S/N of the command baseband output is nominally 20 db for the specified input level.

The cross-strap IF amplifier includes a 150-kHz bandwidth crystal filter, two linear and three limiting stages. When a DCP interrogation signal is present in this channel, it is routed to both UHF transmitters at a nominal level of -15 dbm.

The wideband IF includes four linear amplifier stages, two limiter modules, an 8.2-MHz seven-pole bandpass filter designed for Butterworth response, and an output amplifier stage. It provides a constant output at a nominal level of -7 dbm over a dynamic range from -70 dbm to thermal noise, referenced to the receiver input.

The transmitter performs the functions of modulating an 81.6-MHz carrier signal with the output of the VISSR digital multiplexer, modulating a 94.0-MHz carrier with spacecraft telemetry and combining these signals with the outputs of the repeater channel and the DCP report signal provided from the UHF receiver. The telemetry signal is transmitted continuously at a level 14 db below maximum signal output power. VISSR, WEFAX, and stretched video are transmitted on a time-division basis, that is, only one of these signals is transmitted over a given time interval. During VISSR data transmission, the repeater channel is turned off so the VISSR data captures most of the available output power. During the time the VISSR is pointed away from the earth or turned off, the QPSK modulator is also turned off, and the signal in the wideband channel captures most of the output power.

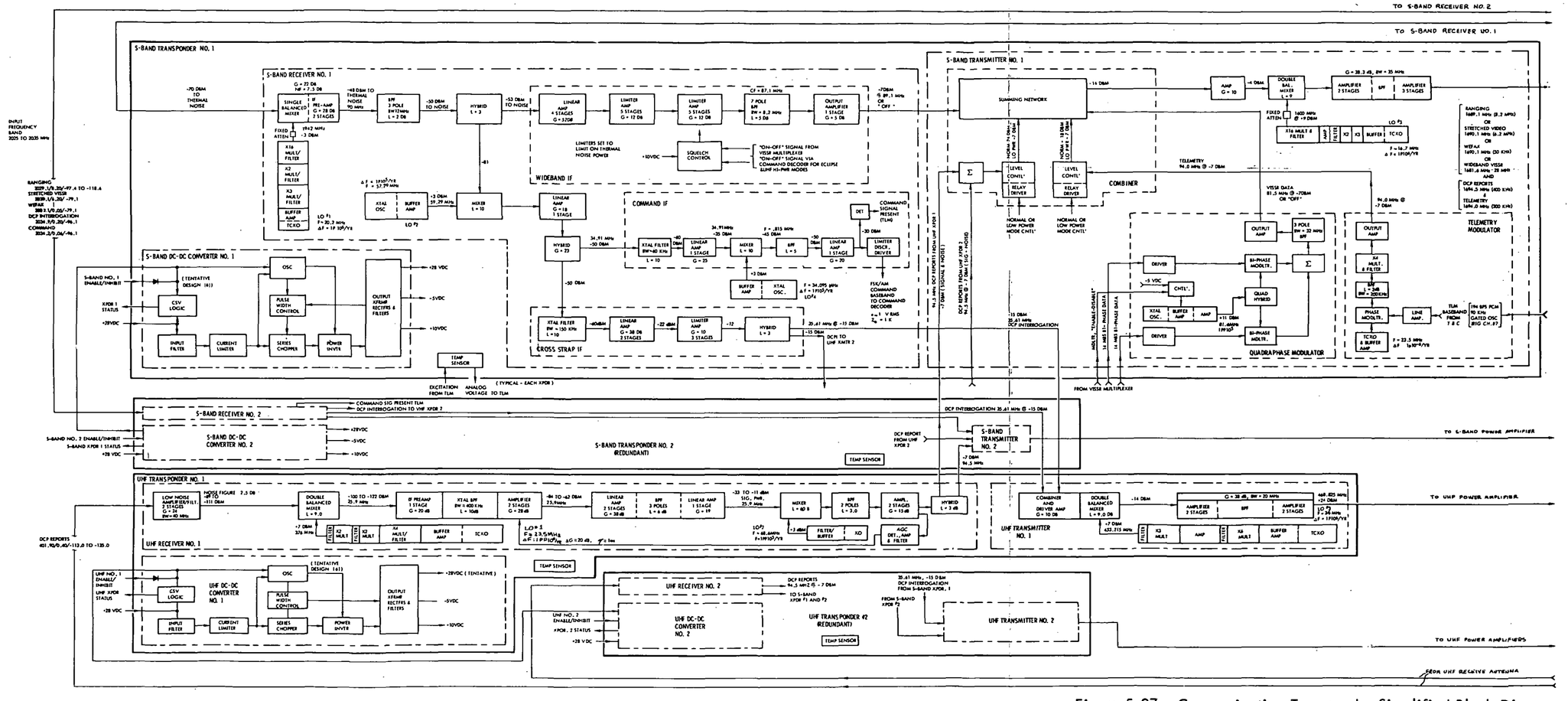

Figure 5-27. Communication Transponder Simplified Block Diagram

An additional control is provided in the transmitter to increase DCP report and telemetry signal levels during UHF high power or eclipse modes of operation. In the normal mode, the telemetry line includes an 11-db pad and the DCP report line a 17 db-pad. In the eclipse mode, the pads are removed and the S-band power amplifier in the antenna is bypassed, thus giving about the same DCP report and telemetry ERP as during the normal mode.

The telemetry modulator uses varactor diodes in a tuned circuit to phase modulate the output of a temperature compensated crystal oscillator (TCXO) with a baseband signal comprised of a 194 b/sec PCM telemetry and IRIG channel B or a 70-kHz gated oscillator signal provided from the T&C subsystem. Peak modulation index is nominally 1.8 radians.

The quadriphase modulator includes an oscillator, two balanced mixers, a quadrature coupler to drive the mixers with the carrier, a summing network, a three-pole bandpass filter, and an output amplfier. The balanced mixers biphase modulate the carriers with the differentially encoded output of the multiplexer. Key parameters in the design are modulator switching times and imbalance between the I and Q channels. Doubly balanced mixers using Schottky barrier diodes provide a switching time <10 ns. Balance is held to within nominally 1.0 db by use of a precision combiner. Nonorthogonality of the I and Q channel carriers also degrade QPSK performance and requires a precision quad-coupler to maintain orthogonality to within $\pm 5.0°$ over $70 \pm 30°$ F.

The upconverter is a standard balanced mixer which is driven by a frequency derived from proven crystal oscillator and multiplier chain. The mixer is operated well below its compression point to assure a linear transfer function. A five-pole bandpass filter centered at 1681.6 MHz attenuates out-of-band spurious and the lower sideband frequencies. The drive to the mixer is nominally -5 dbm and is reduced to about -11 dbm by the mixer conversion loss. This signal is then amplified to a nominal level of 23 dbm and routed to the power amplifier assembly by a coaxial relay. The latter two units are located in the antenna assembly.

5.7.2.3.2 Design Features. Oscillators. Table 5-25 summarizes the oscillators for the communications subsystem. TCXO's are similar to the temperature compensated design employed in the IDCSP transponders (Figure 5-28). The crystal frequency vs temperature curve is compensated over part of its range by $C_1 + C_2$ operating in parallel, and over the rest by C_2 alone. The mechanism which senses and controls is thermistor R_1, which adjusts the effective resistance of D_1 by current bias, thereby cutting C_2 in and out of the feedback path.

Table 5-25

SMS Communications Transponder Oscillator Summary

Type	Program	Frequency (MHz)	Application
XO	ALSEP	34.095	S-band RX, command downconverter
XO	ALSEP	57.290	S-band RX, 2nd downconverter
XO	ALSEP	68.600	UHF RX, upconverter
XO	ALSEP	81.500	S-band TX, quadriphase carrier
TCXO	572, Skynet	16.666	S-band TX, upconverter
TCXO	572, Skynet	20.229	S-band RX, lst downconverter
TCXO	572, Skynet	23.500	UHF RX, downconverter
TCXO	572, Skynet	24.078	UHF TX, upconverter
TCXO	572, Skynet	23.625	Phase mod carrier

Over that portion of the S-shaped crystal characteristic where frequency declines as temperature increases, the diode is turned full on permitting the temperature-compensated capacitors to correct the crystal. This region lies between the lower and upper turning points of the uncompensated crystal (typically +7 and +48° C).

At temperatures below the lower turning point the thermistor increases in resistance, reduces the conductance of D_1, and progressively takes C_2 out of the feedback path. This removal increases with declining temperatures and counterbalances the crystal.

The purpose of D_2 is to drop the voltage applied to D_1 when temperatures become high. This is necessary because R_1 decreases to a very small value and excessive currents become a threat. No crystal compensation occurs above the upper turning point.

Generally, lower order harmonics (2nd, 3rd, and 4th) are used in the multiplier chains to optimize efficiency in generation of local oscillator power. However,

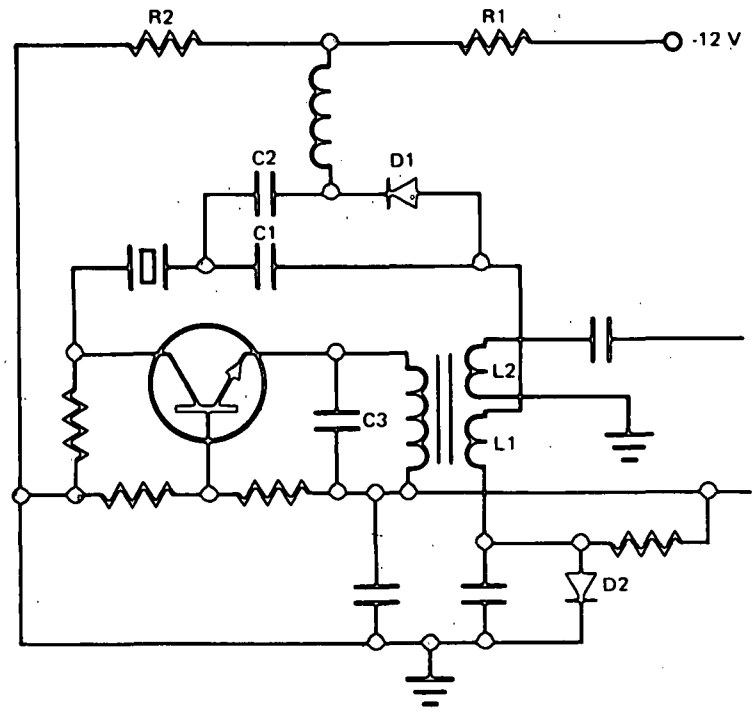

(a) CIRCUIT SCHEMATIC

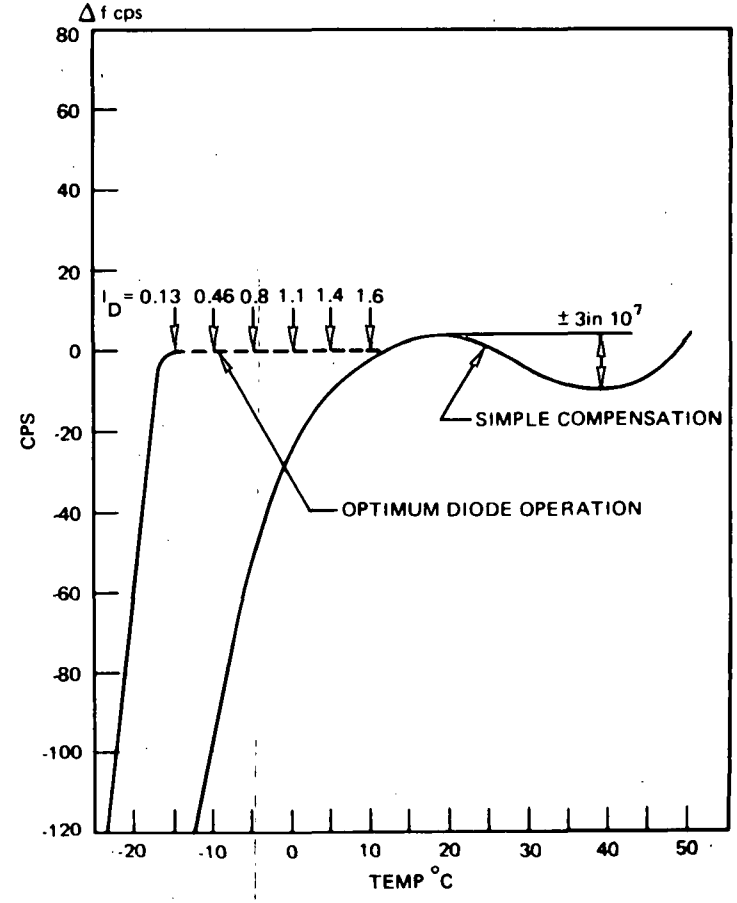

(b) OSCILLATOR FREQUENCY VS TEMPERATURE

Figure 5-28. Temperature Compensated Crystal Oscillator

local oscillator power for the S-band up and downconverters requires a multiplication ratio of 96, and an X16 multiplier was chosen for this application (Figure 5-29). The output filter has a five-pole Cheby-Chev response with 60-db rejection to the 15th (1500 MHz) and 17th (1700 MHz) harmonics of the fundamental input. The center frequency insertion loss of the filter is 1.5 db. The step recovery diode (SRD) comb generator is built on a microstrip-line using TEF or polyguide as a dielectric. The lower order multipliers/filters are conventional design.

IF Amplifiers. Table 5-26 lists each of the four IF amplifiers and summarizes the performance characteristics of each type. Figures 5-30 and 5-31 are a schematic and measured amplitude response, respectively, of this unit. The amplifier is "squelched" when an external command is received to remove the +10 vdc from the circuits. A seven-pole Butterworth filter was chosen as the best compromise between size, weight, selectivity, and delay.

The command and cross-strap IFs are of conventional design and use crystal filters to achieve good selectivity with small size and weight. Conventional designs, using discrete components for the RF stages, are used in both IF's. A Foster-Seeley type discriminator is used in the phase detector circuit to detect the command baseband which is then routed to the command unit of the T&C through an emitter follower. The UHF receiver IF is designed for a linear transfer function since a non-linear IF (limiting or fast automatic gain control) generates intermodulation products when multiple DCP report signals are being received. A slow acting level control is incorporated in the design to compensate for gain variations which occur as a function of temperature and aging. Gain control of about 20 db is adequate for this purpose.

Modulators.

(a) The Quadriphase Modulator. The quadriphase modulator shown in Figure 5-32 modulates the quaternary encoded serial data signal inputs from the digital multiplexer onto two orthogonal carriers, the result being a continuous wave transmission whose initial phase is either 0, 90, 180, or 270 degrees depending on whether the digital input is a one or zero, and whether it originates in line driver A or B. The characteristic impedance of the coaxial input lines is nominally 75 ohms and accounts for the terminating resistors.

The carrier frequency is supplied to either balanced port of the double balanced mixer and after mixing with the data input, it is taken from the other. The logical one and logical zero appear at the third or IF port and act as a gating or switching signal. There is a four-diode

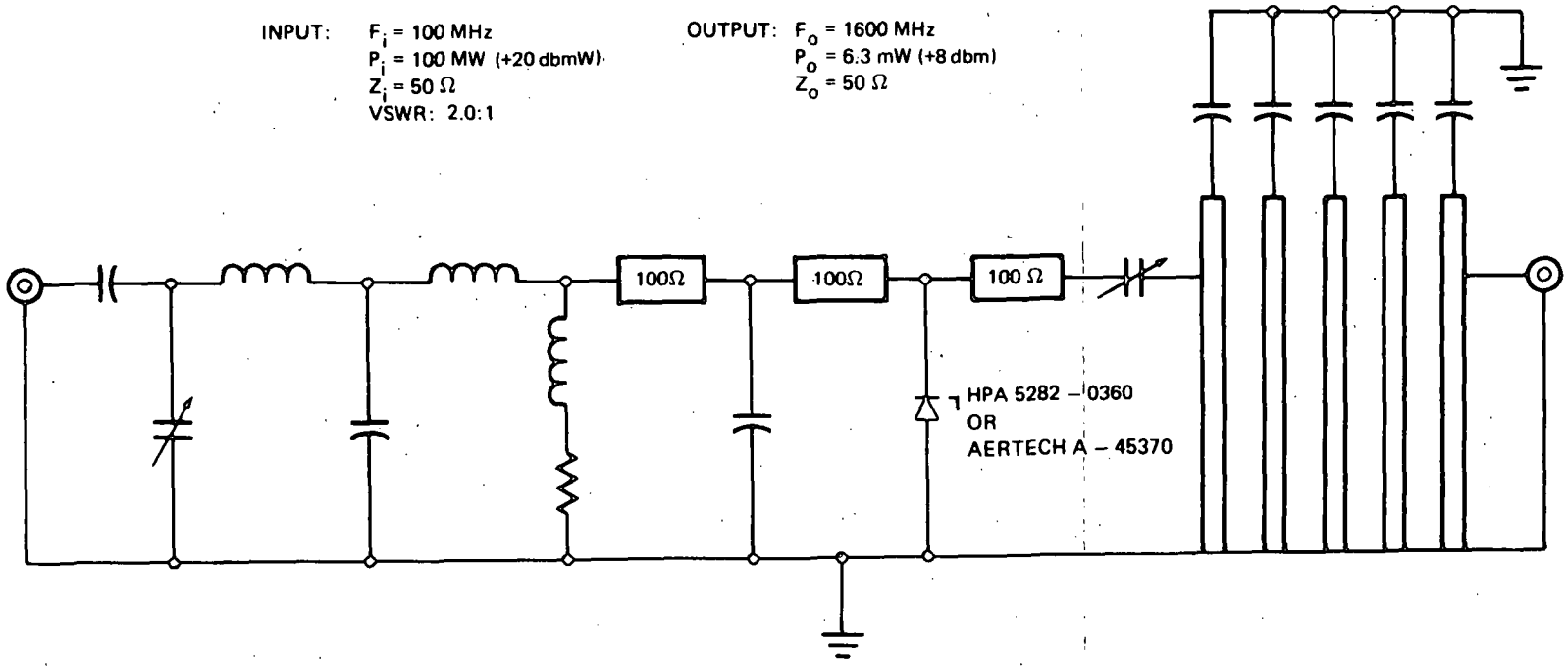

Figure 5-29. Step Recovery Multiplier X-16

Table 5-26

IF Amplifier Summary

	S-Band Receiver			UHF Receiver
	Wideband	Cross-Strap	Command	
Center frequency	87.1MHz	35.61MHz	34.91MHz	25.9MHz
Bandwidth (3 db), min	8.2MHz	150kHz	80kHz	400kHz
Bandwidth (30 db), max	15.0MHz	375kHz	150kHz	1.0MHz
Filter type	7 pole Butterworth bandpass filter	Xtal bandpass filter	Xtal bandpass filter	Xtal bandpass filter
Transfer characteristics	Hard Limiter	Hard Limiter	Hard Limiter	Linear with automatic gain control
Amplitude response	±0.5 db	±0.5 db	±0.5 db	±1.0 db
Dynamic range	-70 dbm to thermal noise	-85 dbm to -105 dbm	-85 dbm to -105 dbm	*-100 dbm to -135 dbm
Control	Squelch "OFF" by external command	None	None	None
Output	IF signal to S-band transmitter	IF signal to UHF transmitters 1 & 2	FSK/AM command baseband to telemetry & command	IF signal to S-band transmitters 1 & 2

*Linearity requirements only to range of -115 to -135 dbm

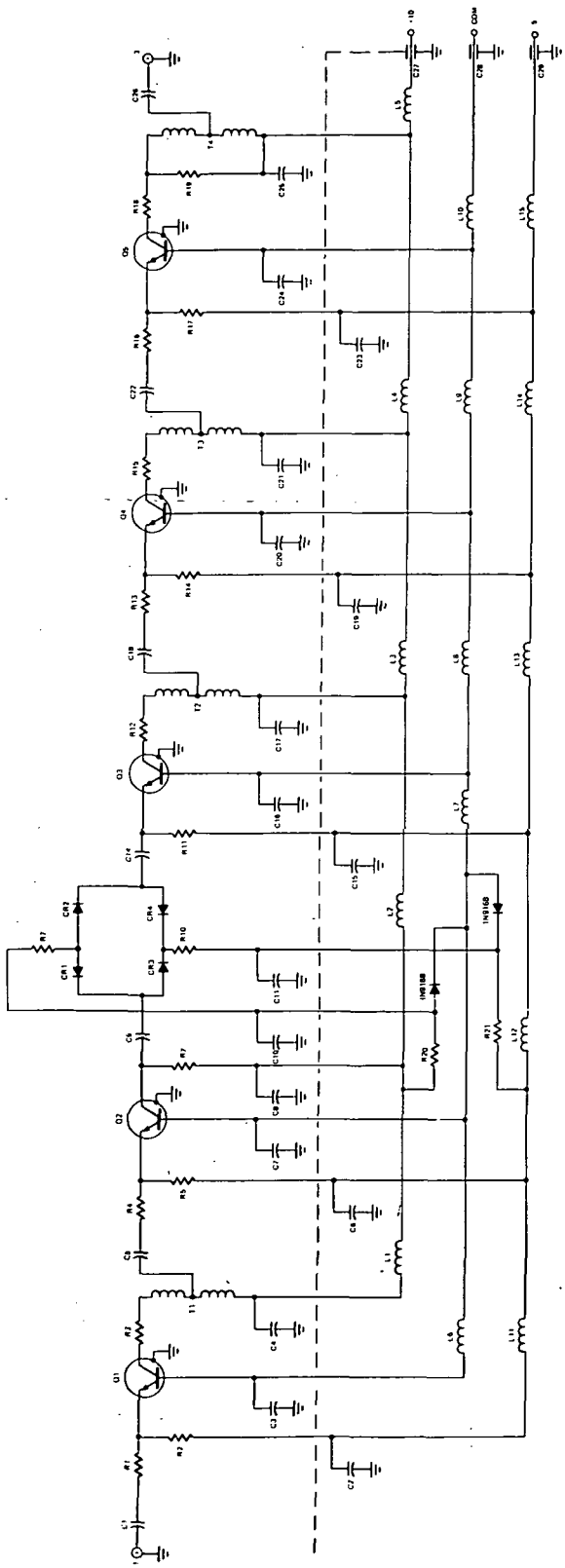

Figure 5-30. Schematic Diagram, IF Limiter Module

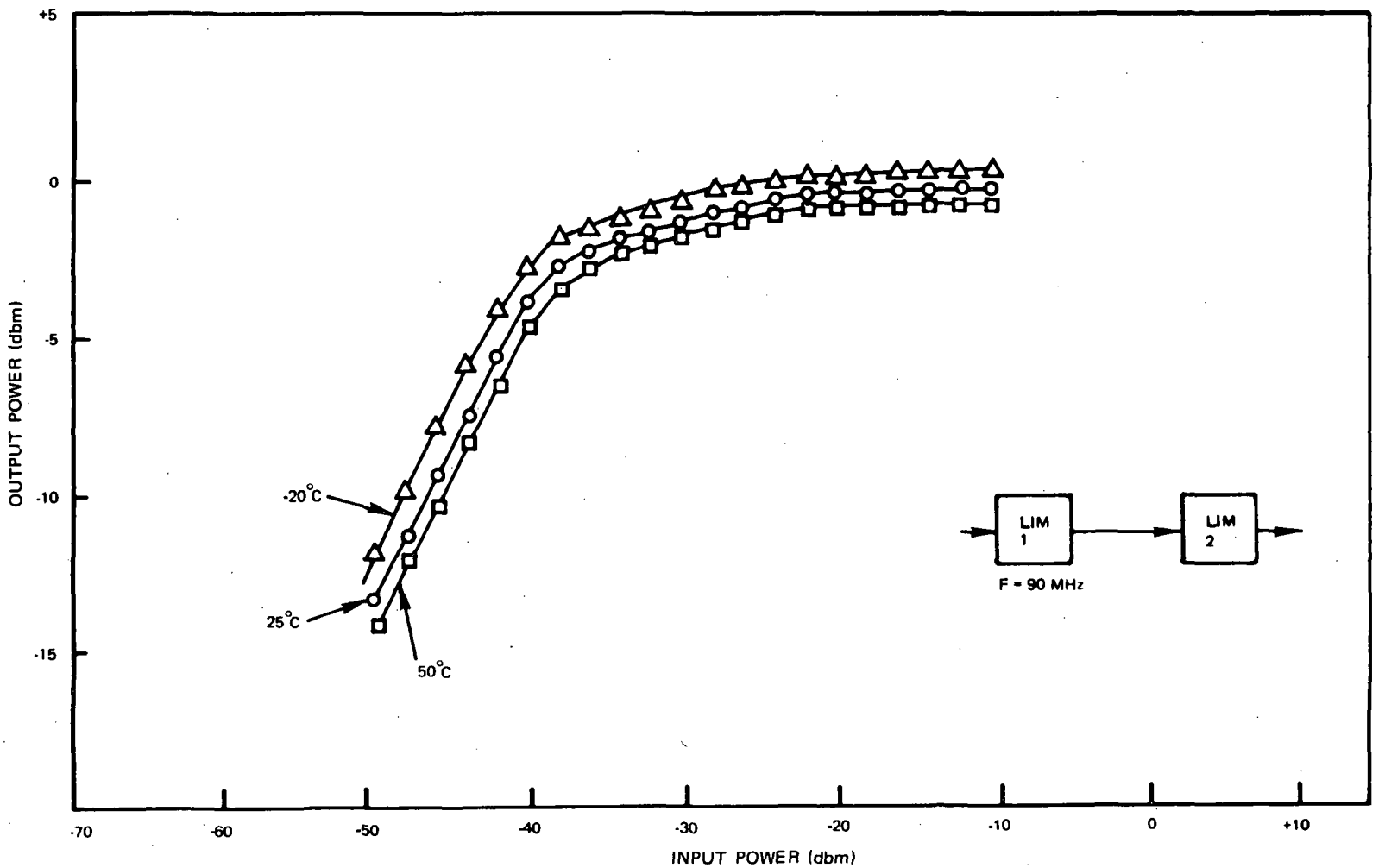

Figure 5-31. Dynamic Range vs Temperature Characteristics

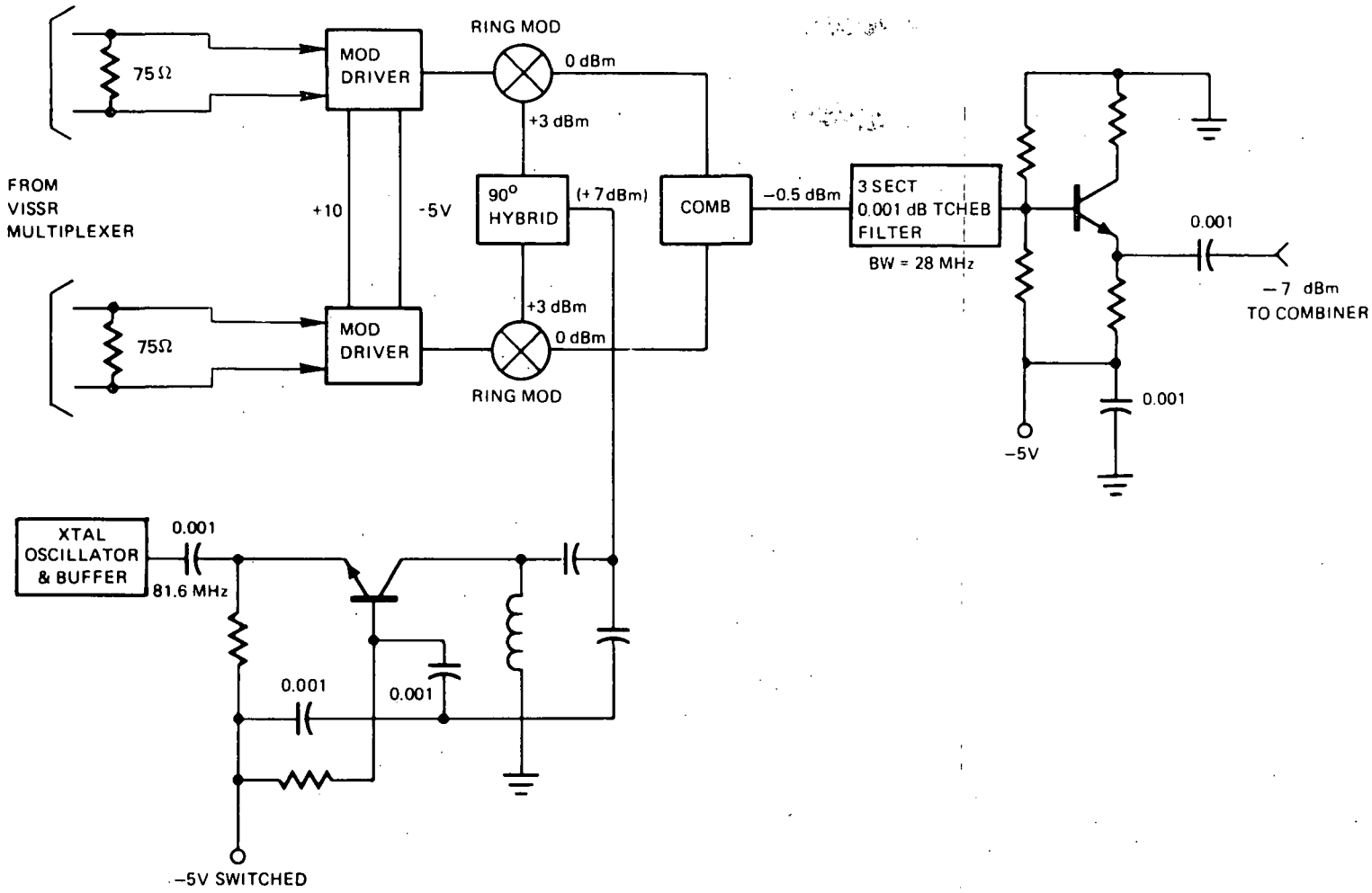

Figure 5-32. Quadriphase Modulator

balanced bridge within the mixer. When a positive signal is presented at the gate, one pair of diodes is forward biased and the other pair is reversed biased. With a negative gate signal conditions are reversed. The sense of current flow through the interval transformers is set by whichever pair of diodes is on. Hence either 0 or 180 degrees carrier phase is determined by the gate polarity. The 90-degree coupler provides the orthogonal carriers to the two mixers as required for QPSK operation.

The information bandwidth around the 81.6-MHz carrier is 28 MHz referenced to the first null of the modulator output spectrum. A 0.1-db ripple Chebyshev with a 3-db bandwidth of 28 MHz is used to reduce sideband levels beyond the first nulls for RFI purposes. A signal provided by the digital multiplexer squelches the modulator by removing dc voltage from the carrier buffer amplifier whenever the multiplexer is off.

(b) Telemetry Modulator. The telemetry modulator is a standard design as shown in Figure 5-33. A temperature-compensated crystal oscillator provides a stable carrier frequency which is phase-modulated by the phase modulator shown in Figure 5-34. The output of the modulator is fed through a crystal filter to a X4 multiplier and emitter follower. The output of the modulator assembly is then routed to the combiner of the transmitter. A crystal filter with a 3-db bandwidth of 200 kHz and shape factor of 2.5 is used to reduce the higher order sidebands to levels which will not degrade DCP report signals in the transponder output spectrum.

Combiner. The combiner is shown in Figure 5-35. It includes a four-port summing network for wideband signals and two-port summing network for the narrowband signals. It also includes latching relays, attenuators and relay drivers for control of telemetry and DCP report signal levels. Relative output levels and level control were discussed in 5.7.2.3.1.

Driver Amplifiers. The S-band and UHF low-level driver amplifiers of the S-band and UHF transmitters are similar in configuration, as shown in Figure 5-36. Three stages of amplification amplify the output of the upconverter to the nominal 200-milliwatt level required to drive the power amplifiers located in the antenna assembly. The first two stages are operated class A while the output stage is operated near class C to reduce power consumption. A bandpass filter is included in each amplifier chain to reduce local oscillator leakage and minimize potential RFI problems. Each filter is a five-section combline similar to those used with the X16 multiplier of the S-band transponder.

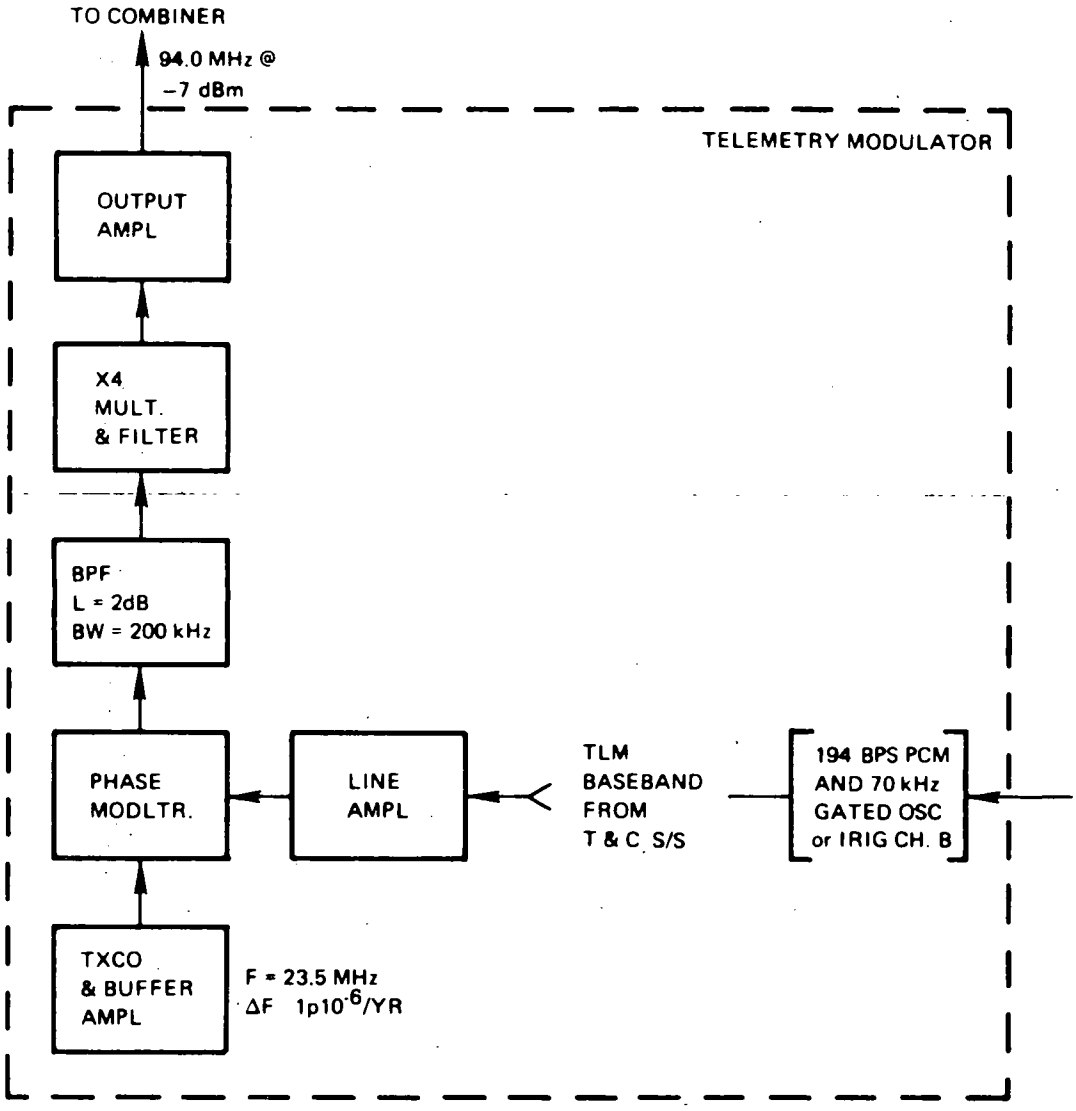

Figure 5-33. Telemetry Modulator

Mechanical Design. There are five transponder packages. Four individual S-band transponder packages include:

1. S-band transmitter 1 and dc/dc converter 1
2. S-band transmitter 2 and dc/dc converter 2
3. S-band receiver 1
4. S-band receiver 2

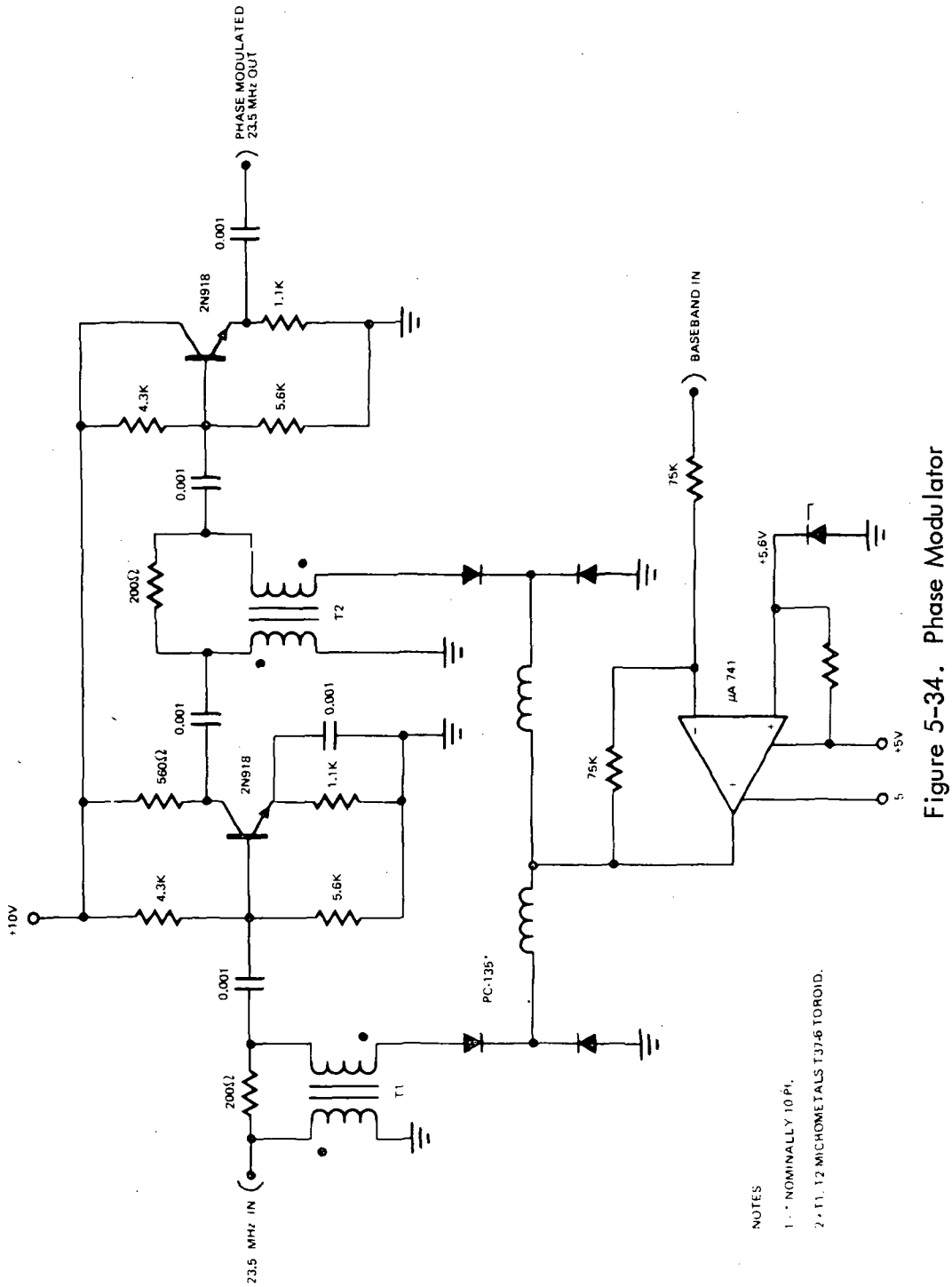

Figure 5-34. Phase Modulator

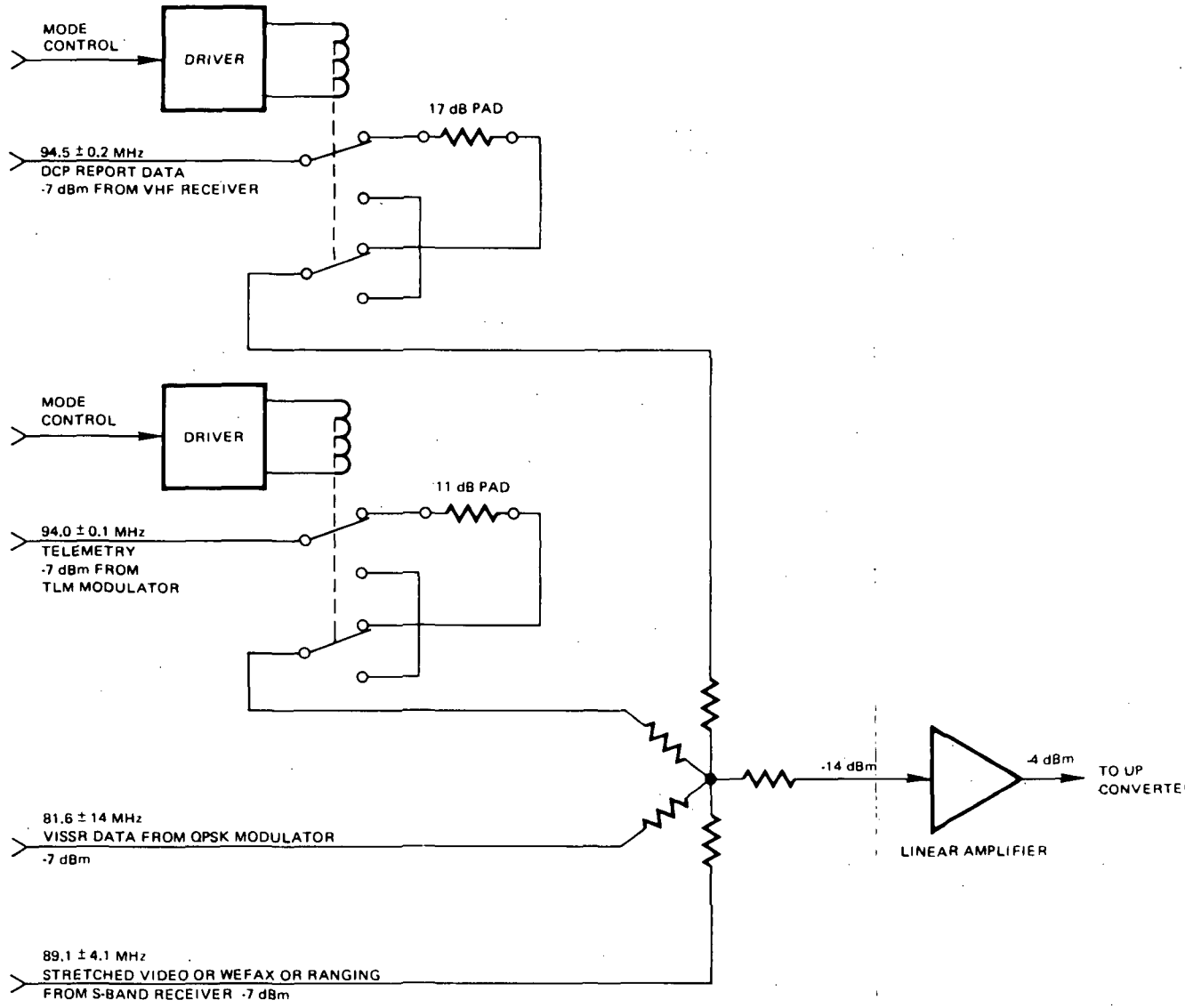

Figure 5-35. Combiner Functional Block Diagram

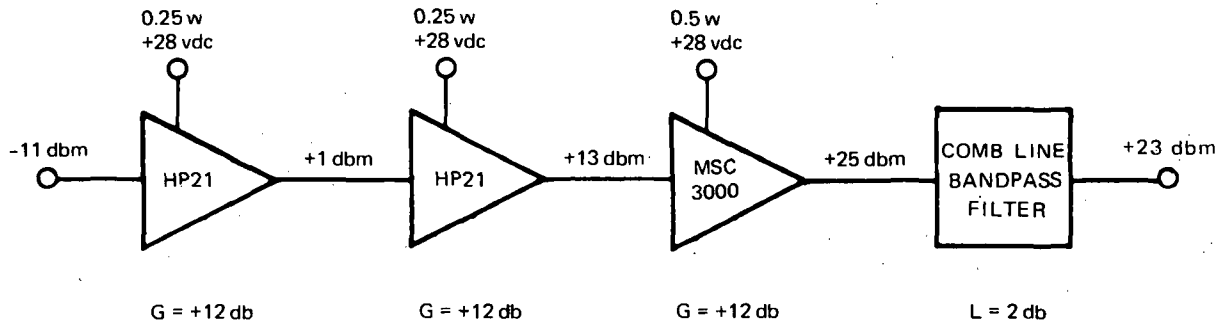

CENTER FREQUENCY = 1681.6 MHz

a) S-BAND TRANSMITTER LOW-LEVEL DRIVER AMPLIFIERS

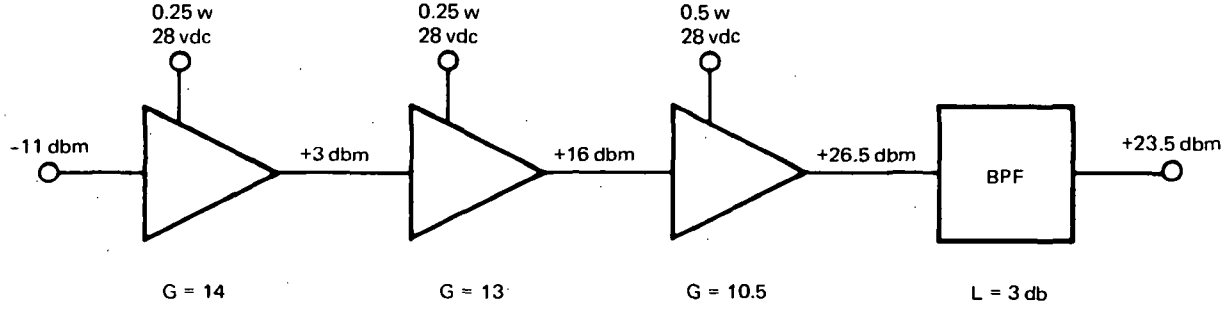

CENTER FREQUENCY = 468.825 MHz
TRANSISTORS: 2N4428

b) UHF TRANSMITTER LOW-LEVEL DRIVER AMPLIFIERS

Figure 5-36. Low-Level Driver Amplifiers

The UHF transponder package includes two dc/dc converters, two receivers, and two transmitters, that is, both UHF transponders are included in one package. The general block diagram of this package is shown in Figure 5-37. Figures 5-38 and 5-39 show a typical subassembly chassis and metal frame module, respectively.

Each of the subassemblies consists of a group of circuit modules mounted on a standard chassis which provides structural support and interconnection for the modules. RF connectors and standard connectors are on the inside and top surfaces of each subassembly.

The standard subassembly chassis are fabricated from either aluminum or magnesium, depending on thermal requirements. The transmitter is aluminum and the other two chassis are magnesium. The circuit module mounting surface is a flat plane, the reverse side of which is milled into compartments for module interconnections. Each of the subassembly chassis are goldplated to reduce any galvanic couples.

The electronic circuits are packaged in:

(a) Miniature metal frame modules

(b) Miniature metal frame modules with a printed circuit insert

(c) Stripline modules

This packaging approach provides:

(a) Separations and shielding between RF and dc components

(b) A good ground plane for parts terminating at ground without excessive wire or lead length

(c) Mechanical integrity to use an encapsulant with a low dielectric constant

(d) Positive thermal control

(e) Shielding for radiated interference

(f) Repeatability

Each module is a functional portion of the total circuit and may be tested, operated, or replaced separately.

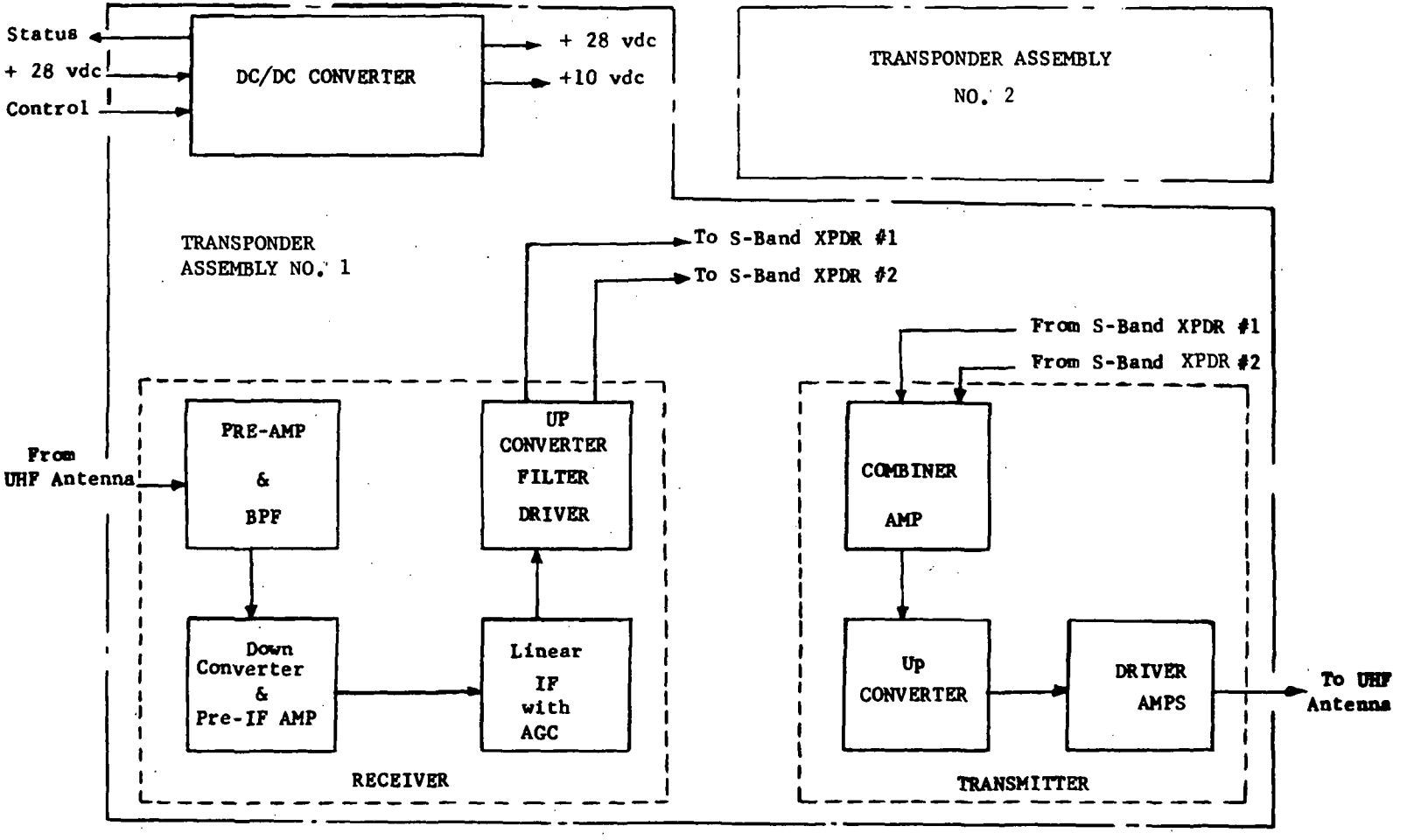

Figure 5-37. UHF Transponder Block Diagram

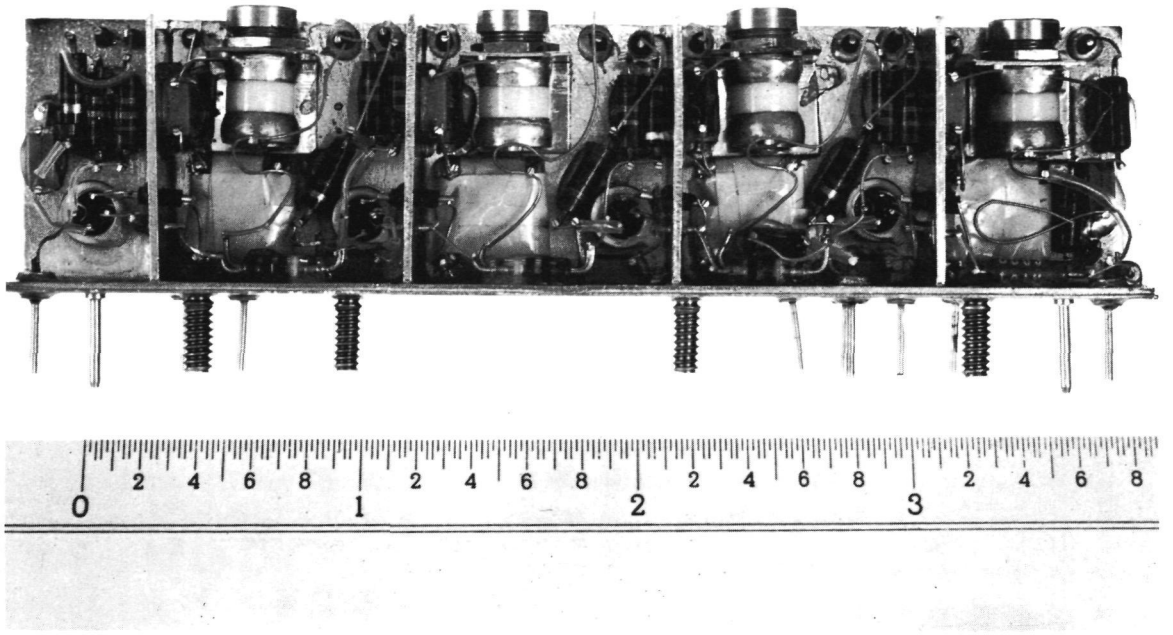

Figure 5-38. Typical Metal Frame Module

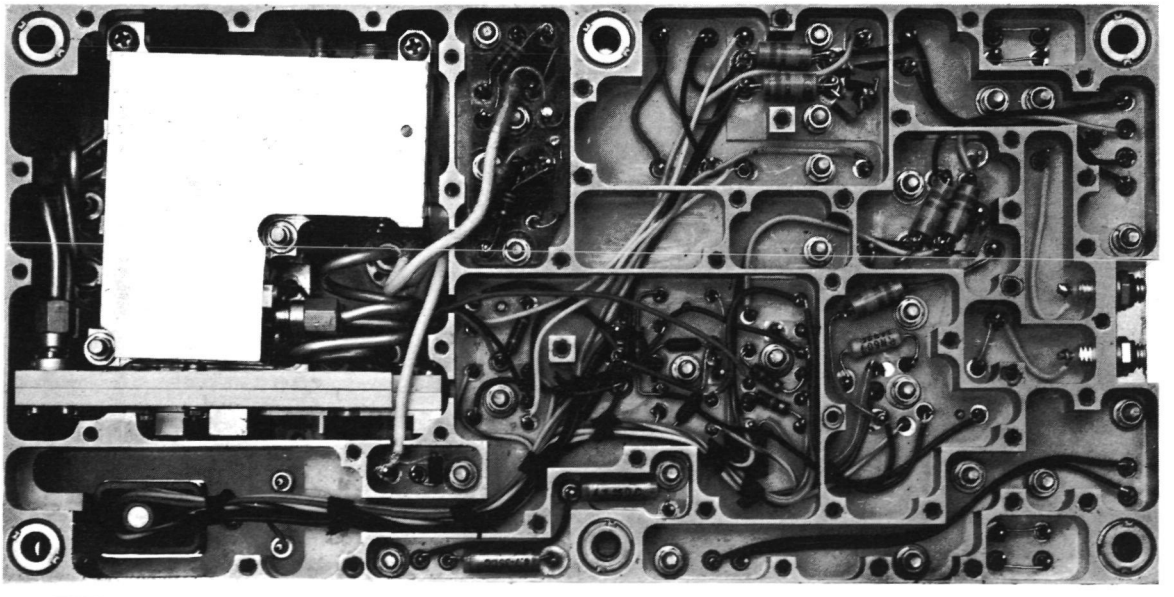

Figure 5-39. RF Interconnect Chassis

A shielding cover is placed over the module assembly and sealed to the mounting flange. The material and thickness of this cover are determined by the use of the shielding equations derived by S. A. Shelkvnoff and adopted by C. S. Vasaka. For the most of Philco-Ford's previous programs, 0.007-inch-thick gold-plated aluminum and 0.005-inch-thick gold-plated copper have been found to be satisfactory.

All transformers and coils are designed with the idea of reproducibility in mind. This is achieved by designing all magnetic components so that they may be installed into the circuit as a tested part. All coils are wound on a form and all transformers are placed into holders with terminals. These parts are then checked electrically against a standard. This standard is an exact duplicate of the part being used, and is the component which was used to set up and test the prototype model of the module.

After the module has been pre-pot tested, it is encapsulated with a 2 lb/ft^3 density, CO_2-blown, polyester-base, slow-reaction foam having a dielectric constant of 1.03. This material was selected by analyzing the tradeoff between the characteristics of density, thermal conductivity, and dielectric constant.

High frequency filters and multiplexers are fabricated using standard stripline techniques. It is standard practice at Philco-Ford to lay out these circuits at 10 times actual size using a coordinatograph to guarantee accuracy.

The interconnections of the modules are accomplished by soldering or welding short jumper wires from one module to the next, except for some special cases where coaxial lines are required. The metal partitions, an integral part of the subsystem frame between the RF and DC portions of the unit, serve as a shield for radiated interference. These partitions also isolate the input and output terminals. The electronic piece parts which filter the conducted interference are wired directly into the interconnection path. The modules are secured to the chassis with threaded fasteners and locking devices so that there is no dependence upon the soldered joints for mechanical security. The module interconnections and their decoupling networks are conformal coated for environmental protection. Upon completion of interconnections and coating, a cover is fastened down over the base opening, providing complete shielding of the system and adding to the mechanical strength. This interconnect system has significantly improved the reliability of RF systems by replacing subminiature coaxial lines and their assorted connectors with short ribbons. Interconnection between subassembly frames is by standard coaxial cable and connectors.

5.8 TELEMETRY AND COMMAND (T&C) SUBSYSTEM

The T&C subsystem[1] (Figure 5-40) includes the functions of telemetry, command, ranging, and tracking. Parallel redundancy is utilized throughout the sustain subsystem operation in the event of a single failure of any unit in the subsystem. The subsystem design is compatible with the Wallops CDA T&C ground station equipment and the GRARR tracking and ranging system. The PCM telemetry function is compatible with the Wallops CDA equipment design and the GSFC PCM Telemetry[2] Standard. The real-time telemetry is IRIG standard frequency-division multiplex on IRIG channels 12 and B and* non-standard on channel E. The command equipment is compatible with the OGO-modified-for-ATS command encoder and the ATS synchronous controller presently in use at the Wallops Station, and in selected STADAN network sites.

The redundant channels of the dual telemetry unit are designated TLM unit 1 and TLM unit 2. These are identical, independent units containing both PCM time-division multiplexing and real-time frequency-division multiplexing to encode routine spacecraft data, and critical control data, respectively. In normal operation, only one of the two telemetry units are on. In case of a failure in one unit, the other unit is commanded on to replace the function of the disabled unit.

In operation, spacecraft telemetry data sources send routine spacecraft data and critical control data continuously to both telemetry units. The PCM telemetry encoder operates in either normal or dwell mode. In the normal mode, routine spacecraft data is time-multiplexed, encoded into 9-bit digital words, and formated into a digital data bit stream at approximately 194 bits per second. A complete mainframe is 64 nine-bit words, or 576 bits long. The first two words of the frame consists of 18 frame-synchronization bit. In the dwell mode the multiplexer is halted at any particular mainframe word (except the first 4 words of the format), and the bit rate remains the same. The first 4 words always occur in their normal time sequence. With the PCM multiplexer in the dwell mode, the real-time frequency-division multiplexer still operates in its normal mode, and both PCM and real-time multiplexer signals are still added and routed to the spacecraft RF equipments. Note that the digital data of words 3 and 4 always appear once each mainframe period (2.97 seconds) both in the normal and the dwell modes of operation.

The outputs of both telemetry units are combined and switched by combining units and routed to four transmitters, two VHF and two S-band units. By

*Channels 12 and B on VHF, channels B and E on S-band. Channel E is non-standard in that channel E is keyed on and off rather than being deviated.

command, this cross-strapping permits either telemetry unit to modulate any one of the four spacecraft transmitters. In normal operation, the telemetry data are transmitted utilizing either of the two S-band transmitters. During transfer orbit, when the S-band coverage is restricted, or in the event of a failure of the S-band links, the telemetry data are transmitted utilizing either of the redundant VHF transmitters. The S-band transmitter transmits the telemetry data down utilizing phase-modulation on a 1694.0 ±0.1-MHz carrier. The relatively high received power levels on the S-band link provide more than adequate link margins and corresponding performance margins for the data subcarrier. The VHF unit transmits the telemetry data, utilizing phase modulation on a 136.38-MHz carrier. In the low-power mode, the transmitter RF output is 2 watts, which provides an EIRP of +26.0 dbm, considering losses and gains of the diplexers, hybrid, and the omnidirectional antenna. The power output of the transmitter is increased by command to 8 watts (+32 dbm EIRP) to meet the worst-case link requirements for simultaneous transmission of real-time and multiplexed data during transfer orbit. The modulation index of the transmitted telemetry carrier is adjusted to achieve optimum performance for each of the combinations of PCM telemetry, real-time telemetry, or ranging. The total downlink modulation, expressed in carrier-peak-phase deviation is listed below for each operational mode:

(a)	PCM telemetry	0.6 radians
(b)	RF telemetry	1.3
(c)	PCM and real-time telemetry	1.9 (0.6 + 1.3)
(d)	Ranging	0.7
(e)	Ranging and PCM telemetry	1.0 (0.7 + 0.3)
(f)	Ranging and real-time telemetry	1.0 (0.7 + 0.3)

In the ranging mode, the telemetry modulation is attenuated in the transmitter modulator during the 4-kHz (holding) tone presence. Table 5-27 is a summary of VHF telemetry downlink performance.

5.8.1 PCM TELEMETRY

The telemetry frame format utilized for the PCM telemetry function in the normal mode is described in Appendix A. The pertinent parameters for this frame format are as follows:

Bit rate	194.18 ±0.05 percent bps
Word length	9 bits

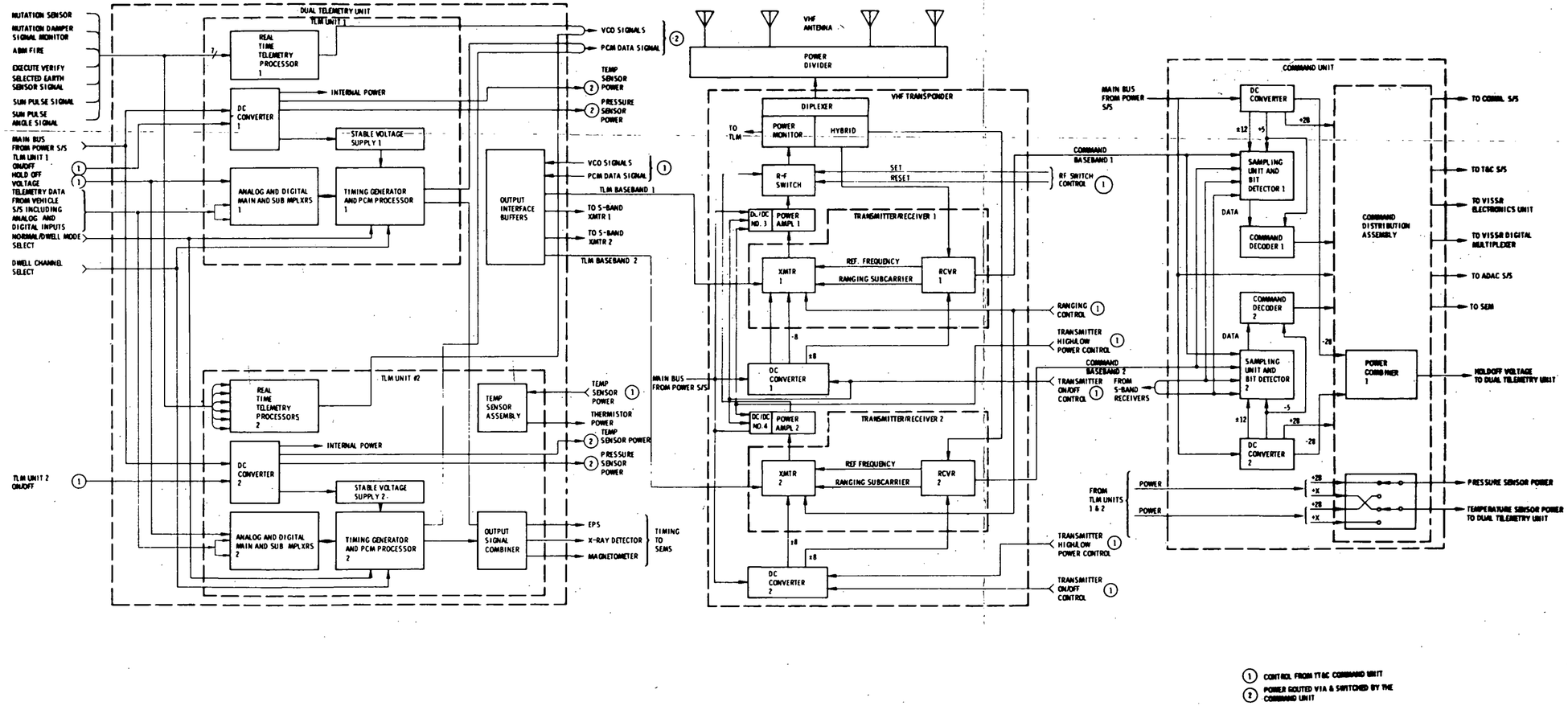

Figure 5-40. SMS Telemetry and Command Subsystem Block Diagram

Table 5-27

Summary of VHF Telemetry Down-Link Performance

	Ranging (sequential)					PCM Telemetry		Real-time Telemetry (Sun pulse)		Fine Range and PCM			Fine Range and Real-time Telemetry			PCM and Real-time Telemetry		
	Acquisition		Tracking															
	Coarse	Fine	Coarse	Fine	Carrier	PCM	Carrier	RTT	Carrier	Range	PCM	Carrier	Range	RTT	Carrier	PCM	RTT	Carrier
Req'd S/N (dB) or E/N_0 (Digital)	13.8	12.4	13.8	35.0	14.0	9.8 $P_e = 10^{-3}$	14.0	8.2	14.0	35.0	9.8 $P_e = 10^{-3}$	14.0	35.0	8.2	14.0	9.8 $P_e = 10^{-3}$	8.2	14.0
Bandwidth (Hz) or Data Rate (b/s)	1.0 t_a = 1.5 sec	10.0 t_a = 0.4 sec	1.0	0.1	10.0	194 b/s	10.0	1000	10.0	0.1	194 b/s	10.0	0.1	1000	10.0	194 b/s	1000	10.0
Req'd Channel S/N_0 (dB-Hz)	13.8	22.4	13.8	25.0	24.0	32.7	24.0	38.2	24.0	25.0	32.7	24.0	25.0	38.2	24.0	32.7	38.2	24.0
Modulation Loss (dB)	-15.6	-15.6	-15.6	-15.6	-1.0	-5.8	-1.7	-2.7	-4.2	-7.1	-12.6	-1.5	-6.9	-14.7	-1.3	-9.9	-4.4	-5.8
Req'd C/N_0 Ratio (dB-Hz)	29.4	38.0	29.4	40.6	25.0	38.5	25.7	40.9	28.2	32.1	45.3	25.5	31.9	52.9	25.3	42.6	42.6	29.8
Margin (dB) from C/N_0 = 47.8 dB-Hz	18.4	9.8	18.4	7.2	22.8	9.3	22.1	6.9	19.6	15.7	2.5	22.3	15.9	-5.1	22.5	5.2	5.2	18.0
Peak Phase Deviation Per Subcarrier (Radians)	0.7	0.7	0.7	0.7	X	0.6	X	1.3	X	0.7	0.3	X	0.7	0.3	X	0.6	1.3	X
Total Peak Phase Deviation (Radians)	0.7	0.7	0.7	0.7	X	0.6	X	1.3	X	1.0		X	1.0		X	1.9		X

f = 136 MHz, ERP = 39.0 dbm (P_t = 8W), G_s = -6.0 db, G_t = 18.0 db

Frame length	64 nine-bit words (576 bits)
Dwell mode operation	Readout at 64 x normal rate (no dwell on words 1 through 4)
Sampling rates	Mainframe — sample each 3 seconds 32-channel submultiplexer — sample each 1.6 minutes 64-channel submultiplexer — sample each 3.2 minutes

Consideration has been given in the main-frame allocation to provide as close to optimum sampling of the solar-environment measurement (SEM) experiment data as possible. The three analog outputs of the magnetometer H_p amp, H_p sun, and H_p quad are assigned 12 words in the mainframe to increase the sampling rate by a factor of 4 over the normal frame rate. In the dwell mode, as noted above, words 5 through 64 are replaced by data from one normal main frame channel to increase the sampling rate. A complete PCM telemetry list is provided in Appendix A. Channels undesignated as to title are spare.

5.8.2 REAL-TIME TELEMETRY

The format for the real-time frequency-division multiplexer is shown in Figures 5-41 and 5-42. The real-time format is not the same for VHF and S-band operation. During ascent and transfer orbit (VHF operation) the nutation sensor data are required continuously. These data are never interrupted except by priority of command execute pulse (secondary) or ABM fire (prime) when it is time shared. These data are on IRIG channel 12. Other data that are required continuously not only during the ascent and transfer orbit, but also for the lifetime of the synchronous orbit, after being placed on station is telemetered on IRIG channel B for both VHF and S-band operation.

5.8.3 COMMAND

The command function is also implemented in a parallel redundant configuration as shown in Figure 5-43. The uplink carrier is received and demodulated by either of two S-band receivers in synchronous orbit, or the two VHF receivers in transfer orbit or in the event of a failure of the S-band links. Both command channels are always in operation and receive baseband input signals from any one of the four spacecraft receivers. Selection of a signal to be processed is made by a signal-sampling assembly in the input section of each redundant channel of the command unit. Figure 5-44 is a block diagram of the redundant sampling units. The presence of the command introduction sequence is detected by

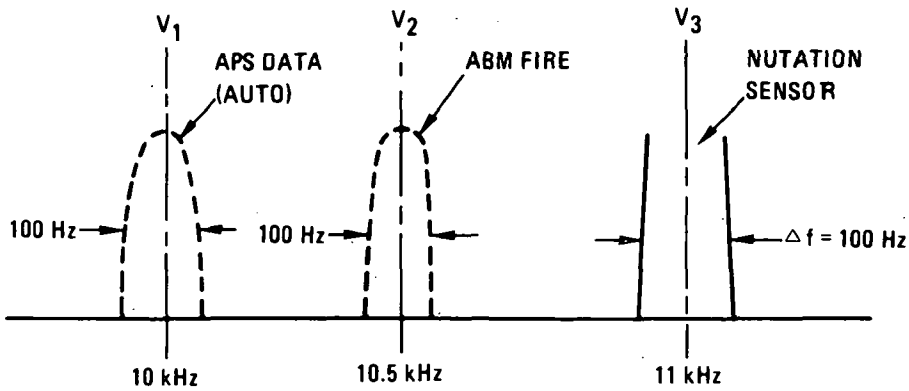

Nutation sensor data on 100 percent of the time. Therefore no idle position is necessary.

Figure 5-41. Channel 12 SCO Output Spectrum (VHF Only)

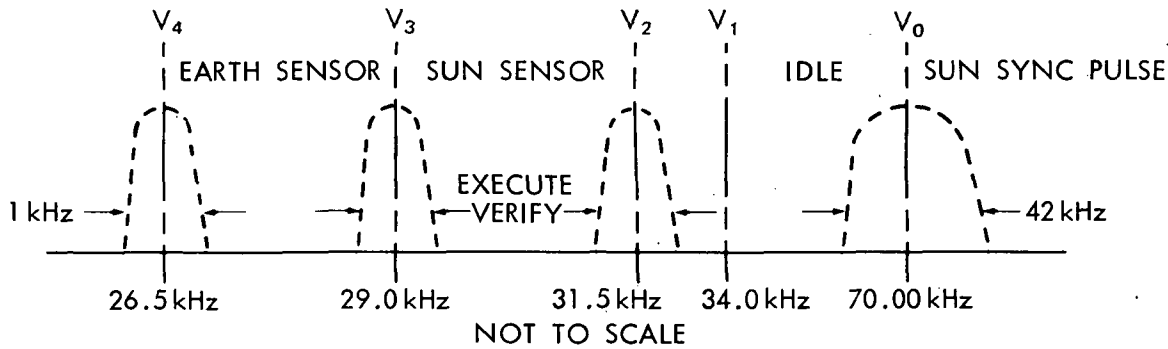

Pulses on V_1, V_2, V_3 and V_4 not on 100 percent of time; therefore idle level is required.

Figure 5-42. Channels B and E Subcarrier Oscillator Output Spectrum (E on S-band Only)

the command decoder, and if the signal is adequate in terms of signal strength and signal-to-noise ratio, the command decoder continues to process the signal. If the signal tone is not present, the signal sampling assembly advances to the next source, repeats the signal measurement, and either stops or advances to the next source, depending on the results of the measurement. Circuits in the command decoders operate on the amplitude and time duration characteristics of the input signals to provide decision criteria for stopping or advancing the sampling units.

Once satisfactory signal acquisition is achieved, the command decoders further process the signals to detect and recognize the command address. Each of the redundant command decoders is enabled by a different command address. The other decoder does not recognize the address in the message and returns to

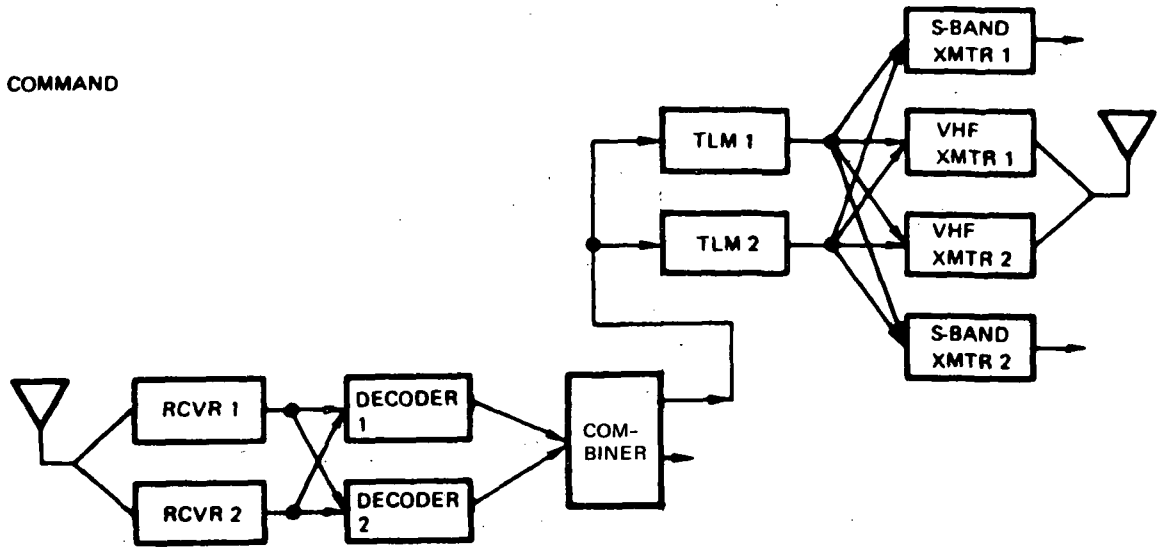

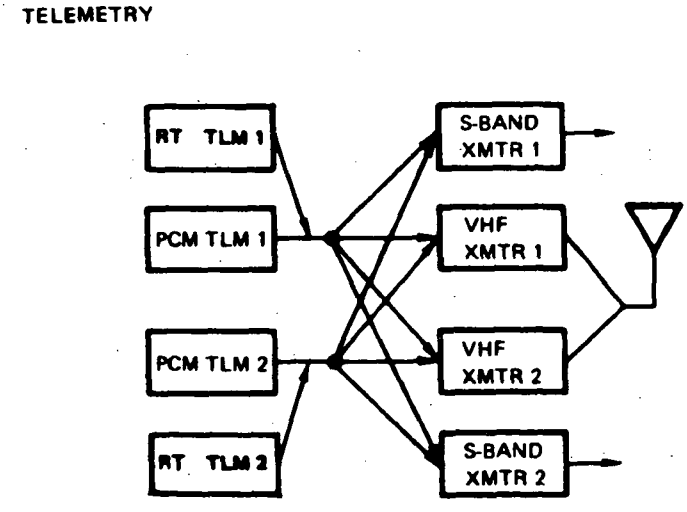

Figure 5-43. Telemetry and Command Functional Cross-Strapping

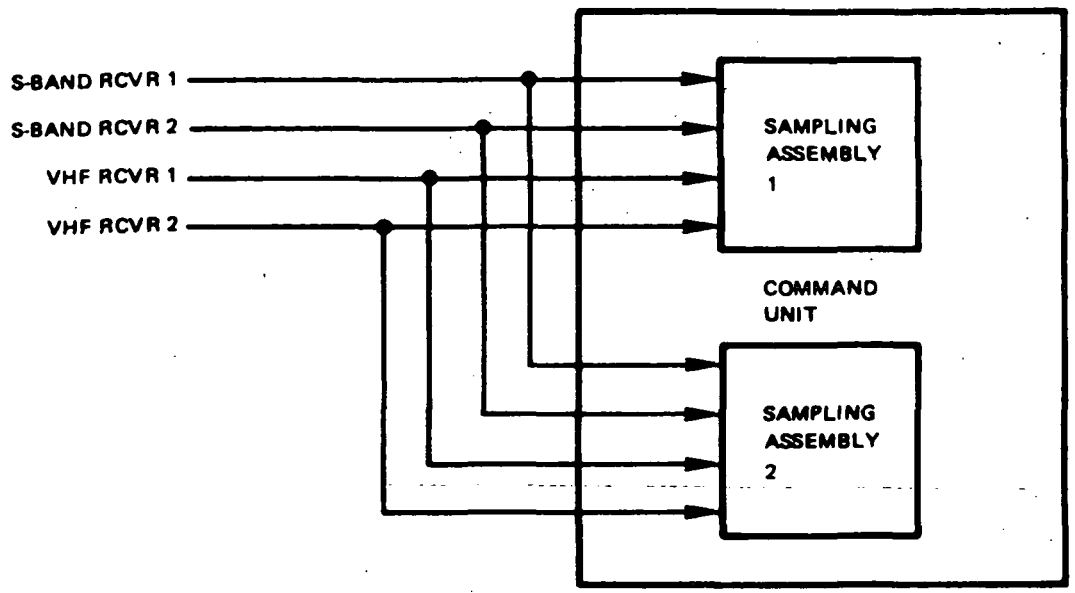

Figure 5-44. Receiver/Command Unit Interface

standby. The enabled decoder detects and decodes the command number. The command number is formatted in the mainframe of the PCM telemetry and transmitted to the CDA station for verification. Following ground verification that the digital command number in the decoder's register is correct, an execute tone is transmitted to the spacecraft. Receipt of the execute tone actuates the command function to the using spacecraft equipment. The received execute tone pulse-shifts the frequency of the real-time telemetry subcarrier oscillator, and sets one bit of a digital word in the PCM mainframe to provide both real-time and stored verification of execute tone presence. In addition, the real-time telemetry provides the duration of execute tone.

The outputs of the redundant channels in the command unit are combined by means of a command distribution (CD) assembly to provide a single output for each command function. The command unit provides 60 relay outputs corresponding to 120 commands. The relay outputs accomplish storage of the command as well as power switching capability and isolation. In addition, the command unit provides 50 pulse commands. The output capability can be expanded to a total of 254 commands (all 0's and all 1's excluded).

5.8.4 IRREVERSIBLE, CRITICAL COMMANDS

Functions which are one-time, critical operations such as commands to fire the ABM or pyrotechnic devices are protected by two measures: the first is that an arm command is executed before a fire command is capable of being executed; the second protective measure is the length of fire execute tone pulse which is

longer in duration than any execute pulse is possible for any other (non-pyrotechnic) functions by a comfortable margin. Thus, two commands must be sent and the receipt of each verified in order. This process is performed in the correct sequence, before a fire command is executed. The much longer time duration of fire executes mitigates against the otherwise possible false recognition of any ordinary function as a critical function to be executed. The present command list appears as Appendix B.

5.8.5 RANGING

A ranging function is implemented with the redundant VHF transponders. Operation starts with reception of the GRARR address tone by both receivers, enabling ranging-mode control circuitry. When a 4-kHz holding tone is subsequently received, the receiver IF channel to the associated transmitter is unsquelched. The ranging sideband modulation on the uplink carrier is translated in the receiver to IF at 800-kHz nominal and, in turn, modulates the operating transmitter (135.565-MHz) for retransmission to the GRARR station. The range tones are not detected in the process of frequency translation, modulation, or retransmission. The 4-kHz holding tone also adjusts the telemetry modulation index at the transmitter modulator to optimize link performance during simultaneous operation of telemetry and ranging. Carrier acquisition is accomplished by ground station acquisition of the VHF transmitter carrier. If required, the telemetry modulation can be commanded off to facilitate acquisition.

5.9 ATTITUDE DETERMINATION AND ANTENNA CONTROL (ADAC) SUBSYSTEM

5.9.1 INTRODUCTION

The ADAC subsystem[1] contains all the necessary sensors and electronic assemblies to perform the following primary functions:

- Provide a measure of spin-axis orientation during transfer, drift and synchronous orbits
- Provide steering reference pulses for pointing both the UHF and the S-band antennas
- Provide necessary timing signals for VISSR operation
- Provide necessary reference for VISSR synchronization of picture-line elements

- Provide necessary timing pulses for SEM control and data processing
- Provide closed-loop active nutation damping during transfer orbit
- Provide reference pulses to the ground for operation of the thrusters by command to accomplish active nutation damping, coarse and fine attitude control, and spin-rate control
- Provide necessary passive nutation damping during synchronous orbit operations.

The subsystem consists of the following functional components which are discussed in more detail in subsequent sections:

- An earth sensor assembly consisting of four infrared sensors, sensitive to radiant energy in the 13.5-to-16 micron region. Two of these sensors are for use only during transfer orbit.
- A sun sensor assembly consisting of two sensors, each having a field-of-view of 117 degrees in elevation. This provides an overlap region of ±30 degrees about the satellite spin plane. Each sensor output consists of a pulse whose duration is a measure of sun angle and whose leading edge is used for timing signal generation.
- A nutation sensor assembly consisting of two redundant accelerometers located to assure the necessary capability for nutation damping during transfer orbit.
- An electronics unit consisting of the complete processing electronics to operate on the sensor outputs and generate the signals to perform the functions outlined above. This electronics unit is completely redundant.
- A passive nutation damper assembly with the necessary caging to enable the damper during synchronous orbit.

The subsystem functional diagram is shown in Figure 5-45.

5.9.2 ADAC SUBSYSTEM FUNCTIONS AND REQUIREMENTS

5.9.2.1 Subsystem Requirements

To perform the necessary functions outlined in section 5.9.1 as per the overall spacecraft requirements, the following subsystem requirements have been established:

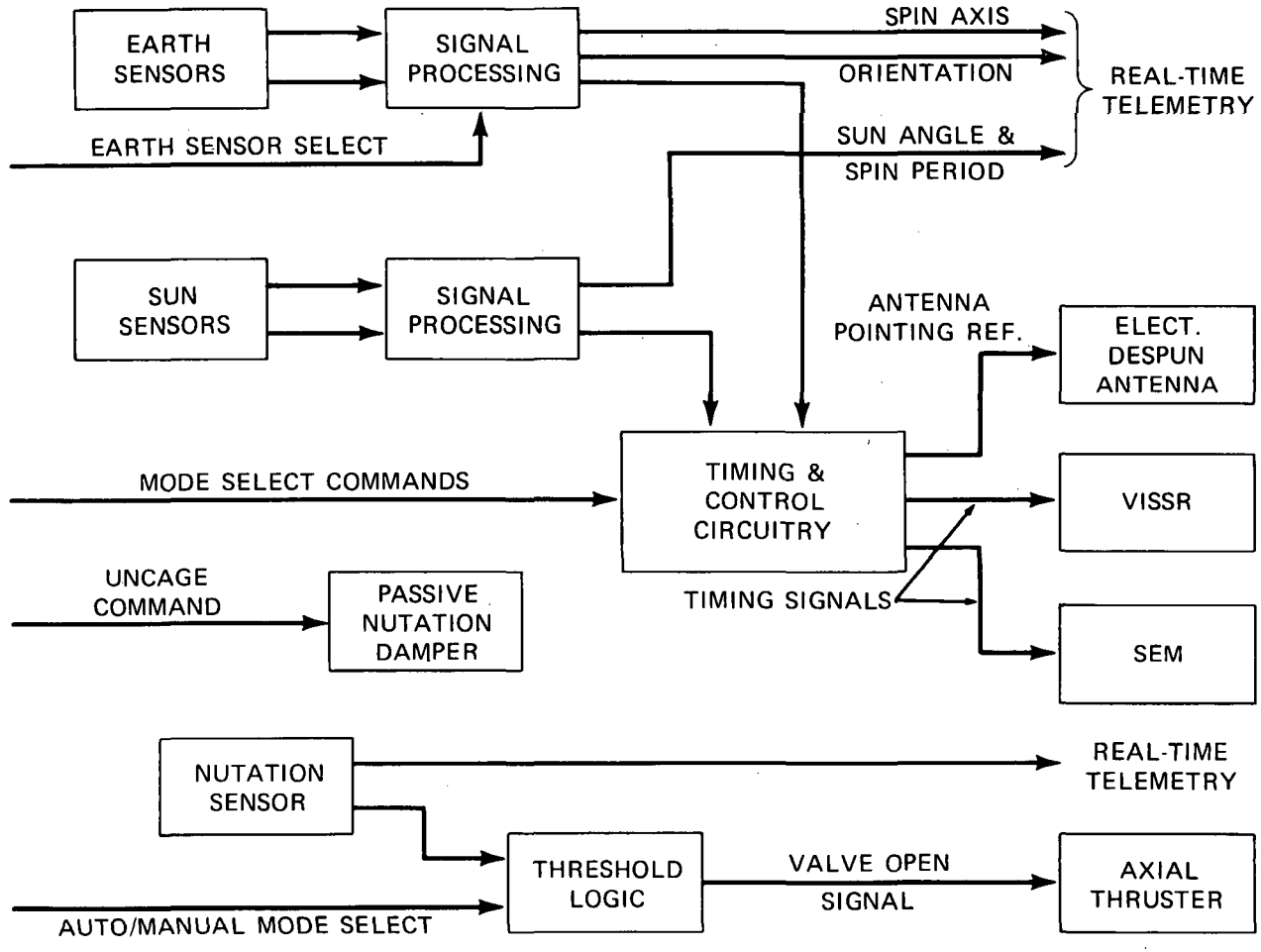

Figure 5-45. ADAC Simplified Functional Diagram

(a) During the transfer orbit, provide means for active control of nutation damping both by automatic closed-loop operation and by real-time ground commanded operation so that nutation can be maintained within a band of 0.1 to 0.4 degree.

(b) Provide coarse spin-axis precession control to perform necessary maneuvers and align spin-axis to orbit normal to within 0.5 degree.

(c) Provide fine spin-axis precession control capability with a resolution of 5 arc-seconds.

(d) Provide means for adjusting spin rate to any desired value in the range of 50 to 110 rpm/min with a precision of 1 rpm/min.

(e) Short-period variations in spin-axis orientation does not exceed 0.0025 mrad during one spacecraft spin cycle, nor 0.025 mrad during a complete picture frame.

(f) A passive nutation damping system has the capability to damp nutational motion following a coarse attitude maneuver to 0.5 arc-second within 7 minutes of time.

(g) The gyroscopic stability of the spacecraft is such that spin-axis precession due to external disturbance torques does not exceed 15 arc-seconds in a period of 24 hours.

(h) The attitude determination system has the capability to measure spin-axis orientation with an accuracy of ±0.5 degree in the transfer orbit, and ±0.1 degree in the synchronous orbit.

(i) Provide a sun pulse to the ground with sufficient stability to meet VISSR line sync requirements (0.025 mrad per frame).

(j) Spin axis orientation measurement accuracy as derived from the earth sensor to within ±0.2 degree -(3σ).

(k) Sun angle measurement accuracy for sun elevations with respect to the spin plane is accurate to within 0.5 degrees.

(l) Timing pulse accuracy for antenna steering is within ±0.25 degree of target location.

(m) Sun sync pulse is stable to within 1×10^{-6} seconds over a period of 20 minutes.

(n) Timing pulses are within ±0.45 degree using earth sensors (3σ).

(o) Timing pulses using sun sensor are within ±0.45 degree (3σ) with an update every 12 hours.

(p) Passive nutation system reduces on-orbit nutation to 0.5 second of arc with a time constant of 2 minutes maximum.

5.9.2.2 ADAC Functional Requirements

ADAC functional requirements are given in the following outline:

(a) Antenna pointing control

1. S-band antenna

2. UHF antenna

(b) Timing-pulse generation

1. VISSR subsystem

2. SEM subsystem

3. VISSR digital multiplexer

(c) Spin-axis orientation determination

(d) Spin-rate determination

(e) Sun-synchronizing pulse

(f) Nutation damping

1. Active

2. Passive

The ADAC subsystem generates timing signals for the VISSR subsystem and the VISSR digital multiplexer. The timing errors in the ADAC generated signals for two modes of operation are:

(a) Earth sensor mode. The earth sensor mode utilizes, as a reference, the centroid of the signal from earth sensor 1 or earth sensor 2.

(b) Sun sensor mode. The sun sensor mode utilizes, as a reference, the leading edge of the signal from sun sensor 1 or sun sensor 2. The electronics receives, by ground command, the delay angle required to delay the sun pulse so that it occurs coincident with the earth centroid.

5.9.3 OPERATIONAL DESCRIPTION

The operation of the ADAC subsystem may be best understood by referring to the simplified functional diagram in Figure 5-45. This diagram illustrates the functions of the subsystem, but does not show the redundancy features.

5.9.3.1 Transfer Orbit Operation

5.9.3.1.1 Spin-Axis Orientation. After injection into the transfer orbit, spin-axis orientation is measured by a pair of earth sensors. The two earth sensors are mounted with their lines-of-sight at angles of +4 and -4 degrees to the equatorial plane of the satellite. The output of the earth sensor is a measure of earth width; the differential readings of the two sensors are translated directly into an instantaneous roll-attitude angle. The sun-angle sensor provides a measure of spin-axis orientation with respect to the sun line as well as a reference pulse for thruster synchronization.

The sensor outputs are conditioned and sent to the ground by the VHF analog telemetry link. This data is smoothed and processed on the ground to give accurate measurements of spacecraft attitude before and after programmed maneuvers.

The attitude is controlled by means of redundant 5-lb axial thrusters which are operated by real-time ground command. Thruster synchronization is controlled by the telemetered sun-pulse data, and the proper thruster delay angle is computed on the ground. Attitude maneuvers are made during the transfer orbit to orient the ABM and, after ABM firing, to place the spin-axis normal to the orbit plane.

5.9.3.1.2 Active Nutation Control. Before the burn and separation of the ABM, the spacecraft has an unstable moment of inertia distribution which leads to a divergent nutational or coning motion. Nutation angle is detected by means of redundant accelerometers located at the outer circumference of the spacecraft and controlled by periodically firing the axial thruster. The telemetered accelerometer data is used as the thruster synchronizing reference.

An automatic nutation-control mode is also incorporated. In this mode, the nutational acceleration is sensed on board, and when the sensor output exceeds

a predetermined threshold, the axial thruster is pulsed in proper phase with the zero crossing of the sinusoidal sensor output. This process is repeated until the acceleration amplitude becomes smaller than a second preselected threshold level. Switching from manual to automatic mode is accomplished by ground command.

5.9.3.1.3 Telemetry Interface. The sensor signals (six sensors in all) utilize a common analog telemetry channel for real-time transmission. The sensor monitored at any given time is selected by command.

5.9.3.2 Synchronous Orbit Operation

Spin-Axis Orientation. After station acquisition has been achieved, the earth sensors are used to detect attitude to an accuracy of better than ±0.1 degree. The 5-lb axial thrusters are then used to make final coarse-attitude adjustment. For the remainder of the mission, 0.5-lb hydrazine thrusters are used for fine attitude corrections at the discretion of the user. These thrusters (with a short moment arm) provide an attitude control resolution of less than 5 arc-seconds, and are operated by real-time commands. The flight-qualified 0.5-lb hydrazine thrusters were selected after an examination of other low-thrust devices. The choice was based on reliability, weight, and complexity. The use of a single propulsion system for all control functions enables greater redundancy and flexibility at minimum cost.

5.9.3.2.1 Timing and Control Functions. The sun pulse (generated once-per-spin cycle) is used as the basic pointing reference for on-board steering of the electronically despun antenna. A 24-hour clock is used for on-board computation of the delay angle between the occurrence of the sun pulse and the earth center. The delay angle is updated by command. In a backup mode of operation (particularly for eclipse operation), either of the two earth sensors are used as the reference for onboard antenna steering. In this case, the delay angle clock is not required. Finally, the antenna is steered by means of a real-time command link. In this case, telemetered sun-pulse or earth-sensor data is used on the ground to generate command steering pulses with the proper phase delay.

The same onboard control circuitry is used to generate timing signals for operation of the VISSR. These signals have fixed-phase relationships with respect to the earth center.

The sun pulse is also used as the VISSR line-sync reference after being received on the ground. By counting the time between a large number of successive pulses, it is possible to obtain a precise measure of spin period. From this operation, a very stable reference pulse is obtained which is delayed as a function of time by the proper earth-sun angle.

5.9.3.2.2 Passive Nutation Damping. A passive nutation damper with a deadband of less than 0.5 arc-second is used to damp nutational motions resulting from operation of the attitude-control thrusters. The damper is caged during launch and transfer orbit, and is uncaged on command.

5.9.3.2.3 Spin Rate Control. Control of spin rate is achieved by applying opposite angular offset to the two radial thrusters to obtain spin-up and spin-down moments. The same is done to the 0.5-lb fine attitude-control thrusters for redundancy.

5.9.3.2.4 Stationkeeping. East-West stationkeeping is accomplished by a redundant pair of 5-lb radial thrusters operating in pulsed mode by real-time command.

5.9.4 PHYSICAL DESCRIPTION

Table 5-28 lists the components that comprise the attitude control subsystem, including the number of units, total weight and power consumed. With the exception of the passive nutation damper there is a completely redundant set of components.

Table 5-28

Attitude Control Subsystem Components

Components	No. of Units	Total Weight (lbs)	Power (Sync. Orbit) (Watts)	Added Power (Transfer Orbit) (Watts)
Earth sensors	2	2.7	0	1.2
Sun sensors	2	0.5	0	0
Accelerometers	2	0.8	0	0.3
Nutation damper	1	2.5	0	0
Electronics unit (redundant)	1	10.0	7.1	0.5
Valve drivers	2	0.5	0	0
	Total	17.0	7.1	2.0

5.10 SMS THERMAL CONTROL SUBSYSTEM

5.10.1 INTRODUCTION

This section describes the design and predicted performance of the SMS thermal control subsystem[1] and development of the VISSR/SMS thermal interface.

5.10.1.1 Spacecraft Thermal Design

The components of the thermal control subsystem for both the synchronous orbit and transfer orbit spacecraft configuration are depicted. Temperature performance of the spacecraft is presented based on a 43-node analytical model. Discussion of thermal control of specific spacecraft components, such as the APS fuel tanks and lines, the S-band and UHF power components, the quad transistor regulators for the PCU, the magnetometer, and the ABM and separation equipment in the transfer orbit are described.

5.10.1.2 VISSR/SMS Interface Thermal Analysis

A summary of the development of the VISSR/SMS thermal interface analysis is described. Included is the revision of VISSR thermal design requirements and the transition of the thermal interface from an ideally isolated VISSR and spacecraft to a partially coupled VISSR and spacecraft.

The development test plan for the thermal control subsystem is also included in this section of the design review data package. The primary purpose of thermal balance tests during the development phase is to verify the thermal design by obtaining a good correlation between test and predicted temperatures from the analytical model for the test environment.

As described in the summary to this section, the design of the SMS thermal control subsystem has drawn on past experience by Philco-Ford, especially the thermal design of the SKYNET spacecraft. In fact, the components of the thermal control subsystem for the APS and ABM are similar to those designed and developed for SKYNET.

5.10.2 SUMMARY

The thermal control subsystem for SMS meets the established design requirements and design criteria; namely, maintaining internal components within a temperature range of 20 ±15°C with a passive thermal control subsystem.

The basic design requirement placed on the thermal control subsystem for SMS is to provide a temperature environment throughout mission life compatible with the operational limits of all spacecraft components and the VISSR. The specific thermal design requirements establishing the design criteria of the thermal control subsystems are summarized as follows:

(a) Maintain the temperature of internal components to 20 ±15° C.

(b) Provide a minimum design temperature margin of 15° C between temperature predictions and qualification design temperature limits of components.

(c) Provide a thermal interface compatible with the VISSR thermal design requirements.

(d) Provide a passive thermal control subsystem (no movable louvers).

Thermal control of SMS is achieved during all phases of the spacecraft mission with a passive thermal design. Spacecraft heat transfer paths are predominantly radiative and are controlled by use of thermal control coatings, thermal shields, and thermal insulation. Gross thermal control of internal spacecraft temperatures is achieved by selective use of thermal control coatings on components and exposed surfaces of the equipment panel and thermal shields located at both ends of the spacecraft. Locally, on the equipment panel, temperature control of specific high-power density components is achieved by providing surface radiators located to increase the conductive heat transfer from the component baseplate to the equipment panel.

Thermal control of the ABM prior to firing consists of the application of thermal control coatings with a selective ratio of solar absorptance to infrared emittance, insulation around the ABM, and a blow-off insulation cap over the ABM nozzle exit plane. This latter component, the blow-off insulation cap, was designed for SKYNET and has undergone extensive development and qualification testing consisting of actual ABM firings in a thermal/vacuum test chamber at simulated space environmental conditions. Temperature control of the ABM and spacecraft is maintained during the transfer orbit by limiting the sun angle (θ) between the limits of +30 to -30 degrees, with a maximum 1.0-hour eclipse. The sun angle is controlled by selective launch windows.

The spacecraft thermal control subsystem provides a compatible thermal interface with the VISSR and the SEM. The thermal control of the VISSR is achieved by thermal coupling with space through the scanner aperture and sunshade, and conductive isolation of the scanner from the spacecraft. The SMS

design also permits energy to be radiated from the radiation cooler end of the scanner directly to space and provides an unobstructed view to space for the radiation cooler. An internal radiation patch on the scanner in the vicinity of the two encoder housings has replaced the proposed forward radiation patch.

The design temperature limits are 5 to 35° C (20 ±15° C) for all internal components of the spacecraft except for the x-ray telescope assembly, the quad-transistor sets, and the S-band and UHF power amplifiers. The x-ray telescope has design temperature limits of -5 to 40° C, the quad-transistor sets have design temperature limits of -40 to 80° C, and the power amplifiers have design temperature limits of -40 to 25° C. The quad-transistor set and power amplifier design temperatures have been modified to both reduce the radiator weights for these components and to reduce power consumption. Each component has been reviewed from a performance and reliability standpoint and have proved to be compatible to the modified design temperature limits. Waivers for changing the design temperature limits from 20 ±15° C for the three components are requested of NASA/GSFC.

For all components, with the exception of the APS hydrazine valves and propellant line, a design margin of 15° C has been achieved between predicted temperature limits and component qualification design temperature limits. The APS hydrazine subsystem has a lower operational temperature limit of 2° C which is determined by the freezing point of hydrazine. During the steady-state synchronous orbit, the minimum temperature of the hydrazine system is approximately 17° C, and the requirement for a 15° C margin is fulfilled. But after a 1.2-hour eclipse following steady-state operation at equinox, the minimum predicted temperature of a propellant line is 4° C and the 15° C margin does not exist; therefore, waivers in maintaining the 15° C design margin during this period of the mission are required.

Presently, heaters are proposed to maintain the axial solenoid valve above the freezing point during summer solstice and prior to equinox eclipse. It is preferred to have the heaters commanded on and off rather than thermostatically controlled to conserve power required of the battery during eclipse.

The primary requirement for a successful SMS mission is to provide a compatible thermal environment for the VISSR. The conceptual design of the thermal interface between the scanner and the spacecraft has developed from a fully isolated VISSR and spacecraft to a design with partial radiation coupling between the VISSR and spacecraft.

5.10.3 SPACECRAFT THERMAL DESIGN

For purposes of the thermal design description, SMS is assumed to consist of a cylindrical solar panel, a cylindrical antenna array panel, a centrally located equipment panel, the VISSR and, in the transfer orbit, an ABM. The thermal design of the proposed spacecraft is based on the constraint that the sun angle θ (defined in Figure 5-46) remains between +25 degrees (winter solstice -25 degrees (summer solstice) in the synchronous orbit with a maximum 1.2-hour eclipse occurring at $\theta = 0°$ (equinox). In the transfer orbit, the sun angle is constrained between -30 and +30 degrees with a maximum 1.0-hour eclipse occurring.

Thermally, SMS consists of two basic configurations: the synchronous orbit configuration and the transfer orbit configuration. Each of these configurations is described as follows:

5.10.3.1 Synchronous Orbit Configuration

The basic thermal configuration of the SMS in the synchronous orbit is shown in Figure 5-46. In the synchronous orbit, the configuration consists of the centrally located equipment mounting panel, cylindrical solar panel, cylindrical S-band array panel, VISSR Scanner, and thermal shields covering the ends of the spacecraft. For purposes of clarity, many subsystem components are not shown in Figure 5-46, but are presented in the discussion of the thermal analysis of the spacecraft.

The overall temperature of the spacecraft is maintained at approximately 20°C by the absorption of solar energy and the emission of thermal energy, primarily by the solar panels, antenna array, thermal shields, and VISSR scanner aperture. The overall solar absorptance to infrared emittance ratio (α_s / ϵ) is such that the spacecraft experiences a minimum temperature excursion for all spacecraft-sun angles. Most of the internal power is dissipated either on the equipment panel, VISSR scanner, or in power amplifiers located adjacent to the antenna array on a separate equipment platform. Energy dissipated by components on the equipment panel is conducted to and along the equipment panel. From the equipment panel, the energy is radiated to the solar panels and/or the end thermal shields and, thence, to space. At equinox, energy from the equipment panel is radiated to both the forward and aft ends of the spacecraft.

The location of the subsystem components on the equipment panel is dictated by three considerations:

(a) Proximity of functional and subsystem components to each other

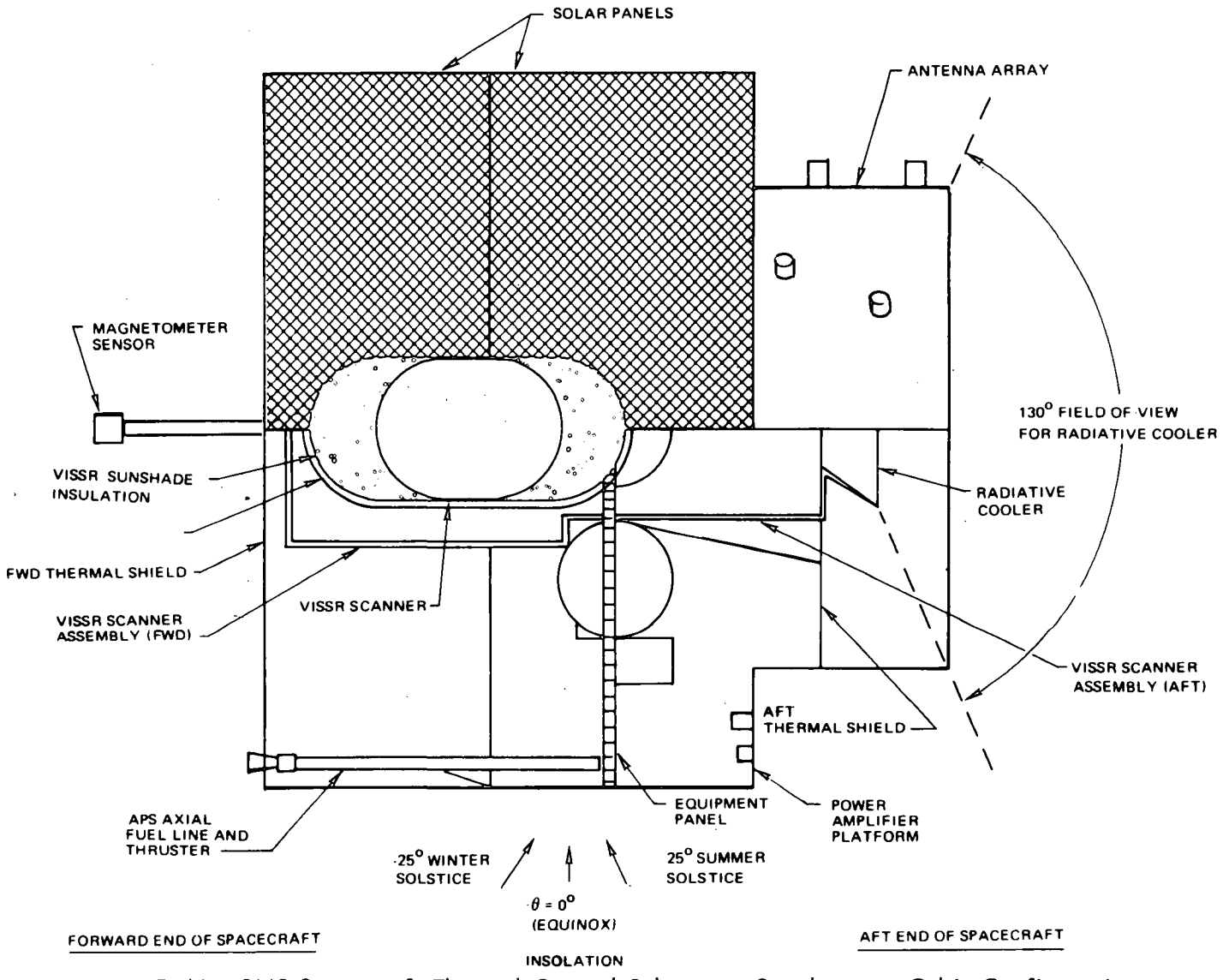

Figure 5-46. SMS Spacecraft Thermal Control Subsystem-Synchronous Orbit Configuration with VISSR Subsystem

(b) Mass properties distribution

(c) Approximate equal distribution of component power dissipation on the panel

The first consideration dictates that, for instance, the communications subsystem components be located in close proximity to each other. The second consideration dictates that the components be located in order to achieve spacecraft balance. Finally, the approximate equal distribution of power dissipation has been achieved as a goal by (1) preventing the location of two or more high power dissipating components (or subsystems) together, (2) location of components with narrow or critical temperature limits (such as the batteries) away from high dissipating components, and (3) clearing of areas around high-power dissipating components to allow efficient thermal radiation from these areas.

The thermal control of components and specific areas of the equipment panel is further achieved as follows:

(a) Increase the face-sheet thickness of the honeycomb equipment panel with doublers in local areas to facilitate thermal conductance from high-power dissipating components along the panel. With the low profile component design achievable with the 75-inch diameter spacecraft, increase of the face-sheet thickness is not required for any equipment panel mounted components. Additionally, heat transfer through the equipment panel is increased in local areas by use of high-conductance plugs, which facilitate heat transfer in the panel's axial direction.

(b) Control the thermal emittance of the components and equipment panel surface. Thermal analyses have shown that to maintain the steady-state temperature of the equipment panel at approximately 25 to 35° C, the average emittance of both sides of the panel are approximately 0.3. It is desired to operate at near 35° C to minimize the thermal subsystem weight. The temperature level of a component or group of components is adjusted by a comparable adjustment of the thermal emittance in the area of the component(s). Components with high-power dissipations and the areas around the components are coated with high-emittance coating, such as black paint. Components with small or no power dissipations and the areas around these components are coated with a low-emittance surface, such as gold plate or aluminum.

(c) Control the thermal conductance between components and the equipment panel. Low-conductance spacers are used under components which dissipate little or no power so that proper thermal balance is achieved,

especially during eclipses. A thermal compound, such as silver-filled silicone, is used to increase the thermal contact conductance between high-power dissipation components and the equipment panel.

(d) Adjust the component temperature limits by waivers to NASA/GSFC. Thermal control of the components and system weight reduction are facilitated, where necessary, by increasing the operating temperature limits of high-power dissipation components above 35° C, such as the S-band and UHF power amplifiers and quad-transistor sets.

(e) APS thermal control is provided by low-emittance coatings on the fuel tanks and fuel lines and solenoid valve heaters. Conformal insulation assemblies are provided for the solenoid valves and the thruster assemblies. The two axial-thruster fuel lines are enclosed in separate radiation shields that are coupled to the solar array. The α_s/ϵ ratio of approximately unity for the solar cells provides a radiation environment temperature of approximately 17° C, prior to equinox eclipse; therefore, for a 1.2-hour eclipse the thermal capacity of the lines and the fuel are sufficient to maintain the lines above the freezing point of the fuel.

5.10.3.2 Transfer Orbit Configuration

The basic thermal configuration of the spacecraft in the transfer orbit is shown in Figure 5-47, and is nearly identical with the synchronous orbit configuration. The major difference between the configurations is the attachment of the separable structure and ABM to the secondary structure. The ABM blocks the aperture of the radiative cooler opening, and the power normally dissipated in the VISSR and communications subsystem (nonoperating in the transfer orbit) is dissipated in the PCU dummy loads. Dummy loads are located on the power amplifier to compensate for the power not dissipated in the amplifiers during the transfer orbit. These dummy loads are controlled by command.

The temperatures of the equipment panels, solar panels, antenna array, and VISSR scanner are maintained in the same manner as they are in the synchronous orbit. The principal requirement during transfer orbit is that the sun angle be restricted to between +30 and -30 degrees with a maximum 1-hour eclipse period (Figure 5-47) for temperature control of the ABM.

The thermal control of the ABM is maintained by thermally isolating the ABM casing, nozzle, and nozzle opening from space, and radiatively and conductively coupling the ABM casing to the separable structure. With the sun angle between +30 and -30 degrees, the outboard surface of the separable structure

NOTE:
COMPONENTS OF SUBSYSTEM AND SURFACE COATINGS COMMON TO BOTH TRANSFER AND SYNCHRONOUS ORBIT CONFIGURATIONS ARE SHOWN IN FIGURE 17-1.

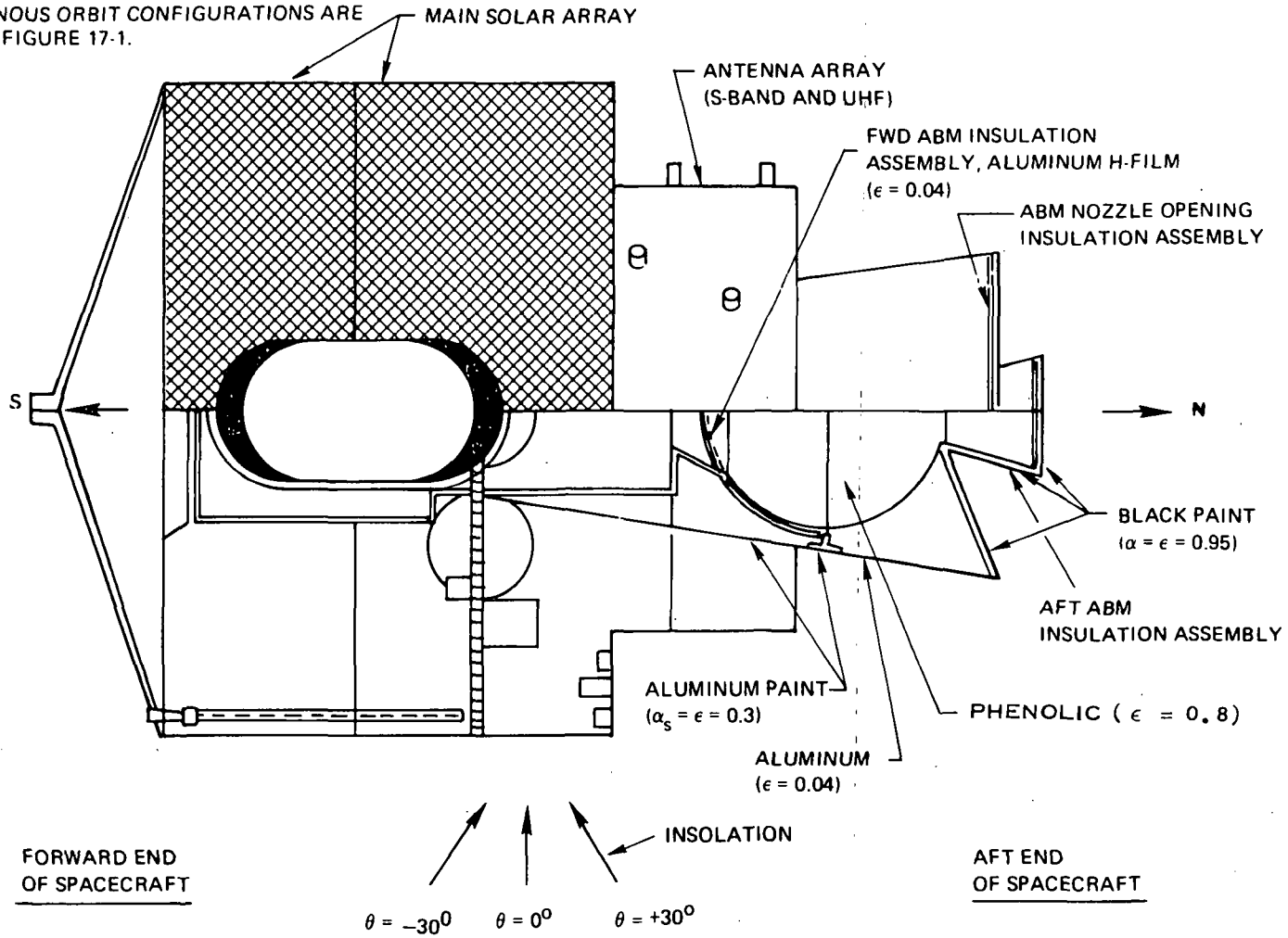

Figure 5-47. SMS Spacecraft Thermal Control Subsystem and Surfaces Coatings for Transfer Orbit Configuration

is always in the sun (except during eclipse periods). The temperature of the structure is controlled by painting the outboard surface with aluminum paint.

5.10.3.3 Spacecraft Thermal Analysis

The conceptual design of the thermal control subsystem utilizes low-emittance coatings on selected interior spacecraft surfaces. These surfaces include portions of the equipment panel, the APS components, the exterior surface of the VISSR and the primary support structure. At the request of GSFC a study was initiated comparing the non-black interior spacecraft to an all black interior spacecraft. This study included the preliminary model of the VISSR supplied by SBRC.

The study of the non-black versus the black interior is summarized in Reference 3. The primary results of the study were that the equipment panel temperature range for the non-black interior spacecraft is controlled between the limits of 17 to 34° C and between the limits of -9 to 25° C for the black interior. The weight of the thermal control subsystem for the black interior spacecraft is 4 pounds heavier than the thermal control subsystem for the non-black interior spacecraft.

Copies of the analyses and design study for the 75-inch diameter were made available at the design review. Preliminary thermal analysis and conceptual design of the thermal control subsystem, based on a 56-inch diameter spacecraft, are reported in reference 4. The thermal design concepts developed during the proposal and initial contract period for the 56-inch diameter spacecraft have been applied to the study of a 75-inch diameter spacecraft. The conceptual thermal design for the large diameter spacecraft has a low emittance surface coating on selected areas of the equipment panel (non-black interiors) with non-adiabatic end shields.

5.10.3.3.1 Power Amplifier Thermal Control. Both the S-band and UHF power amplifiers have power dissipation levels which necessitate the use of a heat rejecting radiator (fin) in order to control temperature; a range of -40 to 40° C was assumed for the study. Since the efficiency of power input to RF output is inversely proportional to operating temperature, a power tradeoff as well as a weight tradeoff study was performed (Reference 5).

The objective of the study was to compare radiator weight and total power difference required for various locations of the radiators on the spacecraft. Six locations were considered: the aft surface of the equipment panel, solar array, forward and aft antenna array, aft thermal shield, and solar array and interface ring of the antenna array. These locations are shown in Figure 5-48.

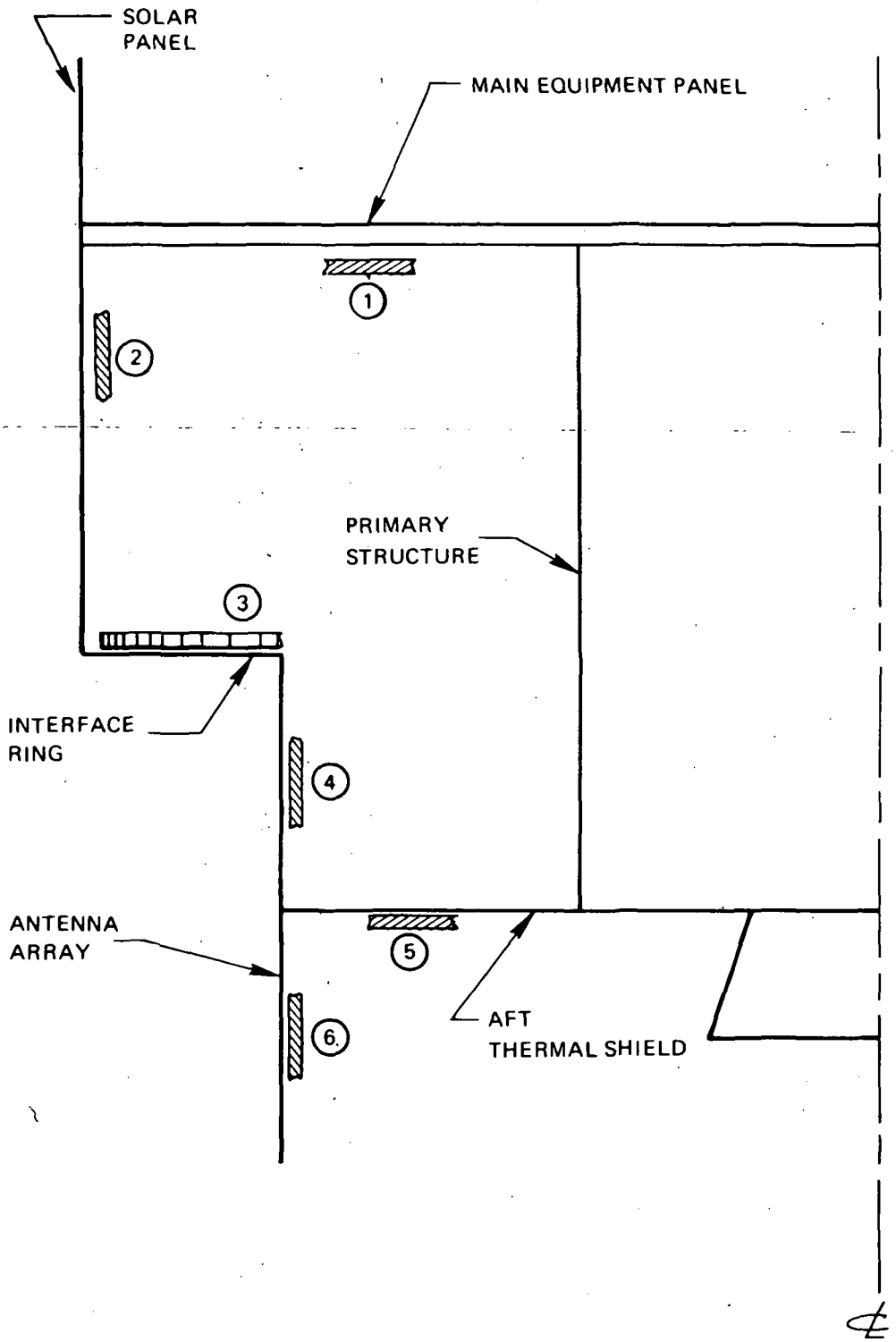

Figure 5-48. Power Amplifier Radiator Location Possibilities

Locations 3, 4, 5 and 6 (Figure 5-48) were disregarded for the 56-inch diameter spacecraft because of adverse effects on moment of inertia ratio by adding weight in these areas. With the increase in the major diameter of the spacecraft, locations 3, 4, 5 and 6 are once again considered because the moment of inertia ratio is no longer between the spin-axis and transverse-axis critical (≤ 1.05).

From a thermal and RF viewpoint, location 3 represents a near-optimum placement. Both the UHF and S-band power amplifiers are located on a single radiator which views space on one side. For a maximum power dissipation of 42 watts, the maximum predicted temperature is 25° C during summer solstice. A minimum temperature of -40° C is predicted at end of a maximum eclipse of 1.2 hours. The size of the radiator is approximately 3.3 ft^2 and occupies approximately a 70-degree segment of the annular area between the antenna array and the solar array. The radiator weight is approximately 2.5 lbs and the surface facing space is coated with a composite thermal-control coating consisting of aluminum and teflon. The assumed emittance and maximum solar absorptance are 0.8 and 0.2 respectively.

5.10.3.3.2 APS Thermal Control. Thermal control of the APS components is primarily concerned with the low temperatures experienced during eclipse, during which period the hydrazine is likely to freeze. The temperature response during eclipse of the axial and circumferential hydrazine lines are shown in Figure 5-49 for both full and empty lines. Both lines are maintained above the freezing point of hydrazine, 2° C, when the lines are full. When the lines are empty, the circumferential line freezes at the end of the eclipse and thaws within 30 minutes after the end of eclipse. The axial line freezes within 24 minutes of start of eclipse and requires approximately 2 hours after eclipse to thaw when the line is empty. Electrical heaters on the two types of propellant lines requires an energy dissipation of approximately 400 mw-hours in order to prevent freezing of the empty propellant lines during a maximum eclipse of 1.2 hours. A decision to incorporate either thermostatic heaters or commandable heaters on the lines is based on system reliability and energy availability during eclipse operation.

The minimum temperature of the hydrazine tanks after eclipse is shown in Figure 5-50 as a function of percentage of hydrazine remaining in the tank. Based on a surface coating emittance of 0.05 the temperature of the tank is above 2° C for 1 percent or more of the fuel remaining in the tank. A surface emittance of 0.05 or less is obtained for a gold surface finish. Considering a degraded surface finish with an emittance of 0.1, the temperature of the tank is above 2° C for 4 percent or more of the fuel remaining in the tank.

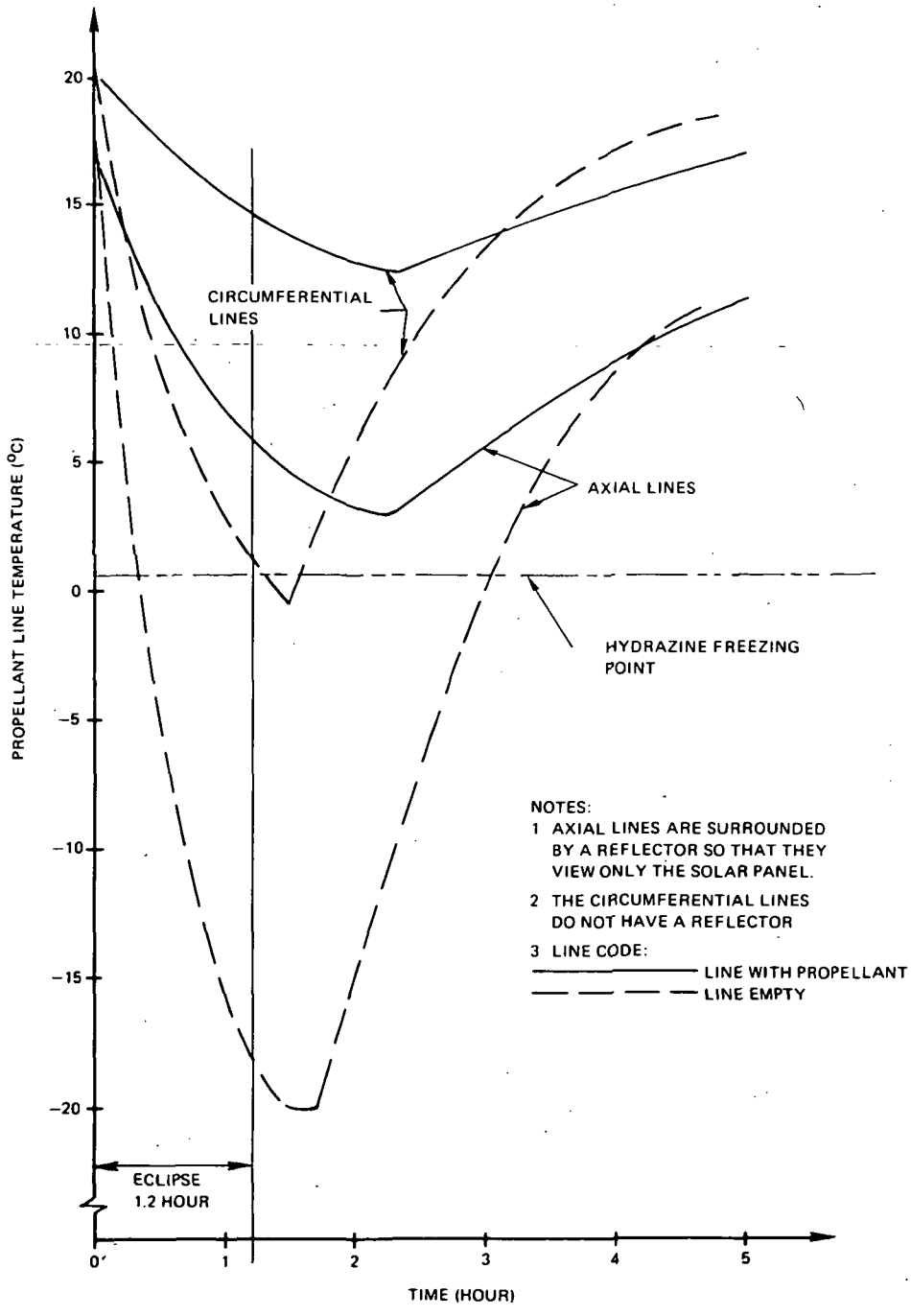

Figure 5-49. APS Propellant Line Temperature Response for a Synchronous Eclipse

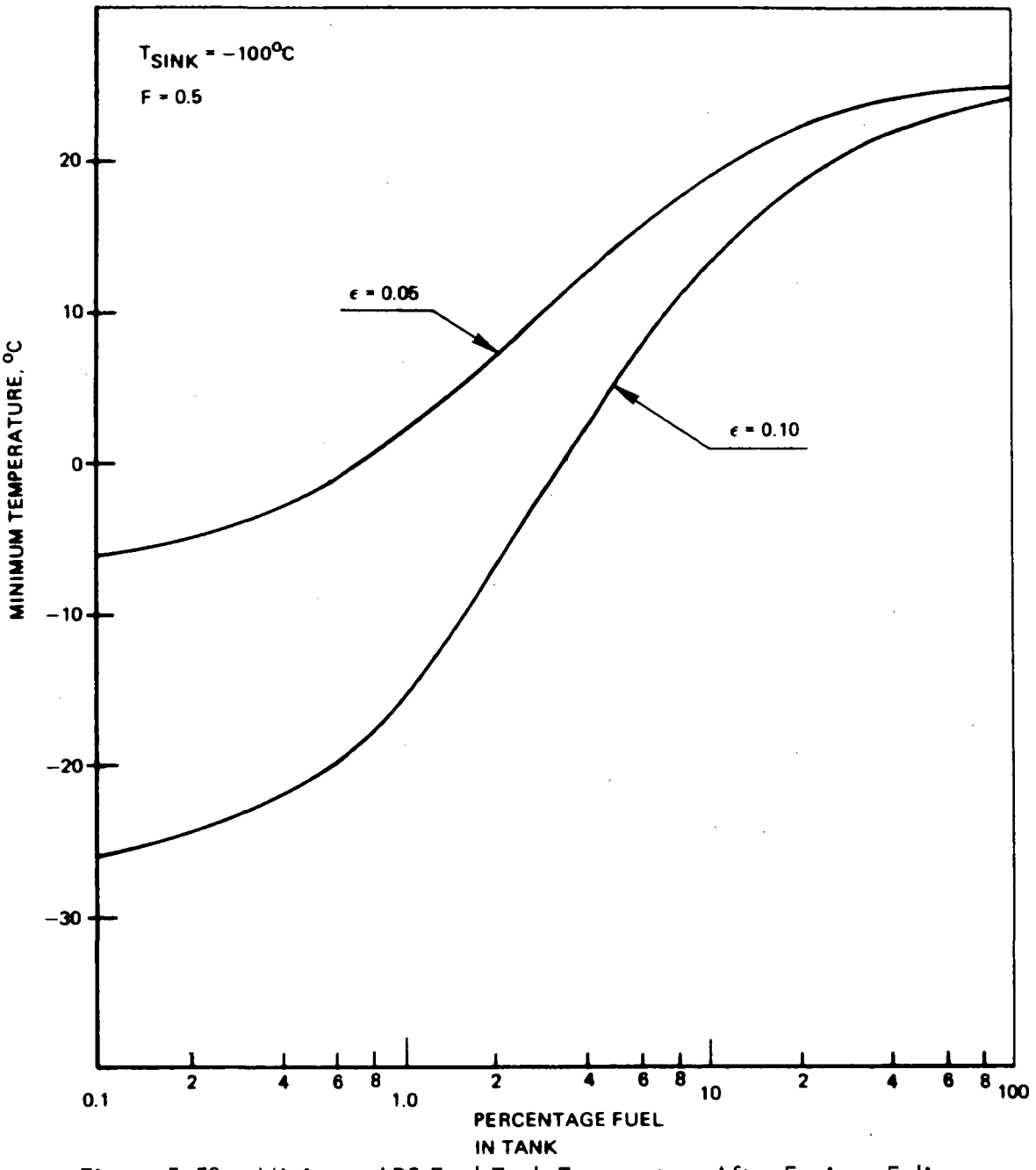

Figure 5-50. Minimum APS Fuel Tank Temperature After Equinox Eclipse as Function of Percentage Fuel by Weight

Heaters on the tanks prevent freezing when the tanks are near empty, and require approximately an energy dissipation of 2.5 watt-hours during a maximum eclipse of 1.2 hours. This figure is excessively high in comparison to the energy available from the battery during a maximum eclipse. In lieu of using a heater on each of the three tanks, the effective emittance is decreased by an order of magnitude by covering the surface area of the tank with multi-layer insulation. An insulation consisting of 10 layers of crinkled aluminized mylar (NRC 2) weighs approximately 0.2 lb for the three tanks.

The primary thermal design requirement of concern for the thrust chamber assemblies (TCA's) of the APS controls the temperature of the catalyst bed above -14° C prior to firing and the solenoid valve above 2° C prior to firing. Thermal control of the radial 5-lb and 0.5-lb thrusters is accomplished by the radiative and conductive coupling between the TCA's and the equipment platform. Incorporating the preliminary thermal math models of the TCA's supplied by the prospective vendor with the thermal analysis of the spacecraft, the temperatures of the TCA radial catalyst bed and valves were predicted. The minimum temperatures for the radial 5-lb thruster catalyst bed and solenoid valve are 19 and 15° C, respectively. The minimum predicted temperatures for the 0.5-lb radial thruster catalyst bed and solenoid valve are 20 and 5° C, respectively.

The thermal control of the 5-lb axial thruster is achieved by radiatively and conductively coupling to the solar array and spacecraft internal environment. During summer solstice and equinox eclipse the environmental spacecraft temperature at the forward end of the spacecraft is a minimum and a 0.15-watt heater is required to maintain the solenoid valve above the minimum design temperature of 2° C. Based on preliminary analyses minimum temperature of the axial catalyst bed and solenoid valve are -19 and -11° C, respectively, without heater power. With heater power of 0.15 watts, the temperatures of the catalyst bed and solenoid valve are -10 and 4° C at summer solstice and -9 and +2° C at end of equinox eclipse, respectively.

5.10.3.3.3 SEM Thermal Control. With the exception of the magnetometer sensor assembly, the components that make up the SEM are located on the spacecraft equipment panel and their predicted temperatures are within the range of 14 to 35° C. The magnetometer sensor assembly is located on a tripod forward of the VISSR and outside of the solar array enclosure. Thermal control of the magnetometer sensor assembly is achieved by utilizing the sensor assembly power dissipation (300 mw), insulation enclosing the assembly, and a low α_s / ϵ ratio surface coating on the exterior of the insulation. When operating in full solar illumination or in the shadow of the spacecraft and during eclipse, the temperature range of the sensor assembly is 0 to 40° C.

5.10.3.3.4 VISSR/SMS Interface Thermal Analysis. A primary requirement of the thermal control subsystem for SMS provides a compatible thermal environment for the VISSR. The outcome of this effort to date has been a better definition of the thermal design requirements for the VISSR/SMS interface and the development of a conceptual design of the thermal interfaces. The summary of definition and understanding of the thermal design requirements for the VISSR/SMS interface is presented in Table 5-29. The primary difference from those proposed and the present are the temperature limits of the VISSR (they were 25 ±10° C and are now 25 ±20° C) and the temperature gradients are now interpreted as maximum blur circle.

Table 5-29

Comparison of Proposal and Present Thermal Requirements for SMS VISSR

Requirement	Purpose	Proposal Requirement	Present Requirement
VISSR temperature limits	–	+15 to +35°C	+5 to +45°C
Temperature difference ΔT_1 = primary mirror temp minus secondary mirror temp	Meet blur circle requirements	±4C°	Nominally ±4C° from initial value following launch (see initial value requirement and blur circle requirements below).
Temperature difference ΔT_2 = primary mirror temp minus aft beryllium table temp	Meet blur circle requirements	±2C°	Nominally ±2C° from initial value following launch (see initial value requirement and blur circle requirements below).
Initial value of ΔT_1 following launch	Meet blur circle requirements	±4C°	Maximum visible channel blur circle = θ_{MB} = $\lvert -3.35\ \Delta T_2 - 0.69\ \Delta T_1 \rvert$ $\leq 70\ \mu$rad
Initial value of ΔT_2 following launch	Meet blur circle requirements	±2C°	Maximum thermal channel blur circle = θ_{MB} = $\lvert 0.107\ \Delta T_2 - 0.022\ \Delta T_1 - 0.098\ \Delta T_3 \rvert$ $\leq 50\ \mu$rad where ΔT_3 is the maximum temperature difference between the primary mirror and preamplifier mounting plate.
Temperature input to visible channel blur circle	Picture quality	None	Maximum visible channel blur circle = θ_{MB} = $\lvert -4.08\ \Delta T_2 - 0.84\ \Delta T_1 \rvert$ $\leq 11.6\ \mu$rad for steady-state conditions and 3.6 hours after the start of an equinox eclipse.
Temperature input to thermal channel blur circle	Picture quality	None	Maximum thermal channel blur circle = θ_{MB} = $\lvert 4.08\ \Delta T_2 - 0.84\ \Delta T_1 - 3.72\ \Delta T_3 \rvert$ $\leq 136\ \mu$rad

The conceptual design of the thermal interface and the thermal analysis is documented in references 6 and 7. The thermal design of the VISSR/SMS interface has developed from a fully isolated scanner and spacecraft to a design with partial radiation coupling as depicted in Figure 5-51.

Based on mutual agreement between Philco-Ford, SBRC and GSFC, the thermal interface is defined as follows:

- Minimum conductance between VISSR and spacecraft equipment panel
- Internal forward thermal radiation patches on encoder covers
- External aft thermal radiation patch on radiation cooler mounting plate
- Low emittance or multilayer insulation (1 or more layers as required to duplicate low emittance) on VISSR exterior surfaces.

The analyses described in reference 7 were performed using the SMS proposal configuration (truncated solar array) and an updated VISSR model. Further analysis incorporates the VISSR model into the recently developed spacecraft model with full cylindrical solar arrays. The analyses were performed (1) to compare the original and updated VISSR thermal models, (2) to determine the effect of VISSR insulation or low-emittance surfaces of VISSR performance, (3) to determine forward thermal radiation patch area requirement, and (4) to determine aft thermal radiation patch area requirements.

The temperature limits for the VISSR in general, and the VISSR mirrors in particular, are +5 to +45° C. The temperature difference between the primary mirror and secondary mirror (ΔT_1) nominally are equal to or less than ±4° C; the temperature difference between the primary mirror and aft beryllium tube (ΔT_2) nominally are equal to or less than ±2° C. The temperature differences ΔT_1 and ΔT_2 are directly related to VISSR performance by use of visible channel and infrared channel blur circles. The visible channel blur requirement is given by

$$\theta_{MB} = \left|4.08\ \Delta T_2 - 0.84\ \Delta T_1\right| \leq 11.6 \mu\text{rad};$$

this requirement applies for all steady state thermal conditions and 3.6 hours after the start of an equinox eclipse. The thermal channel blur circle requirement is given by

$$\theta_{MB} = \left|-3.35\ \Delta T_2 - 0.69\ \Delta T_1\right| \leq 70 \mu\text{rad}$$

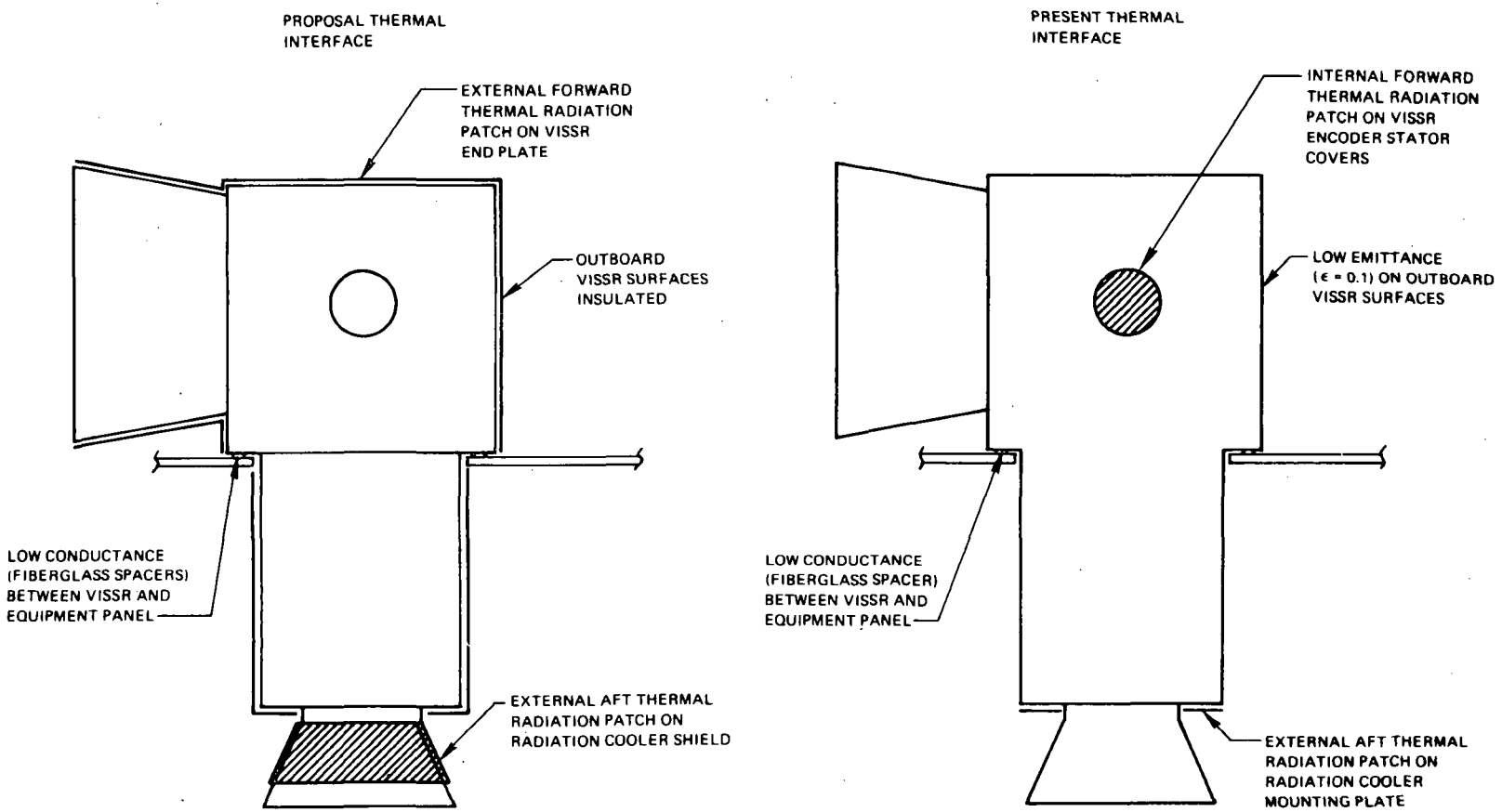

Figure 5-51. Comparison of Proposed and Present SMS Spacecraft-VISSR Thermal Interfaces

and

$$\theta_{MB} = \left|0.107\ \Delta T_2 - 0.022\ \Delta T_1 - 0.098\ \Delta T_3\right| \leq 50\mu\text{rad}$$

The analyses performed to data indicate that the absolute temperature requirements for the VISSR are met for all steady-state conditions; additionally, all VISSR locations meet the absolute temperature requirements during eclipse, with the exception of the secondary mirror, whose minimum temperature limit is exceeded. Using the updated VISSR thermal model, the visible channel blur circle requirement is met for all steady-state conditions but not until 4.3 to 5.0 hours after the start of an eclipse. The thermal channel blur circle requirements are all met, together with the maximum visible and infrared channel requirements immediately following launch. The analyses also indicate the feasibility of incorporating internal forward thermal radiation patches for thermal control of the encoders and an external aft thermal radiation patch, primarily for thermal control of the IR preamplifiers and photomultipliers.

5.10.3.3.5 ABM and Separation Equipment (transfer orbit). ABM temperature control is passively maintained during the transfer orbit within the temperature range of 3 to 24°C. Passive thermal control is accomplished by maintaining the sun angle (θ) within the limits of 0 ±30 degrees and limiting the maximum eclipse to 1.0 hour. Both of these orbit parameters requirements are provided by selection of an appropriate launch window.

The ABM and secondary structure is separated from the spacecraft after ABM firing. Separation is accomplished by squib-actuated bolt cutters located at separation plane 2. The squibs are initiated electrically on command from components located on the equipment panel.

During the transfer orbit the separation equipment survives a 1.0-hour eclipse and experiences predicted temperatures within the range of -70 to 30°C. At apogee, altitude the separation equipment operates within the range of predicted temperatures of -20 to +30°C. The temperature of components located on the equipment panel is controlled within the predicted temperature range of 6 to 30°C throughout the transfer orbit.

5.10.4 THERMAL DEVELOPMENT TESTS

The primary objective of the thermal development test is to verify the thermal analytical model of the spacecraft. Secondly, the development test validates the adequacy of the testing technique for use in the qualification and acceptance testing of the spacecraft.

A full size model of the spacecraft is used for development testing. The engineering model or the thermal/structural model of the VISSR is incorporated into the test spacecraft. The structure in the flight qualification spacecraft is outfitted with thermal mockups of all the spacecraft components. Every aspect of the thermal control subsystem (for example, coatings, insulation, and shields) is included on the test model. The component mockups including the hydrazine tanks and lines duplicate the mass, size, location, surface finish, and mounting configuration of the flight articles. Resistance heaters are used in the mockup of all power dissipating equipment. No operational checks are made on the VISSR performance during these development tests. The thermal response of the VISSR/spacecraft interfaces is studied as the test environment is varied.

The thermal development tests are performed in the Philco-Ford 39-ft space simulation chamber. The chamber features ultra-clean vacuum pumping facilities to maintain the pressure during test below 10^{-5} torr, as well as liquid nitrogen cooled shrouds to simulate the heat sink of space. Simulation of the solar heating on the spacecraft is accomplished with an infrared lamp array and conformal heater blankets. The infrared lamp array is used to simulate the absorbed solar fluxes on the model solar panels and aft antenna array. Conformal blanket heaters duplicate the absorbed solar energy on those spacecraft end surfaces illuminated at solstice conditions.

Closed-loop, automatic controllers are used to regulate the lamps and conformal heaters. Absorbed flux calorimeters are used at each control zone of the lamp array and provide the feedback signal to the automatic controllers. Current sensors monitor the power to the conformal heaters and assure that a constant power level is maintained equivalent to the absorbed solar flux at the heater location. Prior to test, the lamp array is flux-mapped and calibrated in the test chamber.

Instrumentation consists primarily of thermocouples (copper-constantan) and absorbed flux calorimeters. The thermocouples are located on the test model, as closely as practical, to correspond with the nodes established in the analytical model. Briefly, these absorbed flux calorimeters (used not only to control the lamps, but also to measure the absorbed energy at the test model surfaces) are thermally isolated discs, with surface optical properties identical to the test surface on which the absorbed flux is measured. Being thermally isolated, the steady-state temperature of the calorimeter disc is dependent only on its absorbed heat flux and heat leaks through its mechanical supports. Optical measurements (absorptance and emittance) of the calorimeter surface establish its absorbing properties, and vacuum calibration (in a belljar) determines its heat-leak characteristics. These calorimeters have proven to be within 1 percent of National Bureau of Standards (NBS) traceable radiometers.

Four test conditions are imposed on the development model. Sequentially these conditions are as follows:

(a) Nominal conditions

- Solar heating at equinox conditions is simulated
- Components at nominal power levels

(b) Eclipse of 1.2 hours

- No external heating
- Components adjusted to spacecraft eclipse power profile

(c) Minimum thermal conditions

- Solar heating at summer solstice is simulated
- Components at minimum power levels

(d) Maximum thermal conditions

- Solar heating at winter solstice is simulated
- Components at maximum power levels

These four thermal environments provide conditions for evaluating the design bounds of the spacecraft thermal control subsystem as well as provide a quantitative verification of the testing technique. The eclipse test not only provides additional data for analytical model verification, but also allows a direct measurement (by absorbed flux calorimeters) of the effective heat sink extent in the chamber with all test fixtures in place.

Using the development test data, a comparison to predicted temperatures from the detailed math models of the spacecraft is made. Depending on the results of this comparison, either the thermal design of the spacecraft is verified or revisions to the thermal design and/or thermal math models are required.

5.11 POWER SUBSYSTEM

5.11.1 GENERAL

The SMS power subsystem[1] provides all electrical power to the spacecraft loads. It consists of a solar array, battery, power control unit and individual subsystem dc/dc converters; this power subsystem configuration is commonly known as a direct energy transfer (DET) subsystem. As shown in Figure 5-52, the spacecraft loads are fed directly from the solar array; the lack of any series regulating element between the array and the main load bus allows the subsystem to supply the daytime load bus demands at almost 100-percent efficiency.

A body mounted solar array powers a low impedance load bus, which is tightly regulated by a partial shunt regulator. This bus distributes power to the subsystem loads through highly efficient, fault-protected regulating dc/dc converters. A battery is used to sustain eclipse operation, with discharge regulation being accomplished by an active boost converter/regulator. A small section of the solar array is used for battery-charge control. A significant feature of the design is that only eclipse operation is compromised in the event of battery malfunction. The total satellite operational capability is preserved during the illuminated periods of its mission lifetime.

5.11.2 REQUIREMENTS

As in the case of any power subsystem design, certain environmental and performance parameter constraints have been dictated by the projected mission. These constraints are in addition to the load power requirements of the spacecraft subsystems.

Spacecraft power requirements are a function of operating modes. Figure 5-53 depicts the individual load requirements for each operating mode and the total primary power requirements. Included in these loads are electrical integration and power control requirements; in each case, the given subsystem power requirement includes the subsystem's dc/dc converter power losses. In addition, transient power is required for the operation of the ABM and auxiliary propulsion.

The primary environment constraint placed upon the satellite is the requirement for five year operation in the synchronous altitudes' radiation environment. The solar array is capable of providing a minimum power output of 140 watts after withstanding the solar flare, trapped orbital electron and proton produced degradations. This environmental constraint essentially determines the array's solar cell cover glass thickness and series/parallel connection arrangement.

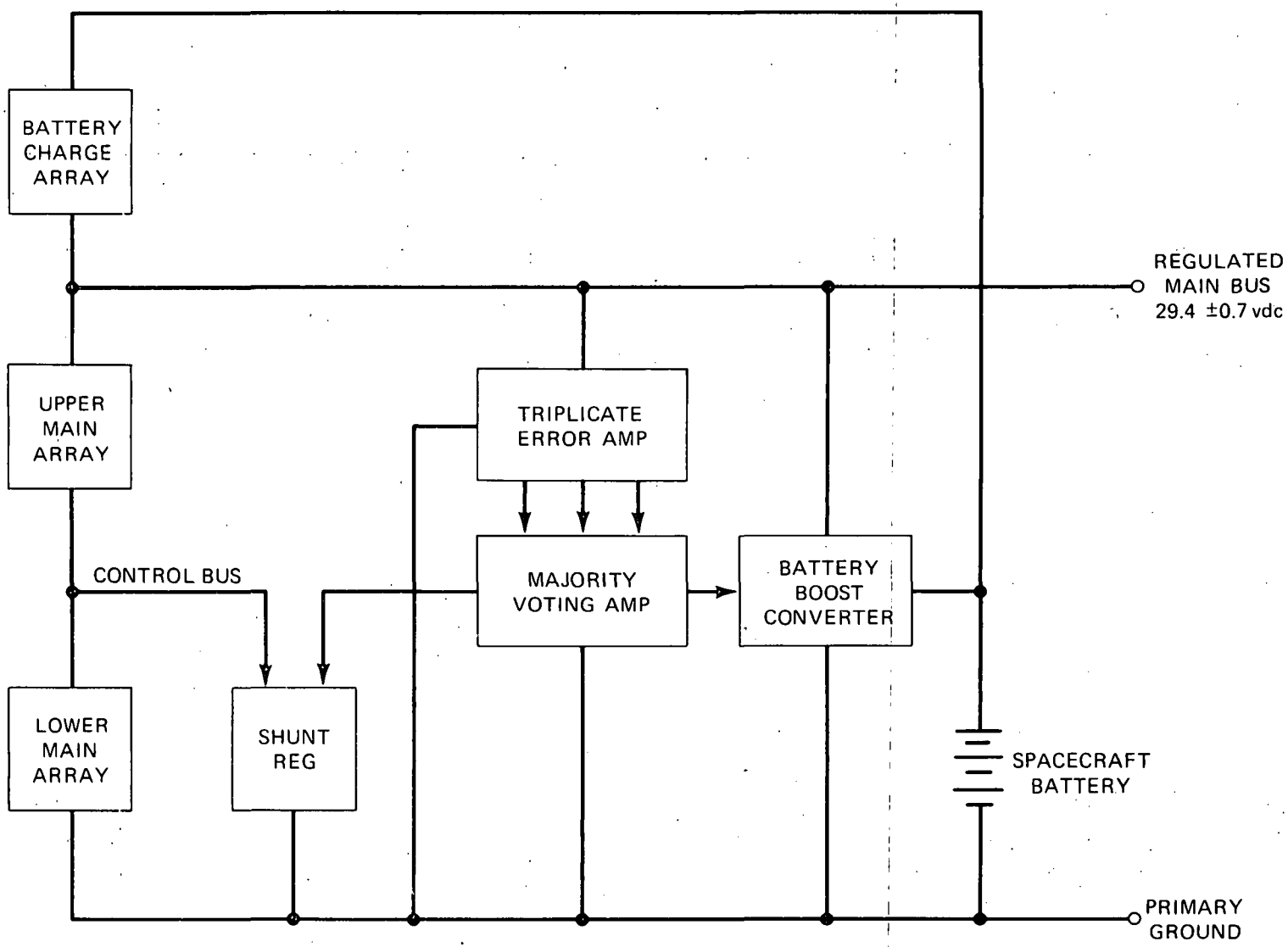

Figure 5-52. Basic Power Subsystem Block Diagram

The five performance parameter constraints are given below:

(a) Satellite configuration constraints. The spacecraft configuration establishes that the solar array be mounted on a 75-inch cylindrical body. Other power subsystem components are mounted on an equipment platform within the spacecraft drum. Size and weight of these components are compatible with the overall spacecraft mechanical design.

(b) Electromagnetic interference. To reduce potential conducted interference problems, between subsystems, the power subsystem meets the following requirements:

- o Source impedance of the load bus ≤ 1.0 ohms
- o Ripple feedback current from the subsystem converters limited to < 5 percent, peak-to-peak average dc current
- o Voltage transients limited to ±5 volts for a maximum duration of 100 microseconds

(c) Battery. The maximum battery depth-of-discharge, for a 72 minute synchronous eclipse period, is limited to 60 percent. The maximum average battery recharge rate is limited to $^{C}/10$.

(d) Load current limiting. Turnon in rush current of any load operating from the power bus is limited to 150 percent of the average steady-state input current. In the event that a fault develops in any subsystem load, the load is disconnected from the primary power source.

(e) Apogee boost motor ignition. The power subsystem provides for ignition control of the ABM.

5.11.3 SUBSYSTEM OPERATION

The power subsystem consists of three major components: a body-mounted solar array, a nickle-cadmium battery and a power control unit. In addition to these components are the dc/dc converters which provide regulated secondary power to the spacecraft loads. Figure 5-54 shows the basic block diagram of the power subsystem.

During the daylight portion of each orbit, the main solar array provides power directly to the spacecraft load bus. This load bus is held at a regulated voltage of 29.4 ±0.2 vdc through the use of a partial shunt dissipator. The shunt dissipator circuitry continuously monitors the load bus voltage; any increase in

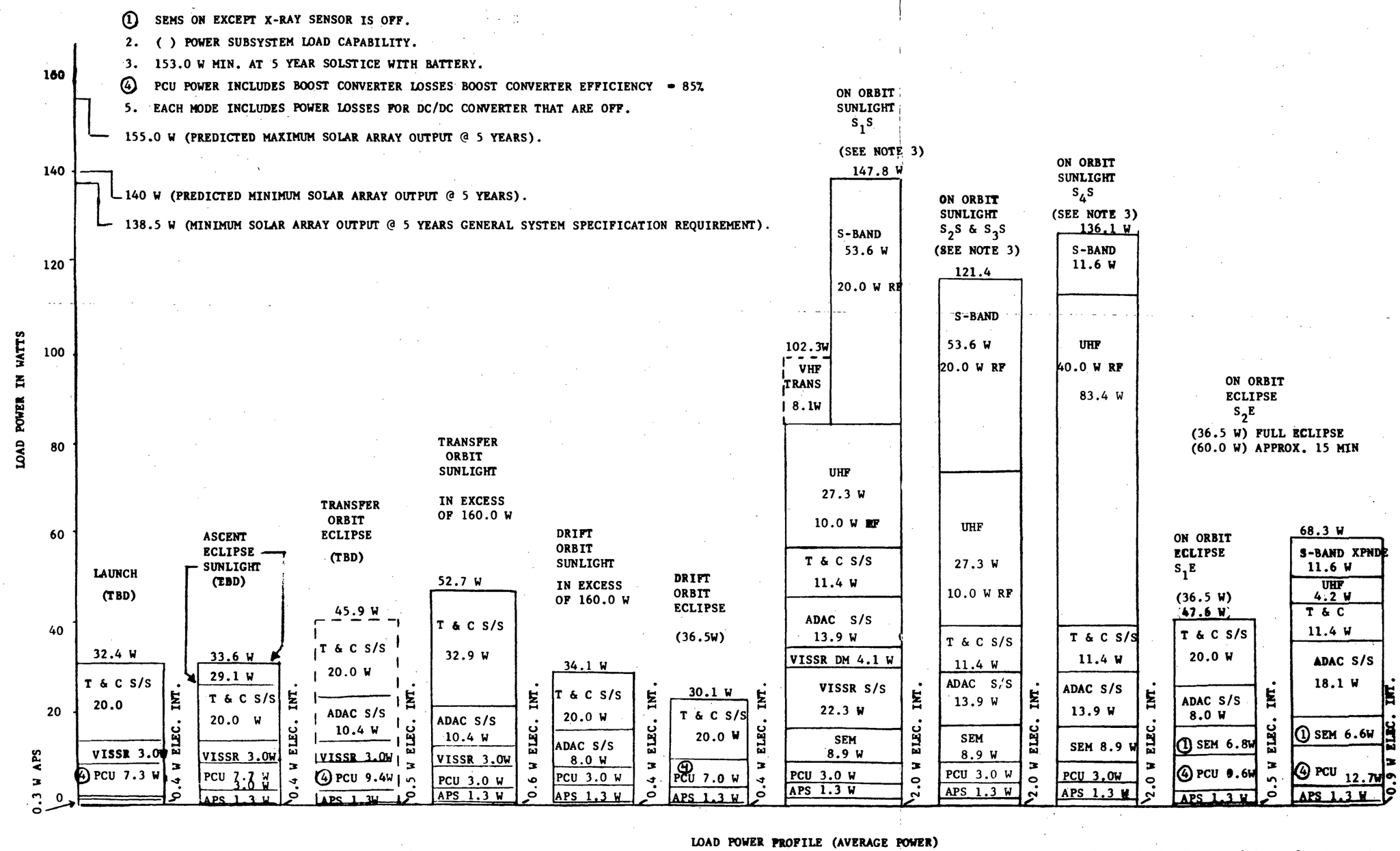

Figure 5-53. Spacecraft Power Requirements

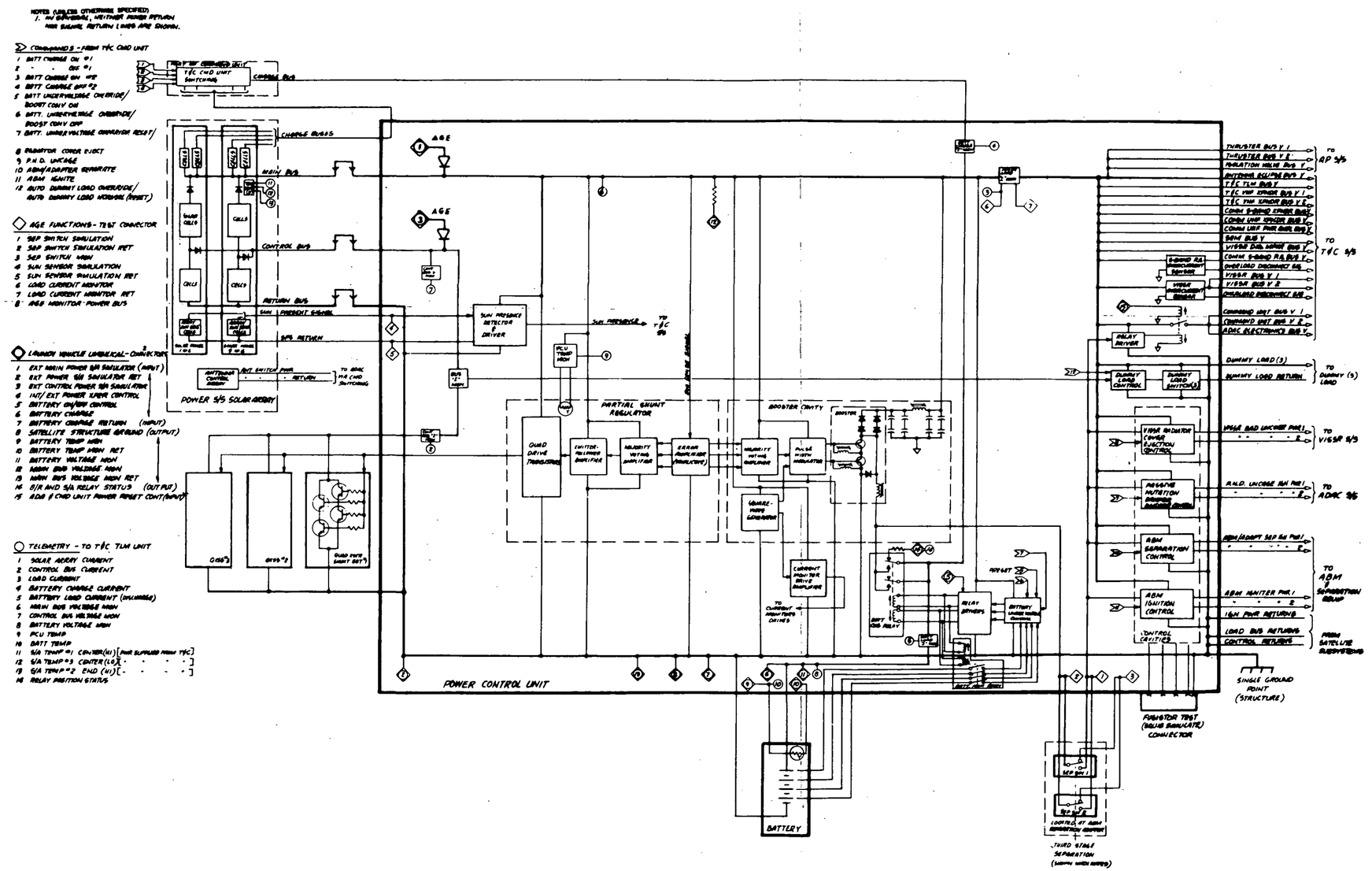

Figure 5-54. Subsystem Block Diagram

array voltage is immediately compensated for by an increase in shunt dissipator current demand, which lowers the bus voltage to within its proper limits. Alternately, an increased load power demand results in a smaller value of shunt dissipator current. Providing a regulated load bus to the spacecraft subsystems has several advantages. Those loads which use regulated voltage directly (for example, the S-band power amplifier) do not require any series regulating element between the load bus and the subsystem load. This results in an efficiency savings of at least 10 percent. Also, the subsystem converters are designed to operate more efficiently by always working from a regulated input voltage, rather a widely varying range of input voltages. In addition, this regulation provides for low power bus impedance; as a result, electromagnetic compatibility (EMC) problems associated with the power subsystem are greatly reduced.

During eclipse periods, and times during the daylight portion of an orbit in which the load power demand exceeds the solar array capability, load bus regulation is provided by means of a battery-boost converter. The converter, which is fed directly from a 20 cell, 3 ampere-hour nickle-cadmium battery, supplies varying amounts of load power to maintain the bus regulation with its proper limits. To preclude the possibility of battery damage due to excessive discharges, a majority of the spacecraft loads are automatically switched off as the spacecraft enters eclipse. Should eclipse operation of any, or all of the normally sun-only loads be desired, the capability of connecting each load to the power bus by ground command has been included. Switch S1 (Figure 5-54) is controlled by a sun-presence detector; this switch is opened, removing power to nominal "sun-only loads." Should eclipse operation of any, or all, of the sun-only loads be desired, switches S2 through S8 need only be ground commanded to the proper position. As additional protection, the battery contains an undervoltage protection circuit. Should the battery voltage fall below a preselected value, the battery is removed from the input to the boost converter. While this results in a temporary loss of spacecraft power, it eliminates the possibility of an excessive load demand permanently damaging the battery.

In addition to the main solar array, two smaller arrays are also contained on the spacecraft's cylindrical drum body. The first of these is the battery charge solar array. This array consists of two small solar cellar circuits which serve as a charge current limiter to the battery. Power from this array is supplied to the battery through a series of ground commandable relays. These relays allow a battery charge current, ranging from $^{c}/10$ to $^{c}/50$ in three discrete steps, based upon the time of year or a particular set of battery/load conditions. As the battery is not normally used extensively during the solstice seasons — when the total solar array capability is the lowest — the battery charge array is switched to its lowest charge mode. This results in an overall increase in the arrays' total available power capability.

The second array also consists of two small sections located adjacent to the battery charge arrays. This array provides a sun-presence signal. Whenever the output from this array drops below a value corresponding to a main array power level of approximately 90 watts, all sun-only loads are automatically removed. An increase in the sun sensor array's output to an equivalent 110 watts of main array power restores power to all of the spacecraft loads.

With the exception of the VISSR and the S-band power amplifier, all spacecraft subsystems interface with the main bus through dc/dc converters. Each of the spacecraft converters provide two functions. First, they convert the primary bus voltage to the voltages required by the user subsystems, providing approximately ±3-percent regulation for both line and load variations. They also provide turnon current surge limiting and output overload current limiting. In the event of a subsystem failure, the converter is automatically removed from the primary power bus, thus preventing a user subsystem failure from causing a satellite failure.

The VISSR and S-band power amplifier receive their power through overload current protection circuits. These circuits operate in the same manner as the protection curcuitry of the dc/dc converters (overload current limiting, and removal of failed subsystems from the primary power bus).

In the event of a battery, or boost converter failure, only the satellite's eclipse operation is affected. The satellite turns on automatically when entering sunlight. This automatic start-up of the individual subsystems is possible in that the maximum power turnon in-rush current is limited to 150 percent of the average steady-state current. This prevents the solar array from locking-up in an unfavorable position, and thus preventing proper spacecraft operation. The present power subsystem operates properly, with or without a battery, for the entire five year mission lifetime.

5.11.4 DETAILED SUBSYSTEM DESCRIPTION

The preceding sections have covered the power subsystem's requirements and operation. This section provides a detailed review of each of the components which make up the power subsystem.

5.11.4.1 Solar Array

The solar array is divided into three portions: main, battery and sun presence. While the three arrays provide distinctly different functions, they are all made up of the same components; the same degradation factors were used in the calculation of each array's power output capability.

The basic array component is the 2 x 2 cm n- on-p silicon solar cells, 0.013 ±0.002 inches thick with a base resistivity of 7-to-14 ohms/cm. These cells exhibit typical conversion efficiencies of 11.2 percent. The cell contacts are solder-coated sintered titanium-silver, with a "corner-dart" n-contact. The cell is covered with Corning 7940 fused silica, 0.006 inch thick. The outer surface of the cover slide has an antireflective coating with a 0.410μ interference filter on the cell side. Less expensive microsheet was not used in this application due to the uncertainties regarding its degradation under particulate and electromagnetic radiation. The solar cell interconnects are made from silver-plated molybdenum; this interconnection material was selected because of its desirable thermal expansion and electrical conductivity characteristics.

The solar cells are formed into modules, the cell arrangement dependent upon array type, and then bonded to array substrates with RTV-511 silicone adhesive. The substrates are formed from 1/8-inch cell aluminum honeycomb with Fiberglass face sheets. The core is 3/8 inch thick. The faces are fabricated from two layers of 0.002-inch thick pre-impregnated Fiberglas cloth. A 0.003-inch thick adhesive film is interposed between the core and face sheets.

Aside from the initial solar cell losses due to coverglass assembly and cell mismatch, the primary contribution to array degradation in space is charged particle irradiation. During the determination of the array degradation, Vette's data (NASA-SP-3024) was used for the trapped elections and protons. A COMSAT Corporation solar flare model, applicable to the 1970 to 1975 period, was selected as the most accurate flare model for the SMS mission. A radiation damage analysis using the information of the above reports yields a total degradation in light-generated current of approximately 15 percent; all three solar arrays degrade an equal amount.

The main array consists of 15,054 solar cells arranged into 62 individual, parallel-connected circuits. Each circuit consists of 2 or 3 cells in parallel and 78 cells in series. Each circuit is connected through redundant isolation diodes to the primary power bus. Each circuit is also center-taped to accomodate the partial shunt regulator; by controlling the amount of array current being drawn through the shunt dissipator, the primary power bus regulation is maintained. The main array is designed to maximize the available power to the load bus at the end of five years. The minimum power occurs during summer solstice, with the VISSR view port pointing directly at the sun. Under these conditions, the array produces a minimum of 140 watts during 5 years in orbit. The minimum power available at the 29.4-volt load bus, corresponding to the condition in which the sun looks directly into the VISSR port, is presented in Figure 5-55. This figure shows the equinox (upper) and solstice (lower) capability versus time in orbit. The actual array output is shown as a cyclic curve, varying between these two extremes.

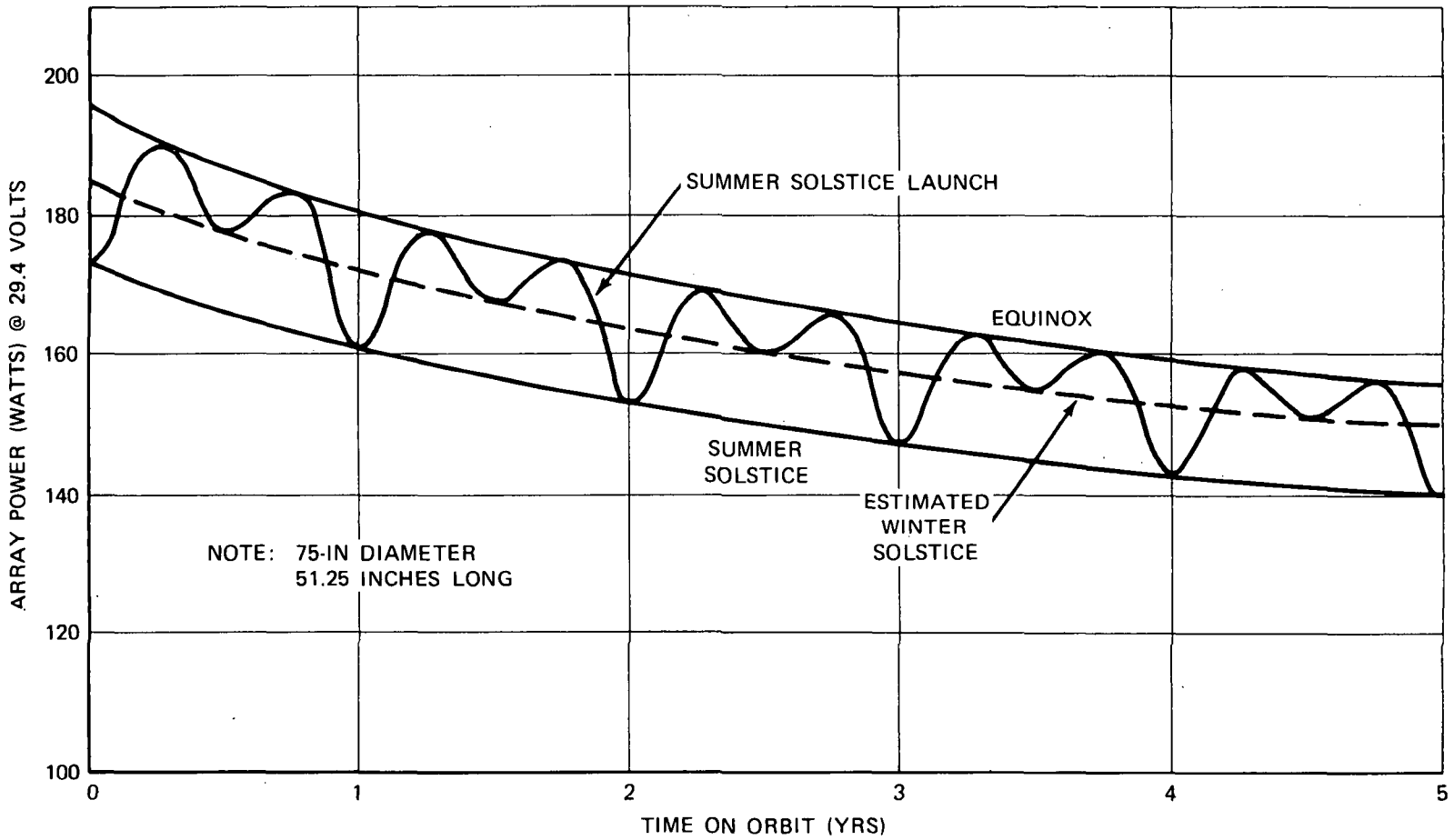

Figure 5-55. Satellite Main Bus Power Versus Time in Orbit

The battery charge control array, which functions as a current limiter, supplies battery charge current in pulses characteristic of full wave rectified alternating current as the satellite spins. Each of the two segments of the charge array are divided into three circuits of four series-connected solar cells which are paralleled in the power control unit. Figure 5-56 shows the battery array charging characteristic at beginning and end of the mission lifetime.

The sun-sensor array's output is shown in Figure 5-57. Each of this array's two segments consists of 8 series-connected solar cells. The output from this array determines whether sufficient power exists to support all of the spacecraft loads.

5.11.4.2 Battery

Two three ampere-hour nickel-cadmium batteries have been selected for use on the SMS satellite. Each battery consists of 20 hermetically-sealed prismatic cells connected in series. Each storage cell is purchased with dual seals; solder lugs are welded to each terminal. The series connections between cells is accomplished by using soft pretinned solid copper intercell connectors, in a strain relief configuration, soldered to the solder lugs. Battery power connections are made to the terminals at the end of the cell series by means of redundant wires leading to the battery/satellite connector. An additional connector permits the monitoring of individual cell voltages during spacecraft ground testing; this connector is sealed prior to spacecraft launch.

Temperature sensing is provided using space qualified precision wafer thermistors. These thermistors have a nominal resistance of 5000 ohms and have a resistance tolerance of ±1 percent from 0 to 50°C, with a temperature coefficient of -4.4 percent/°C. A single thermistor is incorporated into the cell separators located between the two middle cells of each battery. It is positioned to be most responsive to the operational temperature changes of the battery.

The battery packaging assembly is shown in Figure 5-58. The battery case is a milled, black anodized aluminum alloy. The bottoms of each storage cell case are thermally connected to the mounting surface of the battery with thermally conductive epoxy, thereby allowing the heat generated in the battery to be conducted to the satellite structure where it can be radiated to space. This design incorporates maximum heat dissipation characteristics along with minimum weight. The design is based upon flight proven techniques, and represents an optimum battery design for the SMS spacecraft.

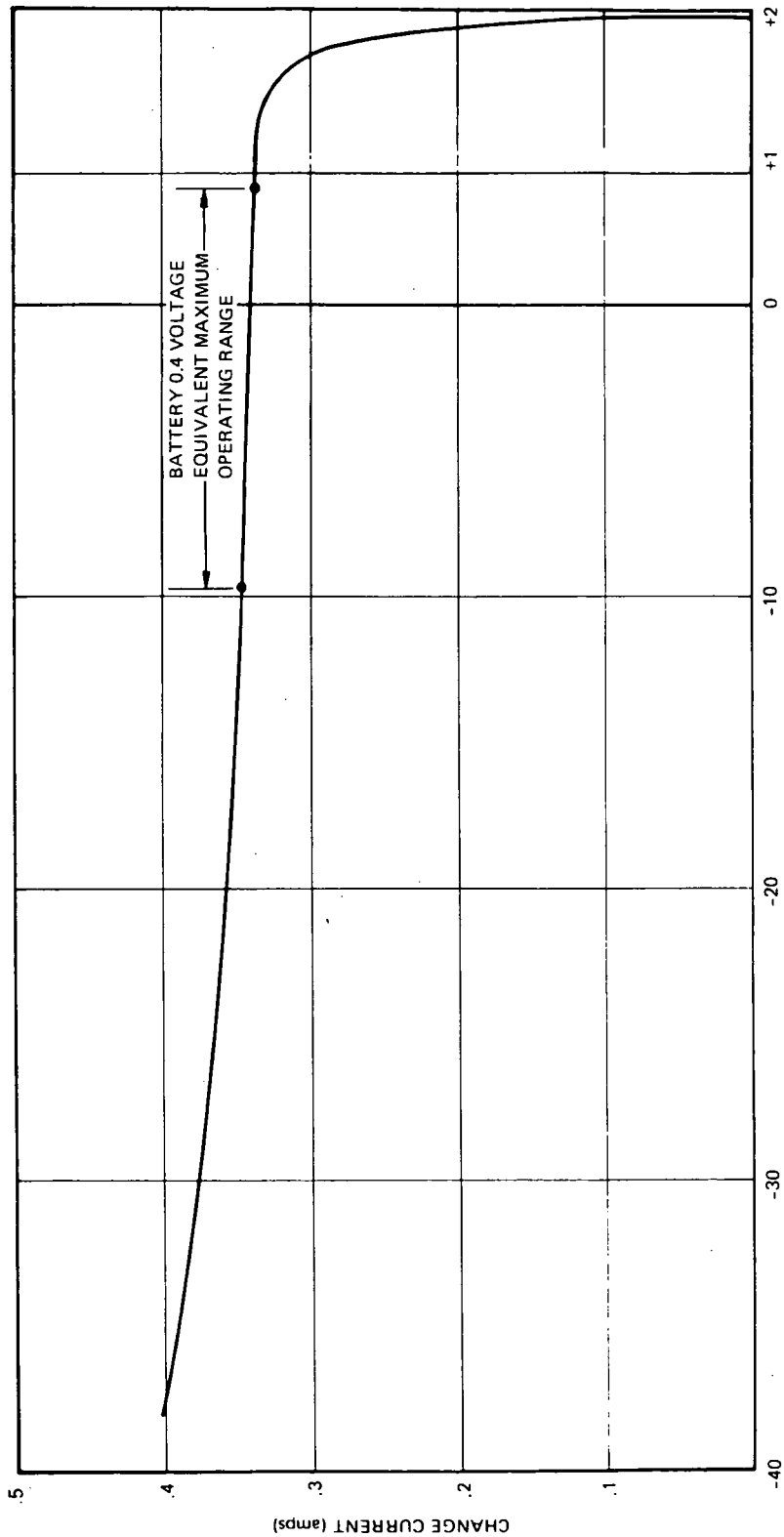

Figure 5-56. Battery Charge Control Array Characteristic Peak Charging Current

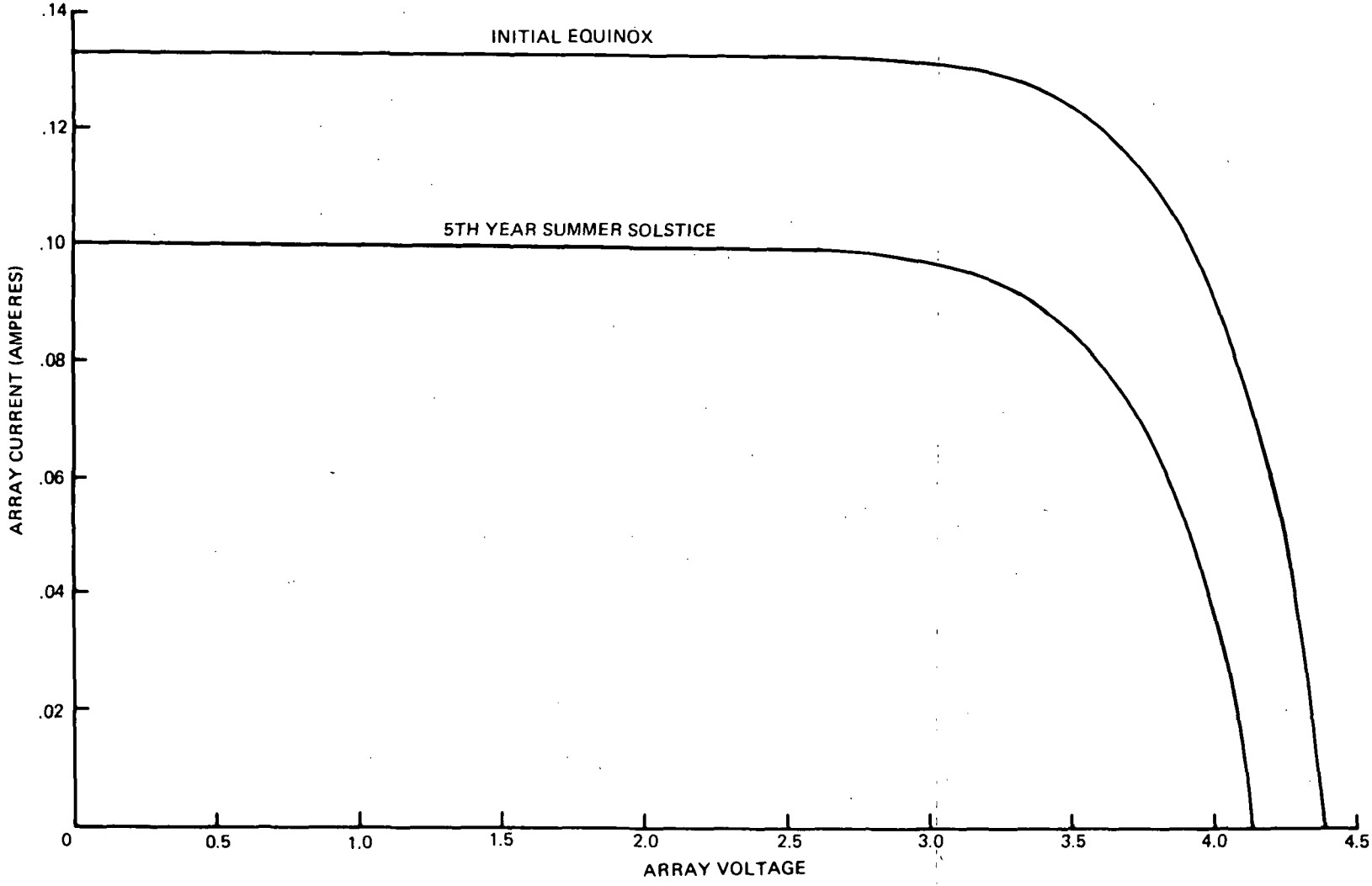

Figure 5-57. Sun Sensor Array Output Characteristics

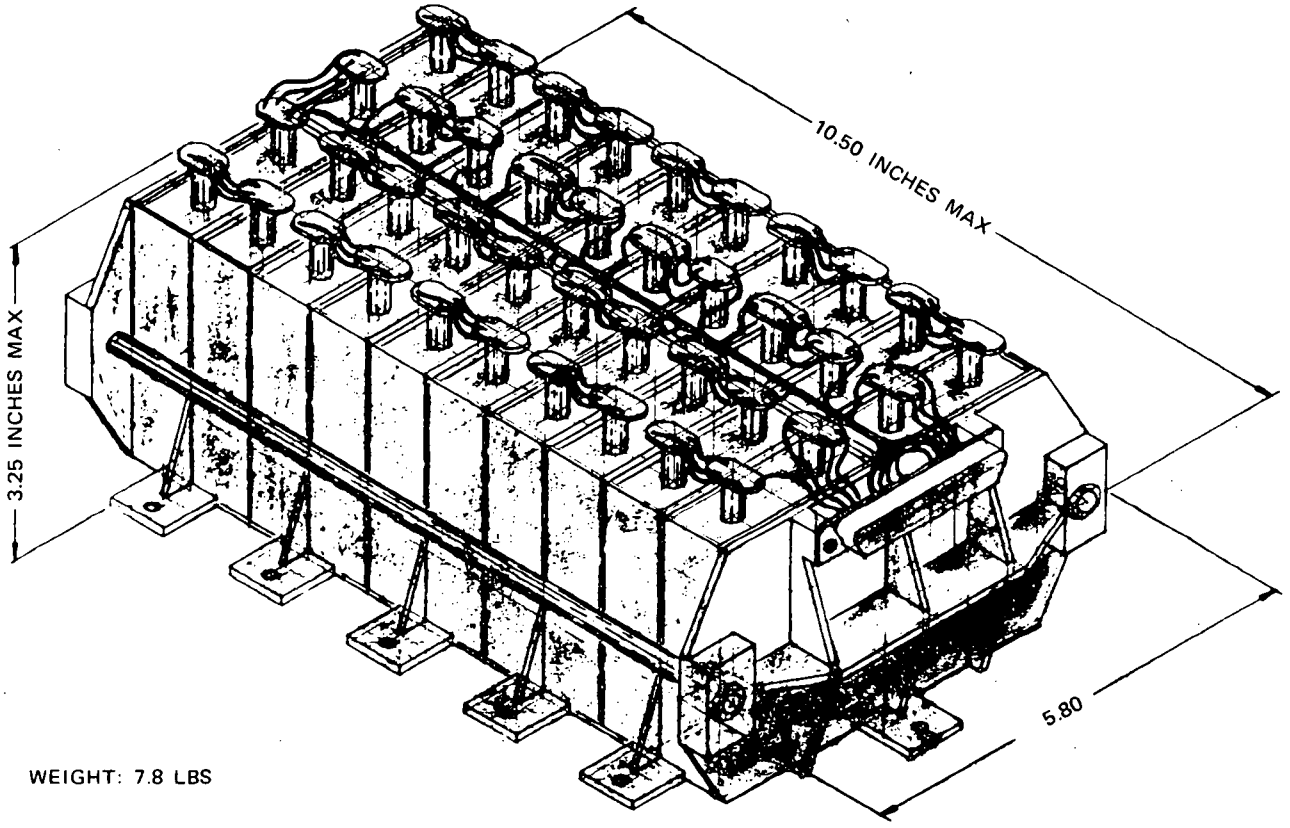

Figure 5-58. Battery Assembly Design

5.11.4.3 Power Control Unit (PCU)

The PCU provides the electrical interface between the solar array, the battery and the spacecraft. Figure 5-59 shows the basic block diagram of the PCU. Circuit simplicity, reliability and utilization of existing flight-proven designs were a major consideration in the design of the PCU. Details of the major circuit functions of the PCU are presented below.

5.11.4.3.1 Partial Shunt Regulator. Array voltage regulation is performed by the partial shunt regulator which consists of the following five sections:

1. Shunt regulator error amplifier
2. Majority voting amplifier
3. Emitter follower amplifier
4. Quad drive transistors
5. Shunt transistor pairs

The first section consists of a group of three differential voltage-sensing amplifiers which sense the level of the main bus voltage. Each of the three independent error amplifiers compares the bus voltage with its reference voltage and produces an output proportional to the error. The error signals from these amplifiers are applied to the majority voting amplifier section; error signals from at least two of the three error amplifiers are required to saturate any one of the three majority voting gates. The outputs of the three majority voting gates are common and provide the error signals to the emitter follower amplifier section.

It should be noted that the triplicate differential amplifier (voltage comparator) and triple majority voting system provide protection against virtually all types of circuit failures. Single transistor failures, whether open or shorted, have no effect on the bus regulation. Many dual-transistor failures also have no detrimental effect on the bus regulation.

The emitter follower amplifier section consists of two emitter follower current amplifier stages. Each stage consists of two fully redundant sets of two series transistors (quads) with a common error-input base drive and a common output to the next stage. This concept greatly enhances reliability. The series arrangement protects against transistor shorts and the parallel redundancy protects against transistor open failures.

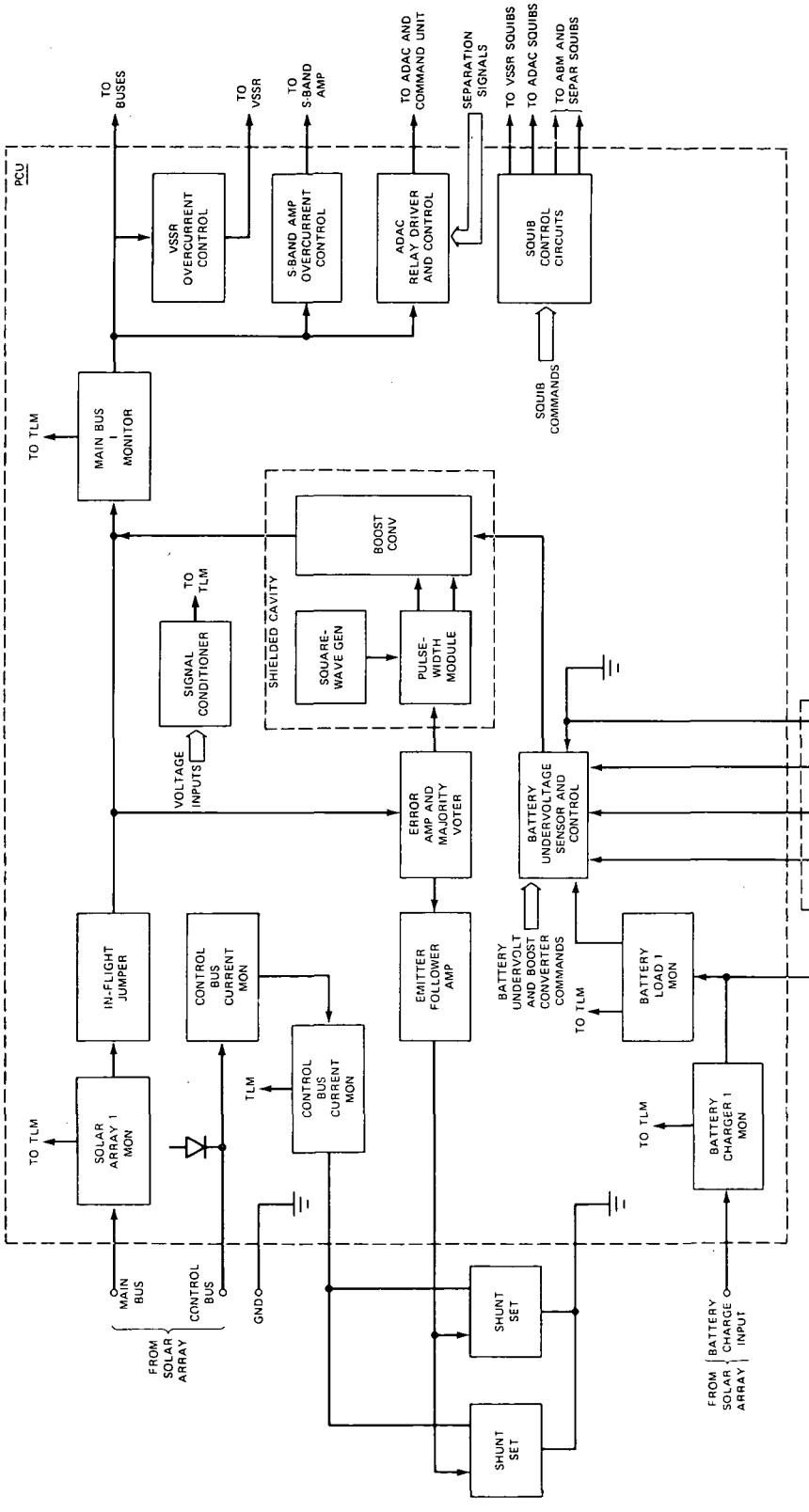

Figure 5-59. Power Control Unit Block Diagram

The quad-drive transistor stage uses stud-mounted power transistors to ensure sufficient base current to the shunt transistor quad sets. Reliability is likewise enhanced in this stage by the use of the quad transistor configuration.

The output quad-drive transistor stage provides base drive power to the twelve shunt transistor pairs. Each of the twelve shunt transistor pairs consists of two series power transistors, with a common base drive from the quad-drive transistor section, to achieve a fully redundant grouping. Series and parallel redundancy is again used to guard against failure, thereby enhancing reliability.

The twelve shunt transistor pairs provide a variable shunt current across the lower portion of the array. This variable shunt current is controlled to increase the shunt current as the main-bus voltage tends to increase. This current shunts the lower portion of the array to the extent necessary to maintain the main bus voltage at 29.4 volts. These twelve shunt transistor pairs are mounted at key locations in the spacecraft to enhance thermal control.

5.11.4.3.2 Battery Boost Converter. During solar eclipse, the main bus voltage is regulated by a battery boost converter. This converter consists of the following five sections:

1. Booster error amplifier
2. Booster majority voting amplifier
3. Square wave generator
4. Pulse width modulator
5. Output stage

The booster error amplifier consists of a group of three differential amplifiers which sense the level of the main bus voltage. The reference voltage for each of these differential amplifiers is obtained from the voltage reference diodes in the shunt regulator error amplifier. The sharing of common references with the shunt regulator ensures that the boost converter regulation point remains at a fixed voltage below the shunt regulator set point. Each of the three independent error amplifiers compares main bus voltage against its reference voltage and produces an output proportional to the error. The error signals from these amplifiers are applied to the majority voting amplifier section. The majority voting amplifier consists of three parts of series-connected PNP transistors driven by the error-signal inputs. Error signals from at least two of the error amplifiers are required to saturate any one of the three majority voting gates.

The outputs of the three majority voting gates are common and provide an error signal to the pulsewidth modulator section. It should be noted that the triplicate differential amplifier (voltage regulator) and triple majority voting system provide protection against virtually all types of circuit failures. Single transistor failures, whether open or shorted, have no effect on the bus regulation. Many dual-transistor failures also have no detrimental effect on the bus regulation.

The pulsewidth modulator is provided with a square wave input from the square wave generator. This input is differentiated by C1, C2, R1, and R2, and combined by CR1 and CR2. The resulting pulses drive the sawtooth generator Q1. The output of the sawtooth generator is combined with the majority voting amplifier output at the base of Q2. Transistor Q2 is switched on for a period which is controlled by the dc bias of the sawtooth ramp. The error signal sets the dc bias of the sawtooth ramp as shown in Figure 5-60.

During the on-time of Q2, base drive is blocked from Q3 by CR4. Emitter followers Q3 and Q4 provide the necessary current gain to drive the output stage. The maximum on-time of the output stage shunt transistor Q1 is limited by the pulsewidth modulator. This is accomplished by setting the amplitude of the sawtooth voltage waveform at Q2, approximately two volts above the zener voltage of CR3. This prevents saturation of the output stage inductor L_1.

The output stage consists of shunt transistor Q1, inductor L_1, redundant flyback diodes CR2 through CR5, and the output filter. Shunt transistor Q1 conducts as a function of the pulsewidth generated by the pulsewidth modulator. During the on-time of Q1, inductor L_1 stores energy. This energy is applied to the bus through the flyback diode quad, when Q1 stops conducting. The pulsewidth determines the on-time of Q1 and the boosted voltage output. The longer Q1 conducts, the greater the energy stored in L_1 and the higher the boost ratio. The output voltage is filtered by a Pi-section filter.

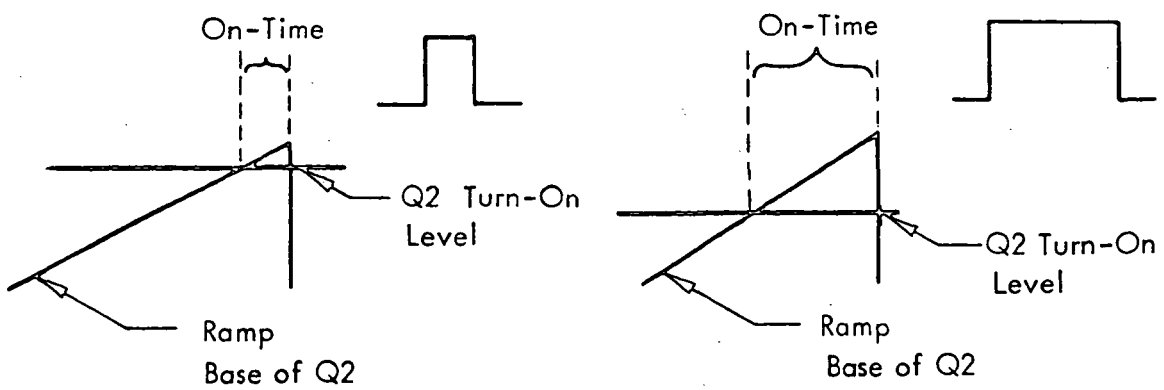

Figure 5-60. Sawtooth Ramp Waveform

5.11.4.3.3 Battery Undervoltage Protection. To protect the spacecraft battery from cell reversal upon discharge, low voltage protection has been incorporated into the PCU. This function disconnects the battery from the boost converter if the battery voltage falls below an average of 1.0 volts/storage cell. A voltage sensor is connected across each five cell section of the battery. If any sensor detects a voltage of less than 5 vdc, the battery is disconnected from the boost converter. The application of the battery undervoltage override on command latches the boost converter relay closed, applying battery power to the converter. Until this command is removed, the automatic battery undervoltage disconnect function is inhibited. Command turnoff of the boost converter is provided by a battery undervoltage override boost converter off command input. This latches the boost converter relay open through the relay driver module.

5.11.4.3.4 Electro-Explosive Device (EED) Actuation Control. Actuation control is provided for the following four EED activated functions:

- Apogee boost motor ignition
- Apogee boost motor separation
- Passive nutation damper uncage control
- VISSR cooler cover removal control

EED control is provided through relays that are actuated upon inputs from the command unit. Upon command, battery current is applied to the EED's through current limiting resistors. Prior to actuation, these EED's are shorted and grounded to prevent inadvertent actuation.

Reduction in the complexity of the EED actuation control circuitry has been made possible by the increased output pulse power capability of the command unit. This allows the ABM ignition, PND uncage, and VISSR cover removal functions to be implemented by driving the associated EED power control relays directly from the PCU command input. The ABM separation function utilizes four power control relays, but these are driven by a 2-out-of-3 majority voting configuration of three teledyne relays. This results in a significant reduction in circuit complexity by eliminating the need for level sensing fail-safe relay drivers.

5.11.4.4 DC/DC Converters

Two basic families of converter design are used to meet the requirements of the system; the primary bus, and the secondary users:

- Linearly pre-regulated converters
- Converters with pulsewidth modulated (PWM) pre-regulators

The linear converter (desirable for its faster dynamic response, simplicity of design, and low-noise characteristics) is utilized except for the following cases. Command and telemetry converters are capable of operation during eclipse with a failed battery boost converter. This condition reduces the primary bus voltage from its normal range of 28.8 to 29.6 vdc to a minimum of 20.0 vdc. To accommodate operation under this condition, an additional 8.8-vdc drop across each affected linear pre-regulator is necessary during normal operation. Such a voltage drop represents an efficiency loss of approximately 30 percent and is intolerable considering that no such loss is incurred using a PWM pre-regulator. Thus, this latter approach is used for all command and telemetry converters. The PWM design is approximately 5 percent more efficient than the linear design. For high power requirements, this higher efficiency results in significant power savings. The VISSR digital multiplexer and the UHF power amplifier represent such high power requirements and are therefore powered by PWM converters.

There are then five linear converters and six of the PWM design; these eleven converters meet the individual user requirements. All users deemed critical are provided with a redundant converter to power the redundant user system. Only the particle detector in the SEM system does not require redundancy and hence employs a single converter.

All converters are hard-wired to the primary bus. On-off capability is obtained with a bilevel biasing signal. Upon application of anominal 28-v signal by the command unit to this single control interface, the converter is biased on; removal of this signal turns the converter off. The command unit is capable of selecting either an automatic eclipse shut-down mode or a manual control mode. For the former, the biasing signal is obtained from the sum presence detector; the latter derives the signal from the main bus.

5.11.4.4.1 Individual Converter Description. Table 5-30 summarizes the eleven sets of secondary power requirements.

5.11.4.4.1.1 Telemetry and Command Subsystem

(a) VHF transponder receiver. The receiver uses a low power, 1.8 w PWM converter of standardized design. No unique requirements are necessary for this unit. Eclipse operation with a failed battery boost converter is required. In-specification operation down to 20.0 v on the primary bus is therefore achieved by the PWM design.

Subsystem User Power Transformer Size	Regulator Type	No. Req'd Per Satellite	Efficiency %	Primary Power (W)	Output Number							Notes
					1	2	3	4	5	6	7	
Telemetry & Command VHF xpdr (xmtr) 18 x 11 mm	PWM	2	74 85	0.38 (rcvr only) 8.8 20.0	0.28w Nom. Either +14 at 3.5w or +28v at 14.0w	8.0v	-8.0					Operation to 20v on input bus; +14 or +28v winding. Operation to +20v on input bus.
VHF xpdr (rcvr) 11 x 7	PWM	2	75	+8v 1.1w				8v 0.24w				
Telemetry & Command Encoder 14 x 8	PWM	2	85	 3.3 nom. 3.8 max. 20 pulse	15v 1.27w 1.425w 3.23w	-15v 0.75w 0.9w 1.3w	5v 0.650 0.75 9.65	-11v 0.077 0.110 1.9	8v 0.064 0.080 0.88			Operation to +20v on input bus.
Telemetry & Command Unit 11 x 7	PWM	2	84	 1.4 nom. 4.9 max. 1.1 min.	29v 0.29w 1.68w 0.28w	12v 0.25w 0.25w 0.25w	5v 0.35w 1.85w 0.05w	-12v 0.25w 0.25w 0.25w	-11v 0.05w 0.05w 0.05w			Operation to +20v on input bus.
COMM 14 x 8, 11 x 7					10v	-5v						
S-band xpdr	LIN	2	75	9.4	4.8w	1.3w	+28v@0.92					Status signals req.
COMM 14 x 8					10v		28v					
UHF xpdr	LIN	2	75	3.5w	1.4w		1.26w					Status signals req.
COMM 22 x 13					28.0v							
UHF pwr amp	PWM	2	85 80	82.5 hi pwr 27.5 lo pwr	70w 22w							
ADAC 14 x 8, 11 x 7					4.0v							
Pin diode	LIN	2	70	10.0 nom. 13.0 max. 5.1 min.	6.97w 9.1w 3.6w 5v	22v	-22v	-40v	15v	-15v		
ADAC and AND	LIN	2	70	6.1 8.6	2.6w	0.9w	0.47w	0.2w	1.33w	0.4 (unswitched 0.13)		(AND during transfer orbit only) Outputs 5 and 6 switched off after transfer orbit.
VISSR					10v	-10v	5v	-5v	10v	-5v	+28	Outputs 1 through 4 switched on once per rotation about spin axis for ≈24 degrees; output 7 relay drive.
Digital multiplexer 18 x 11	PWM	2	78	21.6 peak/40 nom.	5w	5w	0.5w	3.7w	0.5w	2.0w	0.1w	
SEM 11 x 7, 9 x 5					5v	15v	350v	-15v				
Data Processor and particle detector	LIN	1	70	2.4 nom. 2.8 max.	1.3w 1.45w	0.25w 0.40w	0.0816 0.0816	0.075w 0.075w				

Table 5-30
SMS DC/DC CONVERTERS

(b) VHF transponder, transmitter. The transmitter converter is of PWM design to meet the requirement of operation down to 20-v primary bus voltage. It has the added requirement of operation in two modes:

- Low power: 14 volts, 3.5 watts secondary power
- High power: 28 volts, 14.0 watts secondary power

To meet this unique requirement, a common PWM pre-regulator supplies power to two converter-output stages, one of which has a 14-volt output and the other the required 28-volt output. These outputs are diode "OR" ed. On receipt of the command to go to the high power mode, the 28 v section is biased on, back-biasing the diode OR and relieving the 14 v output of its output requirement. Regardless of which mode is operative, a single OFF command by the SPS control interface biases the common pre-regulator off, providing receiver-only capability.

(c) Telemetry encoder. The encoder requires 3.3 watts nominal primary power. The converter is of standardized PWM design so as to operate down to 20.0 v primary bus voltage. Recent design maturation has identified a pulsed power requirement of 17 watts secondary power for 320 microseconds at a repetition rate of 21.56 Hz. This change in user requirements is presently being examined with respect to energy storage needed to sustain the pulsed load requirements.

(d) Command unit. The command unit requires 1.4 watts nominal primary power. The converter is of standardized PWM design so as to operate down to 20.0 v primary bus voltage. The command units operate in active redundancy and are not commandable.

5.11.4.4.1.2 Communications Subsystem

(a) S-band transponder. The communication transponder requires 9.4 watts nominal primary power. Operation is required only with a well-regulated bus, therefore this unit uses a linear pre-regulator. The only unique requirement for this converter is the need for telemetry status signals to indicate which of the redundant units is in operation.

(b) UHF transponder. The UHF transponder converter is of standardized linear design. It has a 3.5-watt primary power requirement, operates from a tightly regulated bus, and provides status signals for telemetry.

(c) UHF power amplifier. The power required for this unit in its high power mode represents the highest demand on any of the user converters

in the spacecraft. At low power, 27.5 watts of primary power is required; at high power, 82.5 watts is required. Though PWM converters are considerably more demanding in their design, the increased efficiency available with this design dictated its use for this major power requirement.

5.11.4.4.1.3 Attitude Determination and Antenna Control (ADAC) Subsystem

(a) Pin diodes. The standard linearly pre-regulated converter design is used to meet the power requirements of the pin diodes. With the elimination of the dedicated array, the pin diodes are powered through redundant 10.0-watt linear converters on the main bus.

(b) ADAC electronics and automatic nutation damper (AND). The ADAC electronics converter also supplies power to the AND through transfer orbit. After transfer orbit the AND power is disabled using secondary switches actuated by relay closure in the command unit. The primary power required of this standard linear design is 8.6 watts while the AND is operative and 6.1 watts after AND disablement.

5.11.4.4.1.4 VISSR Digital Multiplexer — The digital multiplexer has a repetitive peak primary power requirement of 21.6 watts once per rotation during earth scan (42 ms). To accommodate this unique requirement, a common PWM pre-regulator supplies power to two converters. One of these converters supplies the steady-state power required and the other supplies the peak power on command from the ADAC Subsystem. In other respects, the design is the standardized PWM converter design.

5.11.4.4.1.5 SEM Subsystem — The SEM data processor and particle detector's low power (2.4 watts nominal) requirement is met by a linear pre-regulated converter of standardized design.

5.11.4.4.2 Hybrid Packaging. Microelectronics hybrid design is, in actuality, miniature printed wiring boards containing miniaturized electronic parts. In place of the G-10 plastics normally used, aluminum oxide ceramic substrates form the circuit base. Connections between electronic parts are made by soldering. All active devices used are purchased in hermetically sealed packages. The only departure from the ordinary is that the conductors and non-critical resistors are printed and fired on the ceramic substrates. In those critical circuits where special temperature compensating resistors are required, "chip" resistors are used. Similarly, "chip" capacitors are used for circuit functions.

The decision to package the converters using a hybrid-thick film approach realizes many benefits. This approach is intimately connected to the general design philosophy of establishing standardized families of designs. Thick-film resistors are trimmed as a manufacturing process. Thus, to satisfy an entire class of designs over a wide power range, one substrate design is used and variations in resistor requirements is obtained by changing manufacturing instructions for the trimming process.

The families of converters have been modularized. Generally, a converter consists of a pre-regulator substrate, an oscillator-converter substrate, output magnetics, and output rectifier and filter substrates. Thus, particularization of individual outputs is accomplished by modifying the output magnetics and the filter modules. This flexibility in design has been joined with the ability to develop modules in parallel efforts.

The development of breadboards using the hybrid design leads directly to converters meeting the form, fit, and function requirements of the using subsystem. The reactance of interconnecting leads is minimized and tightly controlled in the thick film process. Thus, interfacing the form, fit, and function converters with the user's engineering models is representative of flight hardware. Interaction between the converter and the user is clearly established and corrected, eliminating the added iterations inherent in traditional development methods.

The linear converter design is presently in hybrid development tests with the PWM hybrid design forthcoming. The open planer nature of the substrates has eased the testing process considerably. Visual inspection is also easier in a planer design than in 3-D cordwood packaging. Component parts have been changed or modified easily to achieve the required performance.

Other more obvious benefits of the hybrid approach are size and weight savings and greater flexibility in thermal control through the excellent thermal conduction of the ceramic substrates.

5.12 MULTIPLEXER AND DEMULTIPLEXER SUBSYSTEM

5.12.1 REQUIREMENTS

5.12.1.1 General Requirements

The basic requirement of the VISSR digital multiplexer (MUX)[1] is to sequentially sample the ten VISSR video channels, perform A/D conversion, and generate a quadriphase compatible serial waveform. The signal-to-noise ratio of the

reconstructed video waveforms is not degraded more than 1 db. The end-to-end system consists of the following equipment:

(a) VISSR MUX

(b) Quadriphase modulator

(c) CDA demodulator

(d) CDA demultiplexer

5.12.1.2 VISSR MUX Requirements

5.12.1.2.1 VISSR Video Signals. The GFE VISSR subsystem provides eight visual and two infrared channels. The information bandwidth of the former is 210 kHz and that of the latter is 26 kHz. Pre-aliasing filters are provided to ensure the aliasing error in the reconstructed video is sufficiently reduced so that the system signal-to-noise ratio degradation does not exceed 1 db. The pre-aliasing filter type, the number of poles, and cutoff frequencies are determined by analysis. Additional details of the VISSR interface are contained in part A of Table 5-31.

5.12.1.2.2 A/D Conversion Characteristics. The A/D conversion characteristics are defined in part B of Table 5-31.

5.12.1.2.3 VISSR Line Scan ID Number Signals. The GFE VISSR subsystem also provides 12 encoder signals to the VISSR MUX. The encoder signals contain the line scan identification number which is transmitted once-per-scan to the CDA ground station.

5.12.1.2.4 Operating Modes. The VISSR MUX operates in one of two modes, and mode selection is commandable from the ground. The definition of the modes is contained in Table 5-32.

5.12.1.2.5 Data Format. The data format generated by the VISSR MUX for mode 1 is illustrated in Figure 5-61. Alternate 1's and 0's are generated for a period of 2 ms to allow synchronization of the CDA demodulator. Immediately following is a 56-bit word which contains scan sync and line scan ID number. Video data is then generated, six bits for each visual channel and eight bits for each infrared channel.

The data format for mode 2 is similar to that of mode 1, with the exception that data words 6, 7, 8, and 9 are deleted.

Table 5-31

Digital Multiplexer Specifications

Parameter	Specification
A. VISSR outputs (multiplexer input)	
1. Visual channels	
Quantity	8 each (full capability)
Video bandwidth (3 db)	0.05 Hz to 210 kHz
Peak signal to RMS noise	9 db at black level (noise level 10 mv) 32 db at white level (noise level 120 mv)
Dynamic range	54 db (10 mv to 5000 mv) precompanding 32 db (10 mv to 400 mv) post companding
Minimum noise level	10 mv
Maximum noise level	120 mv (increases as a square root of signal voltage)
2. IR channels	
Quantity	2 each (full capability)
Bandwidth	0.02 Hz to 26 kHz
Peak signal to RMS noise	10 db (target temp. 180°K) 48 db (target temp. 300°K)
Dynamic range	48 db (20 mv to 5000 mv)
Noise level	20 mv
B. Multiplexer	
1. Visual channels	
Encoding	6-bit
Linearity	Companded (≈square root)

Table 5-31 (continued)

Parameter	Specification
S/N degradation	1 db due to quantization (i.e., S/N_Q = 38 db)
Gain stability (per channel)	±0.5 db over any 12-hour interval
2. IR channels	
Encoding	8 bits linear
Linearity	1 percent of full scale from straight line
S/N degradation	≤ 1 db due to quantization and intermodulation (i.e., S/N_Q = 54 db)
Gain stability (per channel)	±0.5 db over any 12-hour interval

5.12.1.3 CDA Demodulator Requirements

The CDA demodulator consists of a quadriphase demodulator, quaternary differential decoder, and a bit synchronizer. General specifications are as follows:

(a) Signal input — 70 MHz ±5 kHz IF at -50 to -10 dbm

(b) Serial data rates — 28 and 14 Mb/sec

(c) Bit-error probability — The bit error probability is not less than 1 bit in 10^6 bits for an E/N_0 of 12.5 db or greater for the 28-Mb/sec operating mode or greater the 14-Mb/sec operating mode

(d) Signal outputs — Two serial data channels at 7 and 14 Mb/sec and clocks

(e) Time-to-lock — 2 msec

Table 5-32

VISSR Multiplexer Data Transmission Modes

Mode	Input[1] Channels	Samples[2] Rate (kHz)	Visible Channel Resolution		Data Mb/sec	Symbol Rate Mb/sec
			N-S (nmi)	E-W (nmi)		
1	8 visible + 2 IR	500	0.5	0.5	28.0	14.0
2	4 visible + 2 IR	437	1.0	0.5	14.0	7.0

(1) Reduction in number of visible channels is accomplished by paralleling individual visible sensor outputs (i.e., 4 visible = 4 groups consisting of 2 adjacent sensors per group; 2 visible = 2 groups consisting of 4 adjacent sensors per group; 1 visible = 1 group consisting of all eight sensors in parallel).

(2) Predicated on 100 rpm spin rate.

5.12.1.4 CDA Demultiplexer Requirements

The CDA demultiplexer reconstructs the VISSR video using a demultiplexer, D/A converters, and lowpass filters. In addition, digital data including clocks and strobes are provided.

5.12.2 DESCRIPTION OF VISSR MUX

The VISSR MUX accepts the eight visual and two infrared analog signals from the VISSR electronics assembly, performs A/D conversion, and provides quadriphase compatible serial outputs. The VISSR MUX operates in one of two modes, as directed by the telemetry and command subsystem, and contains redundant elements to increase the overall MTTF.

The general block diagram of the VISSR MUX is illustrated in Figure 5-62. The unit features input signal multiplexing, redundant A/D converters with their

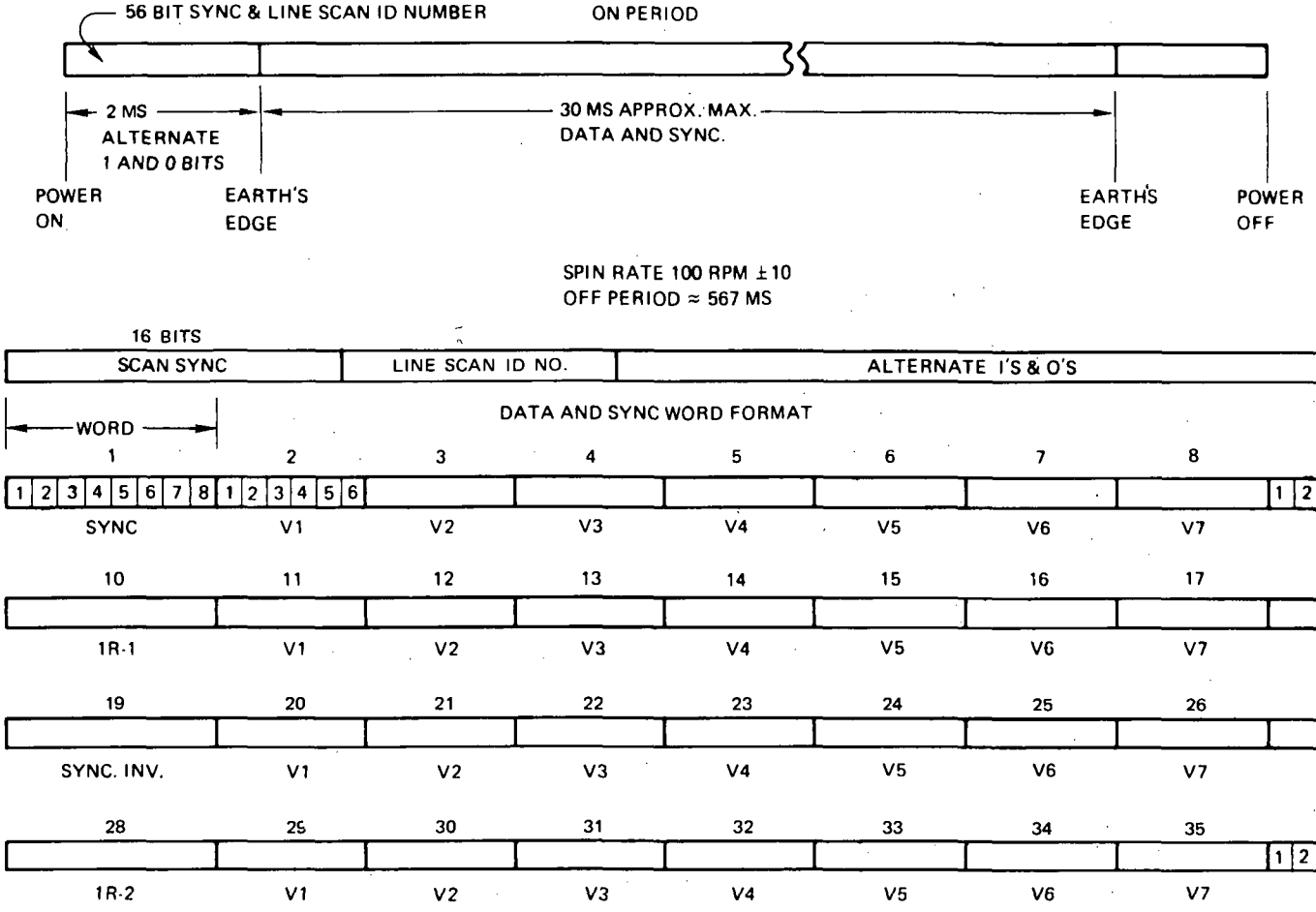

Figure 5-61. SMS VISSR PCM Data Format

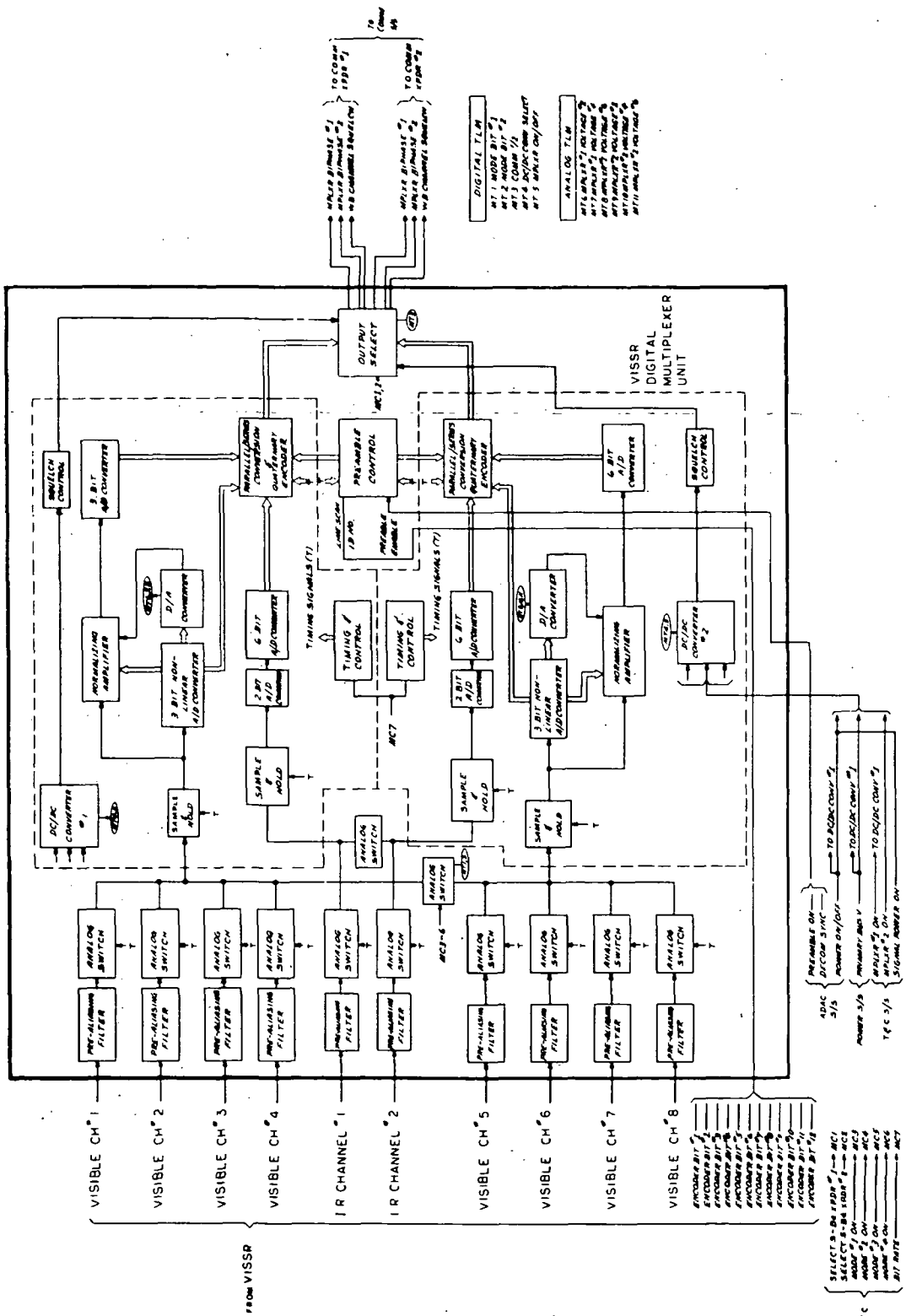

Figure 5-62. SMS VISSR Multiplexer Block Diagram

associated dc/dc converters for reliability enhancement, and output differential encoding for quadriphase modulation. Each VISSR analog output signal to the MUX is bandlimited by pre-sampling filters, which reduce the alias error in the output analog data at the ground station. Analog switches follow each filter and sequentially multiplex each of the input signals to the A/D converters. Track-and-hold elements are inserted between the switches and the converters to provide a constant-amplitude signal during the conversion process. Finally, two types of converters are used: an 8-bit linear A/D converter for the IR channels and a 6-bit nonlinear A/D converter for the visual channels.

5.12.2.1 Pre-Aliasing Filters

The pre-aliasing filter and buffer assembly consists of three stages, A_1, A_2, and A_3, and mode control relays KA have been included where shown. For mode 1, all relays are in the positions indicated by the illustration. If mode 2 is enabled, the KA relay arms switches contacts.

5.12.2.1.1 Pre-aliasing Filter Design. To minimize errors in the VISSR output data because of spectrum folding, five-pole filters are inserted into each channel. Figure 5-63 shows two configurations of the filter for which three basic configurations are needed to implement the total eight-channel pre-aliasing requirement.

The summing of the KA latching relay is the Thevenin summing of the Butterworth filter. The switching of the KA relay adds channels No. 1 and 2, channels No. 3 and 4, channels No. 5 and 6, and channels No. 7 and 8, putting the outputs on No. 1, 3, 5, and 7 respectively. The inputs are halved to keep the full range of the output between zero and five volts.

Figure 5-64 shows the block diagram of the IR channels. The circuit configuration for the filter is the same as the visual channel filter (Figure 5-63 circuit No. 2) with different values of resistors and capacitors to set the corner (-3db of Butterworth) at 30kHz.

Figure 5-65 shows the relay tree and drivers to set the latching relays for the two modes.

A summary of the visual and infrared filter characteristics is contained in Table 5-33.

The pre-aliasing filter, as shown in Figure 5-63 (No. 2), has the following transfer function:

$$\frac{e_{o2}}{e_4} = \left[\frac{1}{R_{S5}R_{I6}R_{D6}C_{B6}C_{F6}C_{D6}S^3 + [(R_{S6}+R_{I6})C_{F6}+R_{S6}(R_{I6}+R_{D6})C_{S6}]C_{D6}S^2+[(R_{S6}+R_{I6}+R_{D6})C_{D6}+R_{S6}C_{S6}]S+1}\right]$$

$$\times\left[\frac{1}{R_{S7}R_{D7}C_{F7}C_{D7}S^2+[R_{S7}+R_{D7}]C_{D7}S+1}\right]$$

where the gain and pole locations can be set to any set of values which are positive real. Three types of active filters are under consideration — Butterworth, Bessel, and Chebyshev. The appropriate filter characteristics are determined by the values of the resistors and capacitors, resulting in no configuration changes. Consider a maximally flat frequency 5-pole Butterworth filter. The normalized transfer function is

$$\frac{e_o}{e_s} = \frac{1}{(S+1)\ (S^2 + 0.618S+1)\ (S^2 + 1.618S+1)}$$

Using this normalized form and the above equation, the values for the resistors and capacitors are determined.

A summary of the pre-aliasing filter characteristics is given in Table 5-33 for both visual and infrared channels.

5.12.2.1.2 Results of Evaluation to Date. Selection of the operational amplifier in each filter element is the major consideration. Analysis determined the circuits necessary to maximize the visual channel bandwidth while holding the errors to less than one bit. The results are as follows:

(a) 10 v/μs slew rate (linear)

(b) 30 ppm/°C components

(c) 1-percent selection of filter capacitors and resistors

(d) $<$ 10 mw per stage

(e) Latching (zero power) relays

Testing of the circuit has revealed the selected amplifier (HA2700), while low in power, is quite nonlinear at frequencies above 20 kHz. In parallel, the discrete

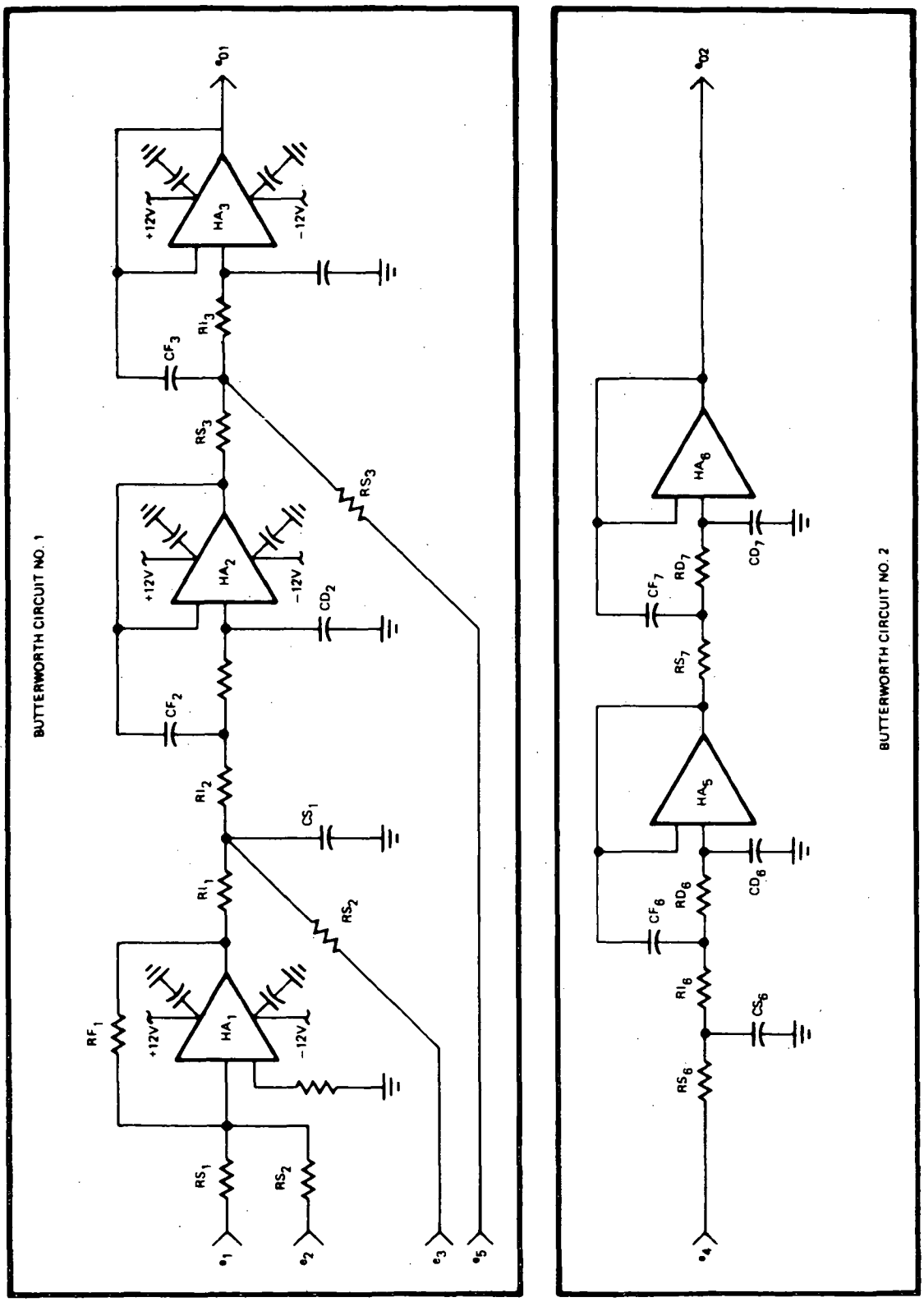

Figure 5-63. Configuration of the Five-Pole Butterworth Filter

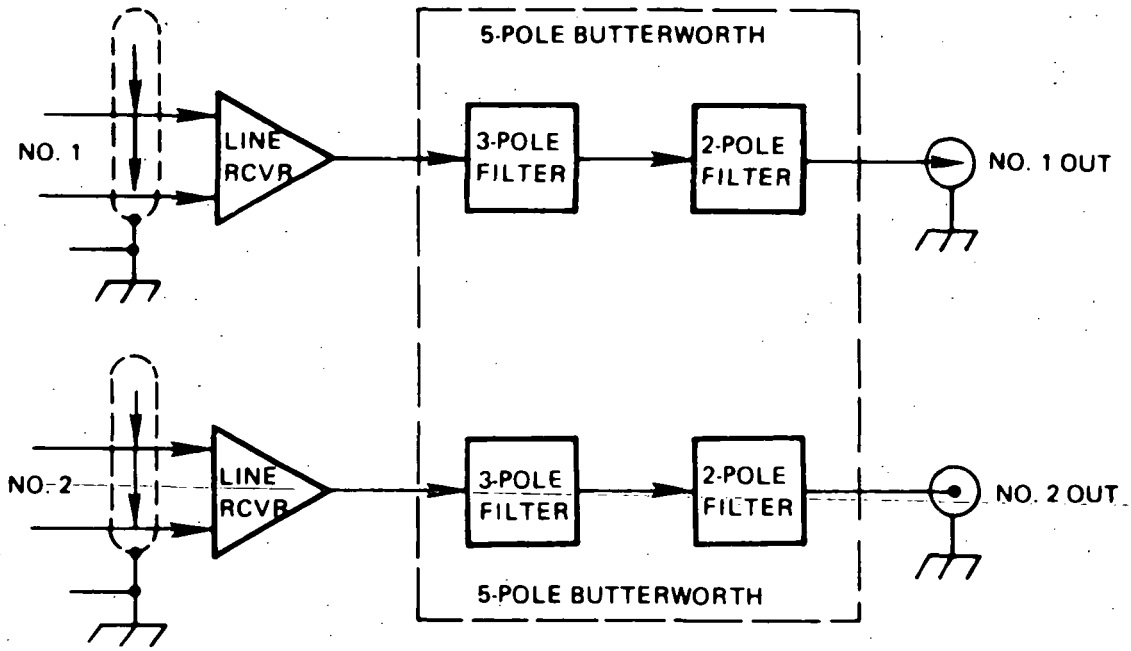

Figure 5-64. IR Channels

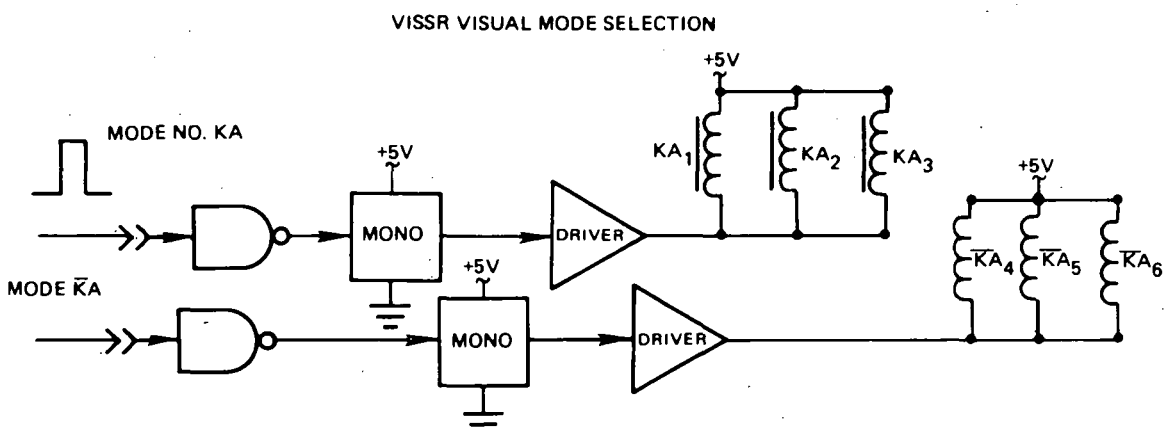

Figure 5-65. Model Select Driver Circuit

circuit is being moved ahead while other amplifiers (LM110) are being investigated. (This nonlinearity problem was verified per telephone conversation with the Harris semiconductor.) Temperature tests were made on this unit with no further degradation to report.

The circuit configuration for the infrared 27-kHz 5-pole filter is the same as the one for the visual channel. The HA2700 amplifier is quite adequate for this circuit.

Table 5-33

Summary of Pre-Sampling Filter Characteristics

Parameter	Visible	IR
Input impedance differential	>100 ohms res & <50 pf cap	>100 ohms res <50 pf cap
Signal	0 v to 5 v dc & 2.5 v pp ac	0 to 5 v dc & 2.5 v pp ac
Gain	1	1
Gain over temp	1 ±0.6 percent	1 ±0.6 percent
Pole locations Over temp (circle ABT location)	Butterworth 5-pole ±1 percent	Butterworth 5-pole ±1 percent
Bandwidth (-3 db) large signal	dc to 210 kHz	dc to 26 kHz
Output resistance	<50 ohms res	<50 ohms res
Power	<1000 mw	<200 mw
Noise (input terminated no signal)	<2 mv RMS in bandwidth	<2 mv RMS in bandwidth TTL
Mode selection Mode selection Interface	Latching relays TTL	Latching relays
DC offset over temp	0 ±10 mv	0 ±10 mv

5.12.2.2 Multiplexer

The analog video multiplexer sequentially combines the eight visual video signals into a sampled video stream for conversion by one of the two redundant nonlinear, 6-bit, A/D converters. Similarly, the multiplexer sequentially combines the two IR signals for one of the two redundant 8-bit linear A/D converters.

5.12.2.2.1 General Description. Refer to the block diagram of the analog multiplexer, Figure 5-66. The visual channels are divided into odd and even groups. A four-input multiplexer is normally assigned to each group, that is, the unit numbered "4 V-1" multiplexes visual inputs 1, 3, 5, and 7, and "4 V-2" the even inputs. The outputs of "4 V-1" and 4 V-2" are connected to two input multiplexers "2 V-1" and "2 V-2". The redundancy control signal energizes only one of these two input multiplexers corresponding to the nonlinear A/D converter currently in use.

The four-input multiplexers also combine a track-and-hold function. In mode 1 (28 Mb/sec and all eight visual signals utilized) one multiplexer is tracking and stabilizing while the other is holding and outputting through the two-input multiplexer to the A/D converter. On the next video conversion, the roles are reversed. Thus the four-input multiplexer has one word time (approximately 214 nanoseconds) to stabilize to the required accuracy of 0.1 percent. As will be seen, this timing remains the same in mode 2 as subsequently described (refer to Figure 5-67).

In mode 2, the data rate drops to 14 Mb/sec, and the even channels are no longer normally nultiplexed. The even-channel signals were previously combined linearly with their odd twins, as described in the section on the pre-aliasing filters. Therefore, the two-input miltiplexer in use does not commutate in mode 2.

The linear averaging function is accomplished in the pre-aliasing filter section, resulting in no change for the multiplexer.

The four SPDT video switches normally connect the inputs of "4 v-2" to the even-numbered channels. In the event of any malfunction affecting multiplexer "4 v-1", the switches are optionally thrown to substitute "4 v-2" thus maintaining 50-percent channel capability for mode 1 and full capability for modes 2, 3, and 4. The redundancy control to the multiplexers "2 v-1" and "2 v-2" allows the system to maintain full capability in the event of malfunction in either of these multiplexers or the related A/D converter.

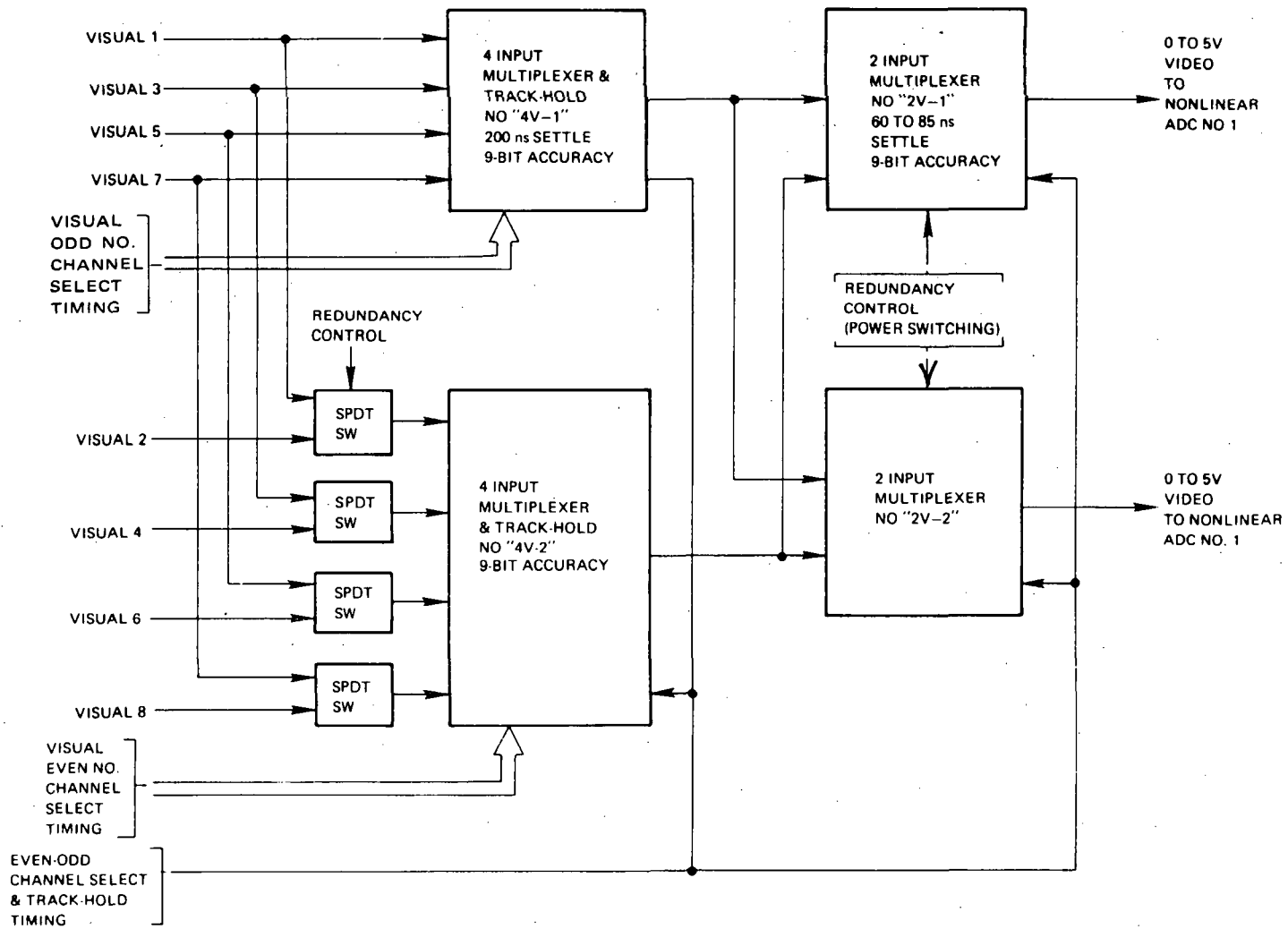

Figure 5-66. SMS VISSR MUX, Analog Multiplexer (Sheet 1 of 2)

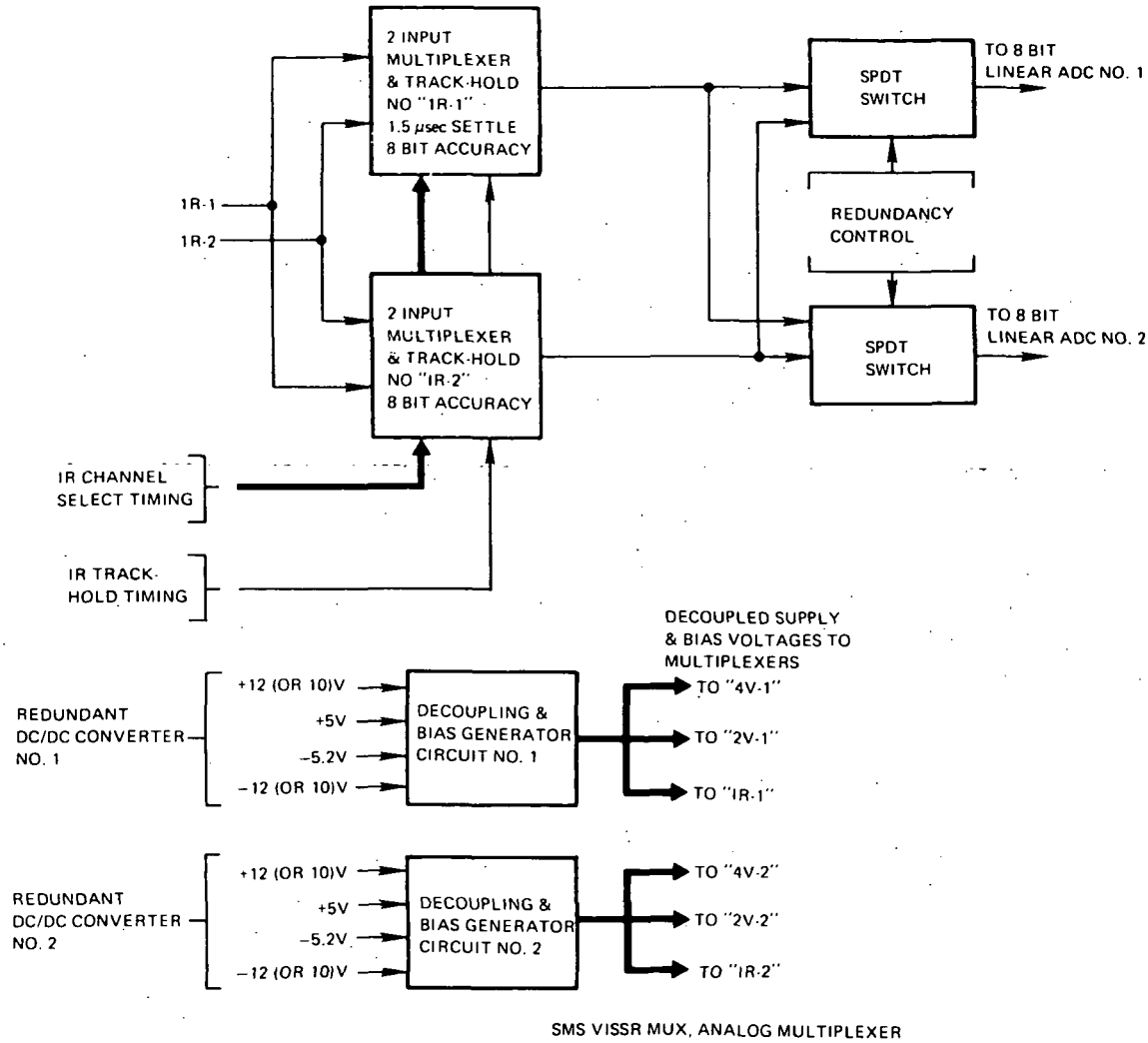

SMS VISSR MUX, ANALOG MULTIPLEXER

Figure 5-66. SMS VISSR MUX, Analog Multiplexer (Sheet 2 of 2)

All multiplexers employ voltage limiting in their analog inputs at approximately +5.8 v and -0.8 v so that erroneous out-of-range input signals do not cause failure on the remaining good channels. To prevent failure in subsequent units, in the event of malfunction, the multiplexer outputs are dc current limited.

The IR channels are handled by two parallel, completely redundant two-input multiplexers and track-hold circuits, "IR-1" and "IR-2". Either is connected to either of the redundant 8-bit linear A/D converters by redundancy control signals applied to the SPDT switches. The IR conversion rate is 250 kHz and up to 1.5 μs is allocated for multiplexers "IR-1" and "IR-2" to stabilize. This is, of course, a relatively conventional speed and presents no difficulty in design.

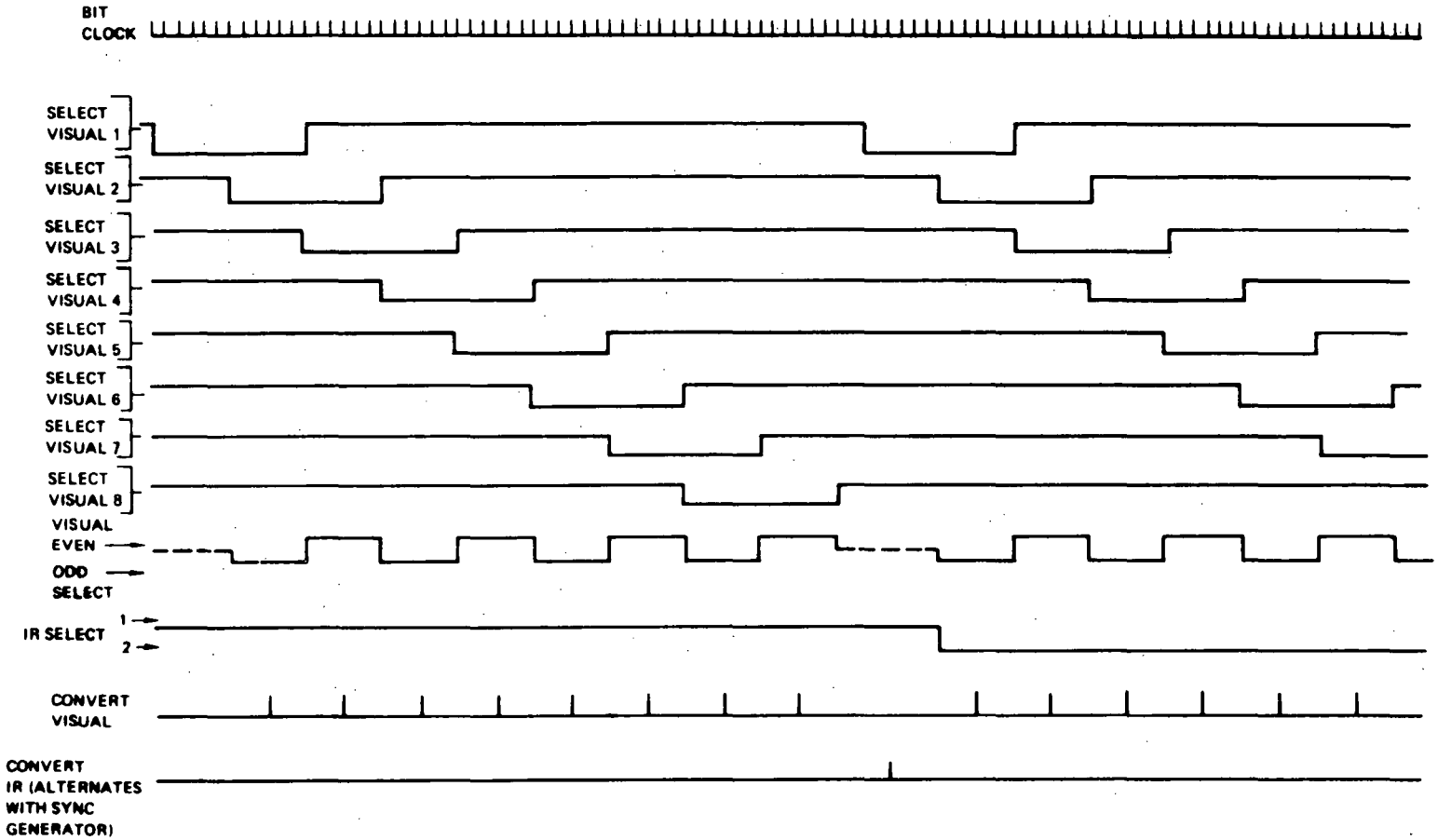

Figure 5-67. VISSR MUX, Timing, Mode, (Full Channels, 28 Mb/sec)

5.12.2.2.2 Results of Design and Evaluation to Date. Development of high-speed analog multiplexers has been undertaken for the SMS VISSR multiplexer. The speed and accuracy requirements are, in combination, approximately state-of-the-art for the visual channels. The sampling rate is 4.68 μs/sec and the system resolution reaches 10 mv out of 5.3 v. This is equivalent to a linear PCM system operating at 44 Mb/sec and 9-bit encoding. The SMS system, however, uses nonlinear encoding to reduce the link bandwidth via a 28 Mb/sec, 6-bit word format.

Experience with fast FET analog switches led to the rejection of this approach. Although FET's are inherently fast, they require typically 10 to 20-v minimum drive signals which in turn require complex driver circuits and excessive power consumption to provide the fast rise and fall switching signals. Further, large switching transients occur due to the charges injected into the collecting bus by the switching waveforms. These transients necessitate an additional trackhold amplifier.

Previous work with an active, feedback track-hold amplifier led to an extension of this approach into an active multiplexer and a combined multiplexer and track-hold. The original track-hold amplifier is shown in Figure 5-68. The block outline indicates an analog gate and a unity follower amplifier placed in the forward gain of the track-hold amplifier. Since these functions are dc stabilized by the loop gain, they are not chosen for either low-offset or long-term dc stability. This greatly widens the availability of fast circuit elements.

Referring to the circuit outline in Figure 5-70, Q1 and Q2 form a differential pair which is biased by the constant current source Q3. Another constant current source, Q4, provides nominally half the current of Q3 and is a load for Q2. Together with the output amplifier, FET Q6, this forms a unity gain amplifier. The circuit operation is converted to holding by causing Q5 to conduct which simultaneously cuts off both Q3 and Q4, and therefore effects the gating function.

The active track-hold amplifier preceding can readily be extended to gated multiple inputs by steering the current from Q3 (Figure 5-68) to multiple differential transistor pairs connected in parallel except for the several inputs (see Figure 5-69). The number of inputs which may be so connected is principally limited by the additive effects of leakage on the holding capacitor (C_{hold}). Power consumption is independent of the number of inputs except, of course, for the control logic. This approach has been chosen for the combined analog multiplexer and track-hold functions in the VISSR MUX. These circuit approaches to multiplexing and its combination with track and hold represent new circuit technologies.

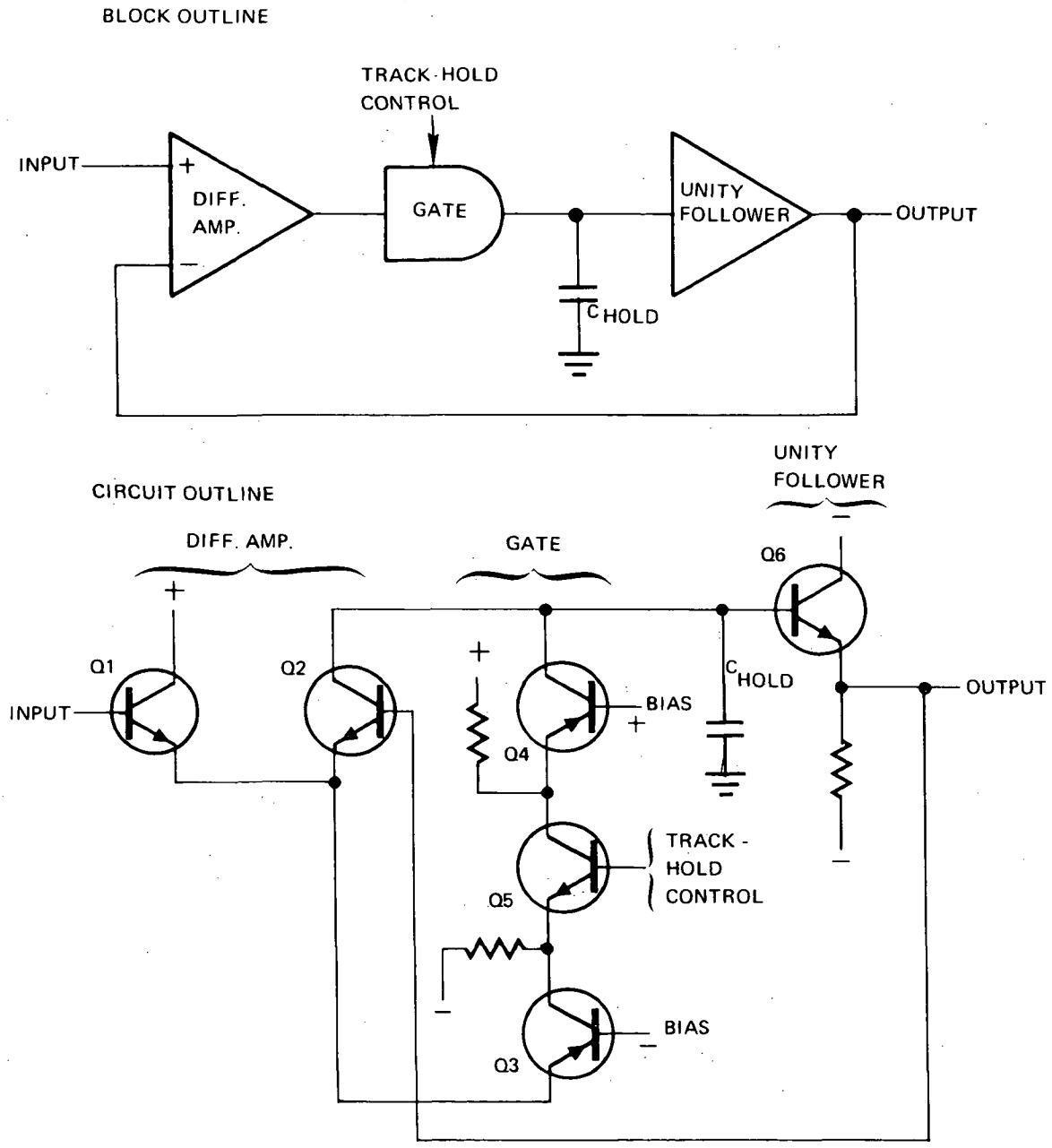

Figure 5-68. Active Track-Hold Amplifier

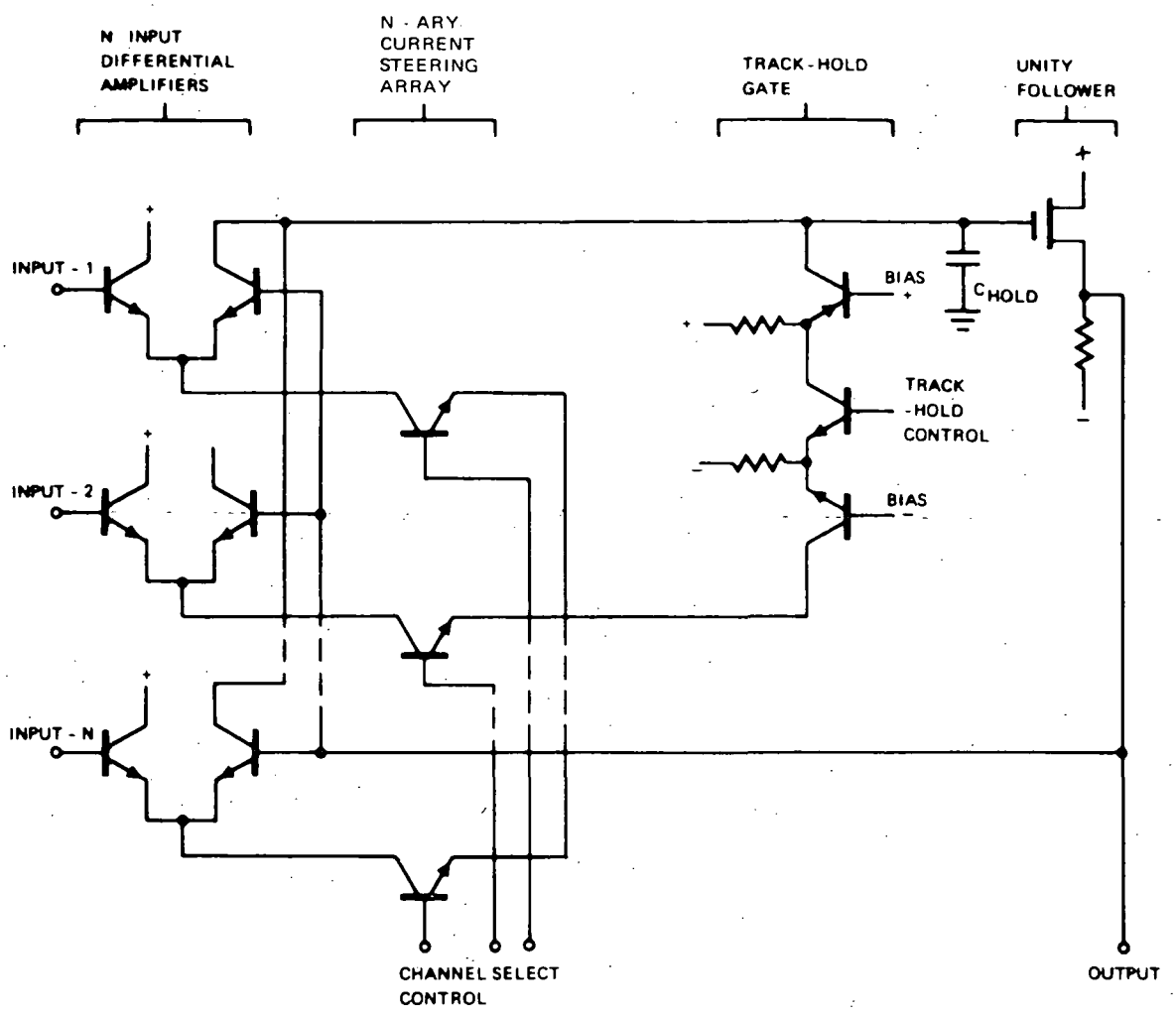

Figure 5-69. Circuit Outline of Gated N-Input Amplifier and Track-Hold

The first design of the two-channel IR multiplexer and sample-hold has been built and is being evaluated. The total IR sample period is 4 μsec. Of this, 2.5 μsec has been assigned to the 8-bit A/D converter and 1.5 μsec to the multiplexer. The system resolution is 8 bits, i.e., about 20 mv in 5.3 v. Since the speed requirements are rather ordinary for this circuit, it employs conventional circuit components and physical layout rather than ultra-compact high-speed techniques. A small offset, approximately 15 mv, occurs during hold and is apparently due to unused charge at the 2N3811 differential-pair emitters.

A two-channel visual signal multiplexer is also under test. Since the speed requirements for this multiplexer are a great deal higher, i.e., it settles to about 5 mv in tp to 85 ns. The devices chosen necessarily have high-gain bandwidth and therefore usually sacrifice dc gain (beta). Since also the varying base currents in the various amplifiers, steering transistors, and constant current

sources cause dc drifts which are aggravated due to low beta, a balanced multiplexer approach is being evaluated (see Figure 5-70). In the balanced approach shown, if matched transistor pairs are used for Q1 and Q2, Q3 and Q4, Q7 and Q8, the effect of the base currents is greatly reduced and therefore wideband, low-capacitance devices are utilized. Only the base-current loss in Q9 remains significant. Also note that the open-loop response control capacitance, which was formerly concentrated in location C_1 as required for holding, is now split into C_1 and C_2. The latter works in conjunction with R_2. The advantage of this split is that since the voltage swing across C_2 is low, the slew rate is considerably improved.

Initial tests have not yet produced the desired settling time. The "turnaround" stage Q9 and the output stage Q10 appear to be contributing additional poles below the required closed-loop bandwidth and probably needs intensive investigation and possible redesign with some ultra-wideband (microwave) components. Note that both of the aforementioned stages are shown in simplified form. Each uses two transistors rather than the one shown. Another problem with the output stage occurs when, during downward slew into the required load of 60 pf, that Q10 cuts off and Q11 conducts. This causes the voltage across C_2 to change substantially and negates much of the advantage of the split described above. If Q11 is replaced by a resistor pull down, the power consumption of the multiplexer is increased inordinately.

5.12.2.3 A/D Converters

Several approaches to the design of both the 6-bit and 8-bit A/D converters were evaluated. The results of the evaluation show that a series-parallel 6-bit nonlinear A/D converter is optimum for the visual conversion process and that a lower-speed 8-bit cyclic A/D converter is the same for the infrared channels.

5.12.2.3.1 Visual Channel A/D Converter. The visual channel 6-bit nonlinear A/D converter element is illustrated in Figure 5-71. The output of the track-and-hold is applied to an eight-level quantizer. The quantizer is made up of 7 high-speed comparators with their thresholds set at nonlinear intervals. The outputs of the quantizer determine the three most significant lists as decoded by logic. In addition to the binary output, one out of eight possible logic signals is applied to a nonlinear A/D converter and also turns on one out of eight programmable-gain amplifiers. By biasing each programmable-gain amplifier with the lower threshold voltage, the residue is formed without the need of a separate D/A converter. The normalized residue of the 3-bit A/D converter is now fed to a linear 3-bit A/D converter which determines the least three significant bits.

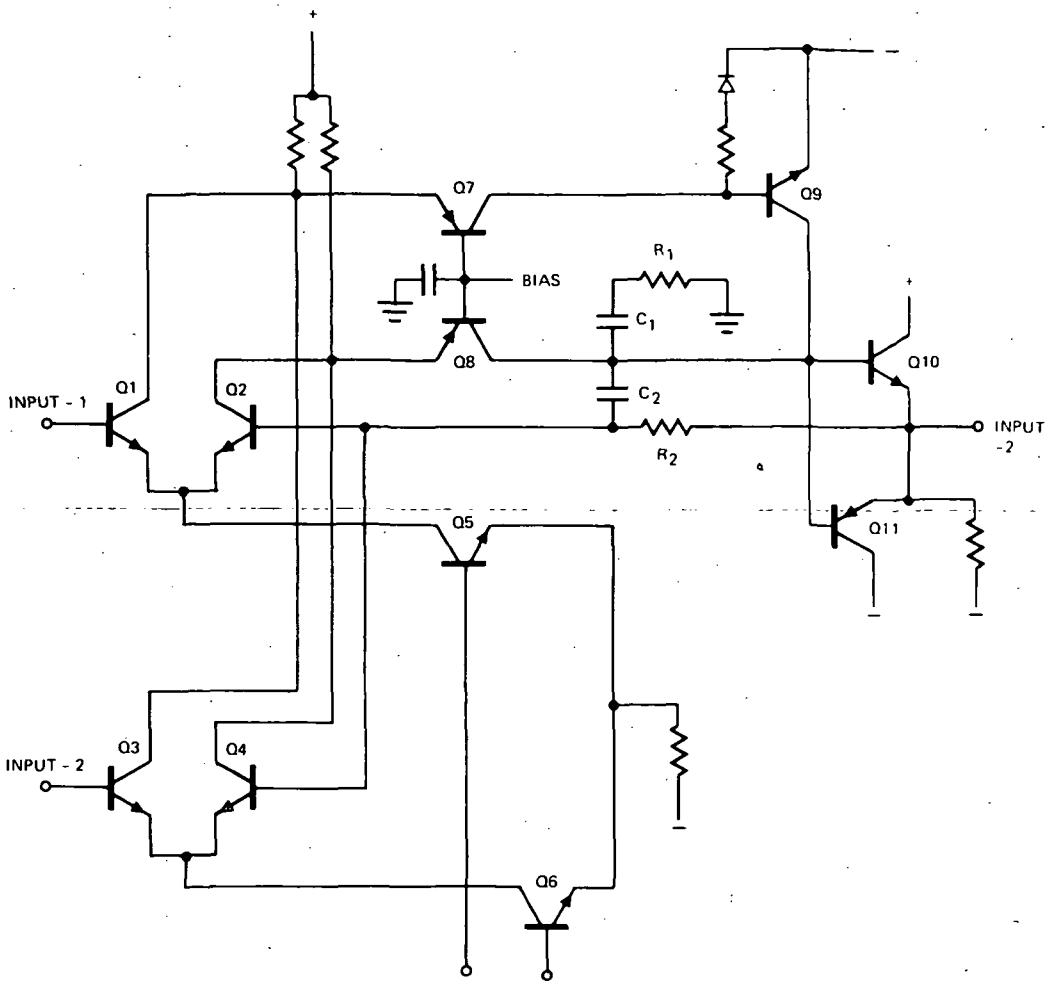

Figure 5-70. Circuit Outline of Two-Channel Visual Signal Analog Multiplexer

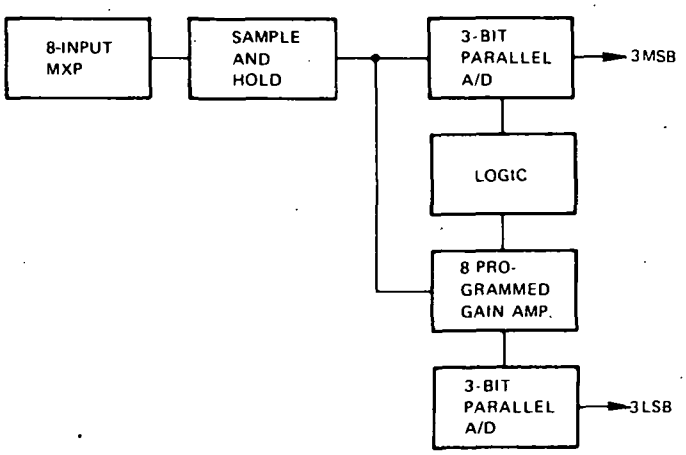

Figure 5-71. A 6-bit Nonlinear A/D Converter

The power dissipation of this element is currently 6 watts. This element completes a conversion in approximately 130 ns, which leaves 74 ns for the track and hold and the multiplexer.

5.12.2.3.2 Infrared Channel A/D Converter. The infrared channel 8-bit cyclic A/D converter is illustrated in Figure 5-72. A circuit diagram of a full-wave rectifier is included for completeness. The input voltage, etc., 1-v full scale, is converted into a current 0 to 40 ma full scale. The input current is compared to 20 ma, half of full scale. The polarity is determined (that is, the input current is determined to be greater or smaller than half of full scale); a logic 1 is provided if greater, and a logic 0 if smaller. The difference between the input current and half scale is full-wave rectified so that the difference, whether positive or negative, is made positive. The output of the first full-wave rectifier is compared to one-quarter full scale, the polarity is again determined, and the residue is again full-wave rectified. This process continues until the input has been quantized to 8-bit accuracy.

The A/D converter is comprised of eight full-wave rectifiers and eight polarity detectors. The logic output is in gray code, which may be easily converted to binary with eight exclusive-OR gates.

5.12.2.3.2.1 Full-Wave Rectifier Operation — The input current is subtracted from $I_F/2$. If the resulting current is directed into the test point TP ($I_{in} < I_F/2$), D_1 conducts, D_2 is cut off, a voltage $(I_{in} - I_F/2)\,R$ is generated across R_1. This same voltage is generated across R_2 in order to maintain the inverting and noninverting terminals of operational amplifier A at zero volts. For R_1 equal to R_2, a current is generated at the collector of Q_3 equal to $I_{in} - I_F$ and flows toward ground.

For the case where I_{in} is greater than $I_F/2$, the resulting difference flows out of the test point, D_1 is cut off, and D_2 is on. With D_1 off, the voltage at the noninverting input of A is zero volts; therefore, the voltage at the inverting input of A is also zero volts. No current flows through R_2 and the difference between I_{in} and $I_F/2$ flows out at the collector of Q_2 again towards ground. It may thus be seen that a full-wave rectification has been achieved. Polarity is determined by comparing the junction of both D_1 and D_2 to ground. A slight amount of current into TP makes D_1 conduct, which causes TP to be positive by 0.4 v with respect to ground. A small amount of current out of TP causes D_2 to conduct, making TP about 0.4 v negative with respect to ground. Q_1 and Q_2 compare the difference between TP and ground, and provide a logic output to storage logic.

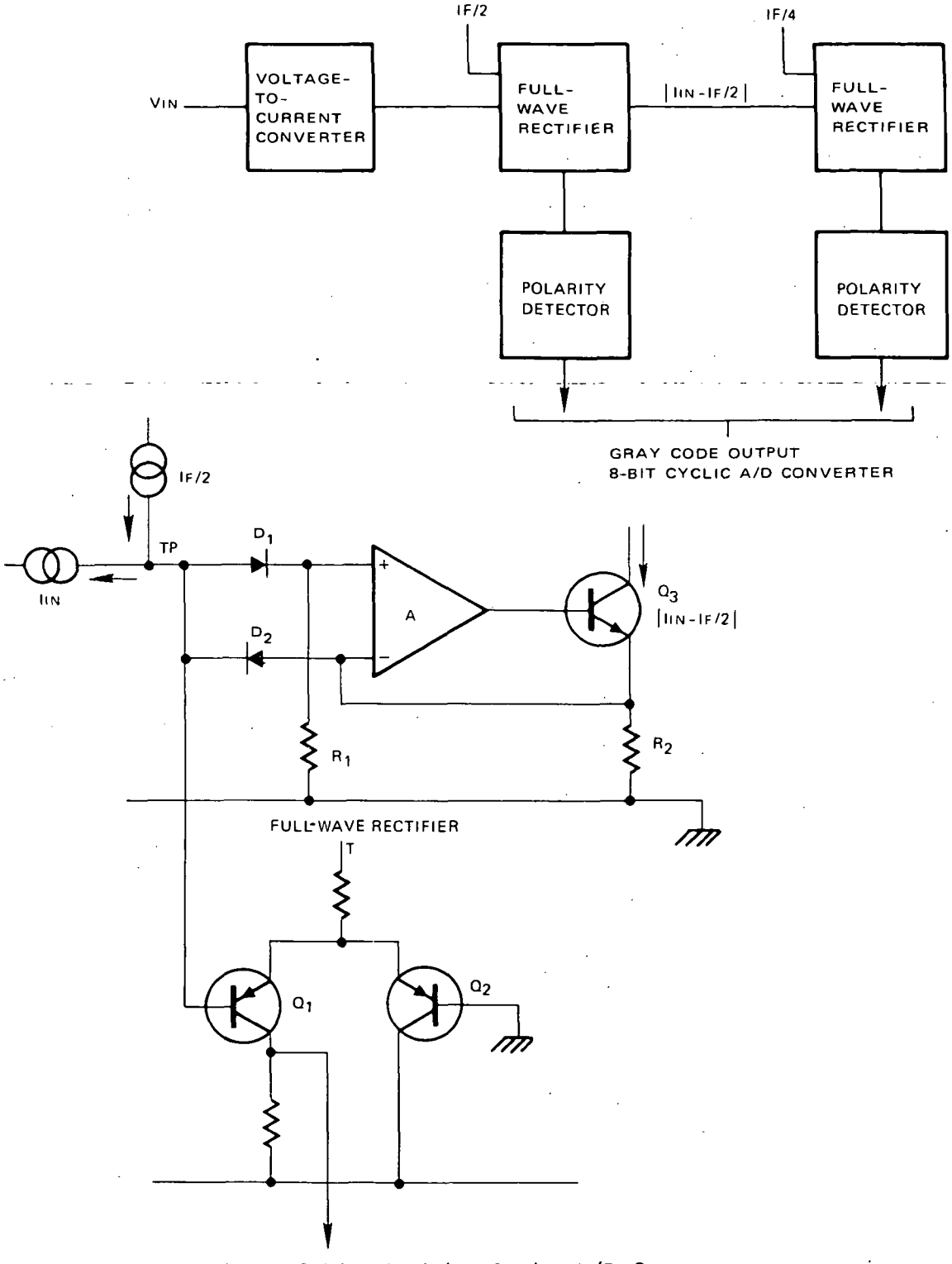

Figure 5-72. An 8-bit Cyclic A/D Converter

5.12.2.3.2.2 Frequency of Operation — The output of the A/D converter is strobed every 4 μs, although the A/D is capable of being operated at 500 kHz.

5.12.2.3.2.3 Power Dissipation — Dissipation is no greater than 2 watts.

5.12.2.3.3 Other Designs. A brief description of other A/D converter designs, which were discarded, is given below:

(a) Square-root companding followed by linear A/D conversion. There was a possibility the VISSR multiplexer could be simplified by incorporating a square-root compander in the visual channels and feeding the output to the IR A/D converter. A paper design was completed; however, the complexity of the design and the possible calibration and timing problems resulted in abandoning this approach.

(b) 2-bit parallel plus 6-bit linear cyclic. This design was developed for the IR channels. It was not known if an 8-bit cyclic converter could be designed with sufficient accuracy or stability for use in the SMS application. Therefore, a 2-bit parallel plus a 6-bit linear cyclic A/D converter was built. The 2-bit parallel conversion takes about 120 ns, and the 6-bit cyclic takes 60 to 70 ns. The power consumption of the 6-bit cyclic circuitry is 3.5 watts.

(c) 8-bit cyclic. An 8-bit cyclic A/D converter is being breadboarded using hi-rel equivalent parts. The results of the 6-bit unit indicates an 8-bit unit could be successfully designed. The estimated conversion time at 4.5 is 100 to 120 ns.

5.12.2.3.4 Logic. Signals generated consist of essentially ten consecutive time intervals which enable the individual channels, visual or IR, to be fed, first to a sample-and-hold and then to either the 6-bit nonlinear A/D or the 8-bit linear A/D. After each conversion, the linear output of the applicable A/D is stored and then checked out two bits at a time into a quadriphase encoder.

Power dissipation has been calculated at 9 watts.

5.12.3 CDA DEMODULATOR DESCRIPTION

5.12.3.1 Carrier Reconstruction Loop

One possible technique for carrier reconstruction is the times-four method in which the carrier frequency is multiplied times four and then phase lock is accomplished at this times-four frequency. The VCO frequency is then divided

by four and is used to provide the reference signal to demodulate the two quadrature data channels.

Another technique is called the Costas loop in which the demodulated data signals are used to derive the phase-lock-loop error signal. This technique has the advantage that the signal processing is performed at baseband. The availability of high quality integrated circuit analog multipliers permits the optimum mechanization of the Costas type carrier reconstruction loop.

The Costas loop mechanization is shown in Figures 5-73 and 5-74. The 70-MHz input signal is amplified and gain controlled and then applied to two double-balanced mixers used as phase detectors. Two signals in quadrature from the VCO are also applied to these two phase detectors. The outputs of the two phase detectors are the two demodulated data signals. These two signals are then applied to two multipliers at the appropriate levels so that one input to each of the multipliers is large compared to the other input. The high-level signal into one input to the multiplier causes the multiplier to perform as a coherent amplitude detector for the low-level input signal. The outputs of the two multipliers used as coherent amplitude detectors are summed to provide the correct phase-lock-loop error signal. This error signal is fed through the appropriate loop filter and thence to the VCO to close the phase-lock loop.

The outputs of these two multipliers are also applied to a third multiplier. This product is the coherent-carrier-frequency amplitude signal. This signal is then used as the input to the AGC amplifier to set the level of the 70-MHz carrier signal into the two input phase detectors, thereby closing the coherent AGC loop.

5.12.3.2 Bit Rate Synchronizer

The optimum technique for recovering the data is to use matched filters for synchronizing with the data and for making the data decisions. The optimum matched filter is the integrate and dump filter. The data is integrated for the full-bit period. The decision is then made as to whether it was a "1" or a "0" and then the integrator is dumped. Since the decision and the dump take a small amount of time, two integrate and dump circuits are used in the "handover" mode. While one circuit is integrating the data, the other circuit is in the decision (hold) and then dump mode. The dumping of the integrator removes any history of the previous data and therefore eliminates intersymbol interference.

The data is also integrated across the transition (in quadrature with the two data integrators) to provide a dc error voltage for the bit-rate phase-lock loop. Three integrate and dump circuits are required for this since the output of these integrators can only be used if there was a transition. The polarity of the error is determined by the polarity of the transition. The transition integrator is then

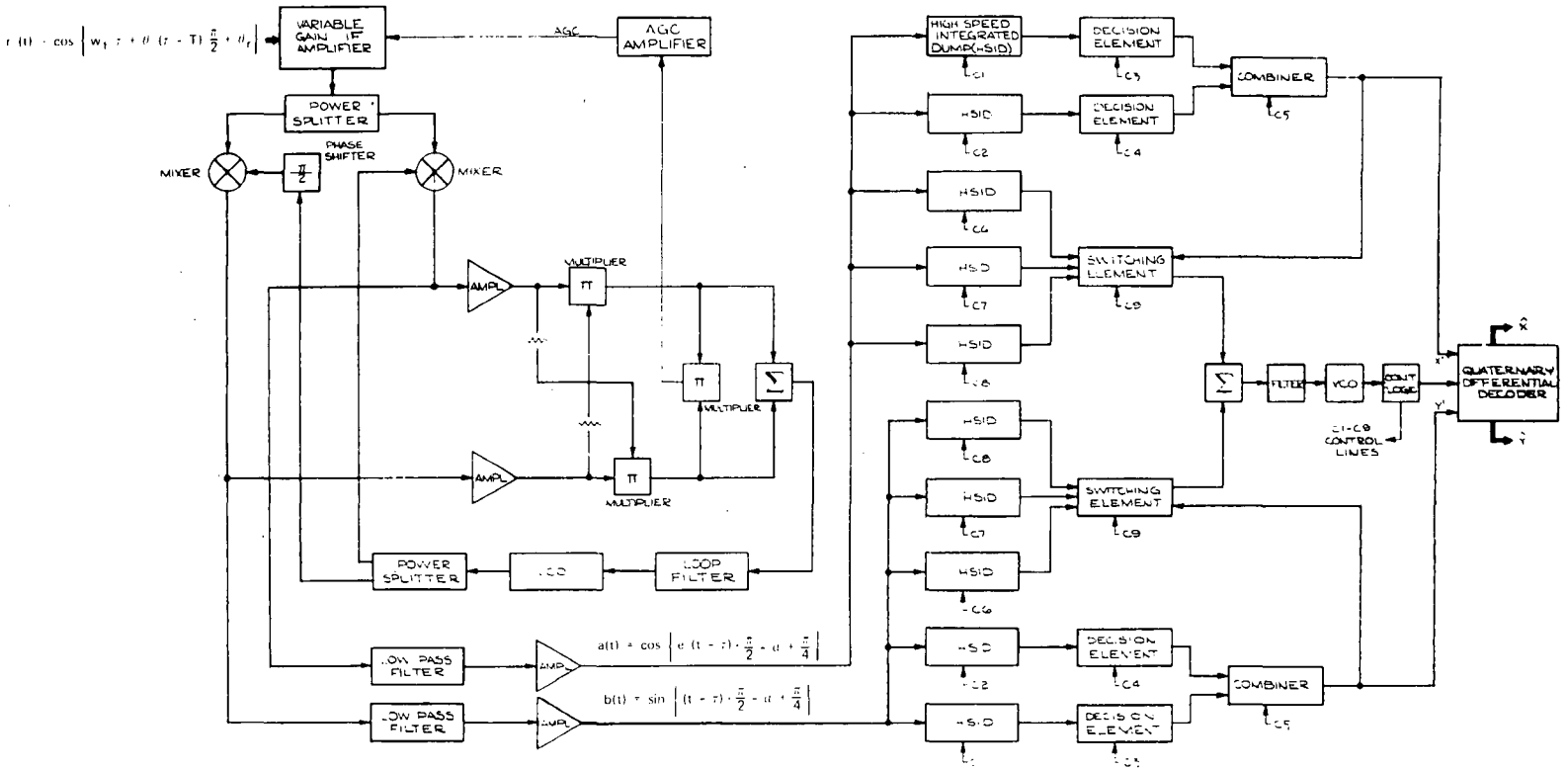

Figure 5-73. Quadriphase Demodulator Block Diagram

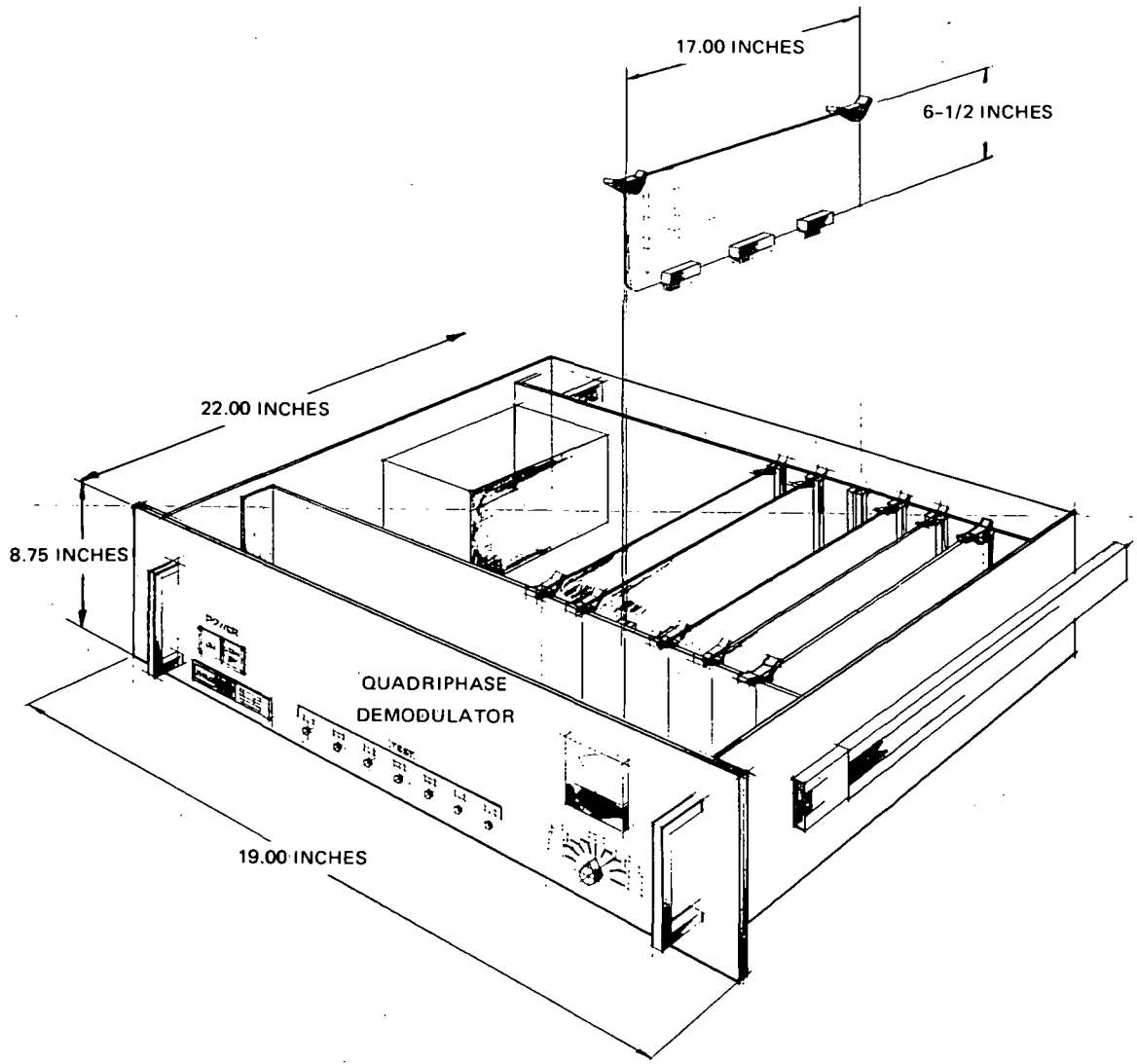

Figure 5-74. Quadriphase Demodulator Package

placed in the "hold" state until it is determined whether it can be used and the correct polarity can be determined. After the signal from an integrator has been transferred to the loop, the integrator is dumped and then used to integrate across another transition time.

Since there are two data channels, the dc error signals from the transition integrators are summed into the loop filter.

5.12.4 CDA DEMULTIPLEXER DESCRIPTION

The VISSR data demultiplexer accepts the outputs from the quadriphase demodulator which consists of two serial-bit streams ($\hat{X}$ and $\hat{Y}$), at 14-MHz clock and

a 28-MHz clock. It demultiplexes the bit streams and generates eight visual and two IR analog outputs. It also provides a digital display of any selected visual or IR data words. A self-check panel provides for checking the demultiplexer in the absence of an input signal.

5.12.4.1 Original Block Diagram Description

The block diagram of the original VISSR data demultiplexer is shown in Figure 5-75. The demultiplexer accepts the output from the quadriphase demodulator which is two bit streams $\hat{X}$ and $\hat{Y}$ and clocks the data into two four-bit shift registers at a 14-MHz rate. The 28-MHz and 14-MHz clock signals are also received from the quadriphase demodulator. The shift registers supply the data as parallel 6- or 8-bit words to eight 6-bit nonlinear D/A converters and two 8-bit linear D/A converters. It also supplies eight parallel bits to the frame-sync detector for detection of frame sync. Bit switches (or a program card) are used to select the proper sync word.

The 28-MHz clock is fed to counters which are controlled by an RS flip-flop. At the start of a frame the control flip-flop is in the "0" state which enables the divide-by-eight bit counter. The clock pulses are then counted, and after eight clock pulses, the bit counter output operates a differentiator which sets the RS flip-flop to the "1" state. The clock pulses then enable the divide-by-six counter and disable the divide-by-eight bit counter. The divide-by-six bit counter is used to count the six-bit words used by the visual channels. The bit counter drives a divide-by-eight word counter for counting the eight visual channels. At the end of the eighth count the word counter output operates a differentiator circuit which resets the RS flip-flop to the "0" state. The cycle then repeats.

The output of the eight word counter also drives a divide-by-four frame counter. The output of the frame counter is used to decode the two IR channels and the two sync channels.

The sync gating logic provides three operating modes for the sync, (a) search, (b) check, and (c) lock. A display light is provided to indicate which mode is operating.

(a) In the search mode the sync gate is open all the time so that the first correct sync word resets the counters.

(b) In the check mode the sync gate is open only at the time when the next sync word is expected. If the correct sync word is received the logic goes to the lock mode. If an incorrect sync word is received, the logic reverts to the search mode. Switching is provided to select the number of frames to be checked, one to three.

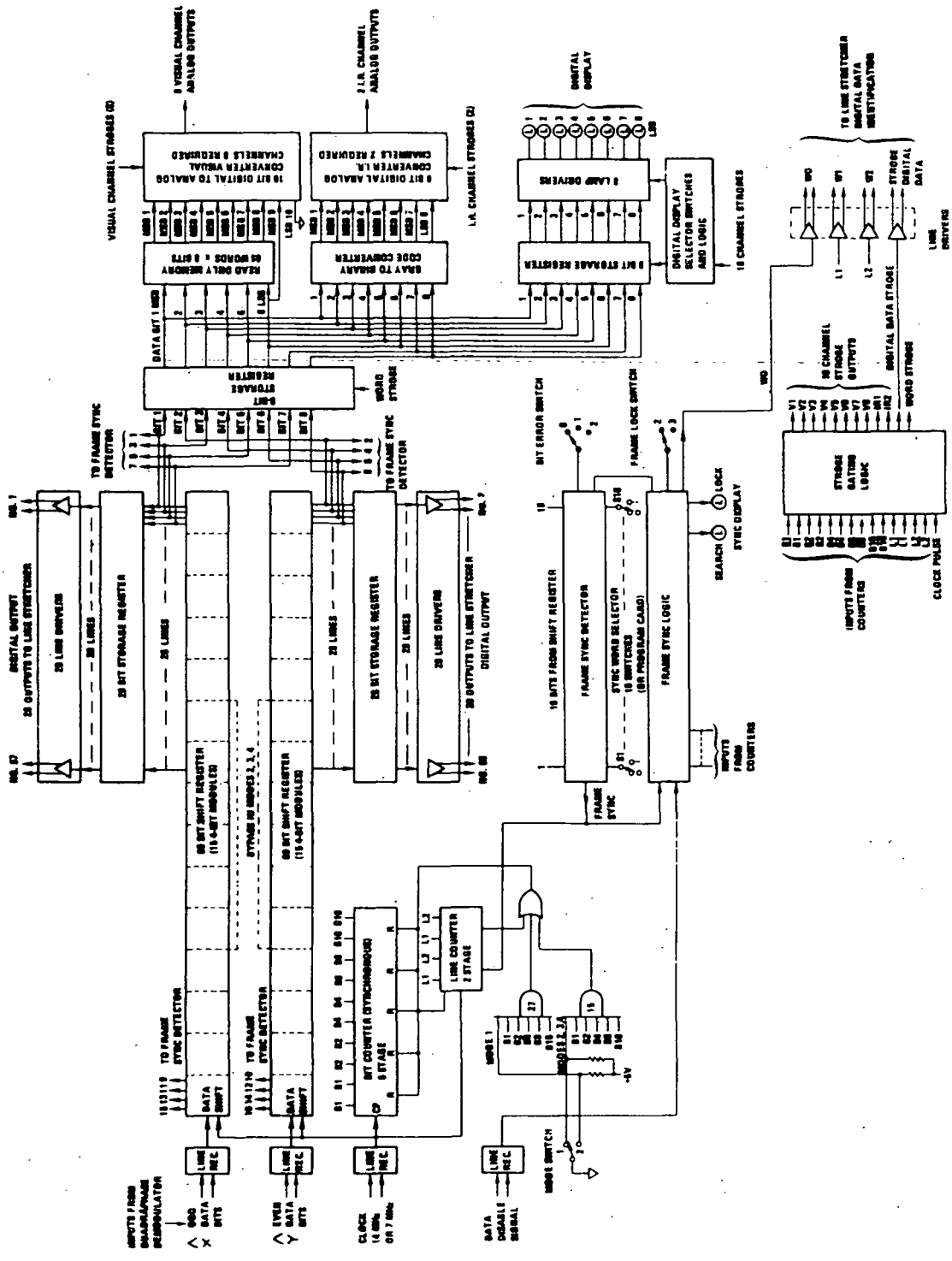

Figure 5-75. VISSR CDA Demultiplexer Block Diagram

(c) In the lock mode the sync gate is open only at the time when the next sync word is expected. If correct sync words are received, the logic stays in the lock mode. If several incorrect words are received, the logic reverts to the check mode. The number of incorrect words are selected from one to four. This mode provides for maintaining lock in the presence of noise which produces occasional sync errors.

Controls are also provided to allow 0 to 1 bit sync error in each of the three modes.

A self-check panel is provided to enable the PCM processor to be checked in the absence of a PCM input. Separate bit switches provide eight bits for the sync and IR channels and six bits for the visual channels. It also provides a 28-MHz clock and 14-MHz clock signal. The duty-cycle generator simulates the duty cycle of the VISSR data.

The selector and binary display consists of a switch for selecting any visual, IR, or sync channel, and eight-bit indicator lights. This is used primarily for trouble-shooting.

5.12.4.2 Description of Improved Version of CDA Demultiplexer

Additional analysis revealed that some modifications to the CDA demultiplexer yields an improved design. Also the requirements of the line stretcher were taken into consideration.

Figures 5-76 and 5-77 show the two frame formats for the two bit rates. The data in each output for the four modes is contained in Figure 5-78.

Because of the dual-bit rate, the counter was redesigned. The count rate was also reduced to half the data rate becuase of the way the data is received from the quadriphase demodulator. At the 28-Mb/sec bit rate the clock is 14kHz. At the 14-Mb/sec bit rate, the clock is 7kHz. The revised counter section consists of a five section synchronous bit counter followed by a two section synchronous frame counter.

In mode 1 the bit counter divides by 28 which at 2 bits per count equals 56 bits per line. In mode 2 the bit counter divides by 16 which at 2 bits per count equals 32 bits per line. The line counter divides by four in mode 2. The frame sync is used to reset both the bit counter and line counter.

Because of the necessity for 56 parallel bits to the line stretcher, the shift register was lengthened. Since the two sync words of eight bits each are reported

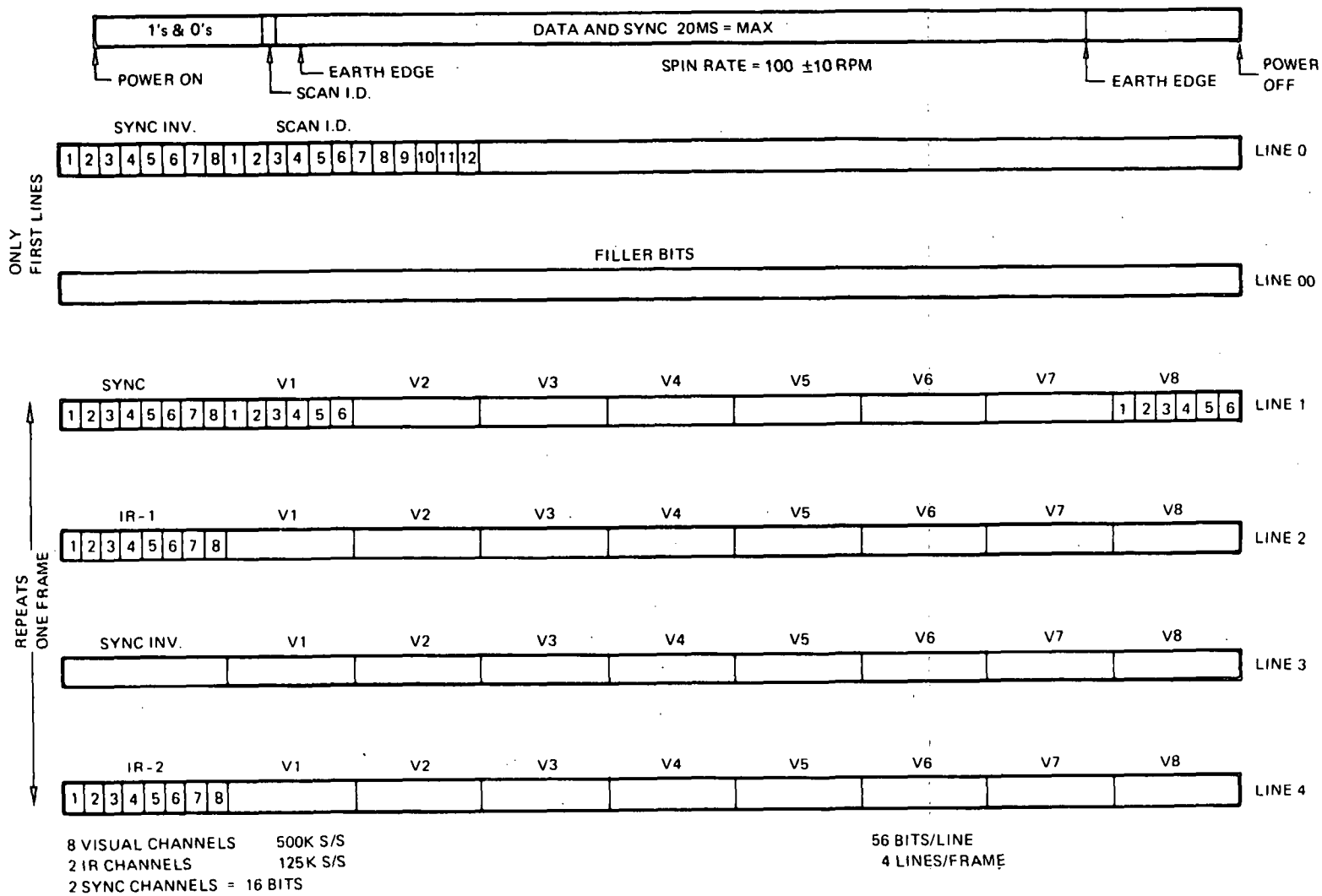

Figure 5-76. A 28-Mb/sec VISSR PCM Data Format

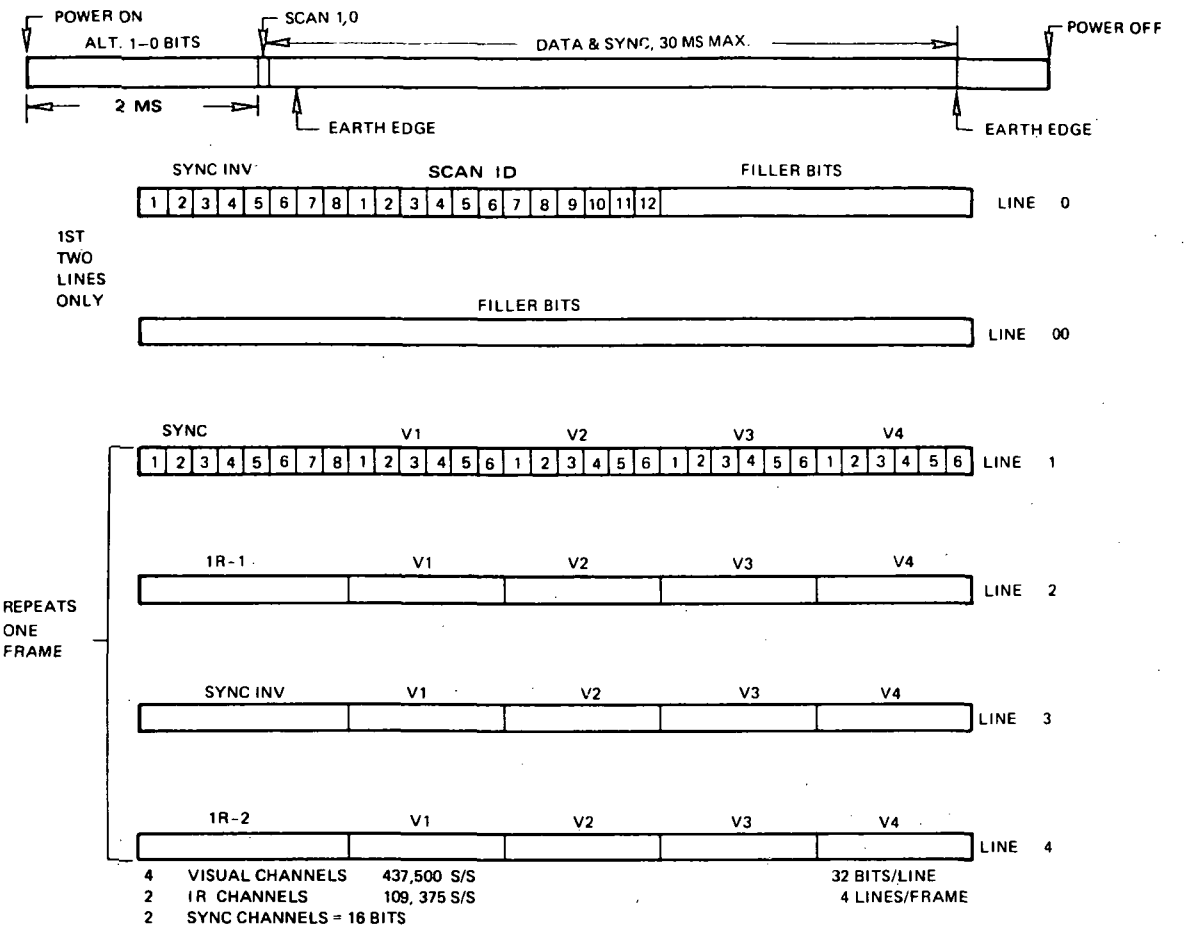

Figure 5-77. 14-Mb/sec VISSR PCM Data Format

by two lines, it was decided to lengthen the shift register so that both sync words are stored in the shift register. Then both words (16 bits) are used to detect initial sync and frame sync. Since the scan identification appears only once per earth scan just after the 1-0 pattern and before the regular data frame begins, it is vital that a very positive sync detector is used to acquire sync the first time it appears.

The shift register consists of 30 four-bit shift registers of two parallel registers 60 bits long, one containing the $\hat{X}$ bits and the other containing the $\hat{Y}$ bits from the quadriphase demodulator. The parallel storage registers consists of 14 four-bit shift registers containing 56 bits from one line of the frame. The storage registers drive line drivers for transmission of data to the remote line stretcher.

The frame sync detector consists of 16 exclusive NOR gates, 16 identical resistors and a comparator. When all 16 bits correspond to the sync pattern,

MODE 1	V1 thru V8 all separate
	1R1 and 1R2 separate
	28 Mb/sec
MODE 2	V1 thru V4
	V1 = sensors 1 and 2
	V2 = sensors 3 and 4
	V3 = sensors 5 and 6
	V4 = sensors 7 and 8
	1R1 and 1R2 separate
	14 Mb/sec

Figure 5-78. Channel Information for Each Mode

the maximum output voltage is developed with a correspondingly smaller output for each bit in error. A selector switch provides for setting the comparator to accept 0, 1 or 2-bit errors. The sync pattern is programmed manually by switches, or by a program card, or fixed wired. The method has not been selected at this time.

After initial sync acquisition the comparator is gated to only look for sync at the appropriate time.

There are two sync modes as opposed to the three initially described. This was chosen due to the use of 16 sync bits rather than 8 as originally planned. The sync logic has two modes: (1) search and (2) lock.

The "lock" light is on if sync lock occurs within 32 μs (four frames) after the scan ID, and sync lock is not lost during the scan period (30 ms).

The "search" light is on if the sync is lost and the logic reverts to search any time between 32 μs and 30 ms after scan ID; or if no scan ID occurs within a 1-second period. A frame-lock switch selects 2 or 3 frames. If the sync signal is lost for 2 or 3 frames, sync lock is maintained; thereafter sync reverts to search. In the search mode the sync gate is open all the time. After the first 16-bit sync word is received, the sync detector is gated to look for sync only from one bit before to one bit after normal sync time. This prevents false sync patterns resetting the counters at the wrong time, which occurs if the data at some time produces a pattern which duplicates the sync pattern.

5.12.4.3 Eight-Bit Linear D/A Conversion

The two IR channels use the linear D/A converter illustrated in Figure 5-79. The eight channel bits are stored in two 8-bit storage registers each time the channel word appears in the frame, and the registers are updated at the IR sampling rate (125,000 samples per second). Storage register No. 1 stores the current word, and storage register No. 2 stores the previous word. Each of the two storage registers drives an associated linear D/A converter which provides an output of 0 to 5 volts. The D/A converter outputs are step functions which change once every sample period. To implement the first order hold function, the output of D/A converter No. 1, the current value V_i and the output of D/A converter No. 2, and the previous value V_{i-1} are applied to the integration and weighting circuit. The functions $K (V_i - V_{i-1})$ and the current value V_i are summed and applied to the low-pass filter. $K = 0.3/\Delta\tau$, and $\Delta\tau$ starts at zero every sample strobe pulse. The low-pass filter is a Butterworth type with 5 poles and has a cut-off frequency of 30 kHz. The mode switching provides for summing both IR channels together.

The IR channels use a cyclic (or Gray) code of eight bits. A circuit for conversion of this code to straight binary is required before converting the data to an analog output. Such a circuit is shown in Figure 5-80. It requires seven exclusive OR gates which would require two DIP integrated circuits.

5.12.4.4 Six-Bit Nonlinear D/A Conversion

The eight visual channels each use the six-bit nonlinear D/A converter illustrated in Figure 5-81. The D/A converter provides the first three most significant bits (eight intervals) in a nonlinear manner as shown in the graph of Figure 5-82. The remaining three bits are encoded in a linear manner in one of the eight applicable intervals. This matches the encoding used in the spacecraft. The six bits are stored in two six-bit storage registers each time the channel word appears in the frame. The registers are updated at the visual channel sampling rate (500,000 samples per second). Storage register No. 1 stores the current word and storage register No. 2 stores the previous word. Each of the storage registers drives an associated nonlinear D/A converter which provides an output of 0 to 5 volts. The D/A outputs are step functions which change once every sample period.

To implement the first order hold function, the output of D/A converter No. 1, the current value V_i and the output of D/A converter No. 2, and the previous value V_{i-1} are applied to the integration and weighting circuit. The function $K (V_i - V_{i-1}) \tau$ and the current value V_i are summed and applied to the low-pass filter. K = between $0.3/\Delta\tau$ and $1.0/\Delta\tau$ (this will be determined later).

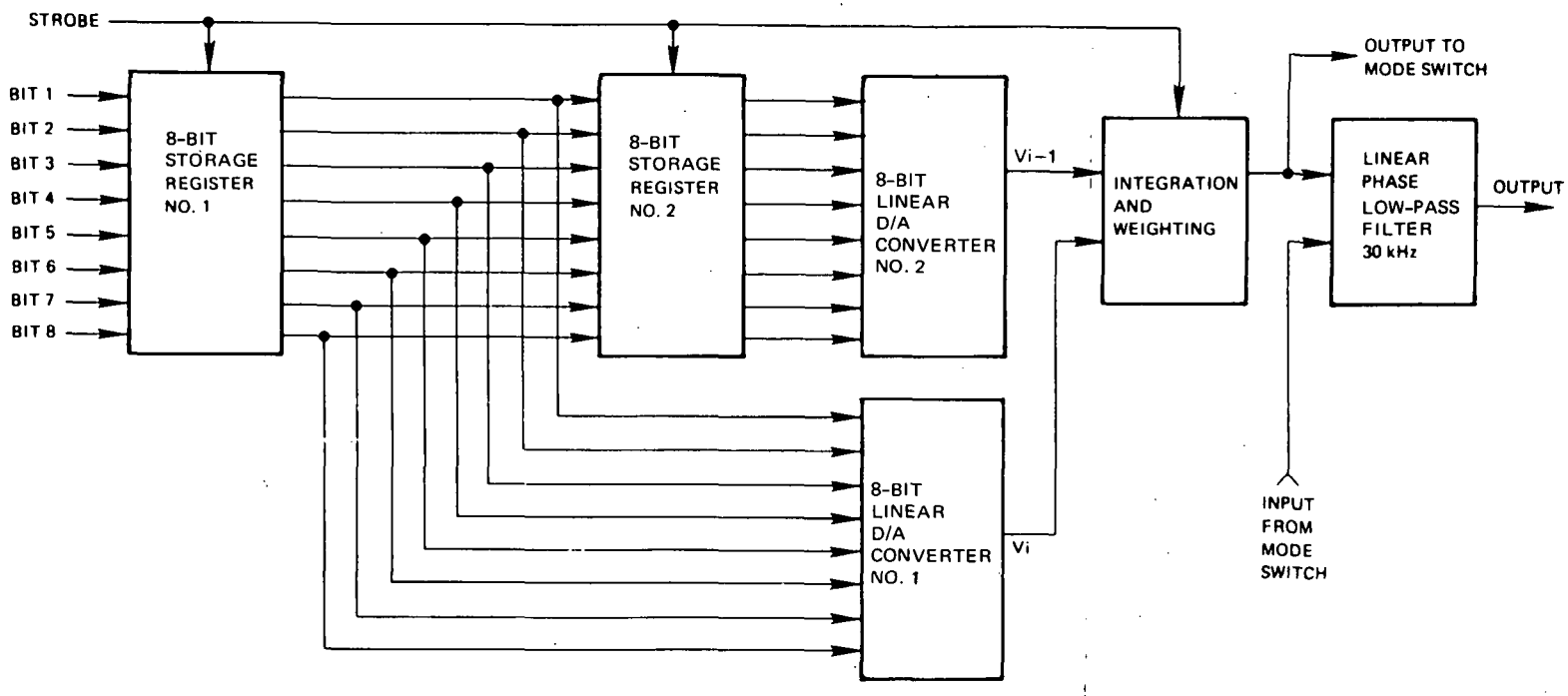

Figure 5-79. Block Diagram of 8-Bit Linear Digital-to-Analog Converter with First-Order Hold, Mode Switch, Connections and Low-Pass Filter

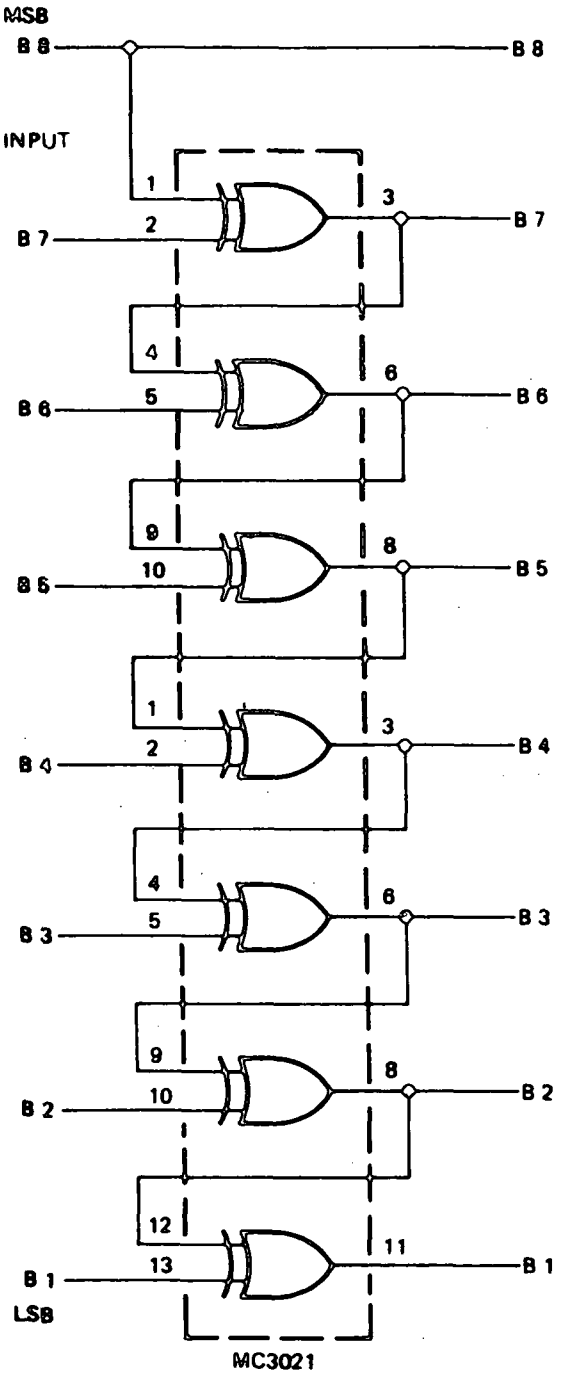

OUTPUT TO D/A CONVERTER

DELAY/GATE = 14ns

$$X \frac{7}{28ns}$$

"EXCLUSIVE OR" LOGIC

3 = 1 2 + 1 2

TRUTH TABLE	
1 2	3
1 1	0
1 0	1
0 1	1
0 0	0

RULES

A. MSB IS SAME IN BOTH CODES.
B. EACH SUCCEEDING BINARY BIT IS THE COMPLEMENT OF THE CORRESPONDING GRAY BIT IF THE PRECEDING BINARY BIT IS "1", OR THE SAME IF THE PRECEDING BINARY BIT IS A "0".

	TYPICAL BINARY	PATTERNS GRAY
0	0 0 0 0	0 0 0 0
1	0 0 0 1	0 0 0 1
2	0 0 1 0	0 0 1 1
3	0 0 1 1	0 0 1 0
4	0 1 0 0	0 1 1 0
5	0 1 0 1	0 1 1 1
6	0 1 1 0	0 1 0 1
7	0 1 1 1	0 1 0 0
8	1 0 0 0	1 1 0 0

Figure 5-80. Gray-Binary Code Converter

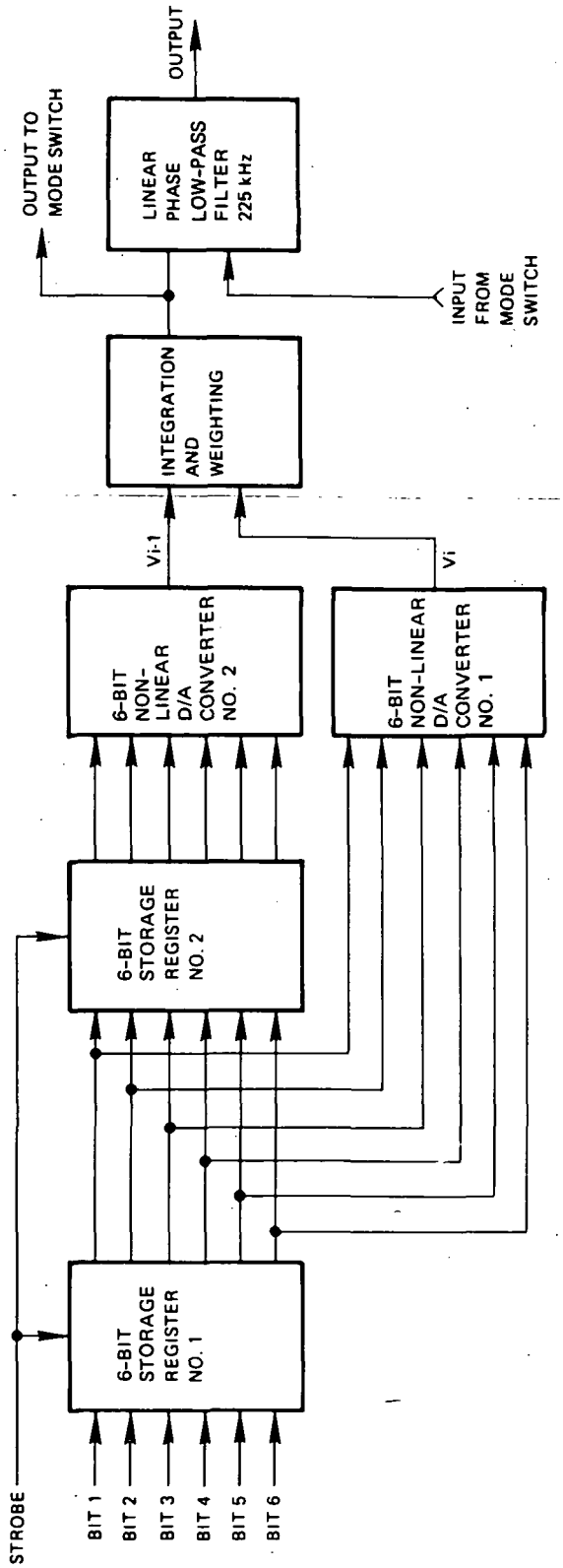

Figure 5-81. Block Diagram of 6-Bit Nonlinear Digital-to-Analog Converter with First-Order Hold, Mode Switch, Connections and Low-Pass Filter

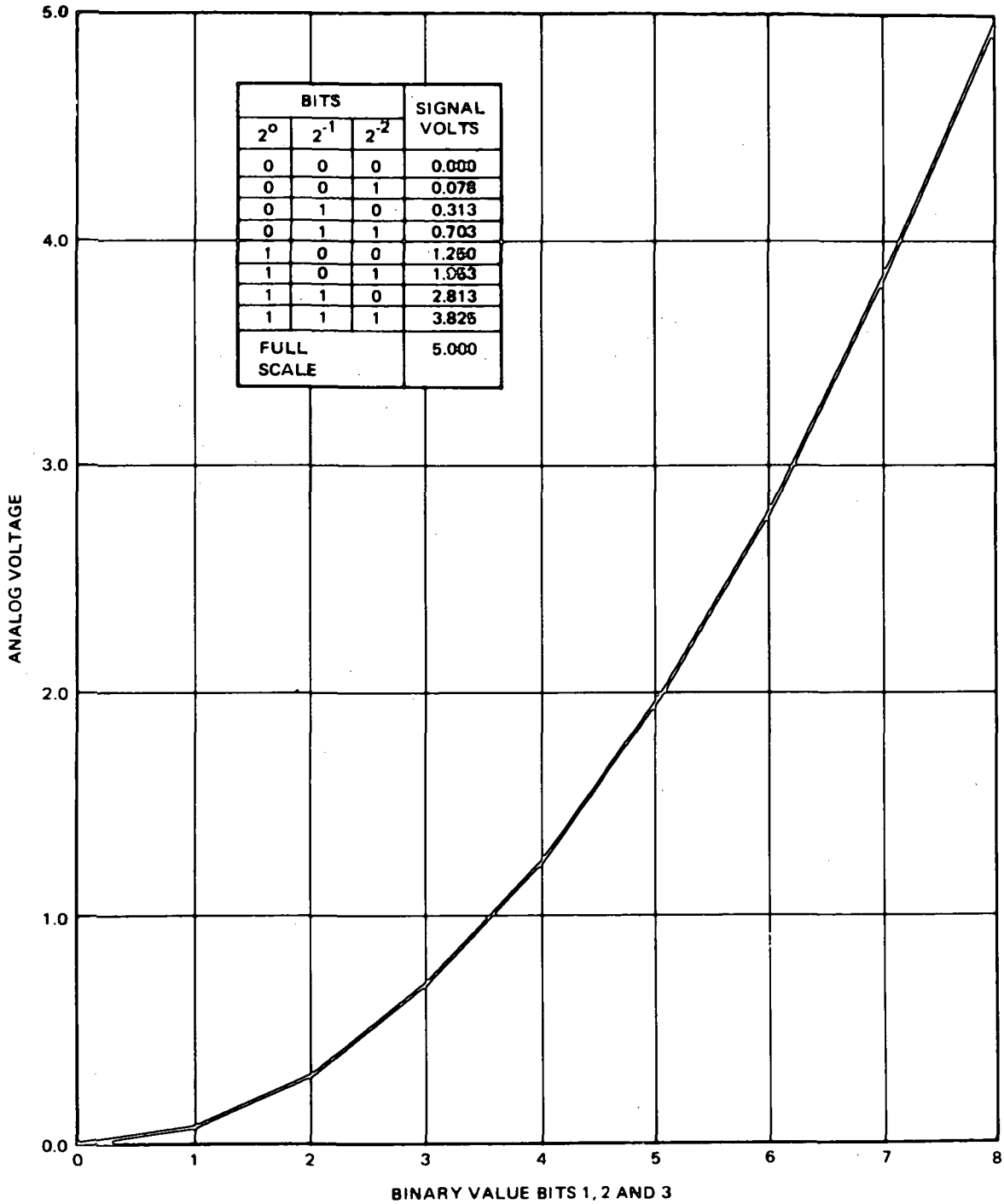

Figure 5-82. Nonlinear A/D and D/A Conversion

$\Delta\tau$ starts at zero every sample strobe pulse. The low-pass filter is a Butterworth type with 5 poles and a cut-off frequency of 225 kHz.

The nonlinear six-bit data was analyzed to discover if a method could be found to use a linear D/A converter. It was found that a nine-bit linear D/A converter provides exactly the right steps necessary for conversion. A read-only memory (ROM) provides the conversion from six bits to nine bits. Two different manufacturers (at least) make ROM's which are field programmable: signetics and monolithic memories. Figures 5-83 and 5-84 show how these two ROM's could implement the six-to-nine-bit conversion. Both ROM's have access times of about 50 ns. Since word time is 214 ns, this is adequate.

Several companies make ten-bit linear D/A converters which have fast settling times and appear adequate for this purpose. Figure 5-85 shows the D/A converters for the visual channel using linear ten-bit D/A converters and one ROM.

5.13 AEROSPACE GROUND EQUIPMENT (AGE)/BENCH TEST EQUIPMENT (BTE)

5.13.1 INTRODUCTION

Equipment required in support of the SMS program is generally categorized into two groups: AGE and BTE.[1] AGE is defined as that spacecraft equipment, both electrical and mechanical, which is required at facilities outside of Philco-Ford and all identical equipments regardless of where they are used. BTE consists of equipment utilized solely within Philco-Ford facilities and in many cases utilizes many items of Philco-Ford capital equipment. BTE includes tooling and fixtures, as well as the conventional bench test equipment.

5.13.2 GENERAL

The electrical AGE consists of the system test complex (STC), ABM squib simulator, ordinance circuit test set solar panel test set, and RF absorber. The system test complex is used for functional tests during satellite assembly, satellite acceptance tests, and satellite qualification tests. The STC consists of power and control equipment, telemetry and command subsystem equipment, communications subsystem equipment, and ADAC subsystem equipment. The complex performs the following functions; provides simulated solar array power to power the spacecraft, generates and applies signals and controls to the spacecraft through the AGE and charge and monitor connectors, monitors all functions on the AGE and charge and monitor connectors, provides simulated sources for the earth and sun sensors, provides system checkout capability of the entire spacecraft, and provides battery "trickle charge" through the charge and monitor connector.

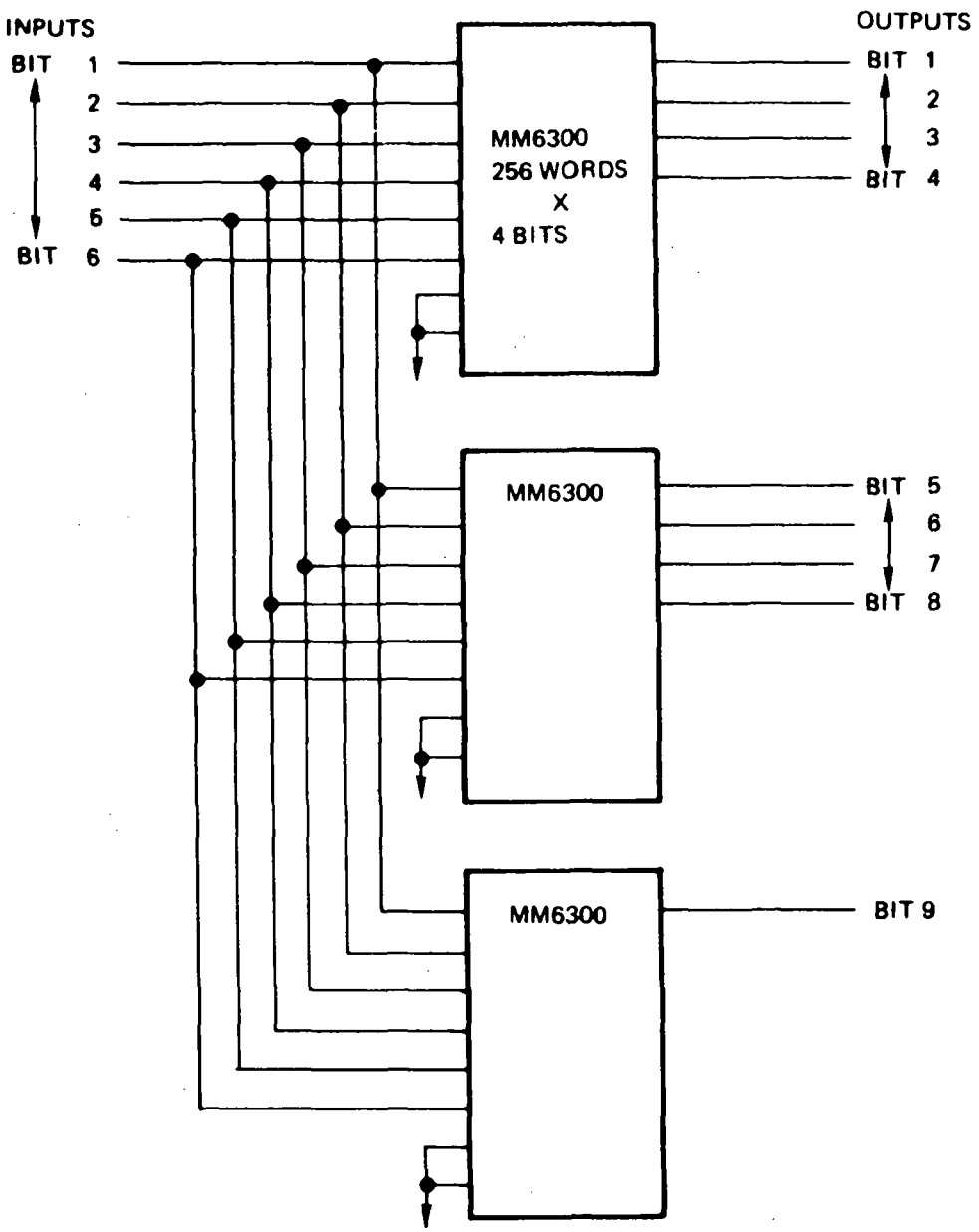

Figure 5-83. A 6-Bit-Nonlinear to 9-Bit-Linear Converter - Monolithic Memories Read-Only Memory

Figures 5-86 through 5-93 are included to illustrate the test setups and test facilities.

The ABM squib simulation (Figure 5-94) contains squib simulating devices which are used to verify the spacecraft system response to separation commands.

The ordnance circuit test set (Figure 5-95) is used to check for stray voltage in the ordnance circuits.

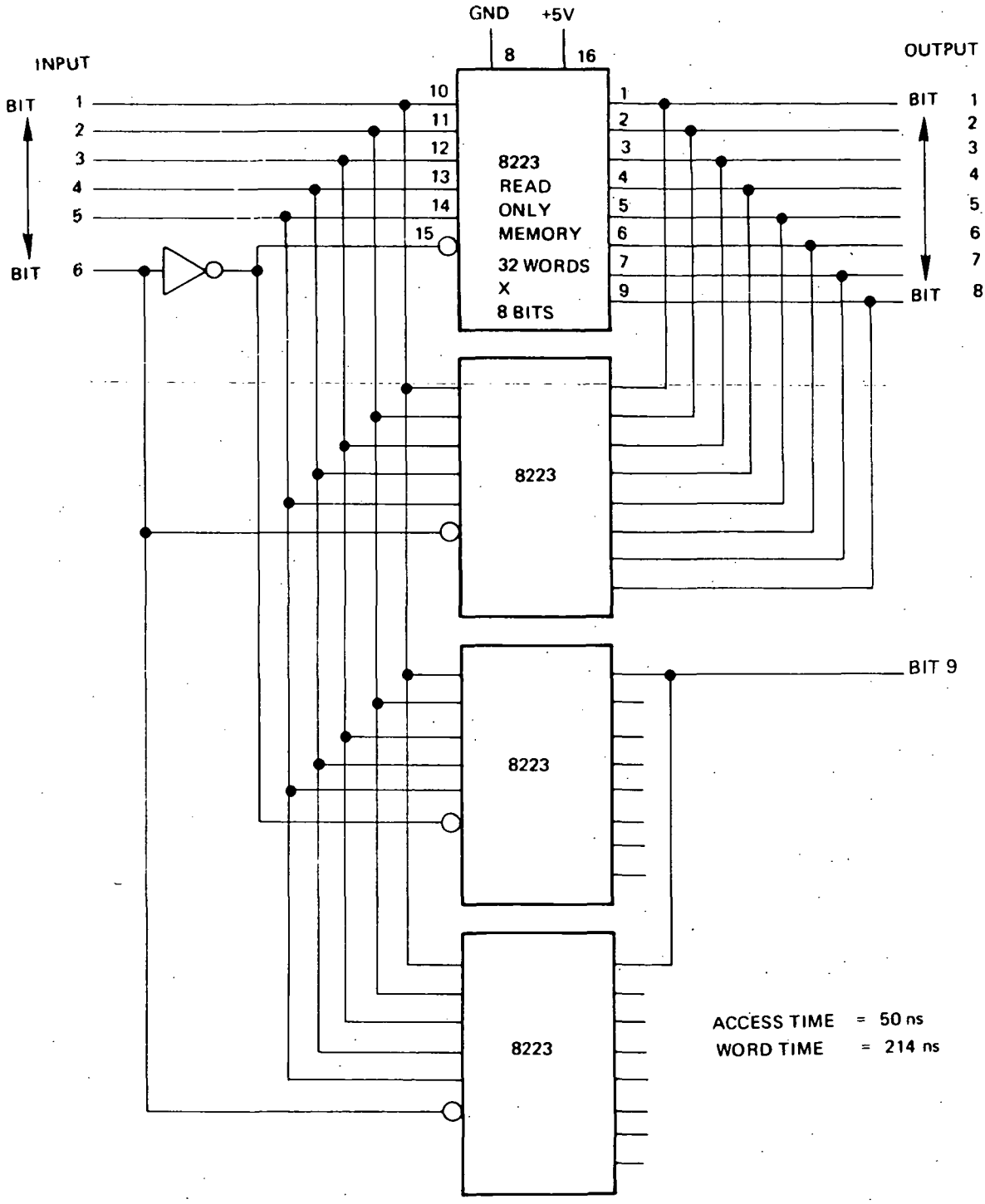

Figure 5-84. A 6-bit-Nonlinear to 9-bit Linear-Converter-Signetics Read-Only Memory

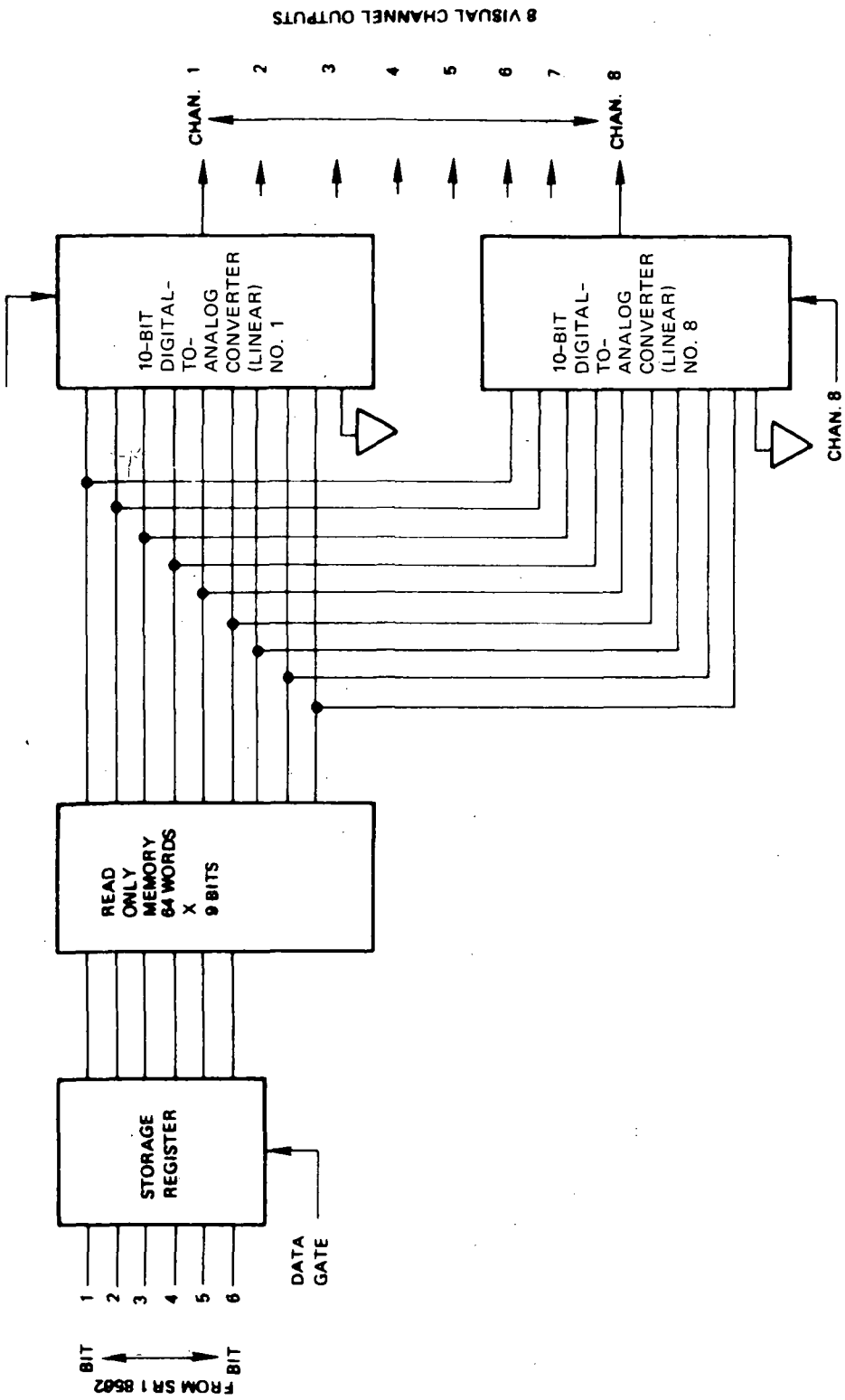

Figure 5-85. Visual Channel Digital-to-Analog Converters Using Field Programmable Read-Only Memory

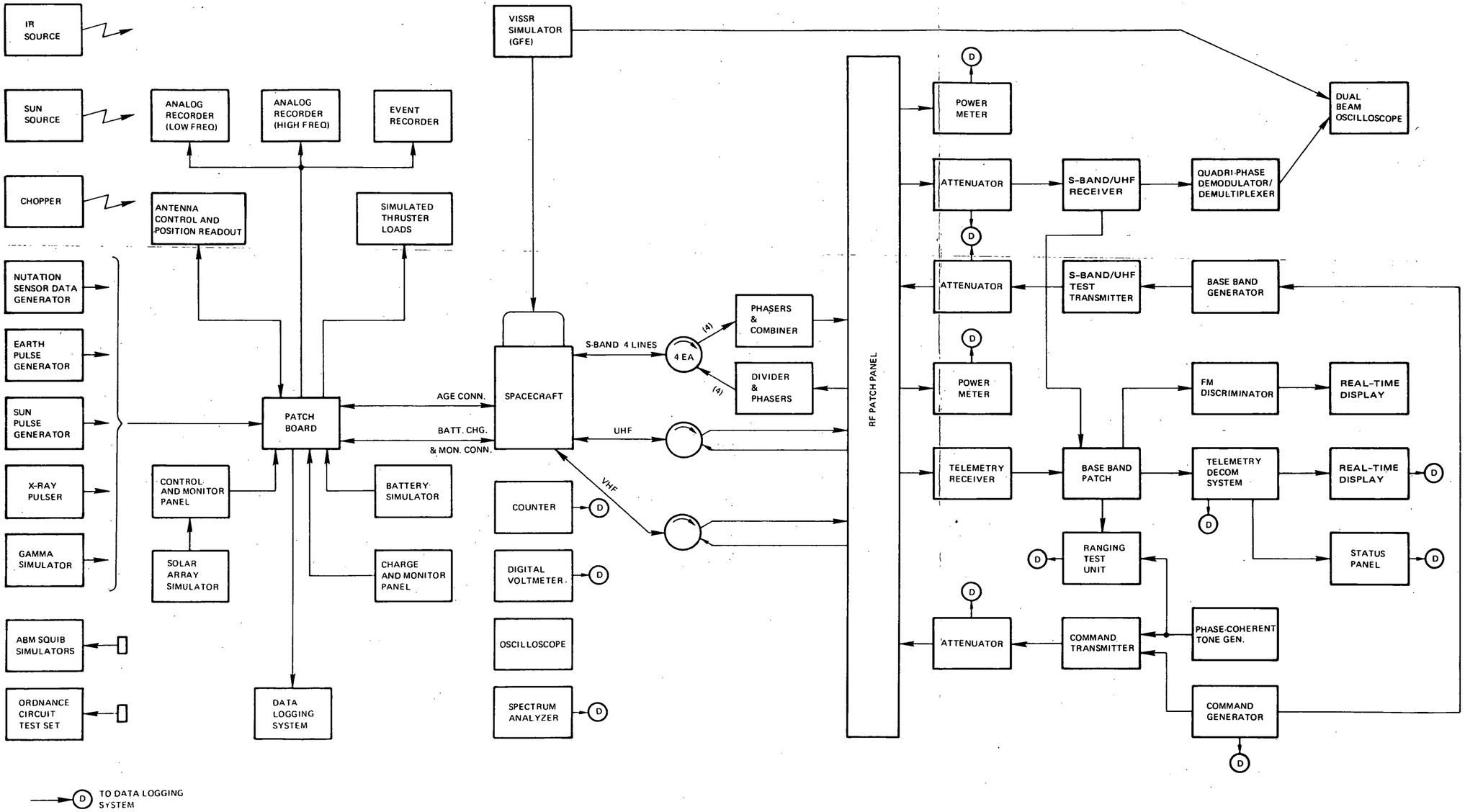

Figure 5-86. System Test Complex (STC), Simplified Block Diagram

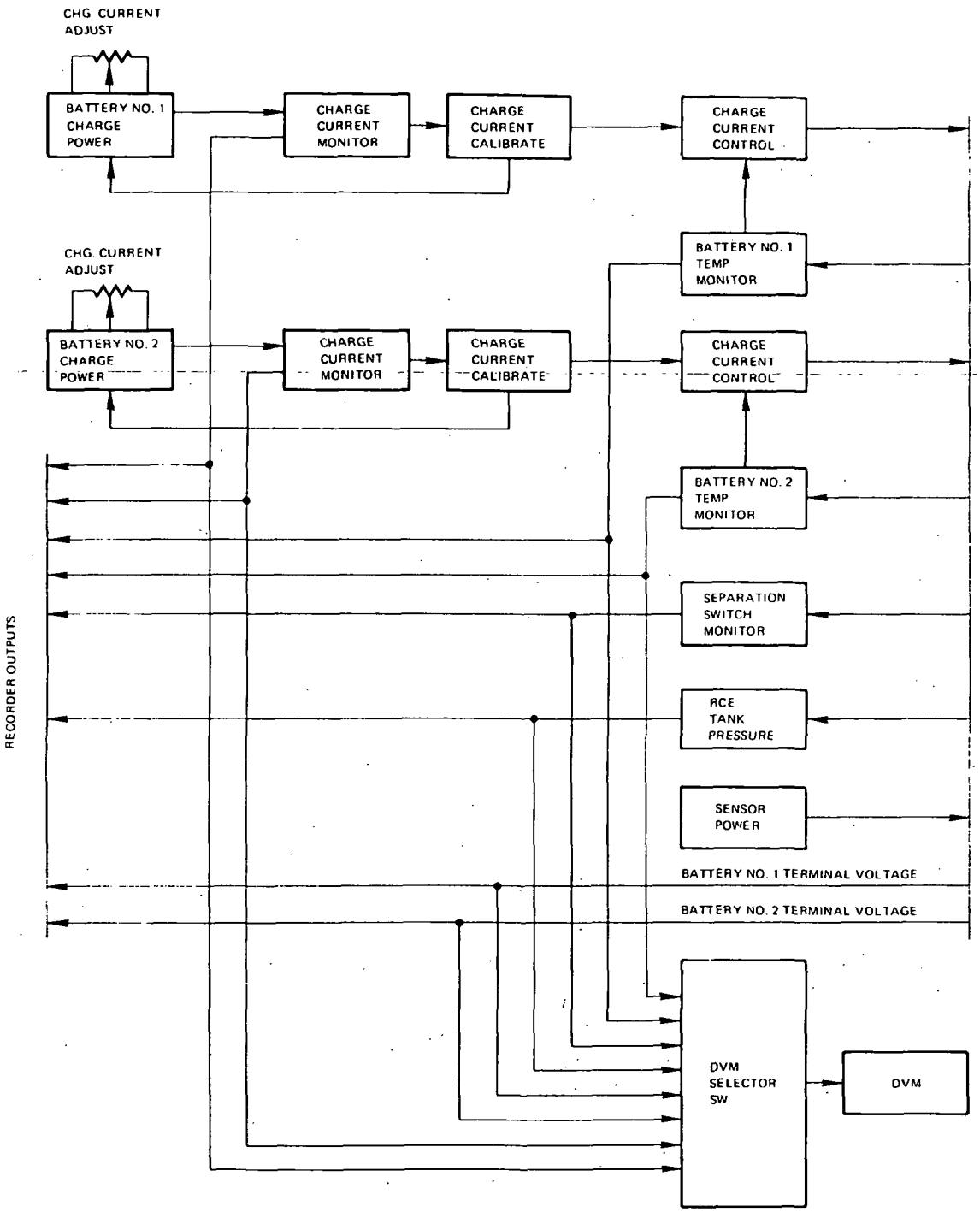

Figure 5-87. Charge and Monitor Panel, Functional Block Diagram

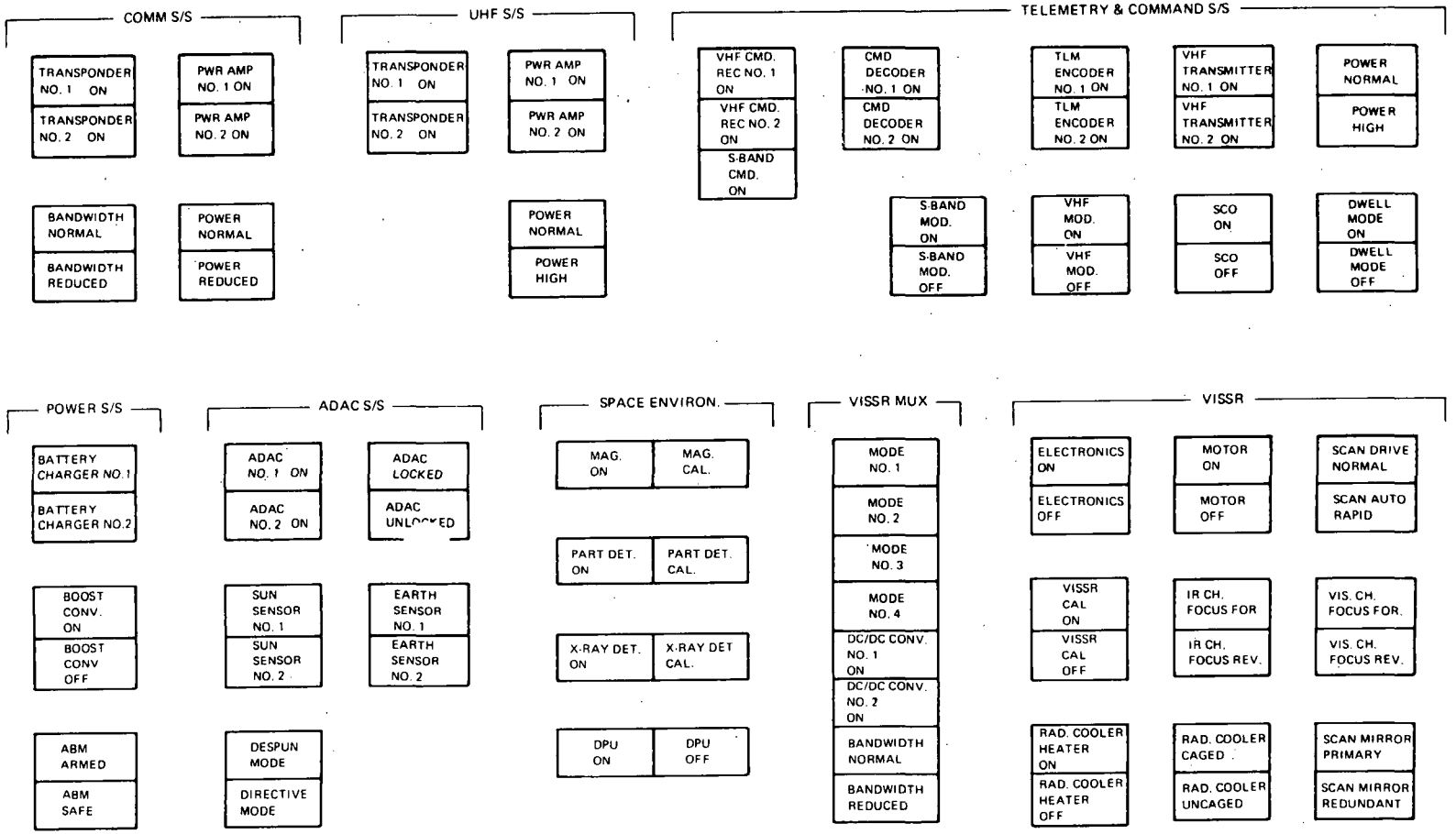

Figure 5-88. Status Panel

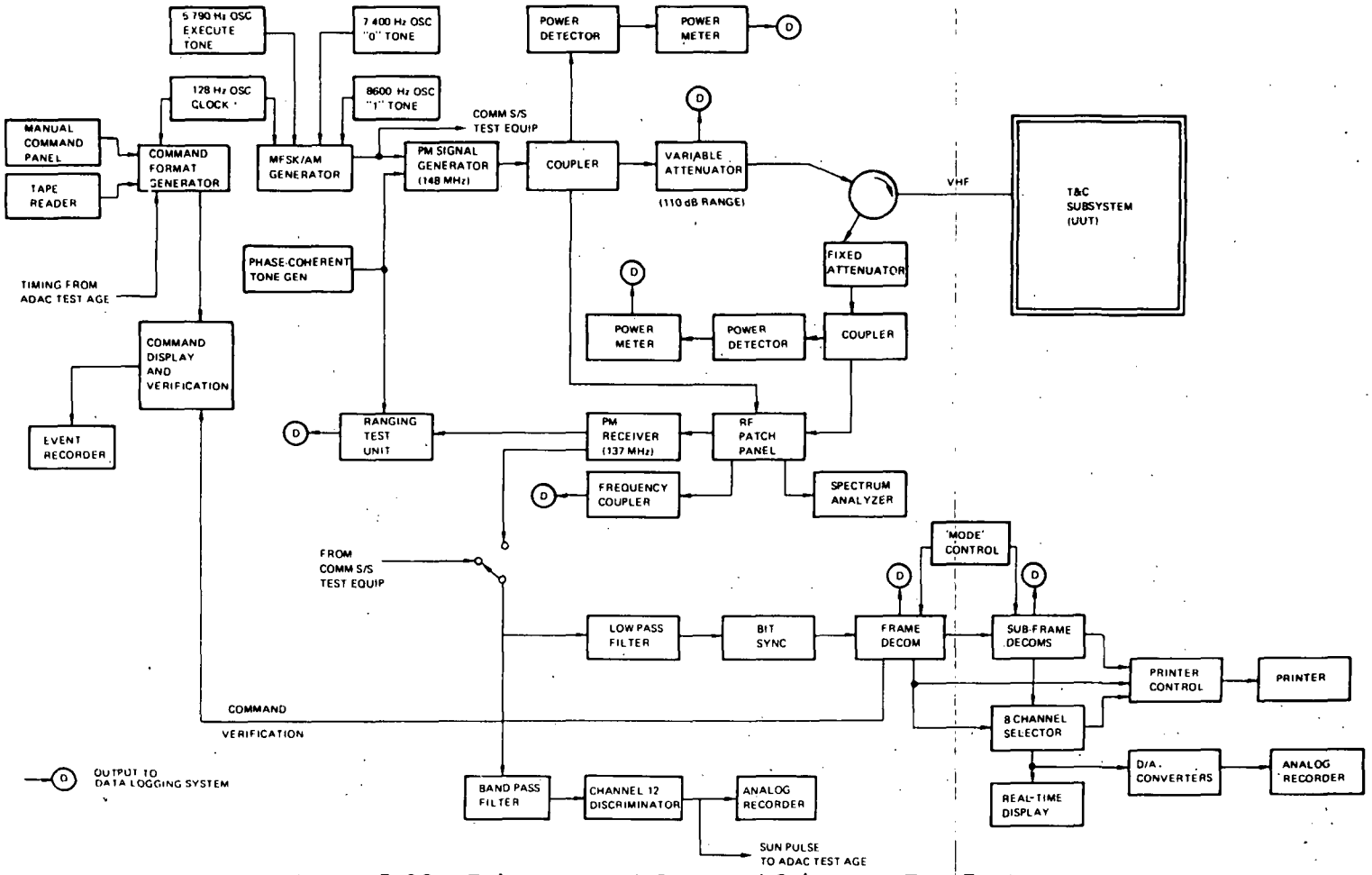

Figure 5-89. Telemetry and Command Subsystem Test Equipment

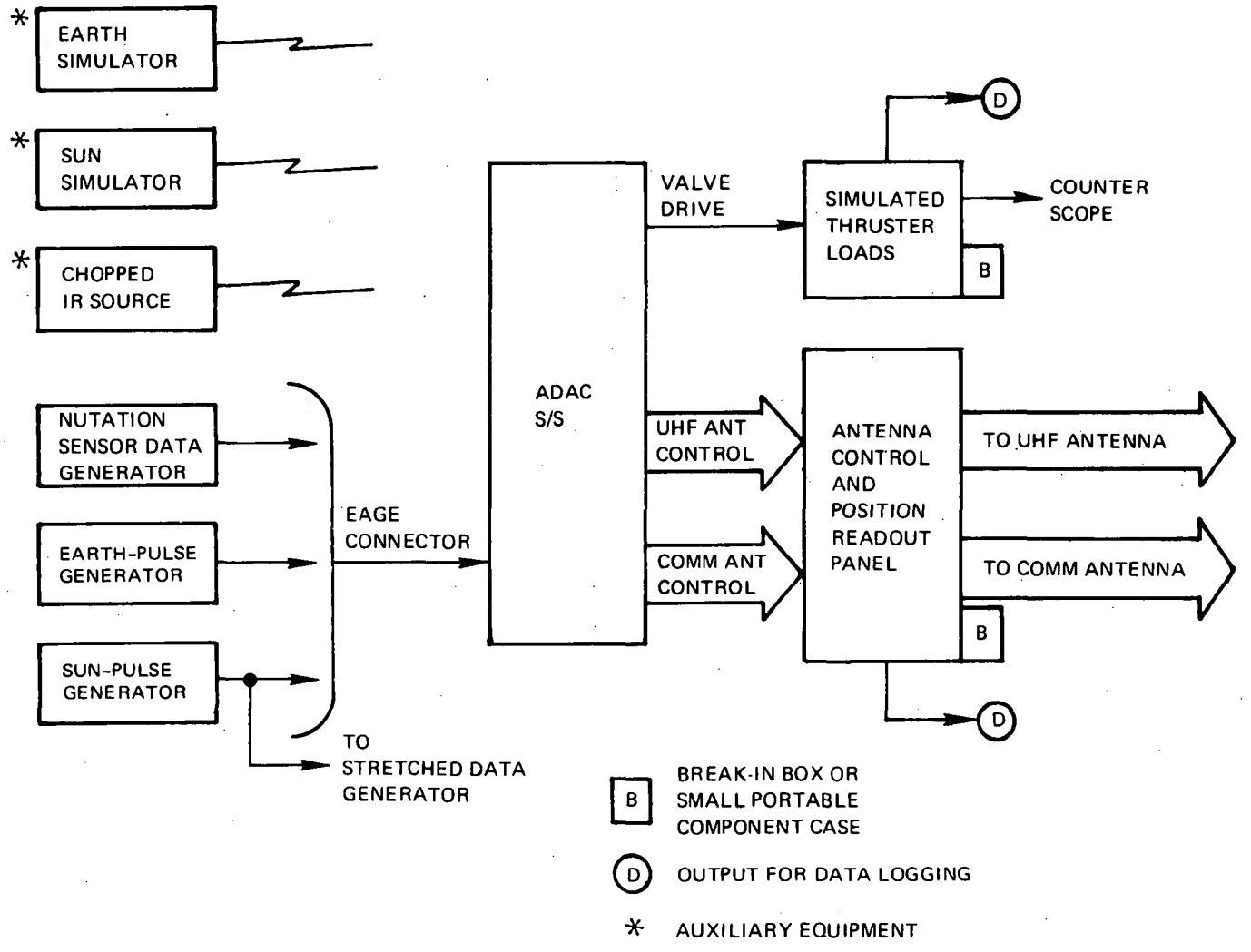

Figure 5-90. Attitude Determination and Antenna Control Equipment

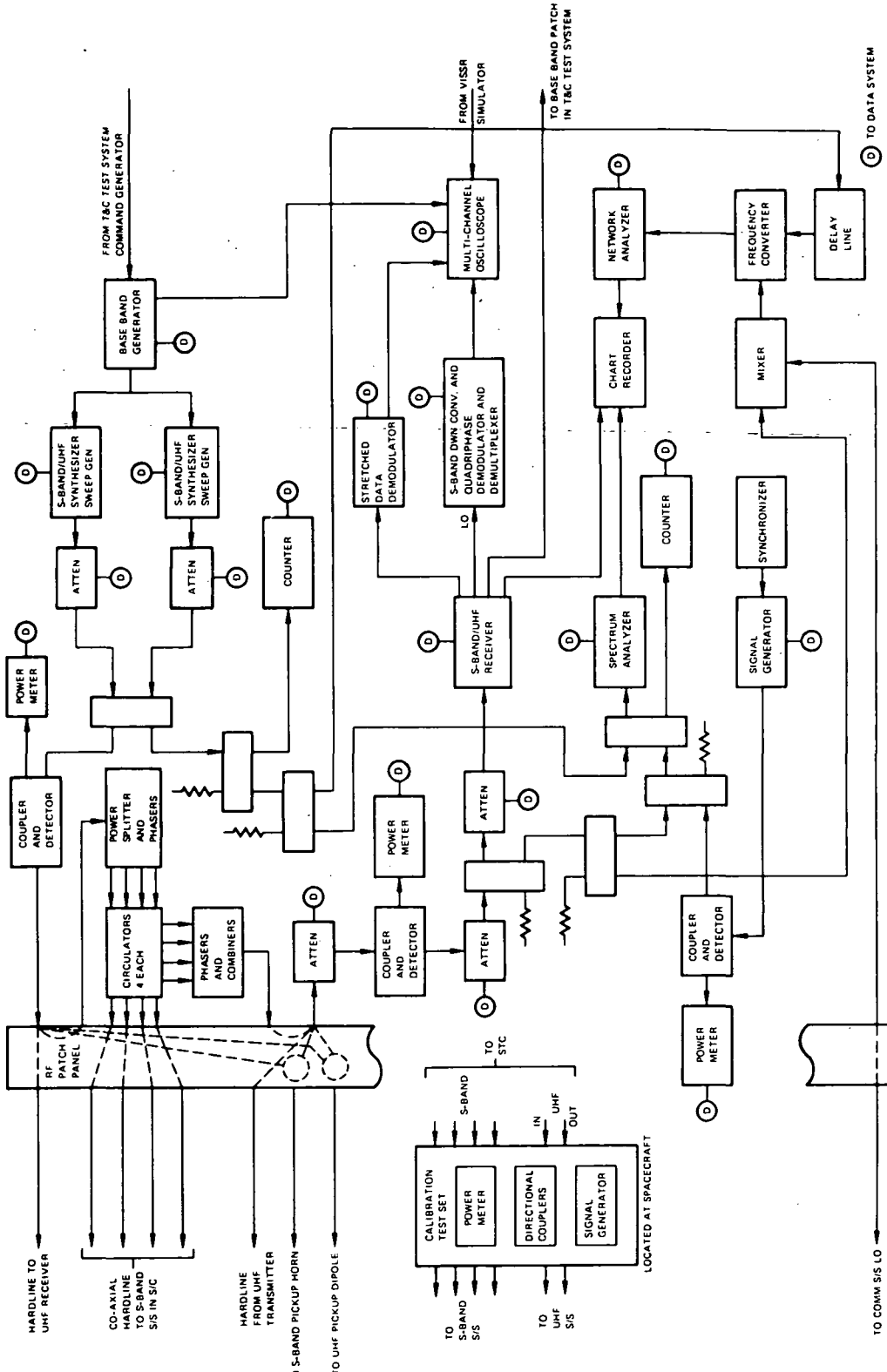

Figure 5-91. S-Band/UHF Communications Subsystem Test Equipment

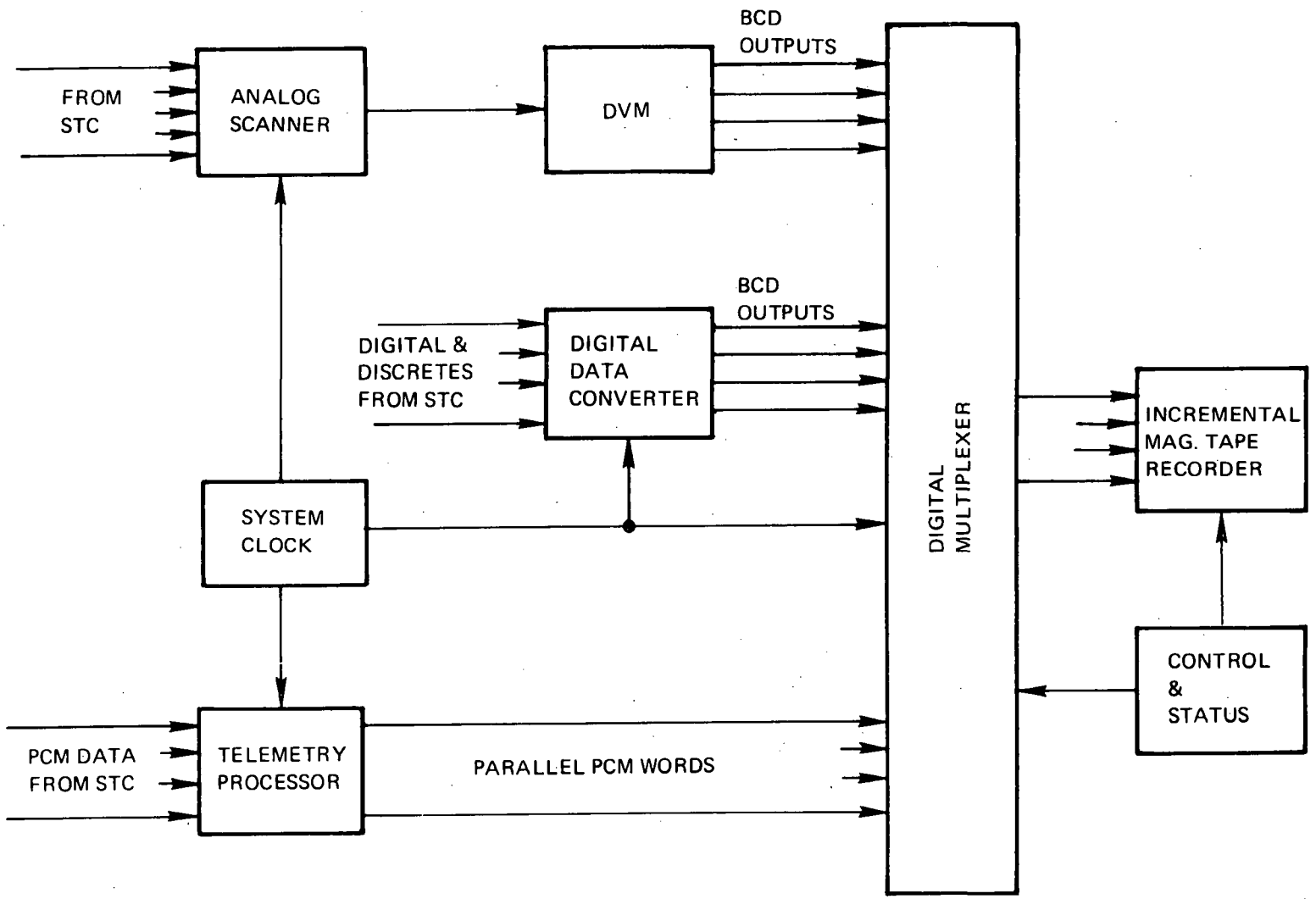

Figure 5-92. Data Logging System

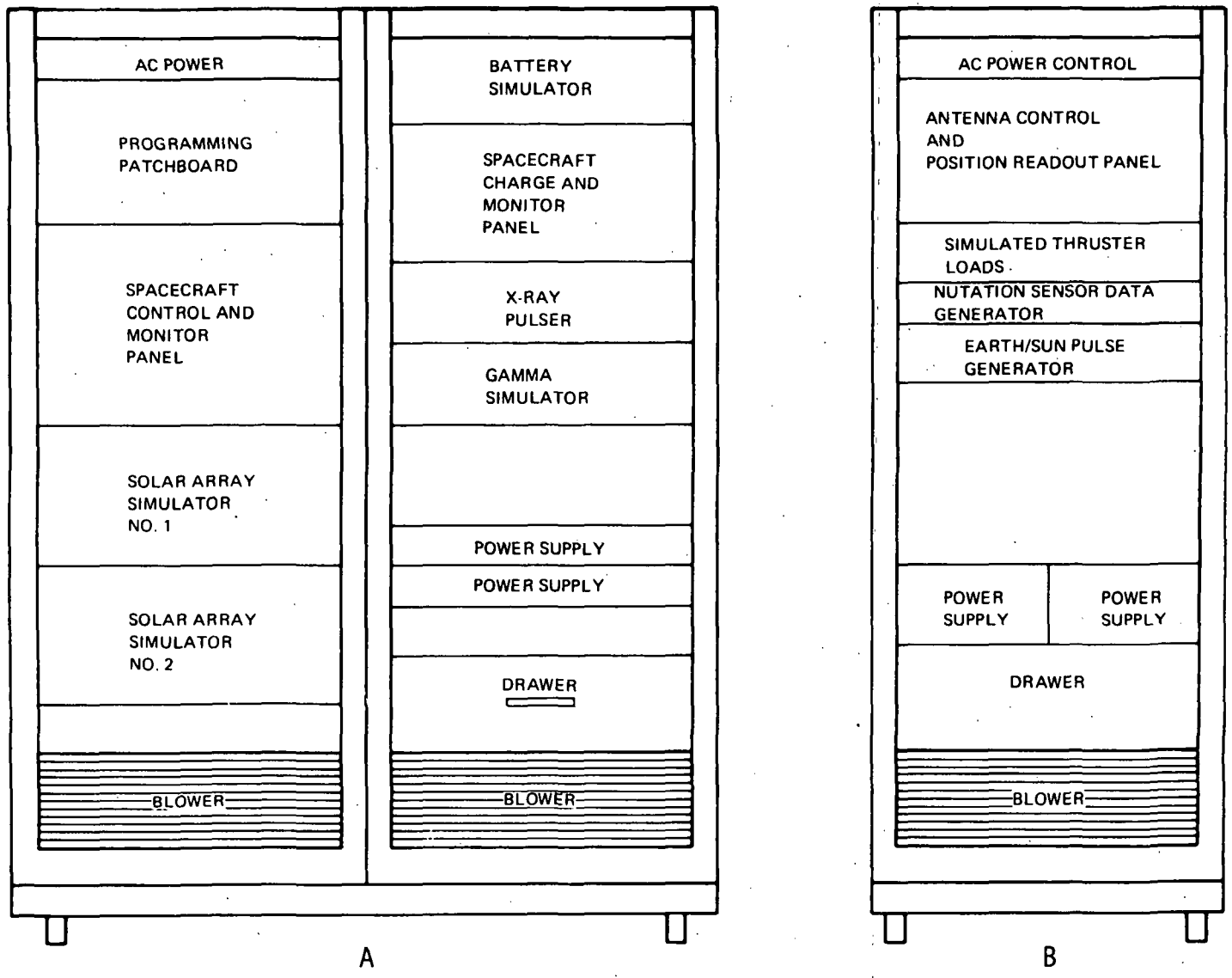

Figure 5-93. System Test Complex Rack Elevation (Sheet 1 of 5)

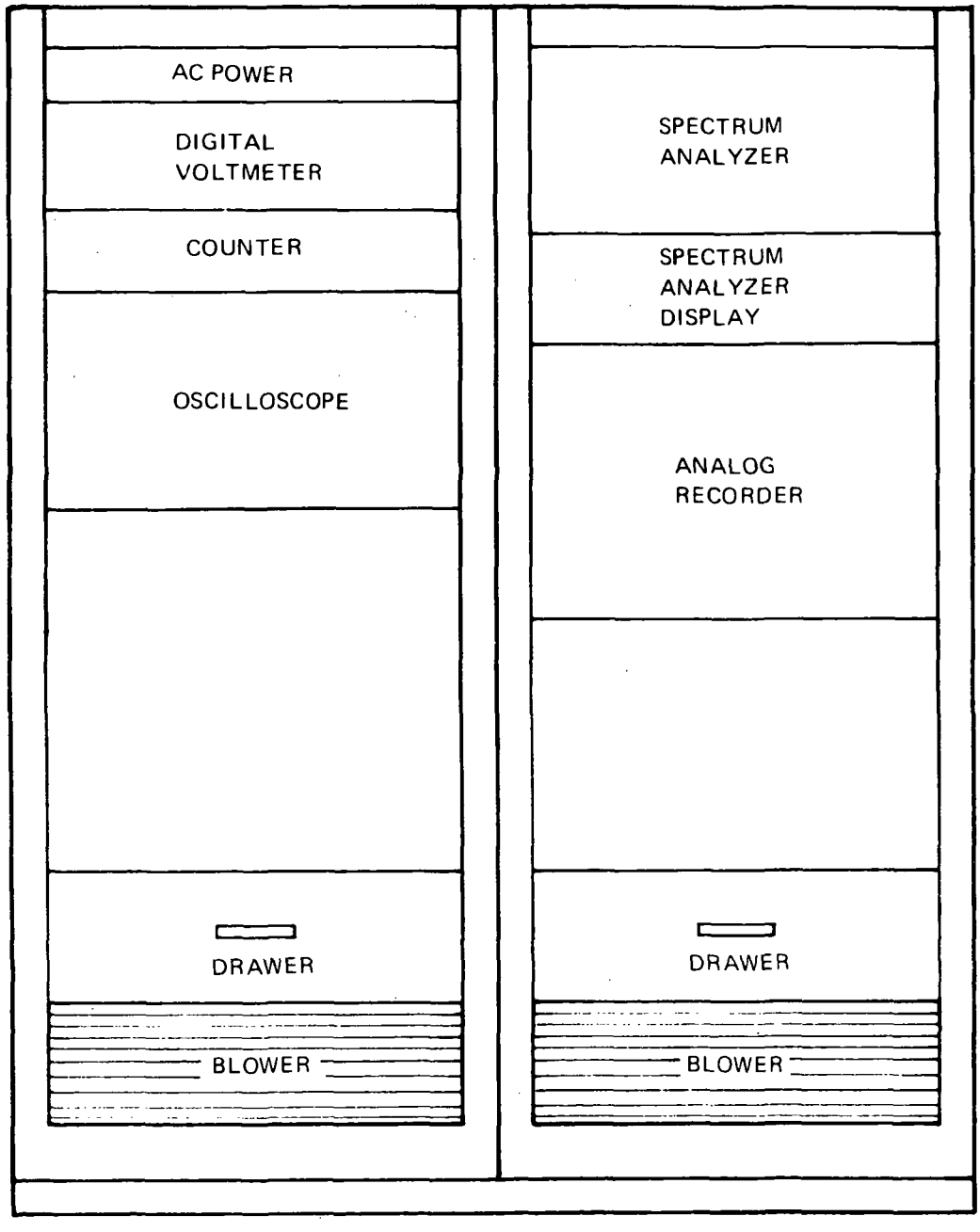

C

Figure 5-93. System Test Complex Rack Elevation (Sheet 2 of 5)

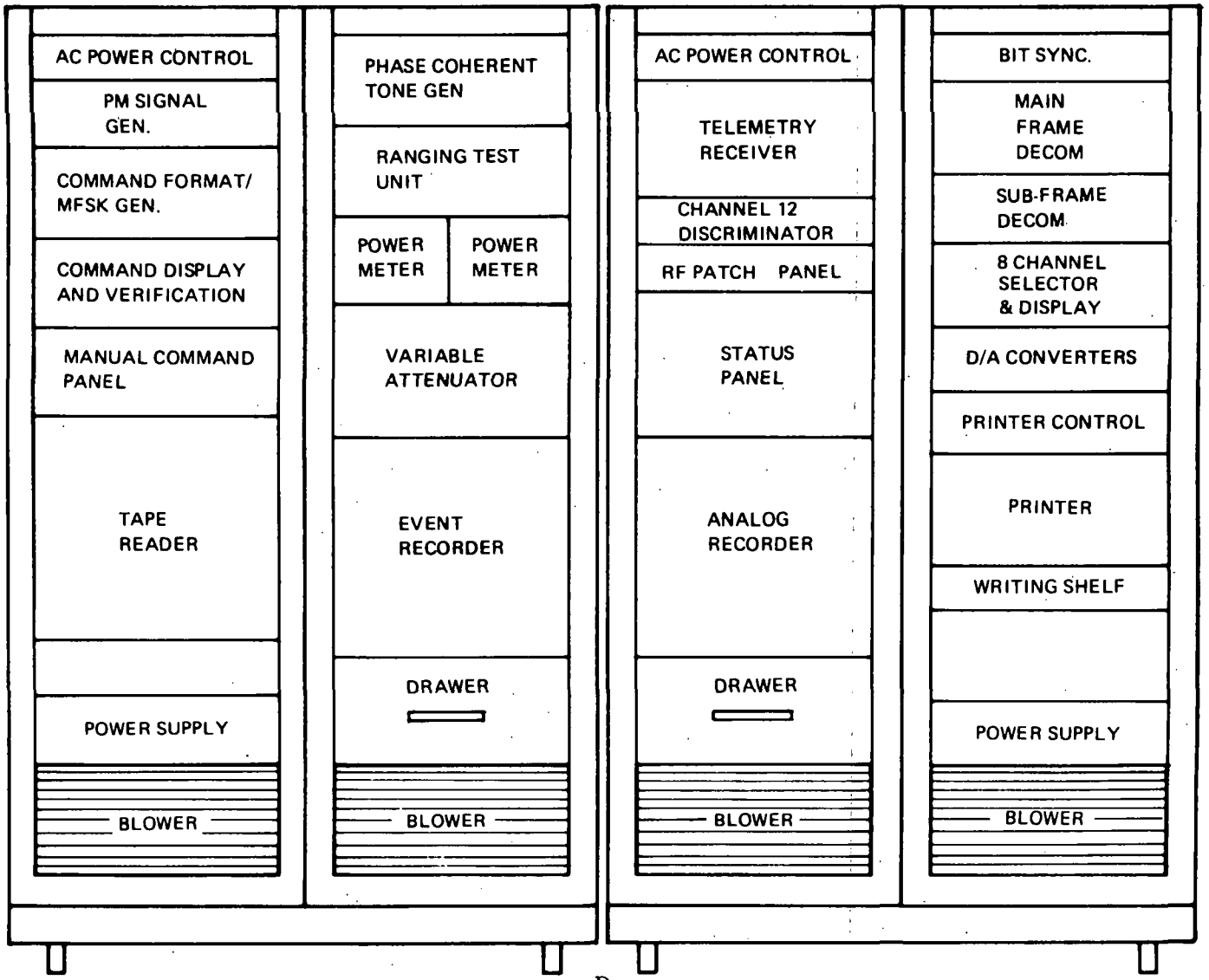

D

Figure 5-93. System Test Complex Rack Elevation (Sheet 3 of 5)

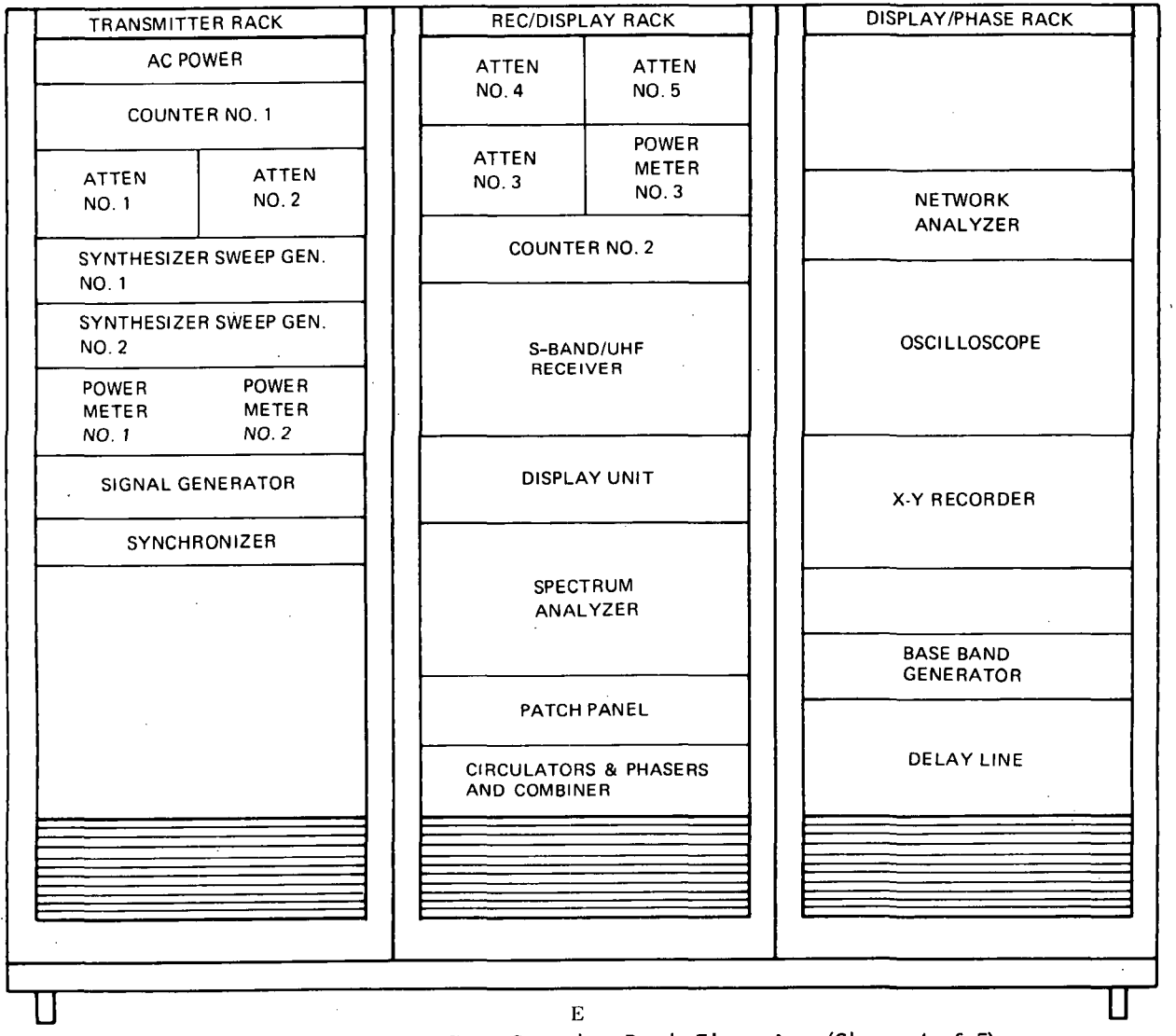

Figure 5-93. System Test Complex Rack Elevation (Sheet 4 of 5)

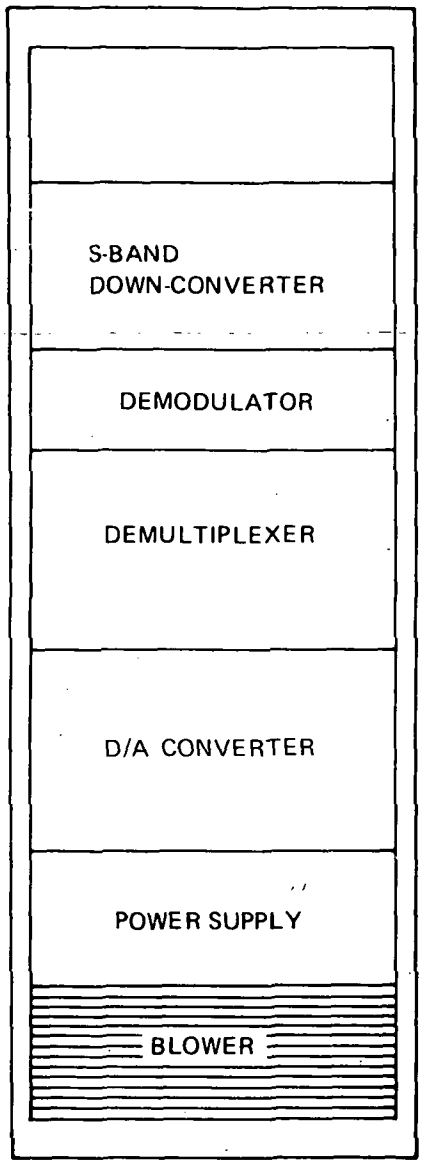

F

Figure 5-93. System Test Complex Rack Elevation (Sheet 5 of 5)

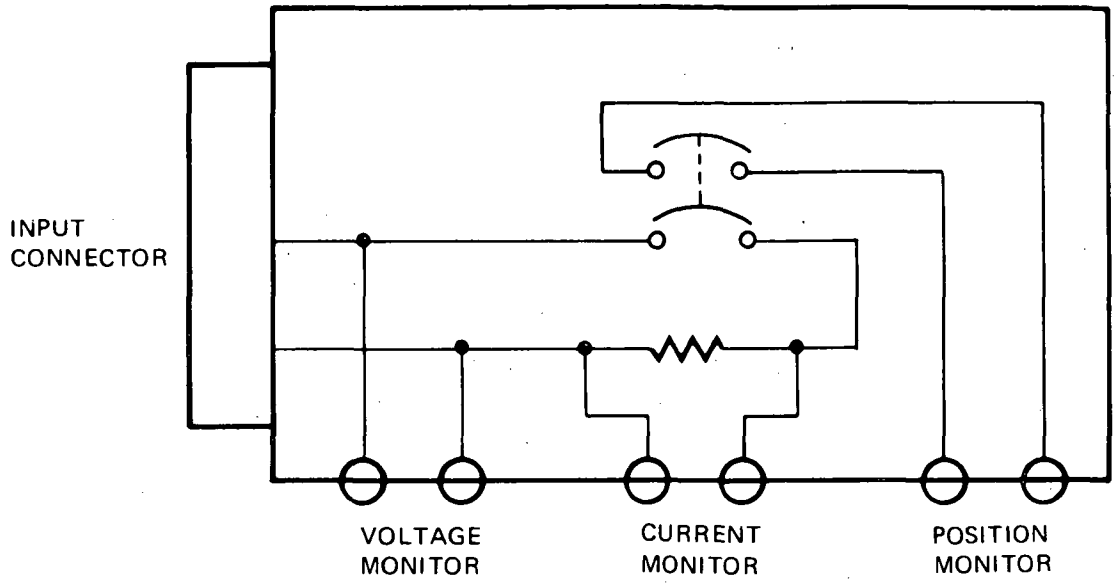

Figure 5-94. ABM Squib Simulator

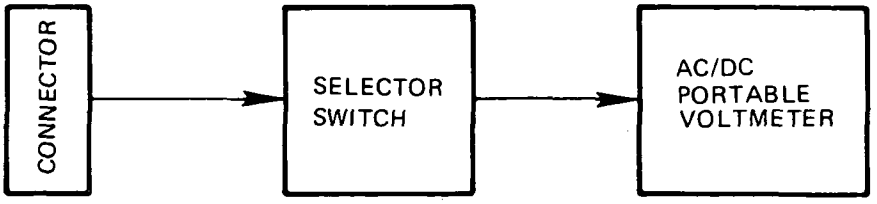

Figure 5-95. Ordnance Test Set, Functional Block Diagram

Testing of the spacecraft solar array is accomplished by selectively illuminating portions of the spacecraft using a solar panel illuminator as shown in Figure 5-96.

A block diagram of the solar panel test set is shown in Figure 5-97 and the solar panel test set rack elevation is illustrated in Figure 5-98.

In addition to the system testing (Figure 5-99), which is performed in the high bay area, additional testing ascertains target acquisition, data processing, and transmission from the satellite.

The electrical BTE is used to fulfill the requirement for test set-ups to provide for component and lower level bench testing. The BTE consists of the auxiliary propulsion test set (Figure 5-100), harness test adapter (Figure 5-101), SEM BTE (Figures 5-102 through 5-121 data processor, X-ray detector, and particle counter BTE), ADAC BTE power BTE (PCU, dc/dc converters, solar array, and batteries), telemetry and command BTE, and UHF communications BTE (communications transmitter, receiver and antenna assembly, and VISSR multiplexer).

Mechanical AGE/BTE is required to support the spacecraft through assembly and test. The equipment provides the following capabilities: handling, supporting, hoisting, positioning, and in-plant movement of the spacecraft, ABM adapter, ABM, and VISSR; pressurizing, loading, unloading, and weighing fuel in the auxiliary propulsion subsystem; shock and environmental protection for the spacecraft during shipment and storage; alignment of auxiliary propulsion subsystem nozzles and sensors; measuring center-of-gravity and moment-of-inertia of the spacecraft; thermal vacuum chamber, vibration, shock, acoustic noise and static load testing of the spacecraft; assembling the spacecraft structure and ABM adapter; molding, forming, fabricating and assembling the thermal subsystem structure and heat shields; protecting the solar panels and antenna from damage during assembly and test; and dynamic balancing of the spacecraft and ABM adapter.

Figures 5-122 through 5-126 depict some of the specialized equipment necessary to support the spacecraft through assembly and test.

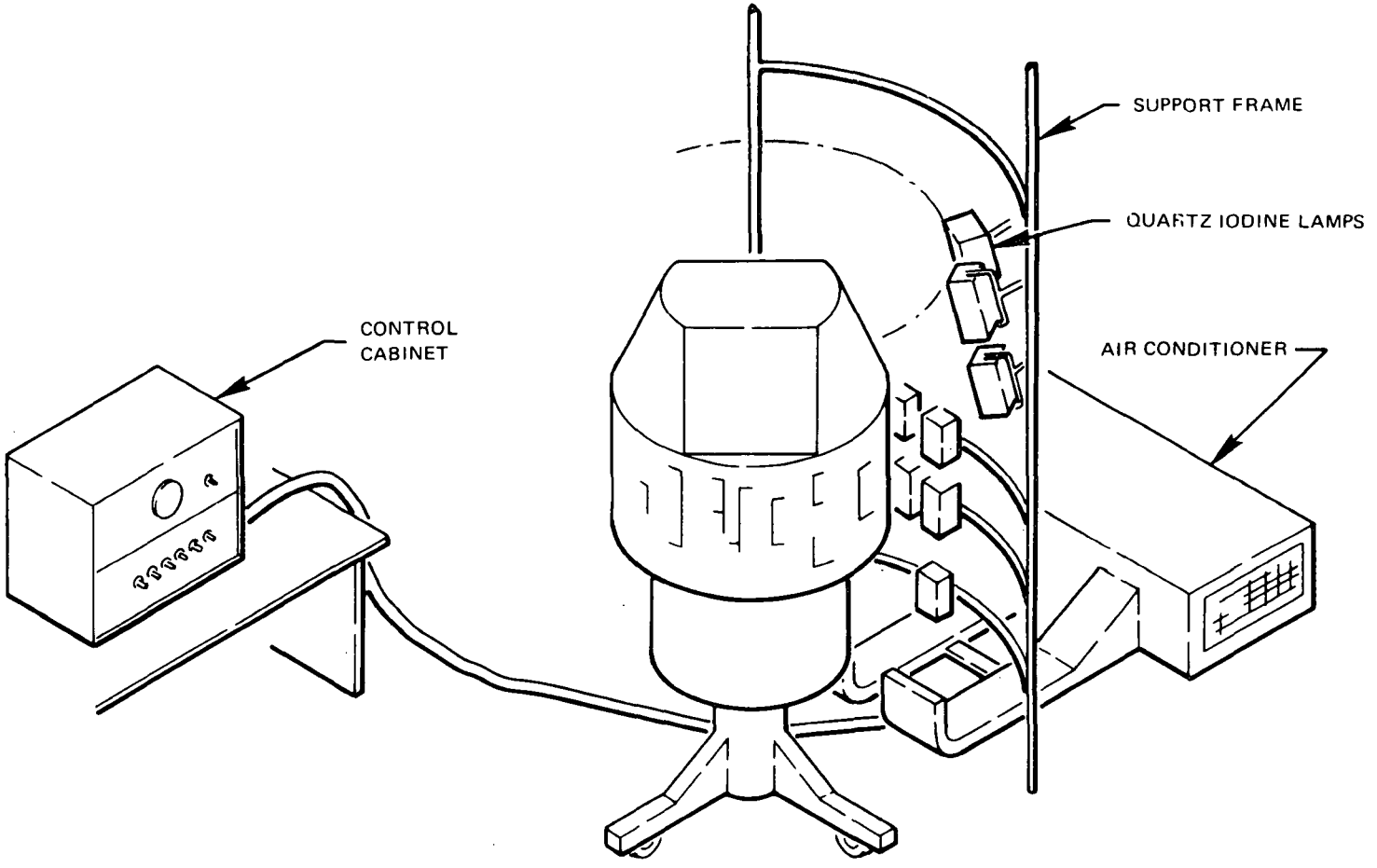

Figure 5-96. Solar Array Illuminator

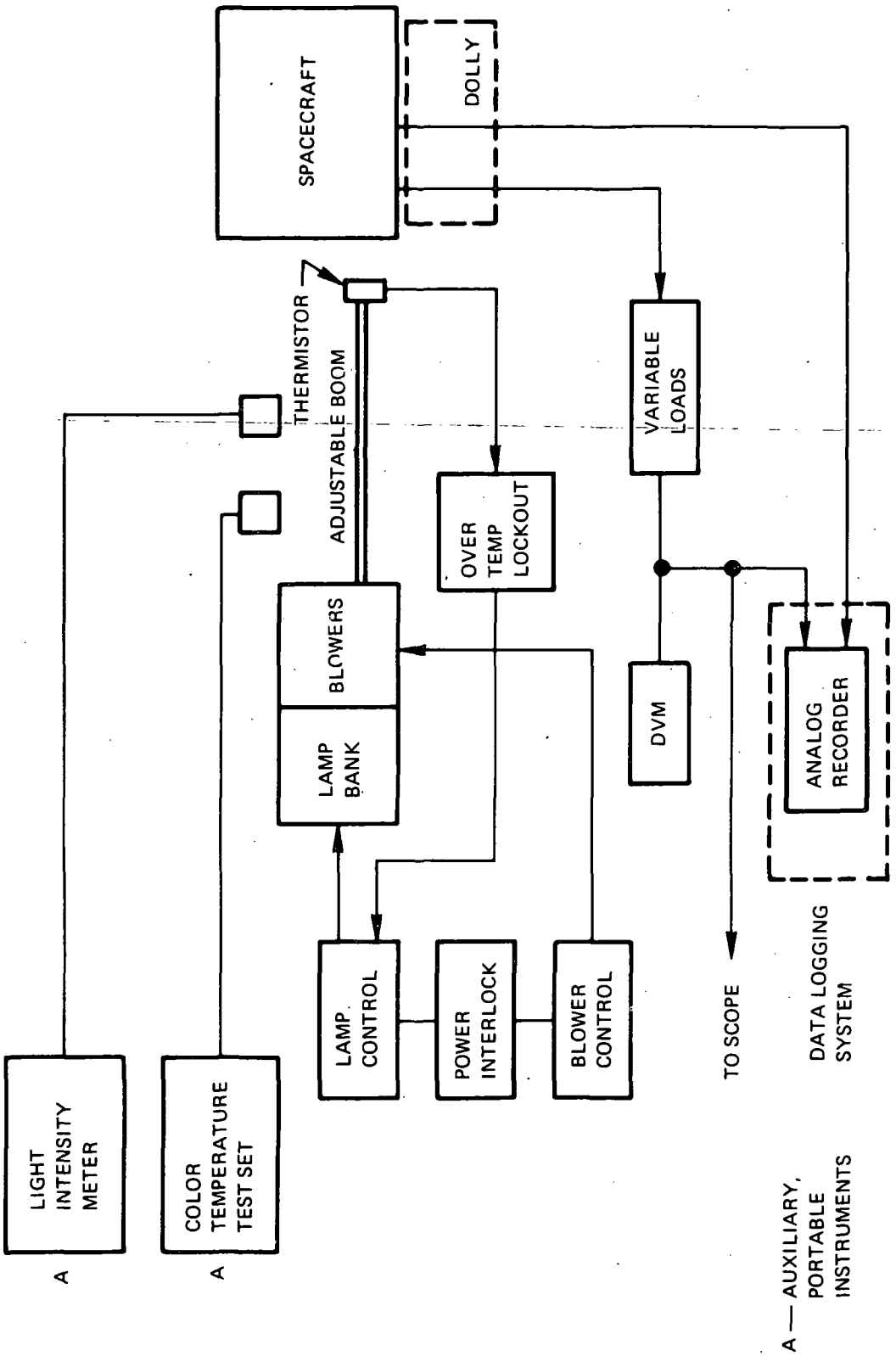

Figure 5-97. Solar Panel Test Set, Block Diagram

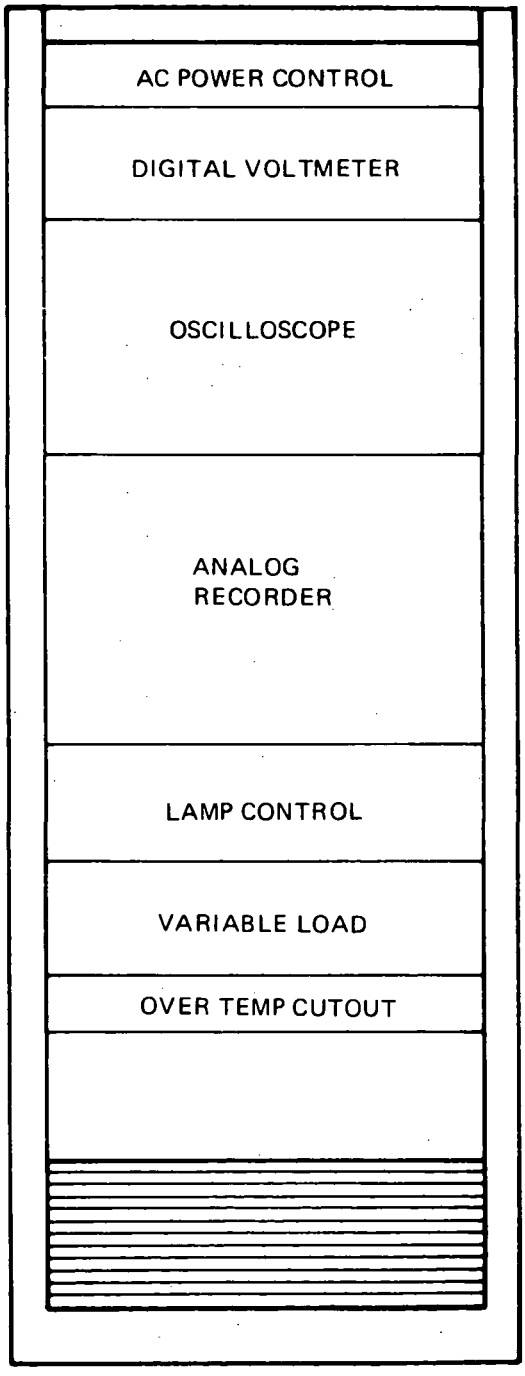

Figure 5-98. Solar Panel Test Set, Rack Elevation

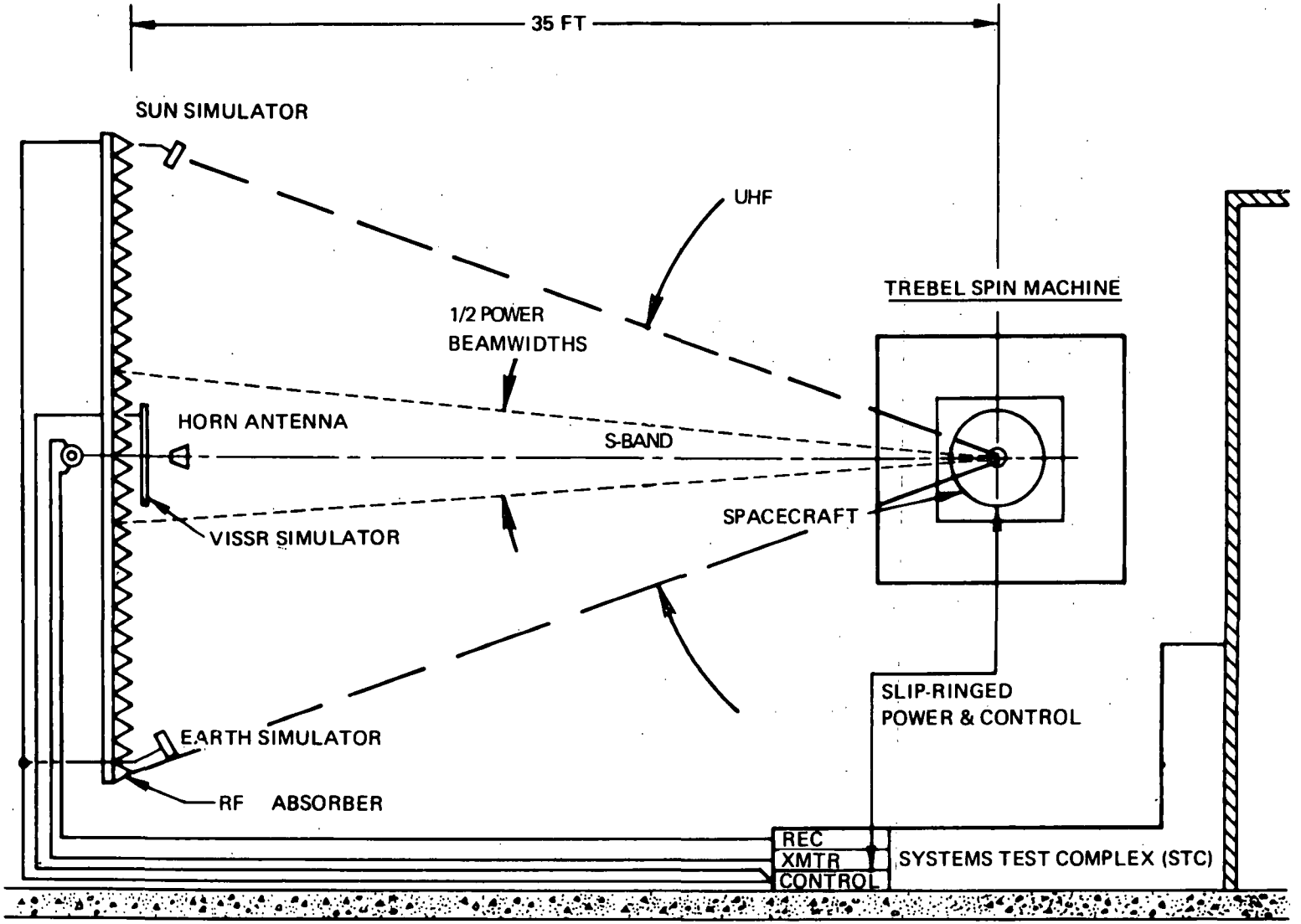

Figure 5-99. Spinup Test Using RF Absorber

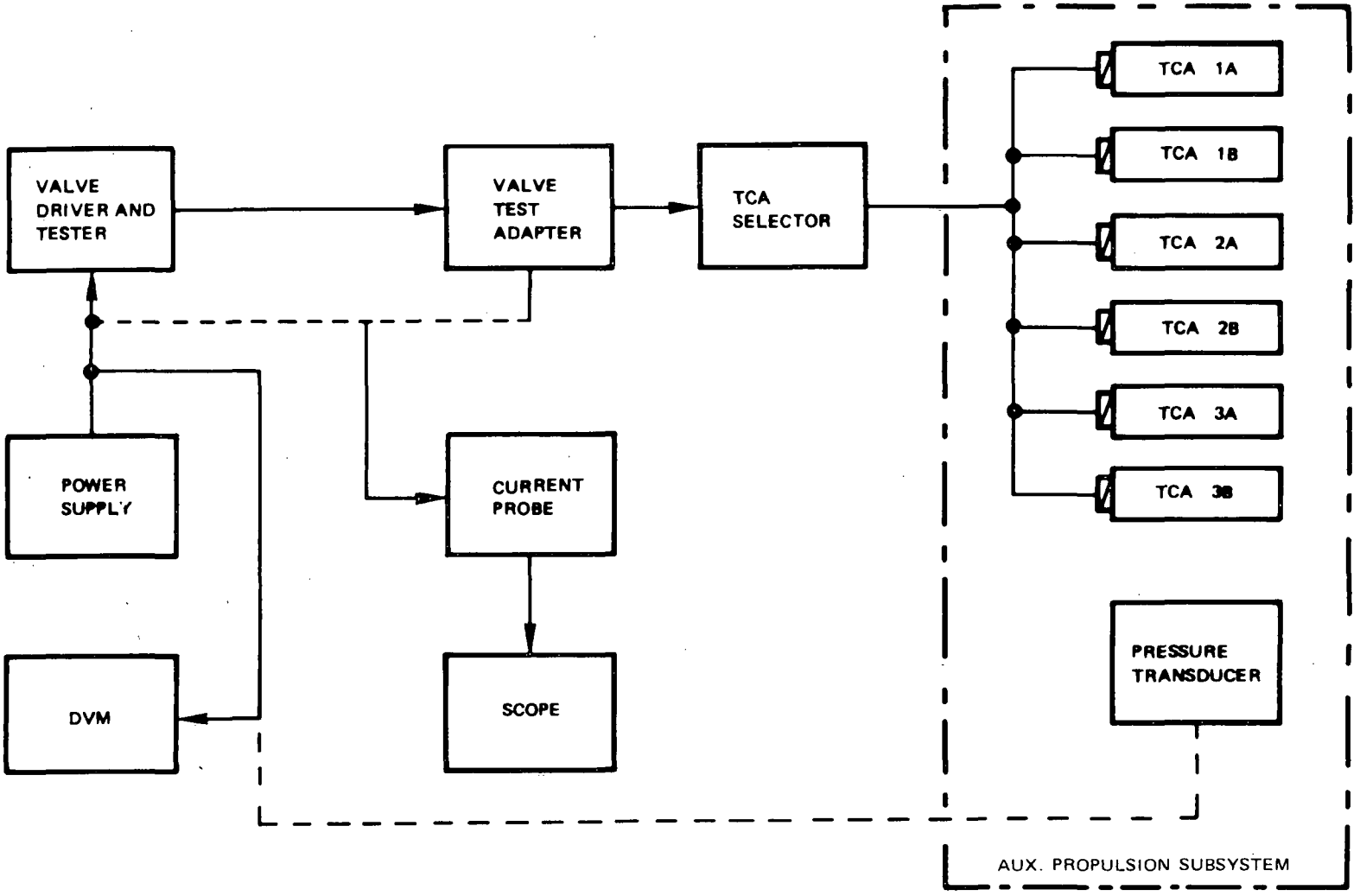

Figure 5-100. Auxiliary Propulsion Subsystem Test Set

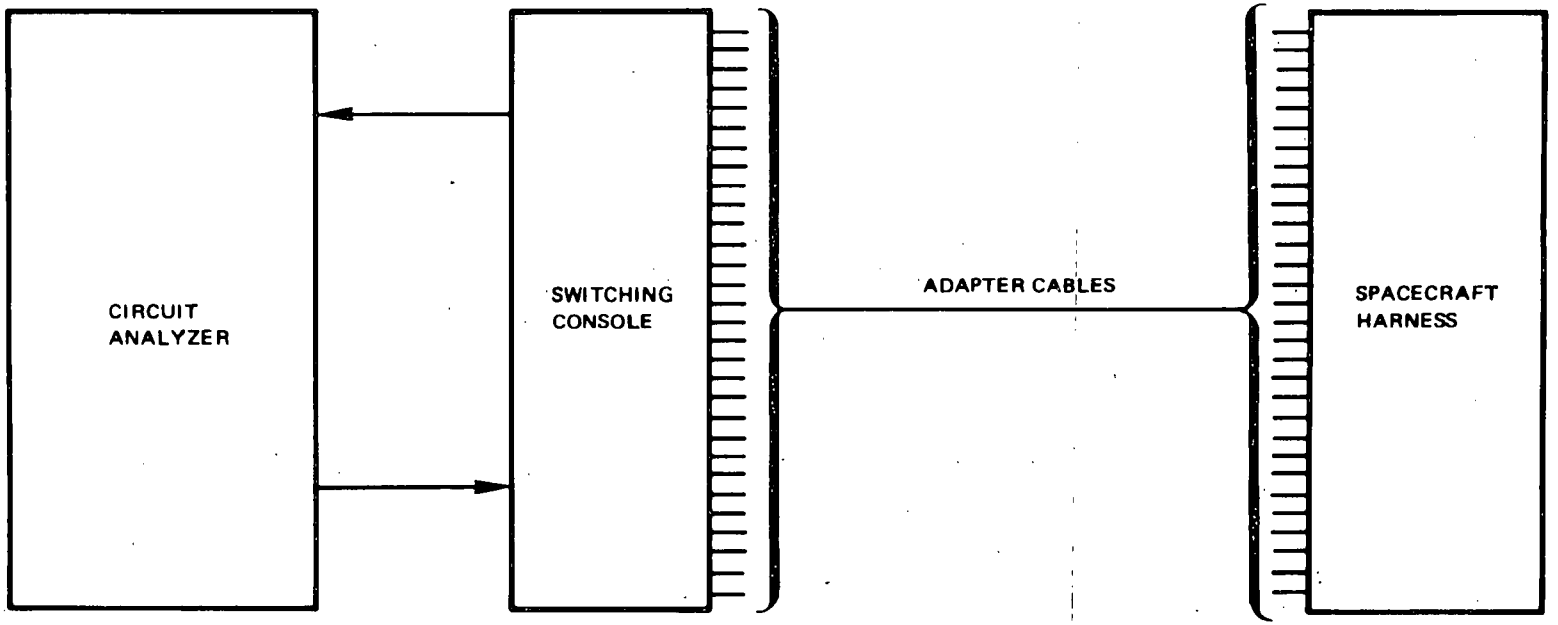

Figure 5-101. Harness Test Adapter, Functional Block Diagram

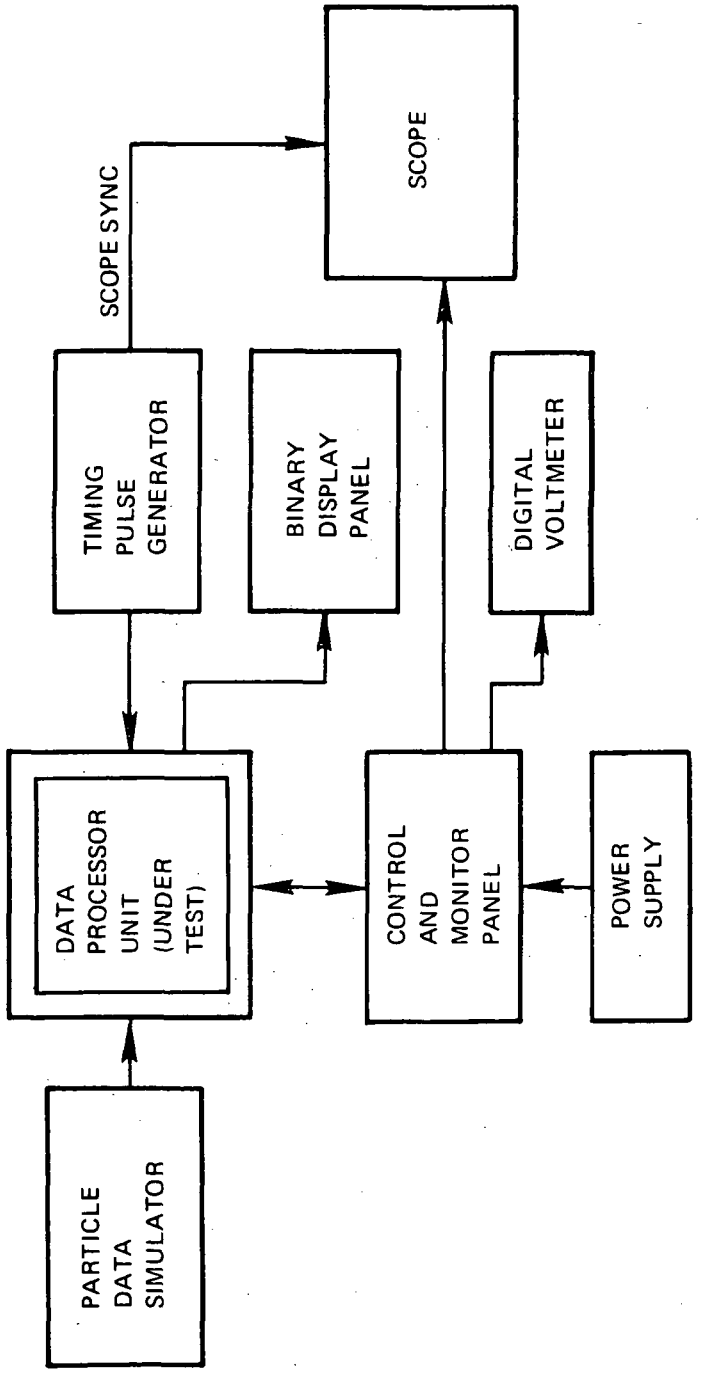

Figure 5-102. Data Processor Unit Bench Test Equipment

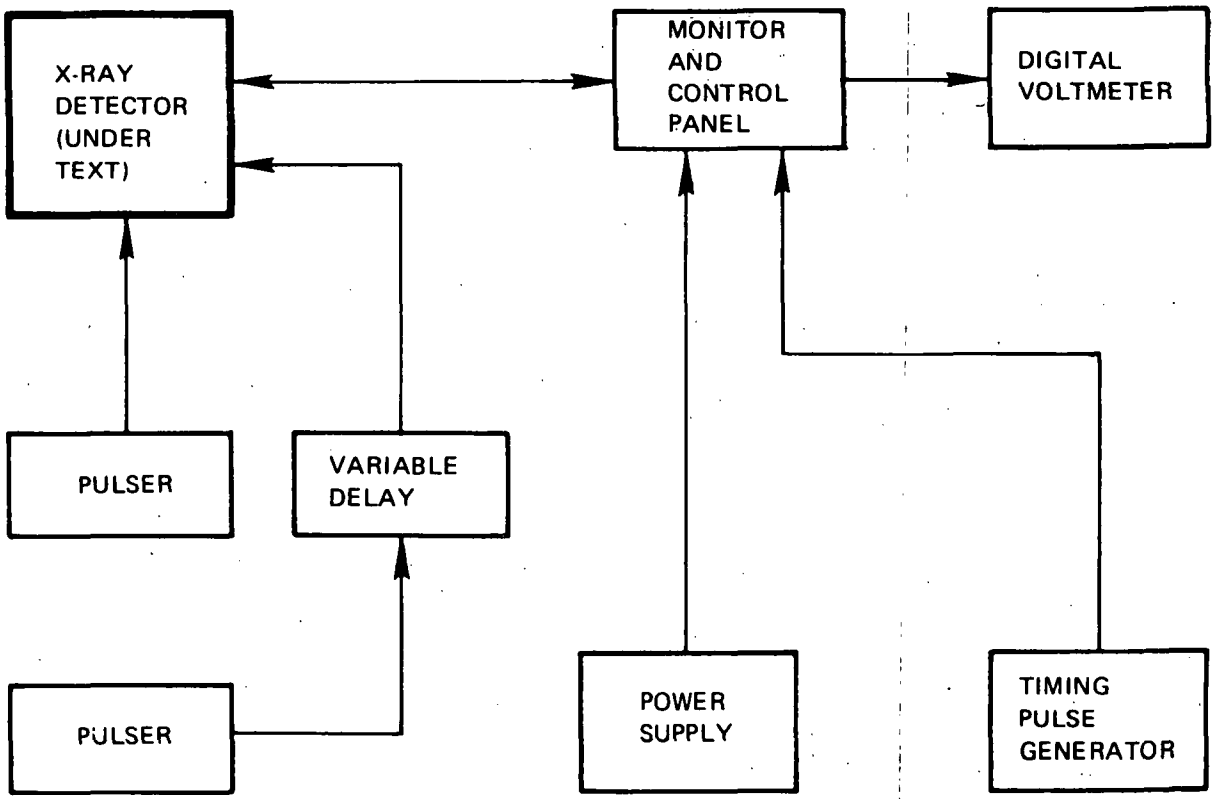

Figure 5-103. X-Ray Detector Bench Test Equipment

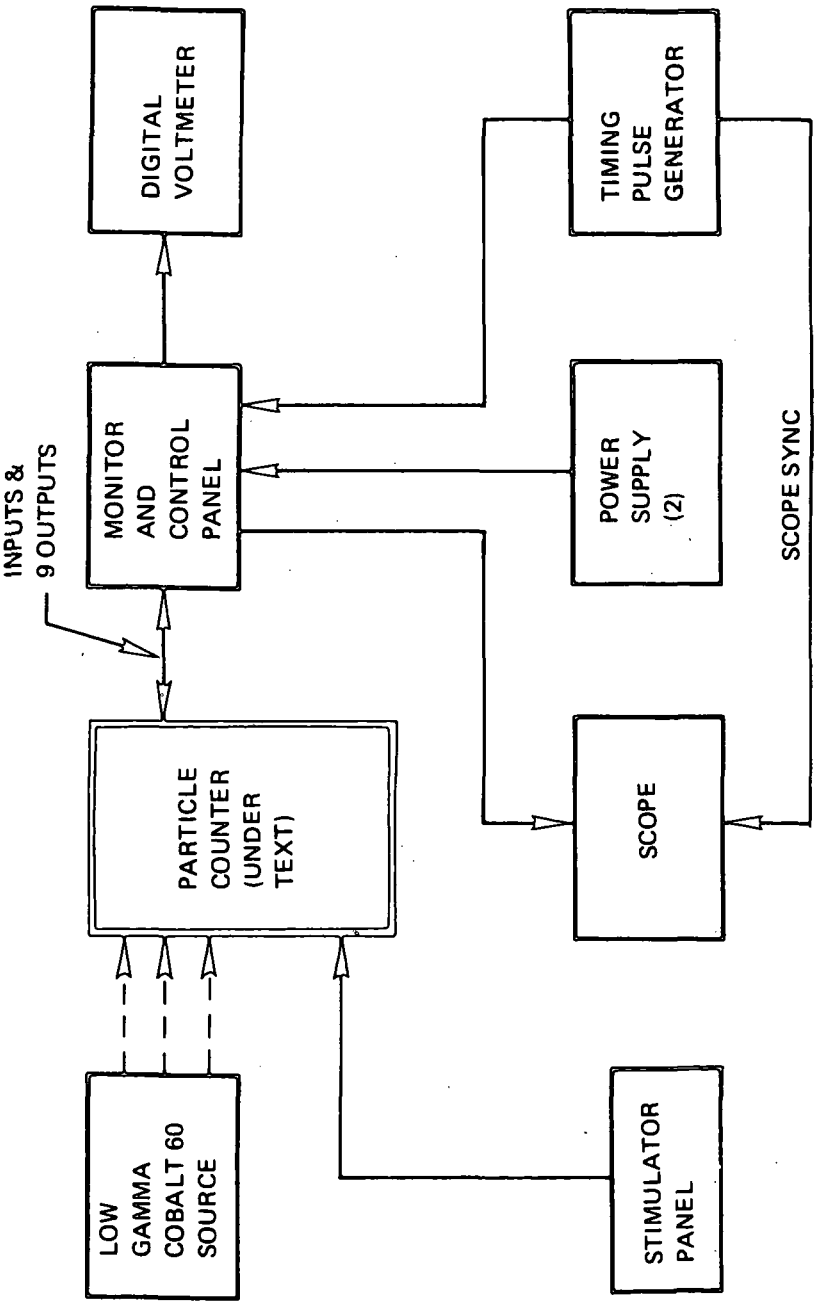

Figure 5-104. Particle Counter Bench Test Equipment

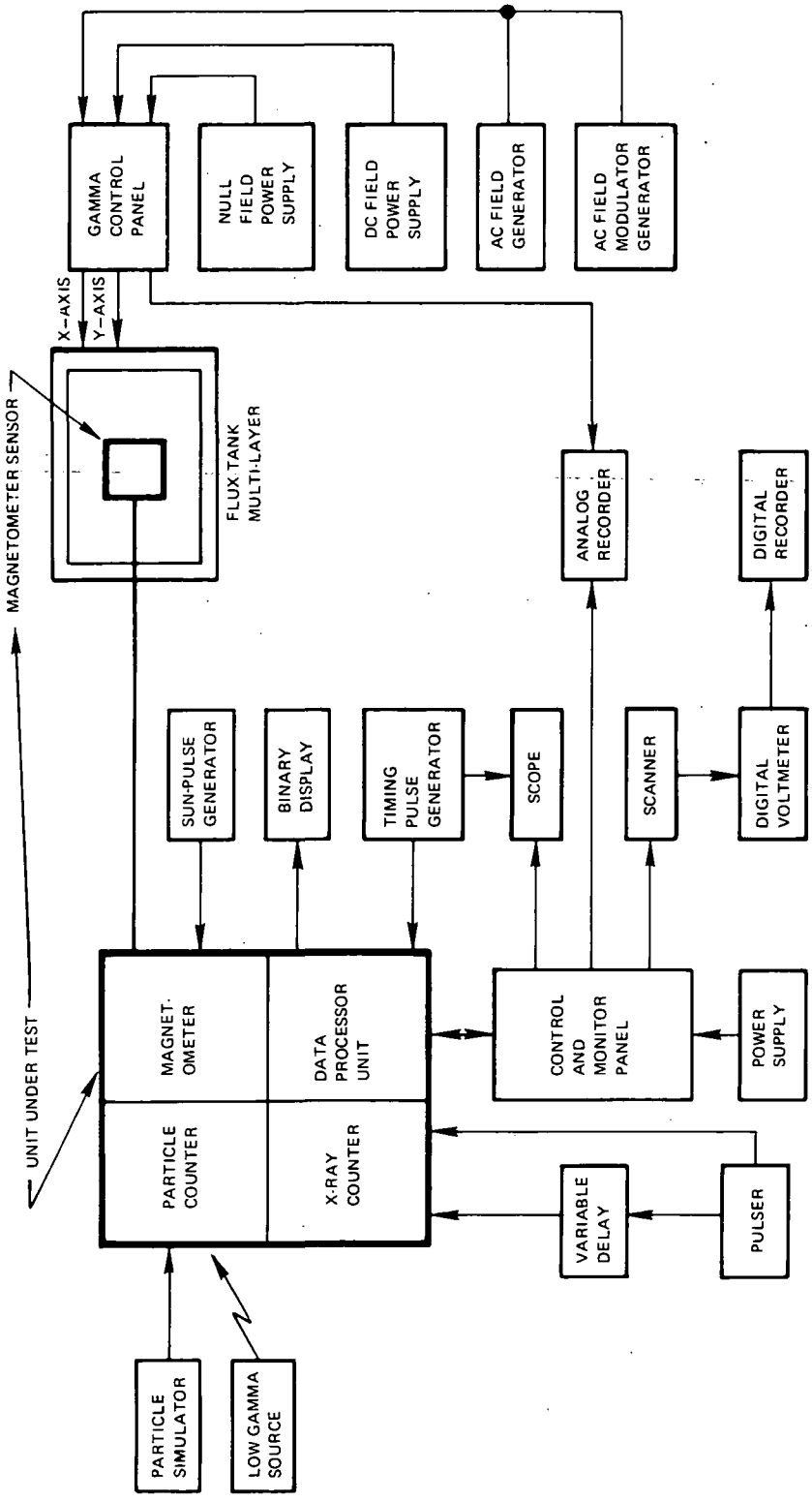

Figure 5-105. Space Environmental Monitor Sub-system Test Configuration

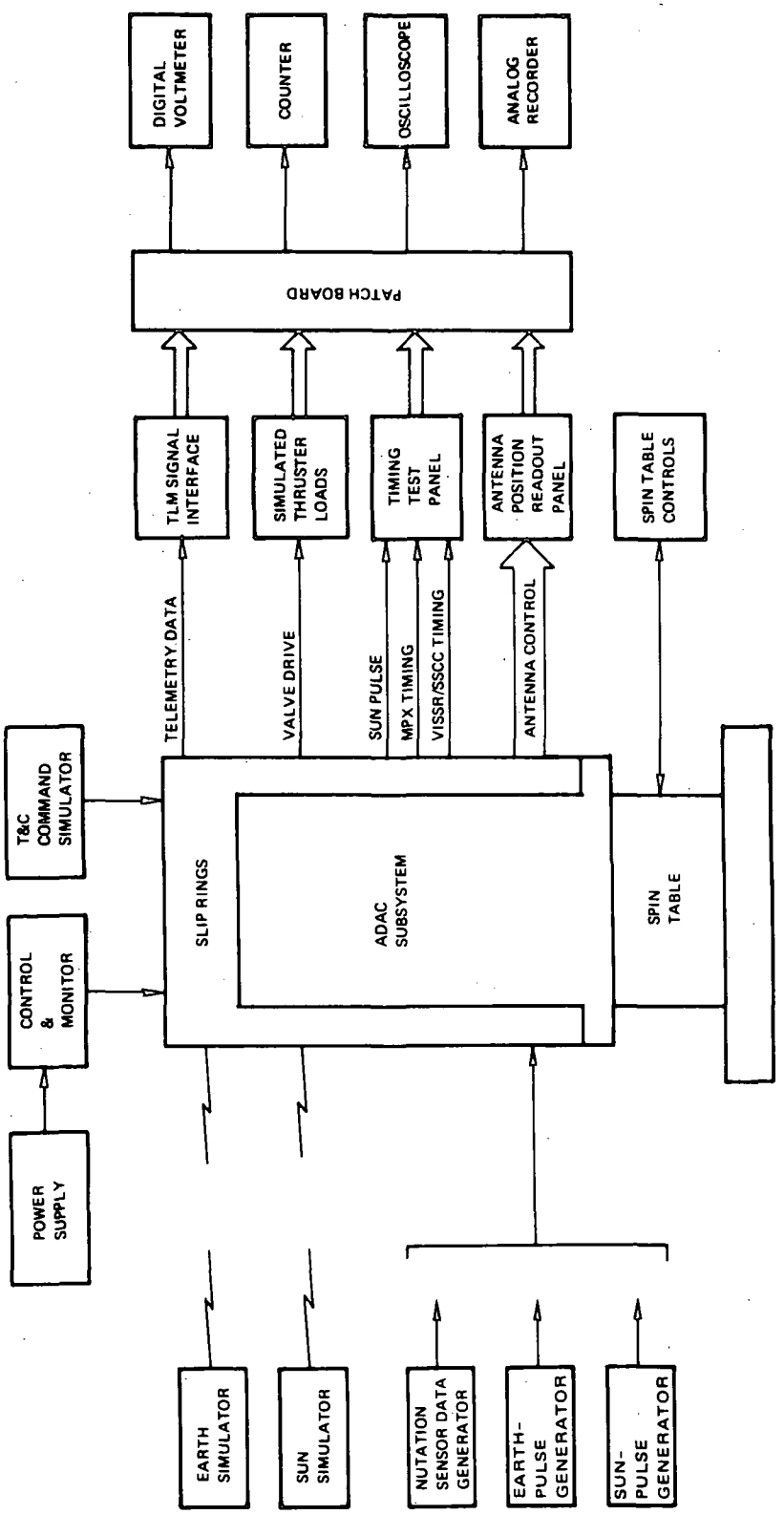

Figure 5-106. ADAC Bench Test Equipment

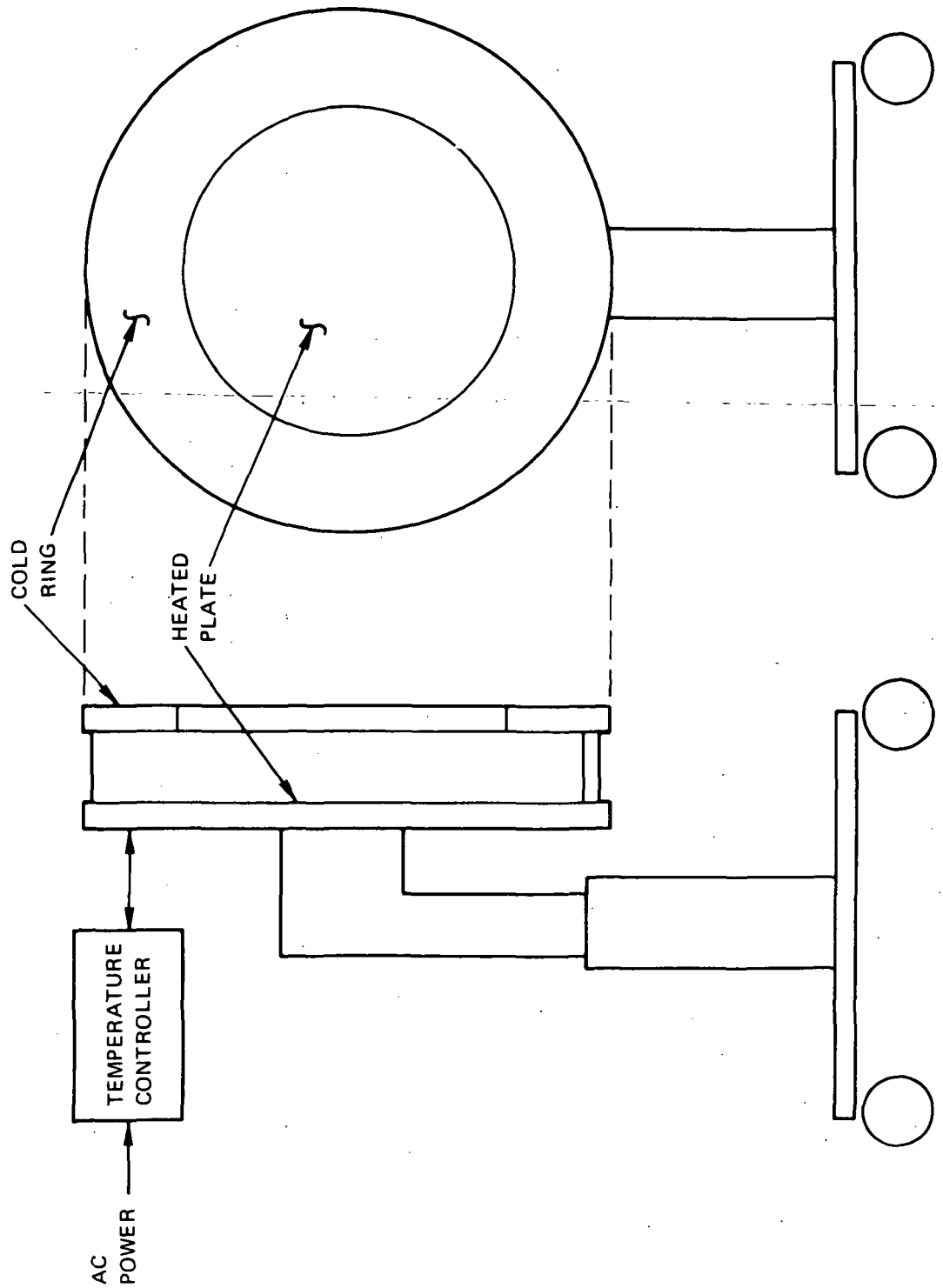

Figure 5-107. Earth Source

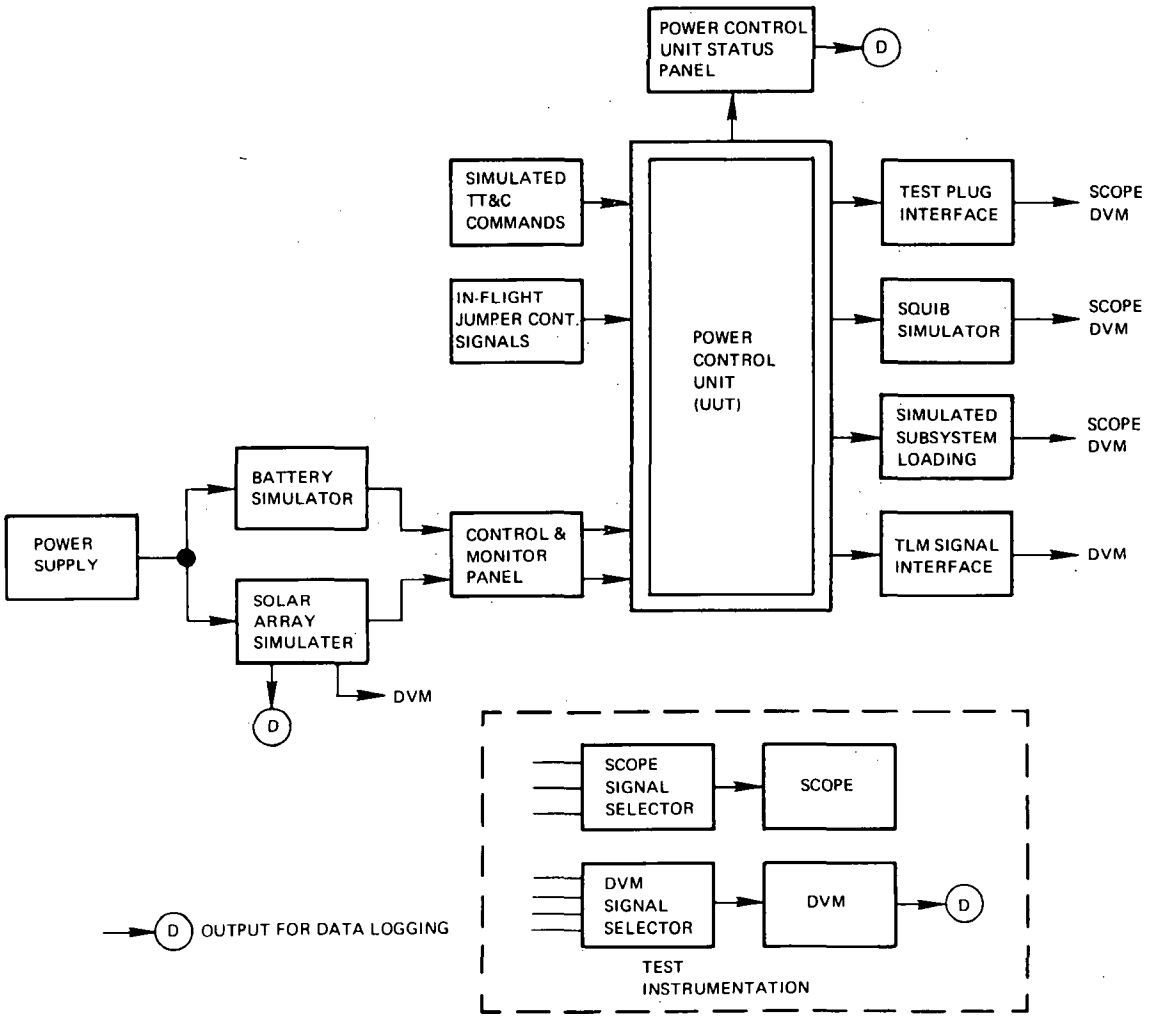

Figure 5-108. Power Control Unit BTE Functions

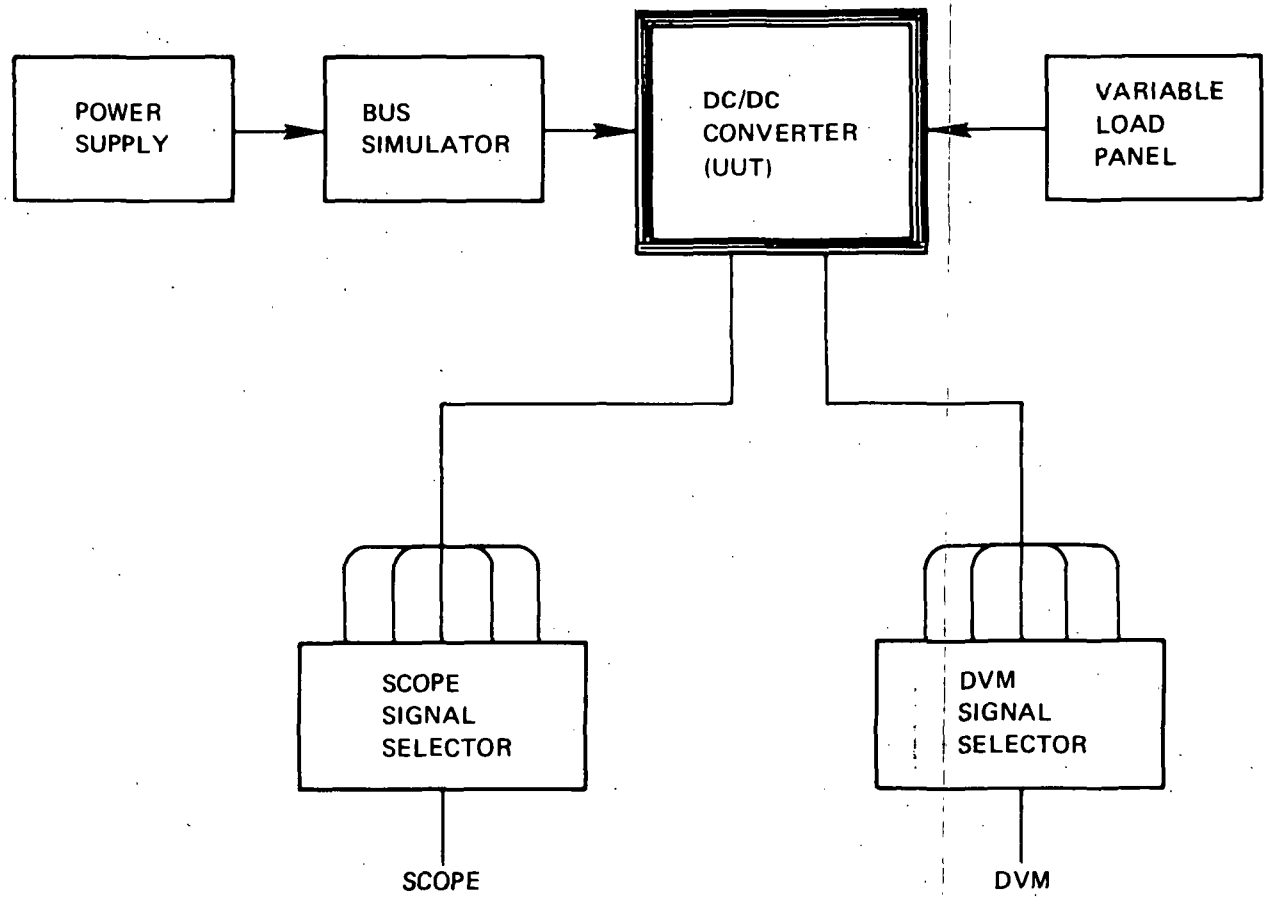

Figure 5-109. DC/DC Converter BTE

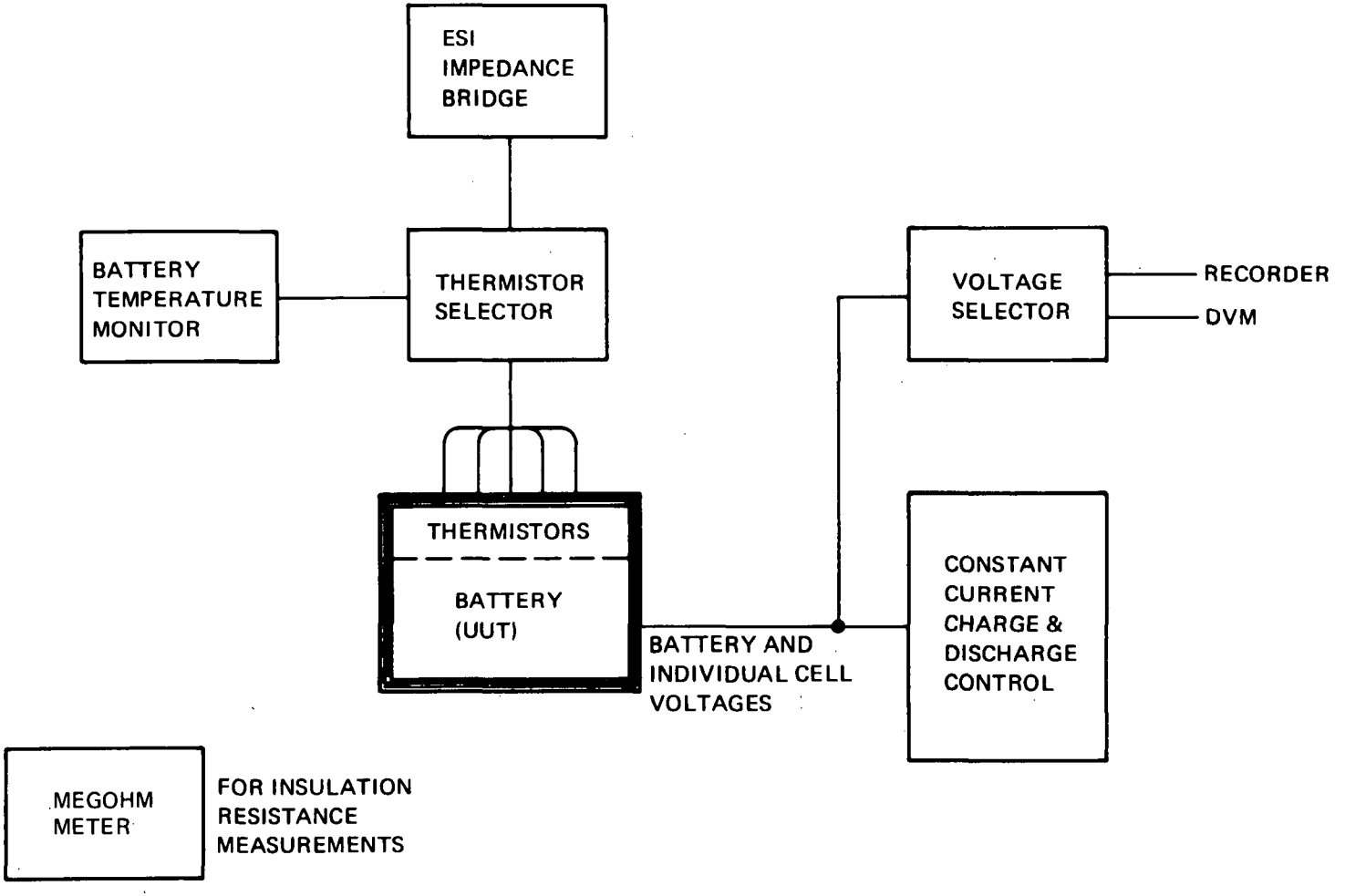

Figure 5-110. Battery Test Set

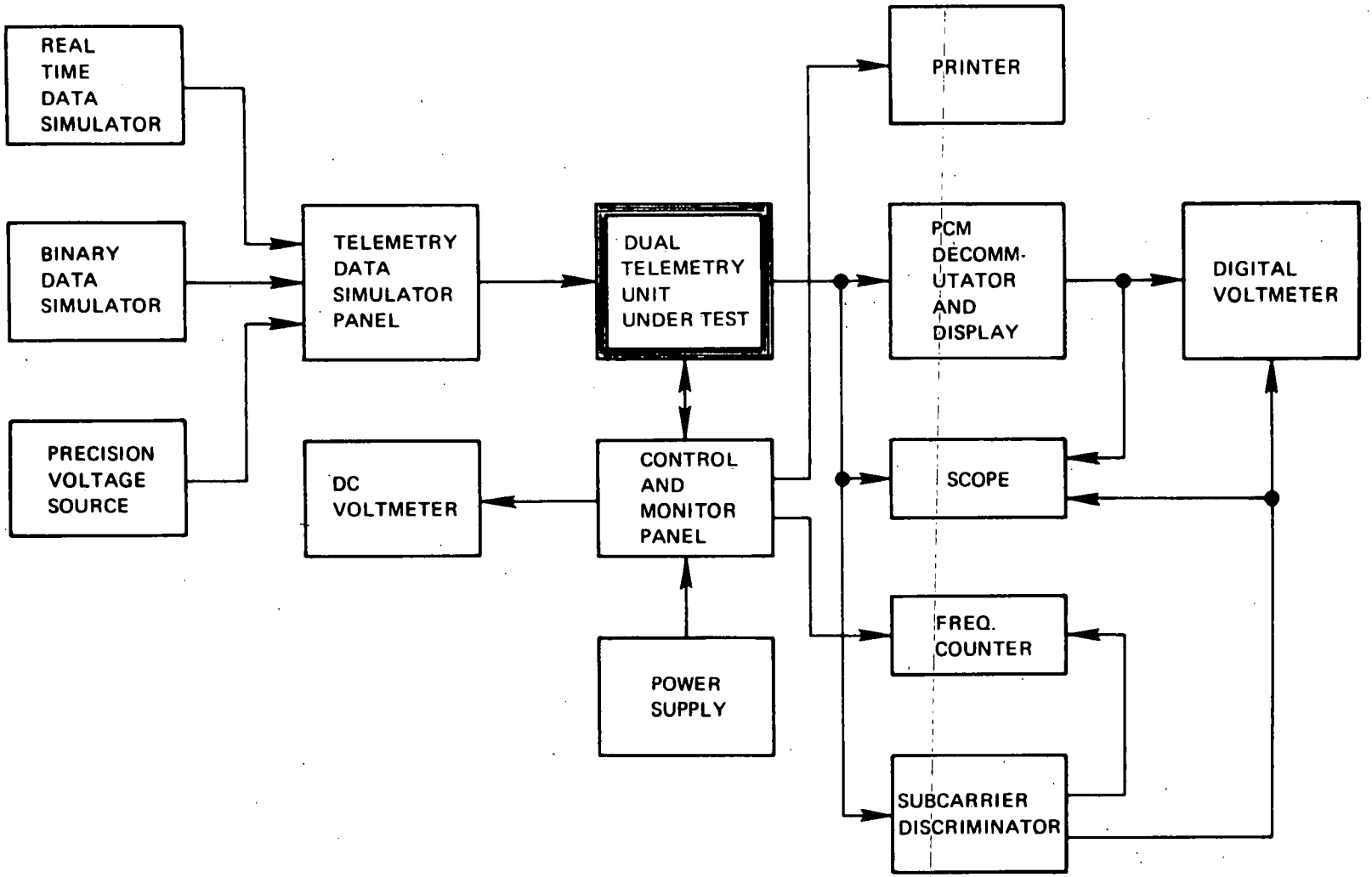

Figure 5-111. Telemetry Unit Bench Test Equipment

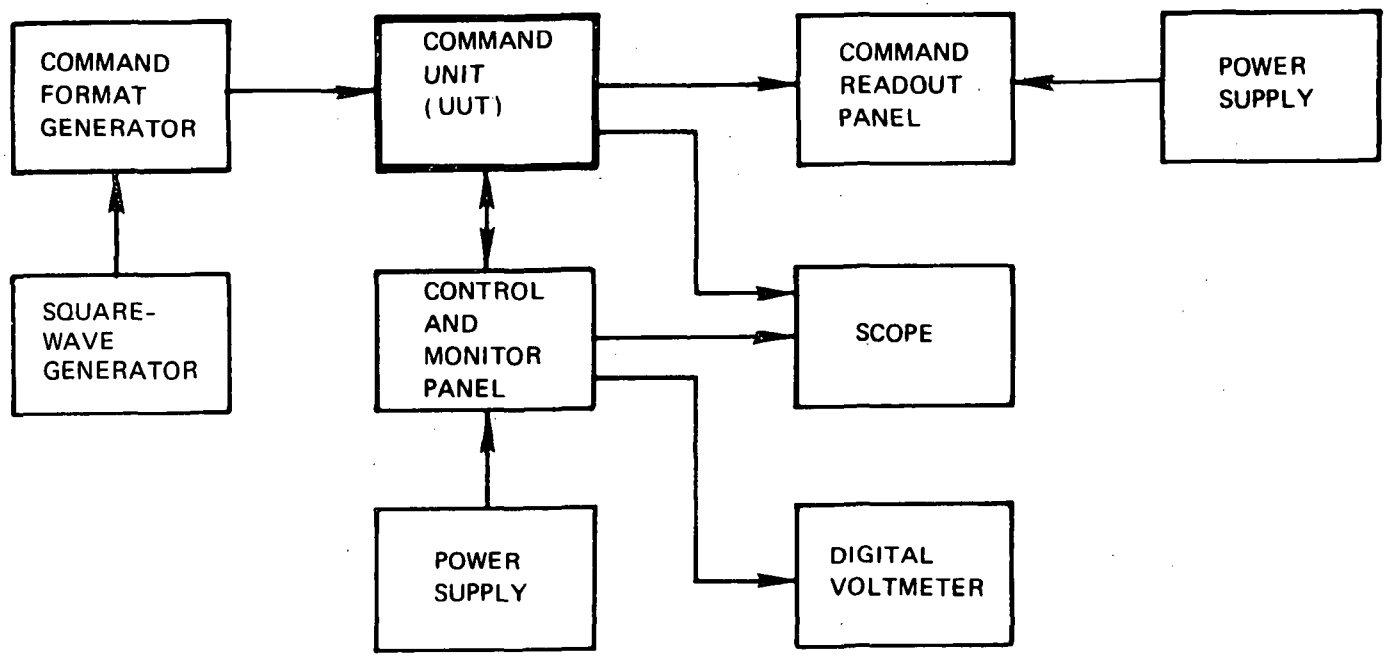

Figure 5-112. Command Unit BTE

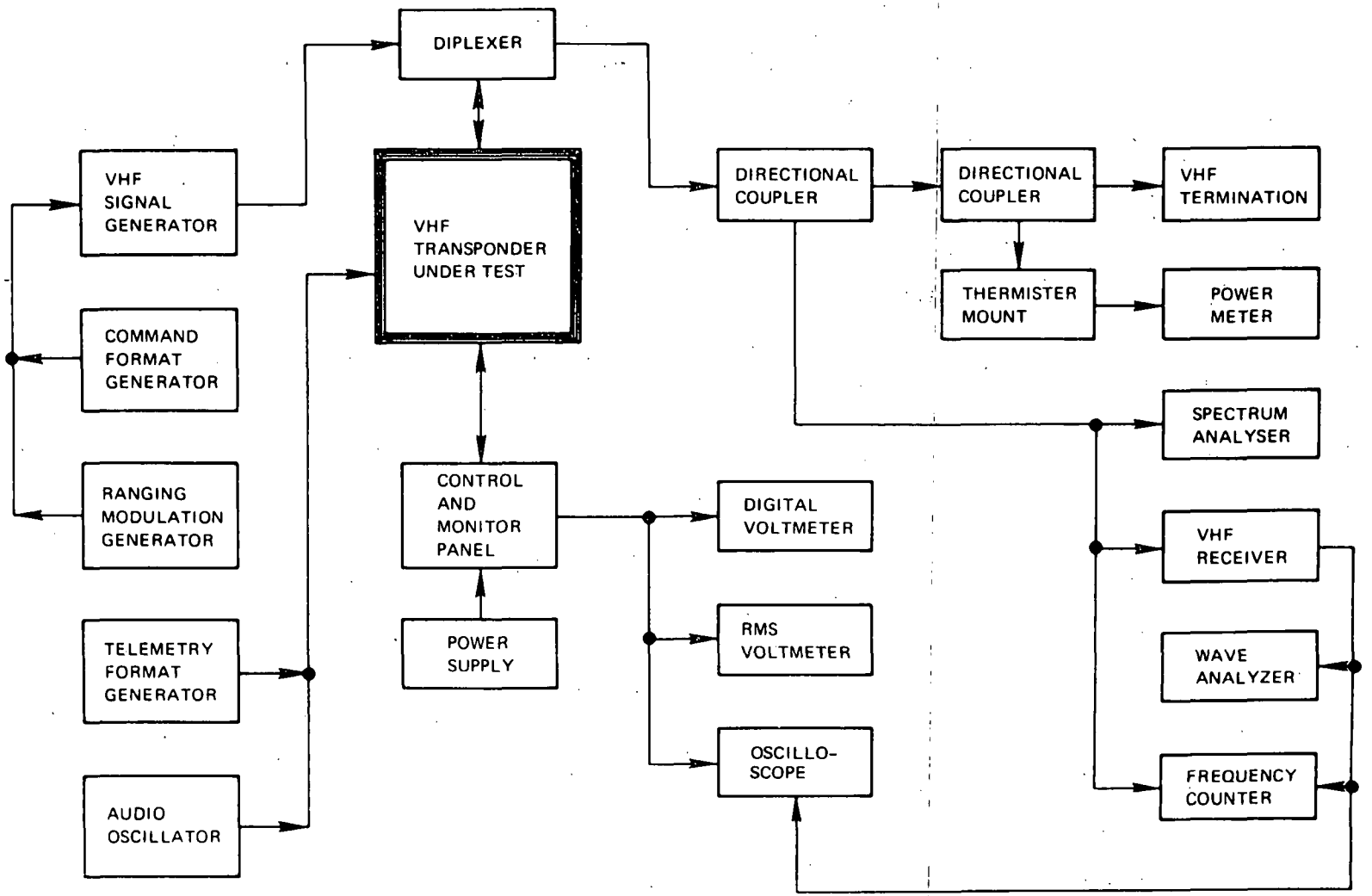

Figure 5-113. VHF Transponder Bench Test Equipment

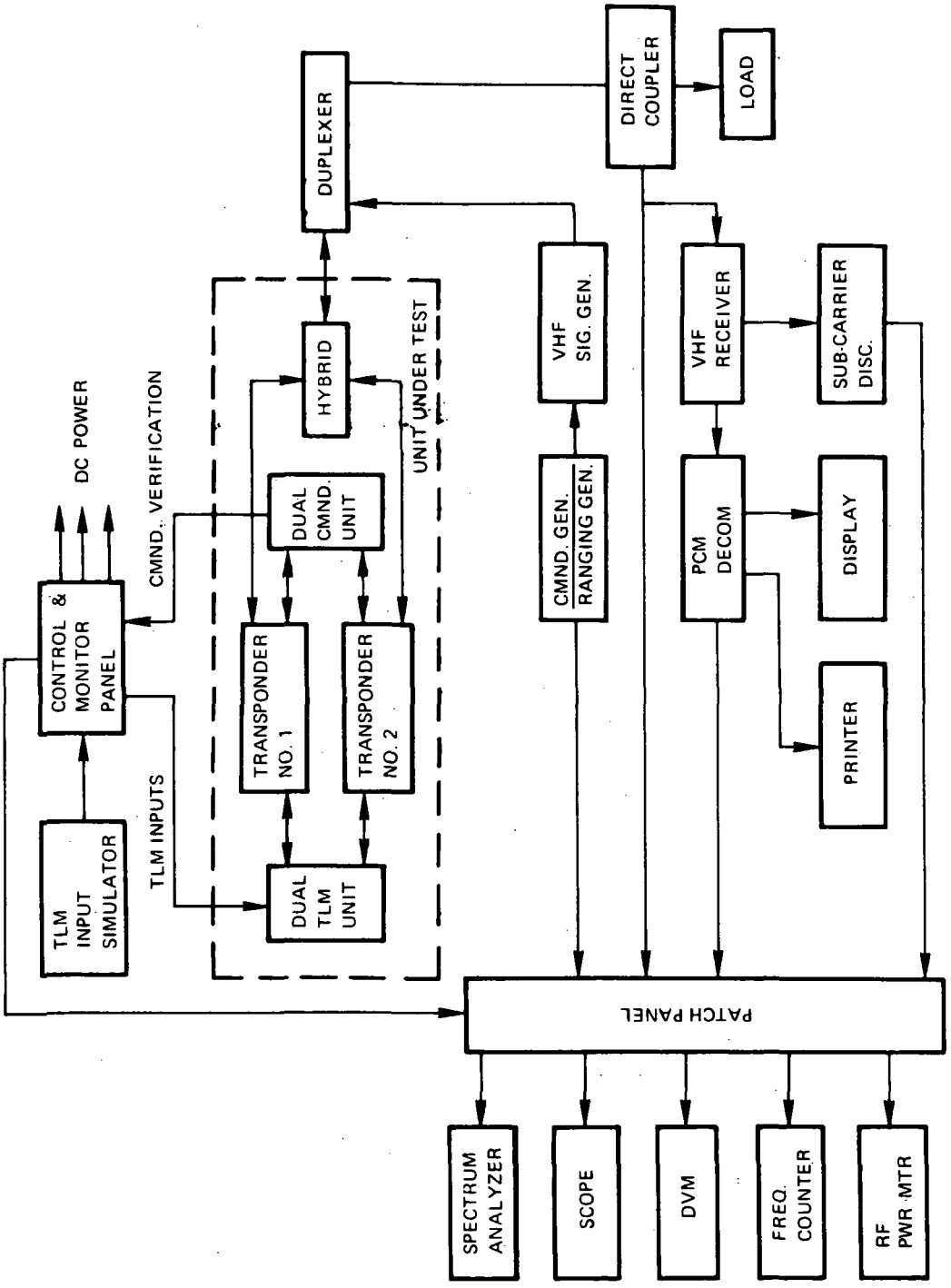

Figure 5-114. Telemetry and Command Subsystem Test Setup

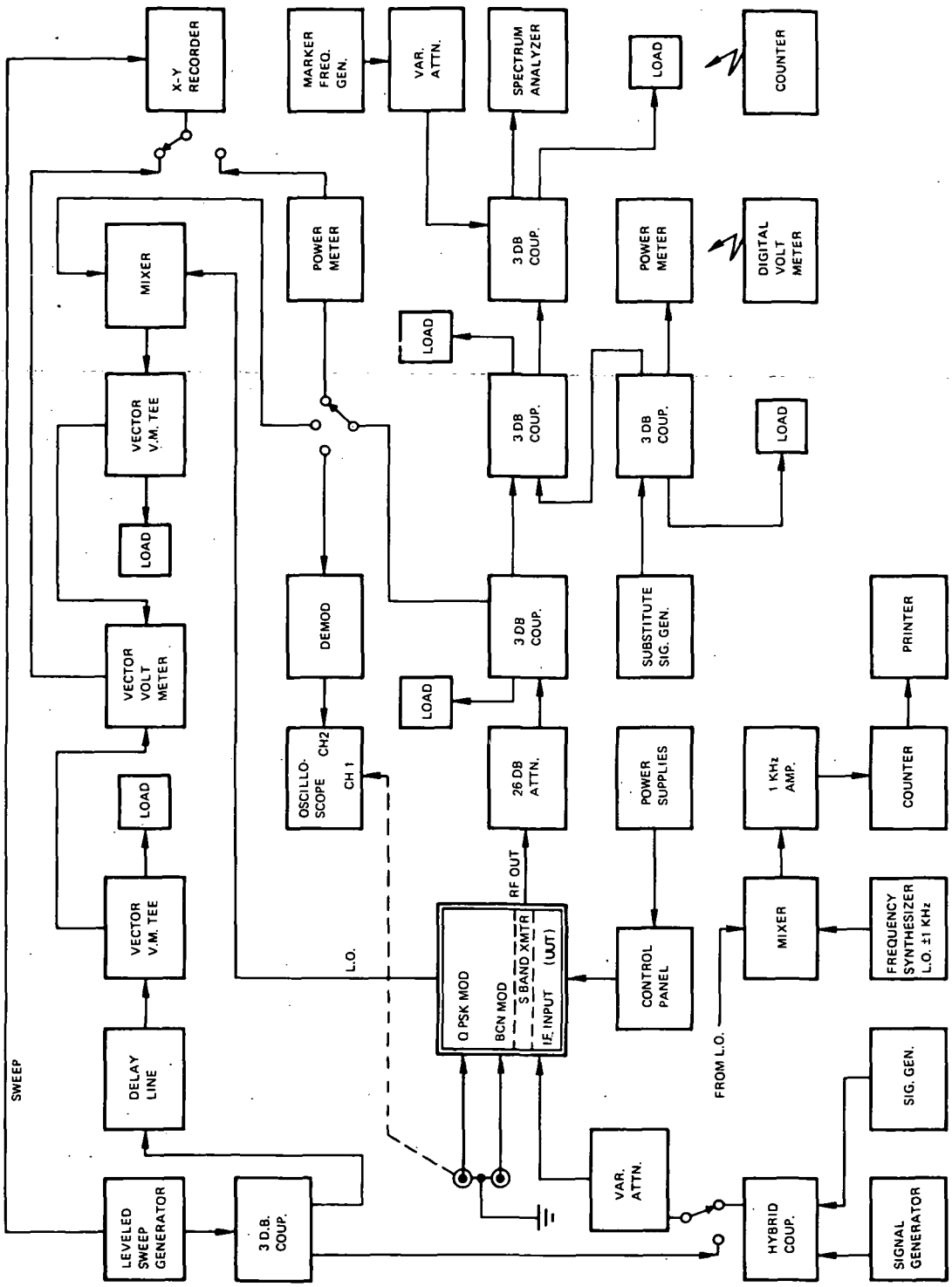

Figure 5-115. S-Band Transmitter Bench Test Equipment

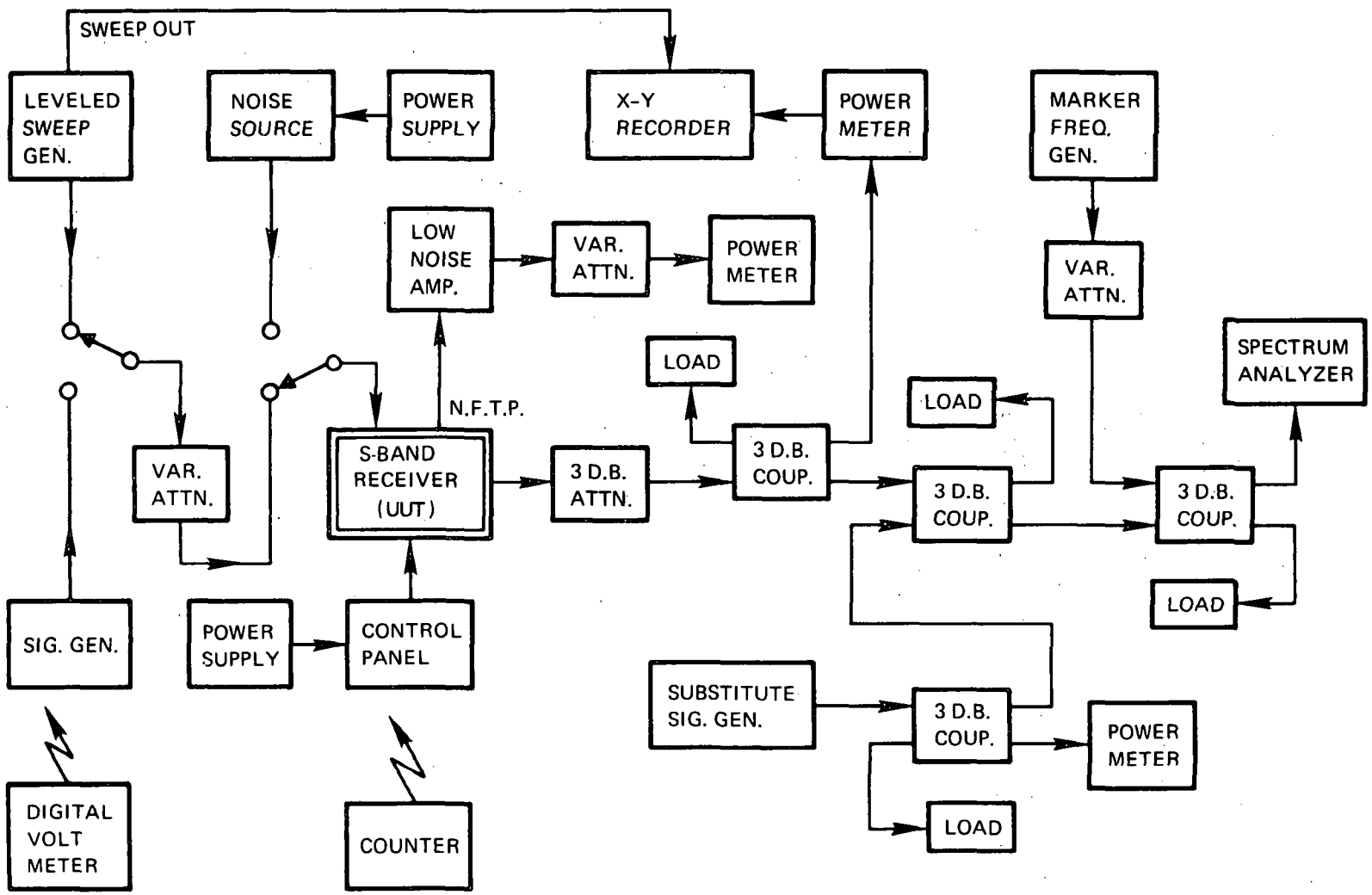

Figure 5-116. S-Band Receiver Bench Test Equipment

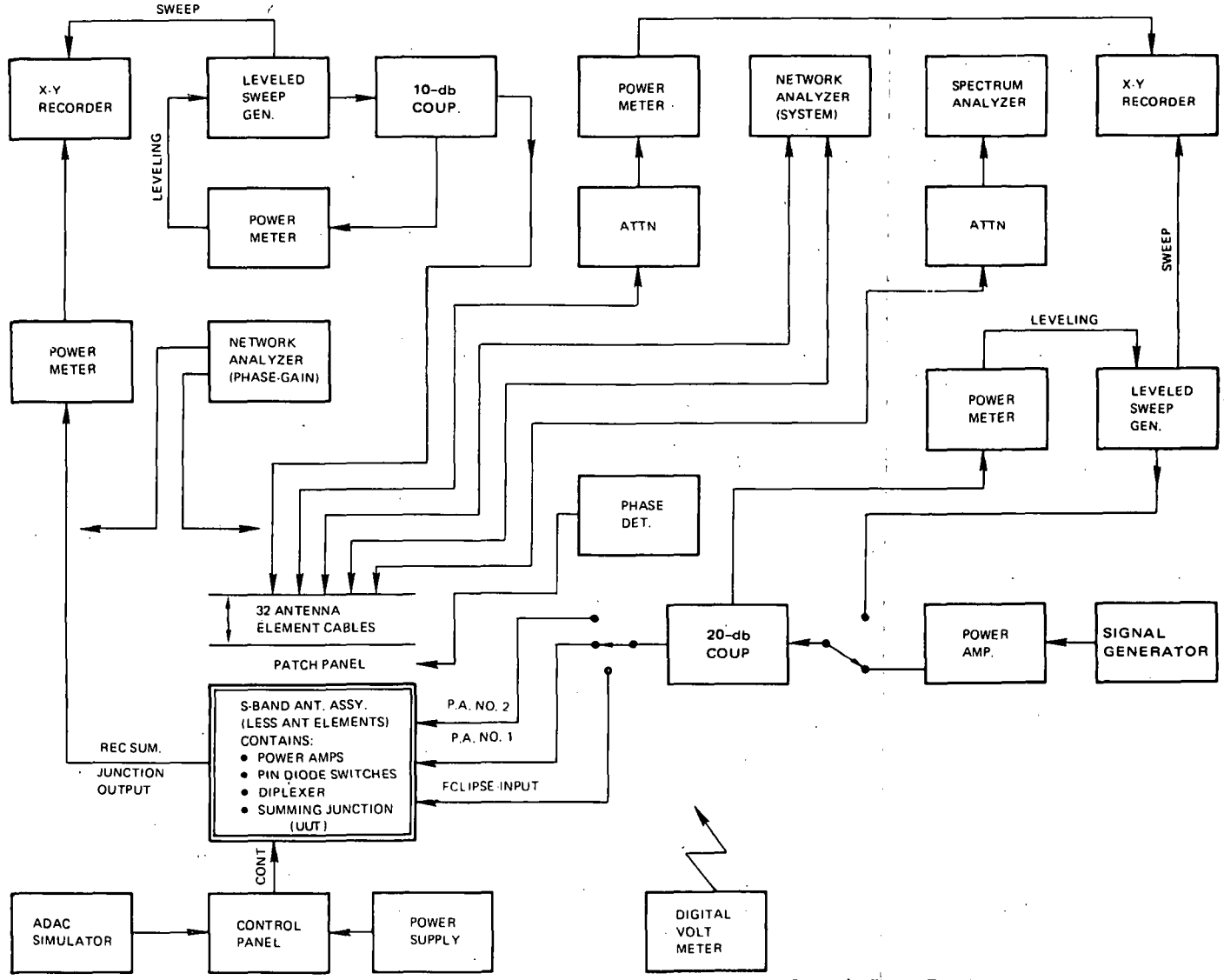

Figure 5-117. S-Band Communications Antenna Bench Test Equipment

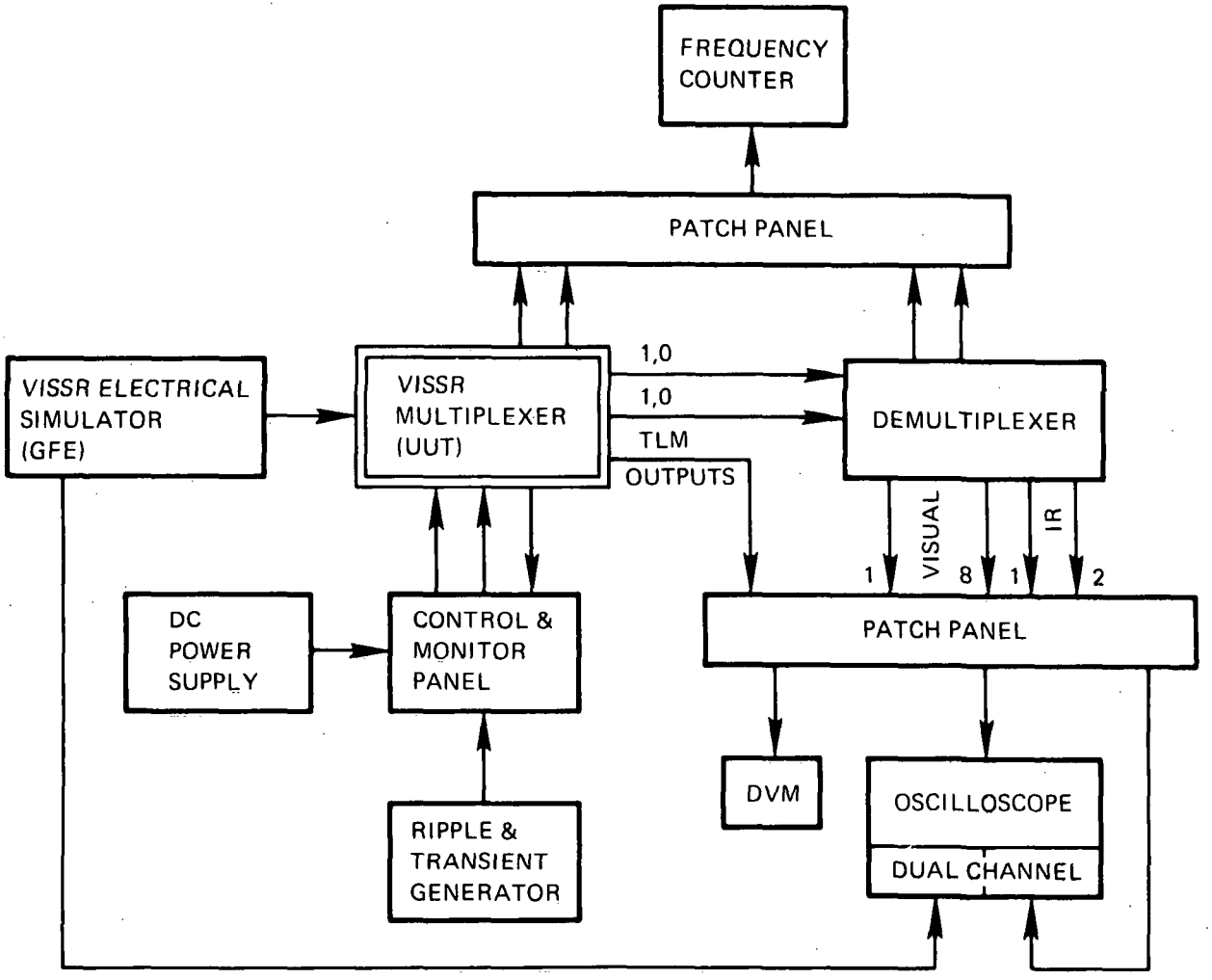

Figure 5-118. VISSR Multiplexer Bench Test Equipment (S-Band)

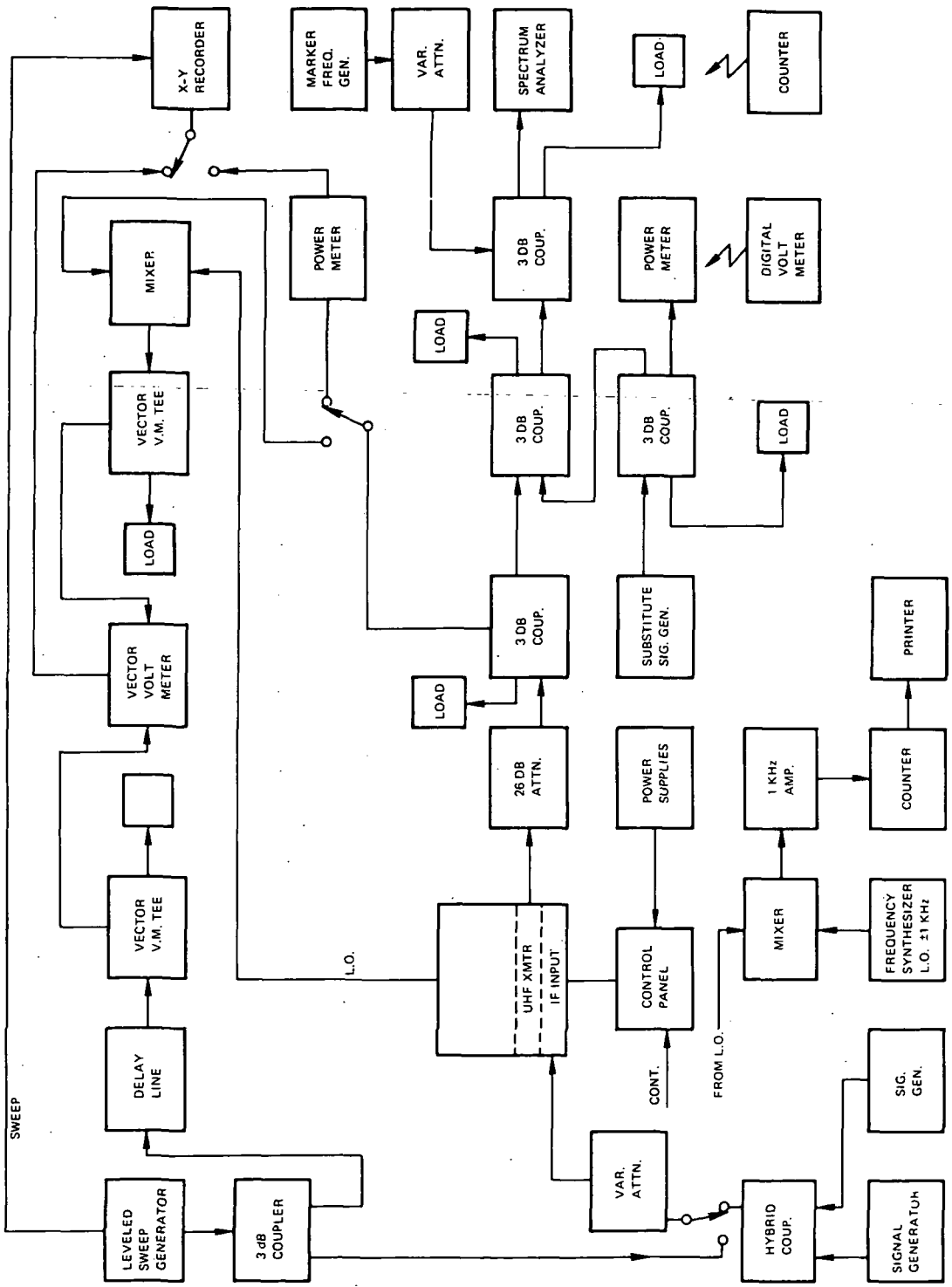

Figure 5-119. UHF Transmitter Bench Test Equipment

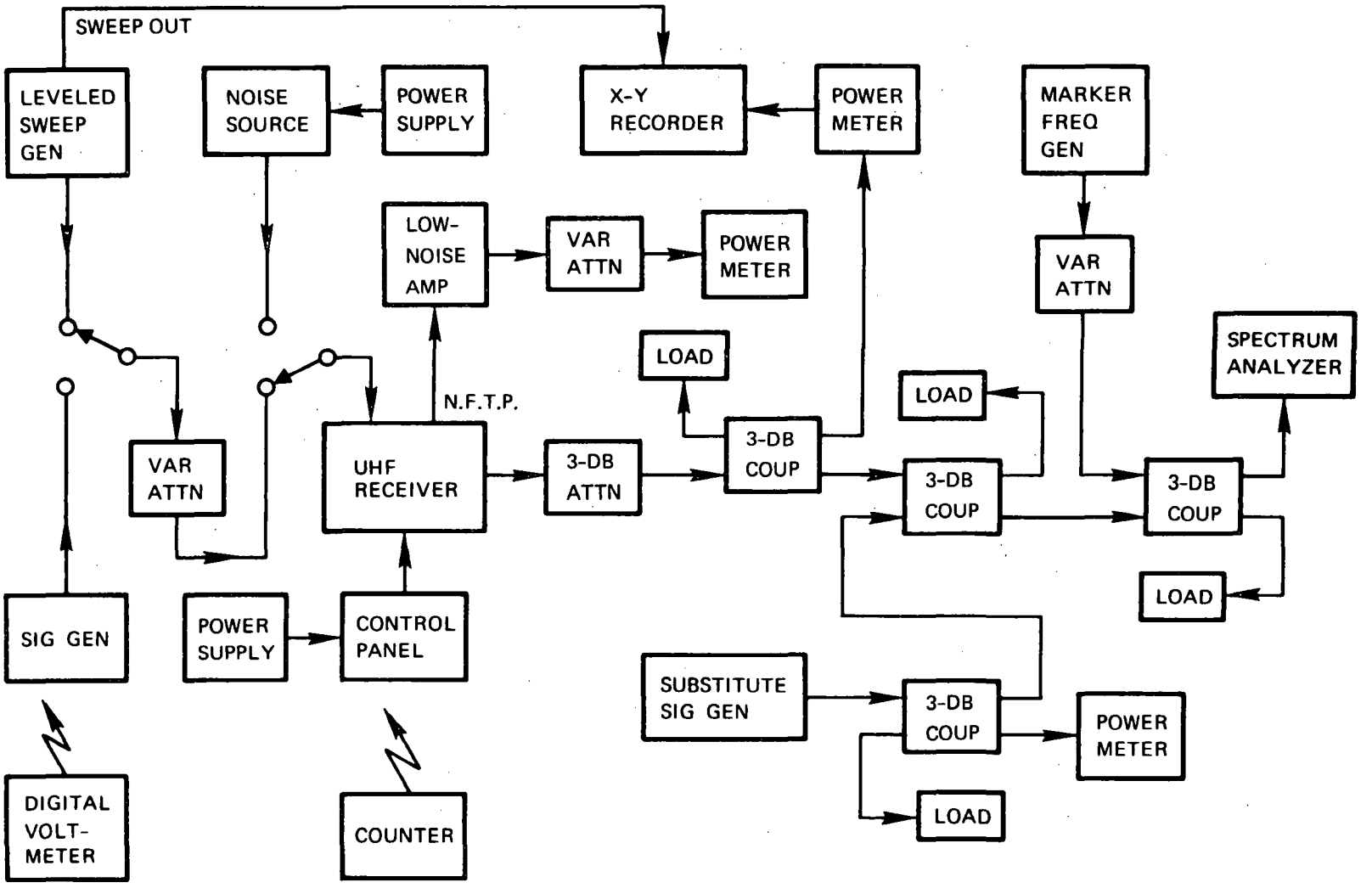

Figure 5-120. UHF Reciever Bench Test Equipment

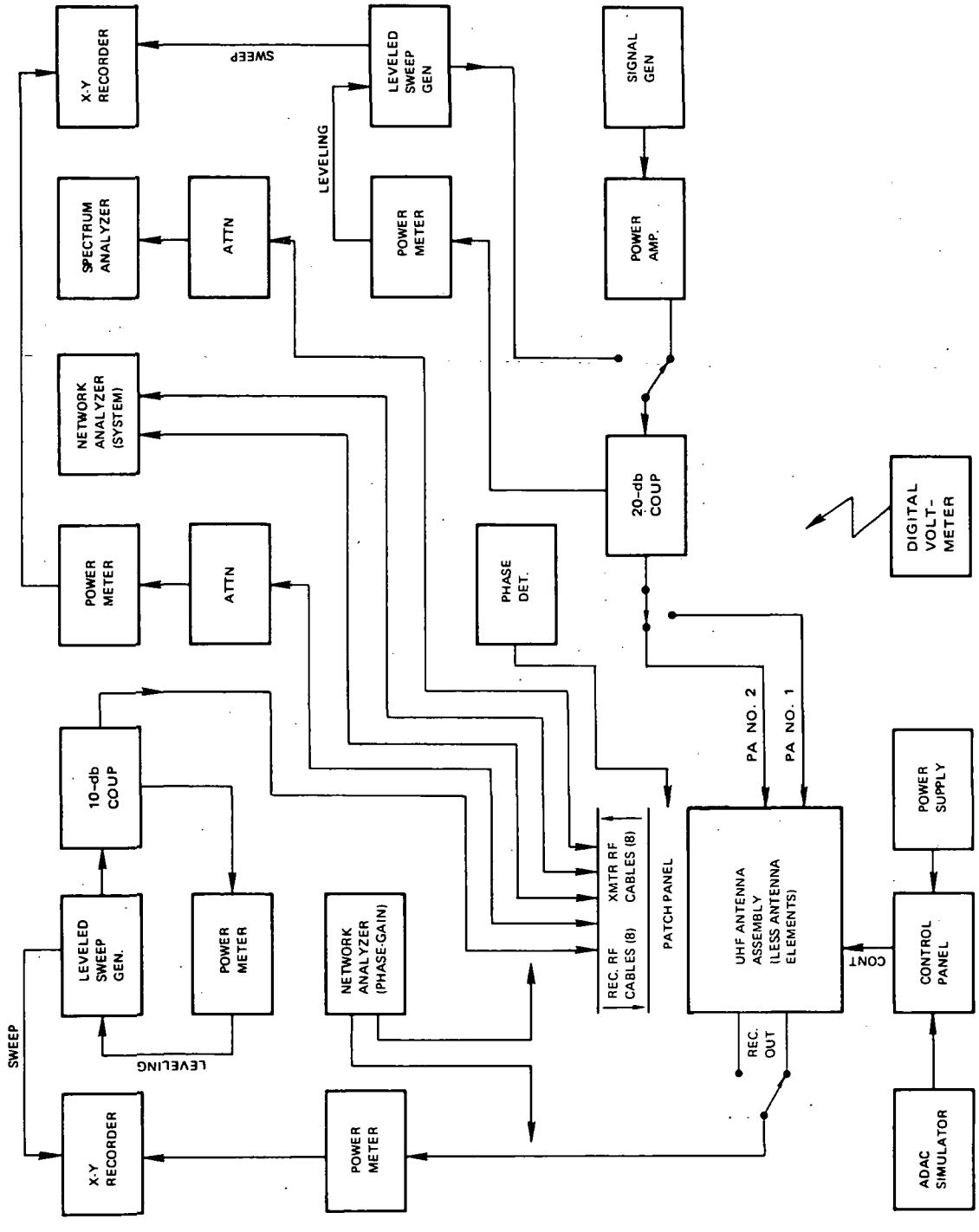

Figure 5-121. UHF Antenna Assembly Bench Test Equipment

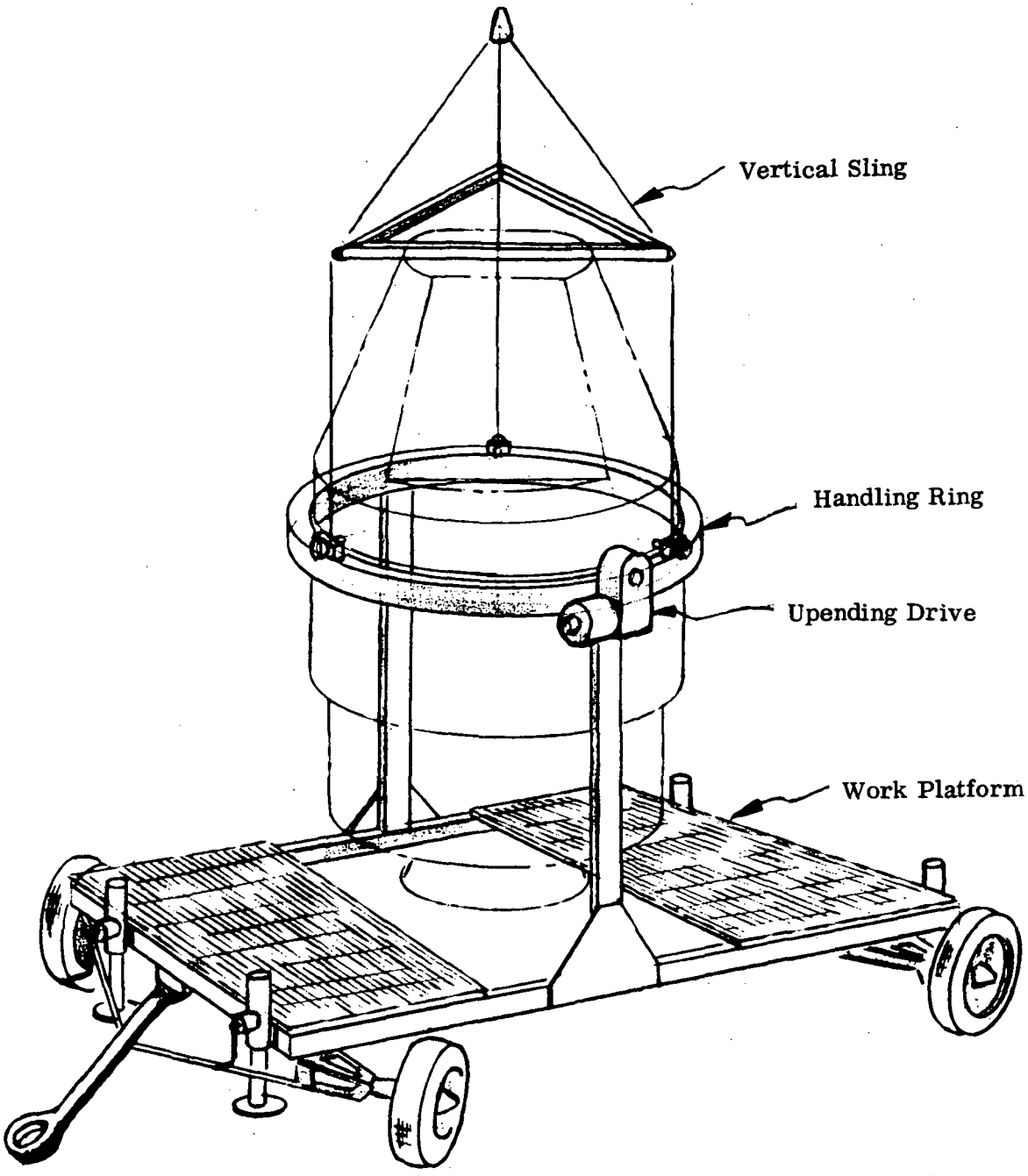

Figure 5-122. Satellite Dolly with Handling Ring

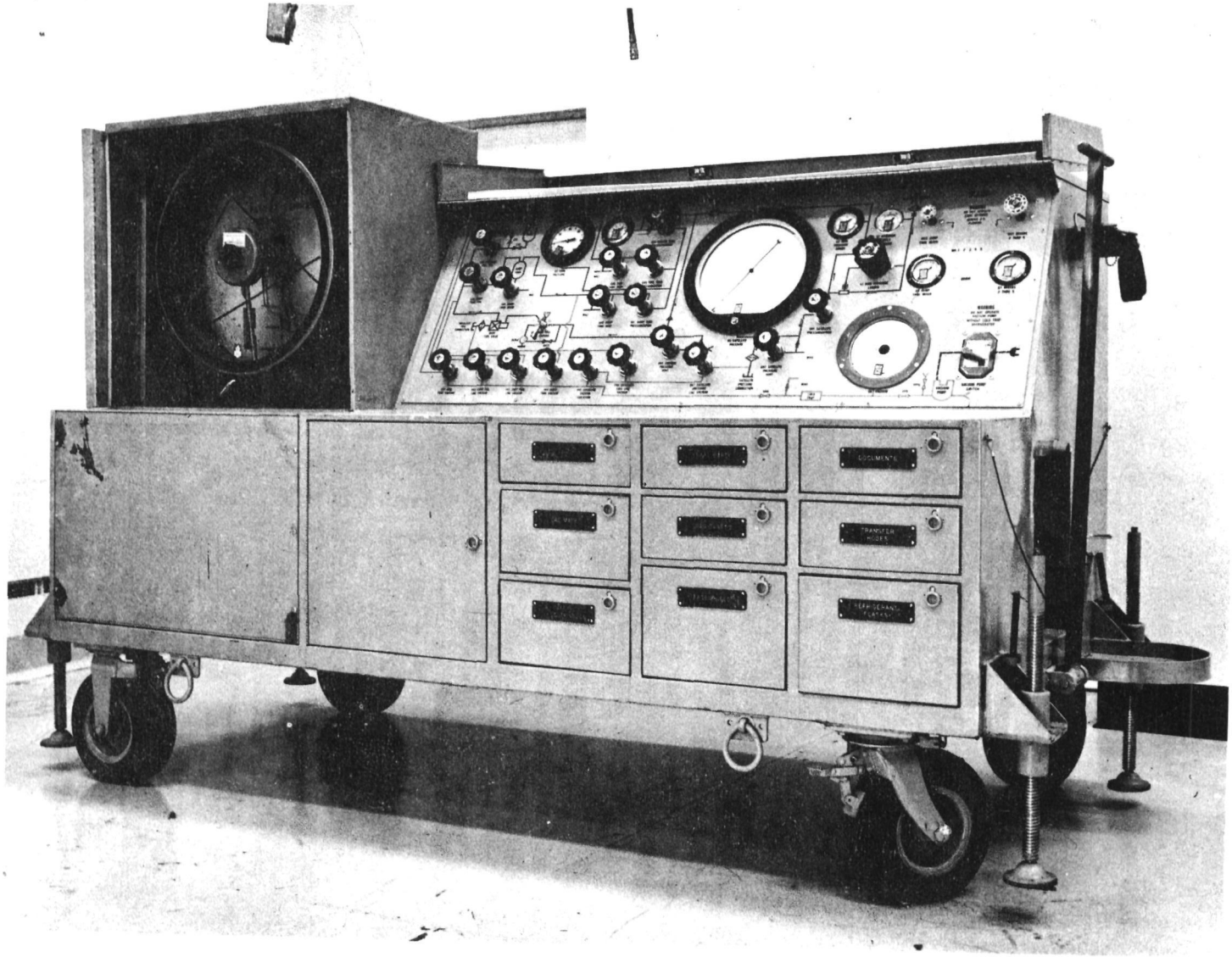

Figure 5-123. Reaction Control Service Cart

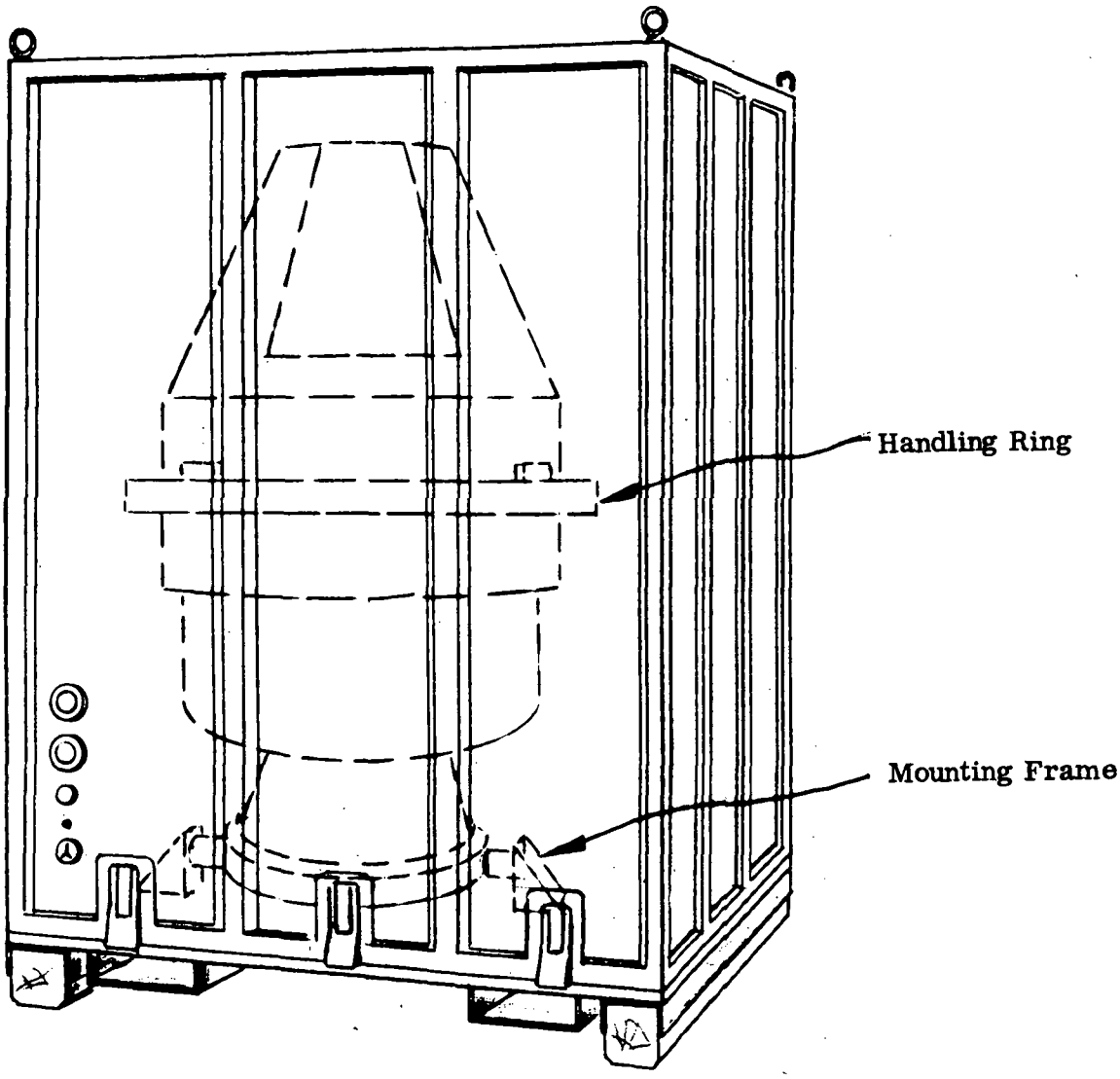

Figure 5-124. Satellite Shipping Container

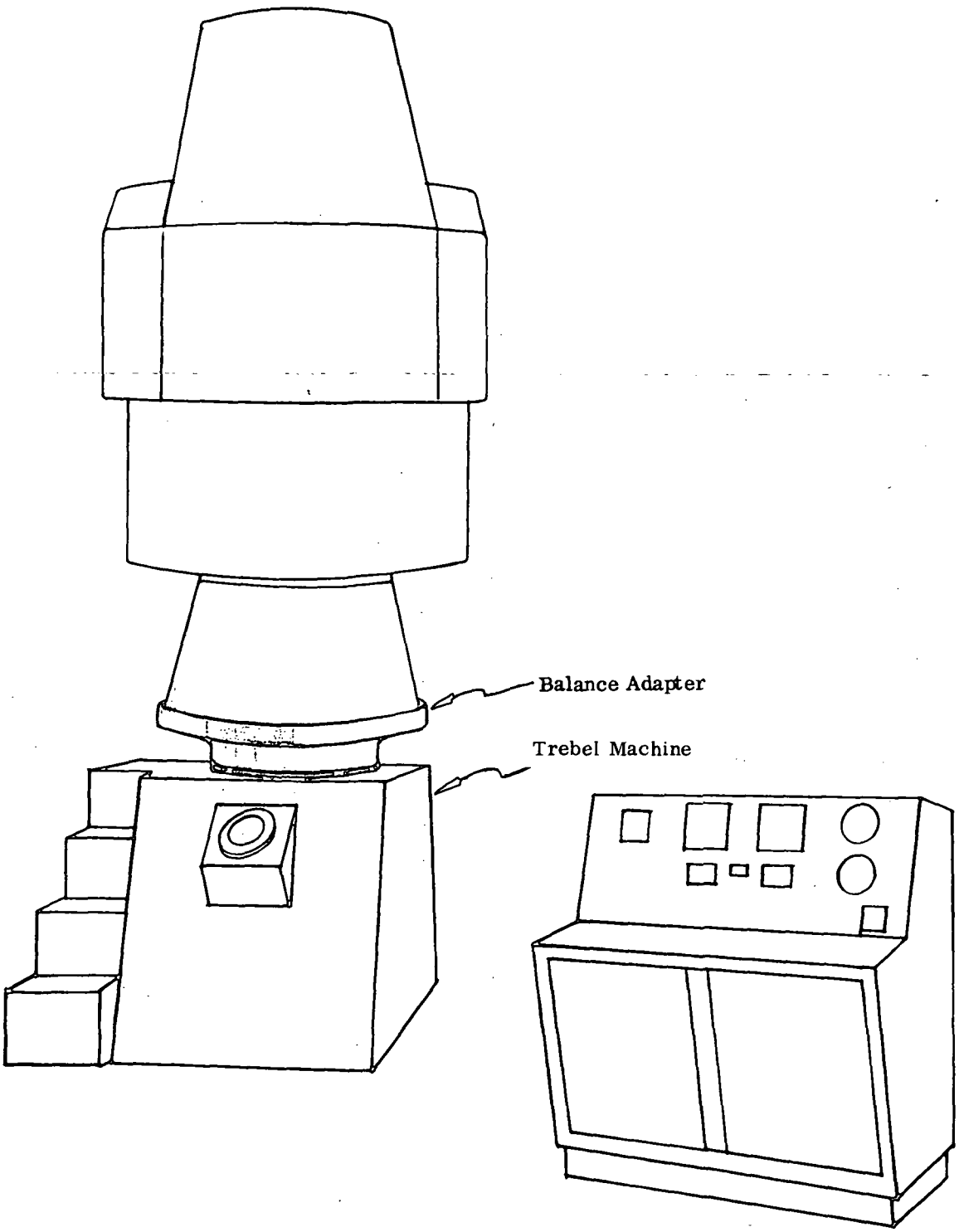

Figure 5-125. Dynamic Balance/Moment-of-Inertia Setup

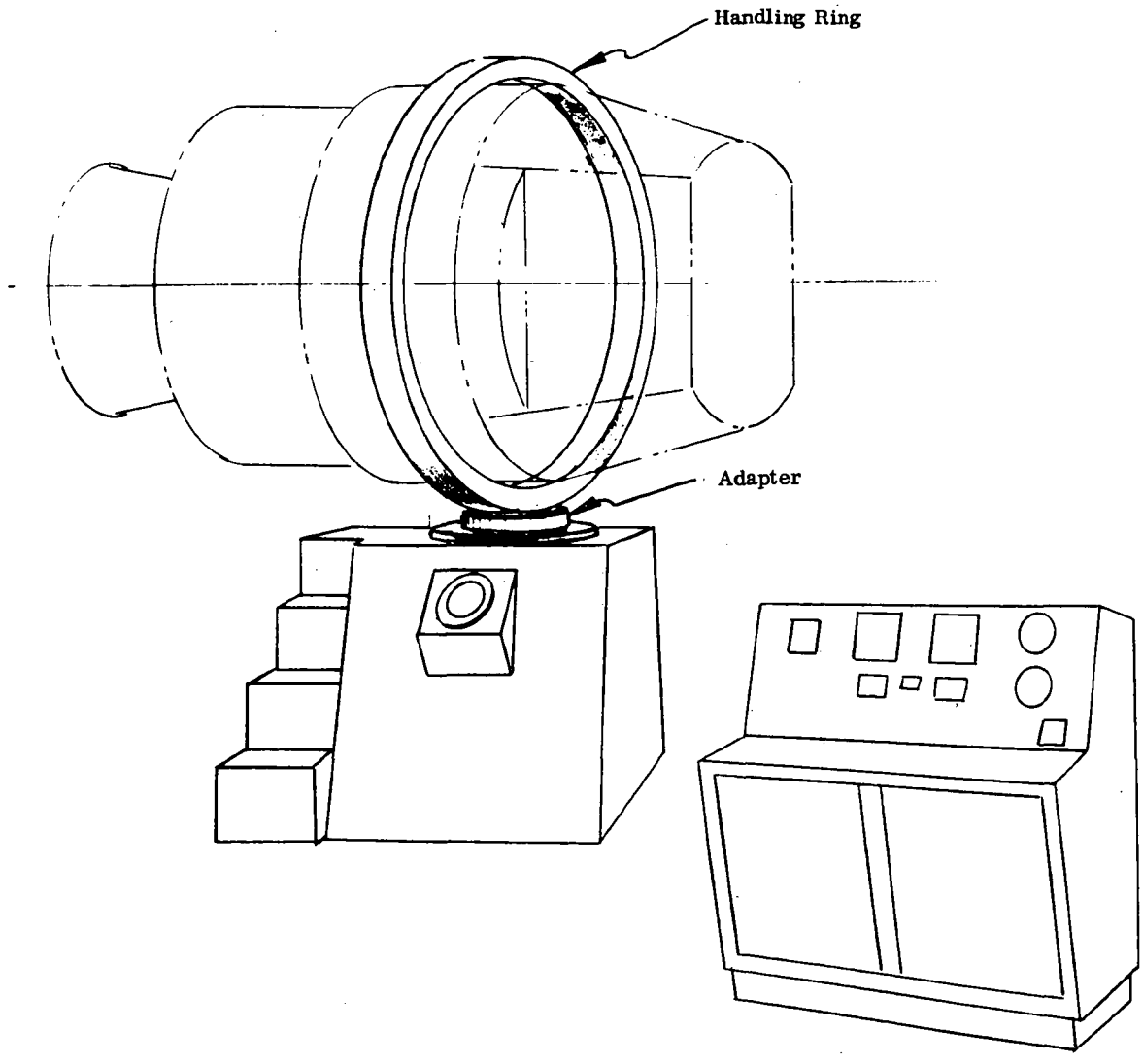

Figure 5-126. Center of Gravity/Moment-of-Inertia Setup

REFERENCES

1. Conceptual Design Review Package for SMS Program. Philco-Ford WDL TR4458A. April 11, 1971

2. Aerospace Data Systems Standards, Part 1, Section 1, Pulse Code Modulation Telemetry Standard. Goddard Space Flight Center, Greenbelt, Maryland 20771. January 27, 1966

3. Summary of Non-Black and Black Interior Spacecraft. TS118, SMS-PCC 1052. January 20, 1971

4. Thermal Mathematical Model for Conceptual Thermal Design of SMS Spacecraft. TS-130, SMS-PCC 1225. February 26, 1971

5. Power Amplifier Integration Optimization Study. TS-126, SMS-PCC 1210. February 23, 1971

6. SMS Spacecraft - VISSR Thermal Interface. TS-109, SMS-PCC 1013. January 8, 1971

7. SMS - VISSR Thermal Interface Analysis. TS-128, SMS-PCC 1222. February 23, 1971

APPENDIX A

TELEMETRY LIST

MAIN FRAME

No.	Type	Title	Remarks
1.	Sync		
2.	Sync		
3.	Bilevel		
4.	Bilevel		
5.	Bilevel		
6.	Analog	H_p amp	
7.	Analog	H_t sun	
8.	Analog	H_t quad	
9.	Analog	VISSR +15 V signal voltage	
10.	Analog	VISSR +15 V aux voltage	
11.	Analog	VISSR +5 V aux voltage	
12.	Analog	VISSR +5 V aux voltage	
13.	Analog	VISSR scanner temp. No. 1	
14.	Analog	VISSR scanner temp. No. 2	
15.	Bilevel		
16.	Analog	X-ray short sun	
17.	Bilevel		
18.	Analog	X-ray long sun	

MAIN FRAME

No.	Type	Title	Remarks
19.	Analog	VISSR scanner temp. No. 3	
20.	Analog	VISSR scanner temp. No. 4	
21.	Bilevel		
22.	Analog	H_p amp	
23.	Analog	H_t sun	
24.	Analog	H_t quad	
25.	Analog	VISSR PMT No. 1 HV MON	
26.	Analog	VISSR PMT No. 2 HV MON	
27.	Analog	VISSR PMT No. 3 HV MON	
28.	64 CH	Submultiplexer	
29.	Analog	VISSR PMT No. 4 HV MON	
30.	Analog	VISSR PMT No. 5 HV MON	
31.	Bilevel		
32.	Analog	VISSR PMT No. 6 HV MON	
33.	Bilevel		
34.	Analog	VISSR PMT No. 7 HV MON	
35.	Analog	VISSR PMT No. 8 HV MON	
36.	Bilevel		
37.	Bilevel		
38.	Analog	H_p amp	

MAIN FRAME

No.	Type	Title	Remarks
39.	Analog	H_t sun	
40.	Analog	H_t quad	
41.	Analog	VISSR CAL TGT temp. No. 1	
42.	Analog	VISSR CAL TGT temp. No. 2	
43.	Analog	VISSR therm. CH DET. temp.	
44.	Analog	VISSR RAD stage 1 temp.	
45.	Analog	VISSR elect Mod temp.	
46.	Analog	VISSR DET temp. control current	
47.	Bilevel		
48.	Analog	Spare	
49.	Bilevel		
50.	Analog	Spare	
51.	Analog	Spare	
52.	Analog	Spare	
53.	Bilevel		
54.	Analog	H_p amp	
55.	Analog	H_t sun	
56.	Analog	H_t quad	
57.	Analog	Main bus voltage	
58.	Analog	Control bus current	

MAIN FRAME

No.	Type	Title	Remarks
59.	Analog	Main bus current	
60.	32 CH	Submultiplexer	
61.	Analog	TLM CAL high	
62.	Analog	TLM CAL low	
63.	Bilevel		
64.	Analog	Spare	

64-Ch Submultiplexer - (all temp data)

No.	Type	Title	Remarks
1.	Analog	Spare	Note 1
2.	Analog	Spare	Note 1
3.	Analog	Spare	Note 1
4.	Analog	Spare	Note 1
5.	Analog	Magnetometer	
6.	Analog	Magnetometer electronics	
7.	Analog	X-ray	
8.	Analog	X-ray electronics	
9.	Analog	Particle counter	
10.	Analog	Particle counter processing unit	
11.	Analog	Battery	
12.	Analog	Spare	

64-Ch Submultiplexer - (all temp data)

No.	Type	Title	Remarks
13.	Analog	Power Control Unit	
14.	Analog	Ant. solar array (high)	
15.	Analog	Solar array fwd (high)	
16.	Analog	Solar array aft (high)	
17.	Analog	VHF transmitter No. 1	
18.	Analog	VHF transmitter No. 2	
19.	Analog	S-band transponder No. 1	
20.	Analog	S-band transponder No. 2	
21.	Analog	UHF transponder No. 1	
22.	Analog	UHF transponder No. 2	
23.	Analog	S-band pwr amp No. 1	
24.	Analog	S-band pwr amp No. 2	
25.	Analog	UHF pwr amp No. 1	
26.	Analog	UHF pwr amp No. 2	
27.	Analog	ABM case	
28.	Analog	ABM case	
29.	Analog	ABM adapter	
30.	Analog	Conical shell	
31.	Analog	VISSR fwd insulation	
32.	Analog	VISSR sunshade	

64-Ch Submultiplexer - (all temp data)

No.	Type	Title	Remarks
33.	Analog	VISSR sunshade insulation	
34.	Analog	Thermal shield aft	
35.	Analog	Thermal shield fwd	
36.	Analog	APS tank No. 1	
37.	Analog	APS 5 RT* No. 1	
38.	Analog	APS 5 RS* No. 1	
39.	Analog	APS 5 RT* No. 2	
40.	Analog	APS 5 RS* No. 2	
41.	Analog	APS .5 RT* No. 1	
42.	Analog	APS .5 RS* No. 1	
43.	Analog	APS .5 RT* No. 2	
44.	Analog	APS .5 RS* No. 2	
45.	Analog	APS 5 AT* No. 1	
46.	Analog	APS 5 AS* No. 1	
47.	Analog	APS 5 AT* No. 2	
48.	Analog	APS 5 AS* No. 2	
49.	Analog	APS propellant line No. 1	

*RT radial chamber temperature
RS radial valve temperature
AT axial chamber temperature
AS axial valve temperature

64-Ch Submultiplexer - (all temp data)

No.	Type	Title	Remarks
50.	Analog	APS propellant line No. 2	
51.	Analog	Solar array fwd (low)	
52.	Analog	Ant solar array (low)	
53.	Analog	Equipment panel quadrant 1	
54.	Analog	Equipment panel quadrant 2	
55.	Analog	Equipment panel quadrant 3	
56.	Analog	Equipment panel quadrant 4	
57.	Analog	Spare	
58.	Analog	Spare	
59.	Analog	Spare	
60.	Analog	Spare	
61.	Analog	Spare	
62.	Analog	Spare	
63.	Analog	Spare	
64.	Analog	Spare	

32-Ch Submultiplexer

No.	Type	Title	Remarks
1.	Analog	S-band RF pwr out No. 1	Note 2
2.	Analog	S-band RF pwr out No. 2	Note 2

32-Ch Submultiplexer

No.	Type	Title	Remarks
3.	Analog	S-band RF pwr out No. 3	Note 2
4.	Analog	S-band RF pwr out No. 4	Note 2
5.	Analog	Magnetometer reference voltage	
6.	Analog	X-ray short background	
7.	Analog	X-ray long background	
8.	Analog	X-ray reference voltage	
9.	Analog	Particle counter reference voltage	
10.	Analog	X-ray elevation	
11.	Analog	Battery voltage	
12.	Analog	Control bus voltage	
13.	Analog	Solar array current	
14.	Analog	Battery charge current	
15.	Analog	Spare	
16.	Analog	VHF RF pwr out	
17.	Analog	Spare	
18.	Analog	VISSR mux 1 voltage 2	
19.	Analog	VISSR mux 1 voltage 4	
20.	Analog	VISSR mux 1 voltage 6	
21.	Analog	VISSR mux 2 voltage 2	
22.	Analog	VISSR mux 2 voltage 4	

32-Ch Submultiplexer

No.	Type	Title	Remarks
23.	Analog	VISSR mux 2 voltage 6	
24.	Analog	ADAC pin diode current mon	
25.	Analog	APS pressure sensor	
26.	Analog	UHF RF pwr output	
27.	Analog	Spare	
28.	Analog	Battery discharge current	
29.	Bilevel		
30.	Bilevel		
31.	Bilevel		
32.	Bilevel		

Word 3 Bilevel

Bit No.	Title	Remarks
1.	TLM mode "NORMAL"	
	TLM mode "DWELL"	
2.	Cmd decoder 1 data accept - yes	
	Cmd decoder 1 data accept - no	
3.	Cmd decoder 2 data accept - yes	
	Cmd decoder 2 data accept - no	
4.	Subframe 1 thru 10 - yes	
	Subframe 1 thru 10 - no	

Word 3 Bilevel

Bit No.	Title	Remarks
5.	Subframe 11 thru 20 - yes	
	Subframe 11 thru 20 - no	
6.	Subframe 21 thru 30 - yes	
	Subframe 21 thru 30 - no	
7.	Subframe 31 thru 40 - yes	
	Subframe 31 thru 40 - no	
8.	Subframe 41 thru 50 - yes	
	Subframe 41 thru 50 - no	
9.	Subframe 51 thru 60 - yes	
	Subframe 51 thru 60 - no	

Word 4 Bilevel

Bit No.	Title	Remarks
1.	Command verification bit 1 ONE	
	Command verification bit 1 ZERO	
2.	Command verification bit 2 ONE	
	Command verification bit 2 ZERO	
3.	Command verification bit 3 ONE	
	Command verification bit 3 ZERO	
4.	Command verification bit 4 ONE	
	Command verification bit 4 ZERO	

Word 4 Bilevel

Bit No.	Title	Remarks
5.	Command verification bit 5 ONE	
	Command verification bit 5 ZERO	
6.	Command verification bit 6 ONE	
	Command verification bit 6 ZERO	
7.	Command verification bit 7 ONE	
	Command verification bit 7 ZERO	
8.	Command verification bit 8 ONE	
	Command verification bit 8 ZERO	
9.	Spare	
	Spare	

Word 5 Bilevel

Bit No.	Title	Remarks
1.	H_p offset bit 1 ONE	
	H_p offset bit 1 ZERO	
2.	H_p offset bit 2 ONE	
	H_p offset bit 2 ZERO	
3.	H_p offset bit 3 ONE	
	H_p offset bit 3 ZERO	
4.	H_p offset bit 4 ONE	
	H_p offset bit 4 ZERO	

Word 5 Bilevel

Bit No.	Title	Remarks
5.	H_p offset bit 5 ONE	
	H_p offset bit 5 ZERO	
6.	H_p offset bit 6 ONE	
	H_p offset bit 6 ZERO	
7.	H_T scale 1 bit 1 ONE	
	H_T scale 2 bit 1 ZERO	
8.	H_T scale 2 bit 1 ONE	
	H_T scale 2 bit 1 ZERO	
9.	Magnetometer "CALIBRATE"	
	Magnetometer "DATA"	

Word 15 Bilevel

Bit No.	Title	Remarks
1.	VISSR PPS - ON	
	VISSR PPS - OFF	
2.	VISSR RPS - ON	
	VISSR RPS - OFF	
3.	VISSR electronics - ON	
	VISSR electronics - OFF	
4.	VISSR scan pwr primary	
	VISSR scan pwr redundant	

Word 15 Bilevel

Bit No.	Title	Remarks
5.	X-ray "CALIBRATE"	
	X-ray "DATA"	
6.	X-ray short scale 1 bit 1 ONE	
	X-ray short scale 1 bit 1 ZERO	
7.	X-ray short scale 2 bit 1 ONE	
	X-ray short scale 2 bit 1 ZERO	
8.	X-ray short sun 1 bit 1 ONE	
	X-ray short sun 1 bit 1 ZERO	
9.	X-ray short sun 2 bit 1 ONE	
	X-ray short sun 2 bit 1 ZERO	

Word 17 Bilevel

Bit No.	Title	Remarks
1.	VISSR CAL CMD On	
	VISSR CAL CMD Off	
2.	VISSR CH 1 Position 1	
	VISSR CH 1 Position 2	
3.	VISSR CH 1 Position 3	
	VISSR CH 1 Position 4	
4.	VISSR CH 2 Position 1	
	VISSR CH 2 Position 2	

Word 17 Bilevel

Bit No.	Title	Remarks
5.	VISSR CH 2 Position 3	
	VISSR CH 2 Position 4	
6.	X-ray long scale 1 bit 1 ONE	
	X-ray long scale 1 bit 1 ZERO	
7.	X-ray long scale 2 bit 1 ONE	
	X-ray long scale 2 bit 1 ZERO	
8.	X-ray long sun 1 bit 1 ONE	
	X-ray long sun 1 bit 1 ZERO	
9.	X-ray long sun 2 bit 1 ONE	
	X-ray long sun 2 bit 1 ZERO	

Word 21 Bilevel

Bit No.	Title	Remarks
1.	VISSR CH 3 Position 1	
	VISSR CH 3 Position 2	
2.	VISSR CH 3 Position 3	
	VISSR CH 3 Position 4	
3.	VISSR CH 4 Position 1	
	VISSR CH 4 Position 2	
4.	VISSR CH 4 Position 3	
	VISSR CH 4 Position 4	

Word 21 Bilevel

Bit No.	Title	Remarks
5.	VISSR CH 5 Position 1	
	VISSR CH 5 Position 2	
6.	VISSR CH 5 Position 3	
	VISSR CH 5 Position 4	
7.	VISSR CH 6 Position 1	
	VISSR CH 6 Position 2	
8.	VISSR CH 6 Position 3	
	VISSR CH 6 Position 4	
9.	VISSR RAD cover latched	
	VISSR RAD cover unlatched	

Word 31 Bilevel

Bit No.	Title	Remarks
1.	CMD decoder 1 on	
	CMD decoder 1 off	
2.	CMD decoder 2 on	
	CMD decoder 2 off	
3.	APS valve 1 open	
	APS valve 1 closed	
4.	APS valve 2 open	
	APS valve 2 closed	

Word 31 Bilevel

Bit No.	Title	Remarks
5.	CMD sample LSB bit 1 ONE	
	CMD sample LSB bit 1 ZERO	
6.	CMD sample MSB bit 1 ONE	
	CMD sample MSB bit 1 ZERO	
7.	Spare	
	Spare	
8.	Spare	
	Spare	
9.	Arm (one)	
	Safe (zero)	

Word 33 Bilevel

Bit No.	Title	Remarks
1.	EPS CAL on	
	EPS CAL off	
2.	EPS E_1 P_1 bit 1 ONE	
	EPS E_1 P_1 bit 1 ZERO	
3.	EPS E_1 P_1 bit 2 ONE	
	EPS E_1 P_1 bit 2 ZERO	
4.	EPS E_1 P_1 bit 3 ONE	
	EPS E_1 P_1 bit 3 ZERO	

Word 33 Bilevel

Bit No.	Title	Remarks
5.	EPS E_1 P_1 bit 4 ONE	
	EPS E_1 P_1 bit 4 ZERO	
6.	EPS E_1 P_1 bit 5 ONE	
	EPS E_1 P_1 bit 5 ZERO	
7.	EPS E_1 P_1 bit 6 ONE	
	EPS E_1 P_1 bit 6 ZERO	
8.	EPS E_1 P_1 bit 7 ONE	
	EPS E_1 P_1 bit 7 ZERO	
9.	EPS E_1 P_1 bit 8 ONE	
	EPS E_1 P_1 bit 8 ZERO	

Word 36 Bilevel

Bit No.	Title	Remarks
1.	Spare	
2,	Spare	
3.	Spare	
4.	Spare	
5.	Spare	
6.	Spare	
7.	Spare	

Word 36 Bilevel

Bit No.	Title	Remarks
8.	Spare	
9.	Spare	

Word 37 Bilevel

Bit No.	Title	Remarks
1.	VISSR CH 7 position 1	
	VISSR CH 7 position 2	
2.	VISSR CH 7 position 3	
	VISSR CH 7 position 4	
3.	VISSR CH 8 position 1	
	VISSR CH 8 position 2	
4.	VISSR CH 8 position 3	
	VISSR CH 8 position 4	
5.	VISSR heater No. 1 on	
	VISSR heater No. 1 off	
6.	VISSR heater No. 2 on	
	VISSR heater No. 2 off	
7.	VISSR heater control on	
	VISSR heater control off	
8.	VISSR mirror stow latched	
	VISSR mirror stow unlatched	

Word 37 Bilevel

Bit No.	Title	Remarks
9.	VISSR mirror stow CMD on	
	VISSR mirror stow CMD off	

Word 47 Bilevel

Bit No.	Title	Remarks
1.	VISSR CH-1 high voltage supply on	
	VISSR CH-1 high voltage supply off	
2.	VISSR CH-2 high voltage supply on	
	VISSR CH-2 high voltage supply off	
3.	VISSR CH-3 high voltage supply on	
	VISSR CH-3 high voltage supply off	
4.	VISSR CH-4 high voltage supply on	
	VISSR CH-4 high voltage supply off	
5.	VISSR CH-5 high voltage supply on	
	VISSR CH-5 high voltage supply off	
6.	VISSR CH-6 high voltage supply on	
	VISSR CH-6 high voltage supply off	
7.	VISSR CH-7 high voltage supply on	
	VISSR CH-7 high voltage supply off	
8.	VISSR CH-8 high voltage supply on	
	VISSR CH-8 high voltage supply off	

Word 47 Bilevel

Bit No.	Title	Remarks
9.	Spare	
	Spare	

Word 49 Bilevel

Bit No.	Title	Remarks
1.	VISSR radiator cage latch	
	VISSR radiator cage unlatch	
2.	VISSR thermal focus limit reverse	
	VISSR thermal focus limit off	
3.	VISSR thermal focus limit forward	
	VISSR thermal focus limit off	
4.	VISSR thermal CH focus CMD forward	
	VISSR thermal CH focus CMD off	
5.	VISSR thermal CH focus CMD reverse	
	VISSR thermal CH focus CMD off	
6.	VISSR visible focus limit reverse	
	VISSR visible focus limit off	
7.	VISSR visible focus limit forward	
	VISSR visible focus limit off	
8.	VISSR visible CH focus CMD forward	
	VISSR visible CH focus CMD off	

Word 49 Bilevel

Bit No.	Title	Remarks
9.	VISSR visible CH focus CMD reverse	
	VISSR visible CH focum CMD off	

Word 53 Bilevel

Bit No.	Title	Remarks
1.	Spare	
2.	Spare	
3.	EPS proton and alpha particles bit 1 ONE	
	EPS proton and alpha particles bit 1 ZERO	
4.	EPS proton and alpha particles bit 2 ONE	
	EPS proton and alpha particles bit 2 ZERO	
5.	EPS proton and alpha particles bit 3 ONE	
	EPS proton and alpha particles bit 3 ZERO	
6.	EPS proton and alpha particles bit 4 ONE	
	EPS proton and alpha particles bit 4 ZERO	
7.	EPS proton and alpha particles bit 5 ONE	
	EPS proton and alpha particles bit 5 ZERO	
8.	EPS proton and alpha particles bit 6 ONE	
	EPS proton and alpha particles bit 6 ZERO	
9.	EPS proton and alpha particles bit 7 ONE	
	EPS proton and alpha particles bit 7 ZERO	

Word 63 Bilevel

Bit No.	Title	Remarks
1.	X-ray on sun yes	
	X-ray on sun no	
2.	EPS - proton and alpha particles bit 1 ONE	
	EPS - proton and alpha particles bit 1 ZERO	
3.	EPS - proton and alpha particles bit 2 ONE	
	EPS - proton and alpha particles bit 2 ZERO	
4.	EPS - proton and alpha particles bit 3 ONE	
	EPS - proton and alpha particles bit 3 ZERO	
5.	EPS - proton and alpha particles bit 4 ONE	
	EPS - proton and alpha particles bit 4 ZERO	
6.	EPS - proton and alpha particles bit 5 ONE	
	EPS - proton and alpha particles bit 5 ZERO	
7.	EPS - proton and alpha particles bit 6 ONE	
	EPS - proton and alpha particles bit 6 ZERO	
8.	EPS - proton and alpha particles bit 7 ONE	
	EPS - proton and alpha particles bit 7 ZERO	
9.	EPS - proton and alpha particles bit 8 ONE	
	EPS - proton and alpha particles bit 8 ZERO	

Main Frame 60

32-Ch Submultiplexer - (all temp data) Word 29

Bit No.	Title	Remarks
1.	S/A - BATT relay open	
	S/A - BATT relay closed	
2.	ABM not fired	
	ABM fired	
3.	VHF rec. 1 signal present	
	VHF rec. 1 signal not present	
4.	VHF rec. 2 signal present	
	VHF rec. 2 signal not present	
5.	VISSR MUX mode bit 1 ONE	
	VISSR MUX mode bit 1 ZERO	
6.	VISSR MUX mode bit 2 ONE	
	VISSR MUX mode bit 2 ZERO	
7.	VISSR MUX dc/dc converter select 1	
	VISSR MUX dc/dc converter select 2	
8.	VISSR MUX on	
	VISSR MUX off	
9.	VISSR MUX to comm 1	
	VISSR MUX to comm 2	

Main Frame 60

32-Ch Submultiplexer - (all temp data) Word 30

Bit No.	Title	Remarks
1.	S-band transponder 1	
	S-band transponder 2	
2.	UHF transponder 1	
	UHF transponder 2	
3.	S-band power low	
	S-band power high	
4.	UHF power low	
	UHF power high	
5.	S-band receiver 1 signal present yes	
	S-band receiver 1 signal present no	
6.	S-band receiver 2 signal present yes	
	S-band receiver 2 signal present no	
7.	Spare	
8.	Spare	
9.	Spare	

Main Frame

32-Ch Submultiplexer - (all temp data) Word 31

Bit No.	Title	Remarks
1.	ADAC ANT bias bit 1 ONE	
	ADAC ANT bias bit 1 ZERO	
2.	ADAC ANT bias bit 2 ONE	
	ADAC ANT bias bit 2 ZERO	
3.	ADAC ANT bias bit 3 ONE	
	ADAC ANT bias bit 3 ZERO	
4.	ADAC ANT bias bit 4 ONE	
	ADAC ANT bias bit 4 ZERO	
5.	ADAC ANT bias bit 5 ONE	
	ADAC ANT bias bit 5 ZERO	
6.	ADAC ANT bias bit 6 ONE	
	ADAC ANT bias bit 6 ZERO	
7.	ADAC - spacecraft normal	
	ADAC - spacecraft inverted	
8.	Active nutation damping "Auto"	
	Active nutation damping "Manual"	
9.	Active nutation damper "On"	
	Active nutation damper "Off"	

Main Frame 60

32-Ch Submultiplexer - (all temp data) Word 32

Bit No.	Title	Remarks
1.	ADAC on	
	ADAC off	
2.	ADAC #1 on	
	ADAC #2 on	
3.	ADAC freq lock loop "in lock"	
	ADAC freq lock loop "not in lock"	
4.	ADAC reference "earth"	
	ADAC reference "sun"	
5.	On sun sensor 1	
	On sun sensor 2	
6.	ANT dc/dc converter on	
	ANT dc/dc converter off	
7.	ANT control bus "normal"	
	ANT control bus "eclipse"	
8.	ADAC reference pseudo earth on	
	ADAC reference pseudo earth off	
9.	17° earth sensors on	
	17° earth sensors off	

NOTES: 1. Not Sampled in Dwell mode
2. Sampled every other frame in dwell mode

APPENDIX B

COMMAND FUNCTION LIST

VISSR MUX

Command	Output Characteristics
Select mode 1	Relay driver
Select mode 2	Relay driver
Select mode 3	Relay driver
Select mode 4	Relay driver
VISSR mux ON	Latch relay 0.1 amp
VISSR mux OFF	Latch relay 0.1 amp
Select VISSR mux 1	Latch relay 0.1 amp
Select VISSR mux 2	Latch relay 0.1 amp
Select normal bit rate	Pulse
Select reduced bit rate	Pulse
VISSR mux auto eclipse	Latch relay 0.1 amp
VISSR mux auto eclipse override	Latch relay 0.1 amp
Select S-band transponder 1	Pulse
Select S-band transponder 2	Pulse
Mux normal	Latch relay 0.1 amp
Mux ADAC override	Latch relay 0.1 amp

VISSR Subsystem Command List

Command	Output Characteristics
Mirror stow on	Relay driver
Scan mirror stow off	Relay driver
Radiator cover eject	Pulse
Radiator heater No. 1 on	Relay driver
Radiator heater No. 2 on	Relay driver
Radiator heaters and temperature control off	Pulse
Primary power supply on	Relay driver
Redundant power supply on	Relay driver
Power supplies off	2 relay drivers
Radiator temperature control on	Relay driver
Visible channel electronics on	Relay driver
Visible channel No. 1 high voltage supply on	Relay driver
Visible channel No. 2 high voltage supply on	Relay driver
Visible channel No. 3 high voltage supply on	Relay driver
Visible channel No. 4 high voltage supply on	Relay driver
Visible channel No. 5 high voltage supply on	Relay driver
Visible channel No. 6 high voltage supply on	Relay driver
Visible channel No. 7 high voltage supply on	Relay driver
Visible channel No. 8 high voltage supply on	Relay driver
Visible channels off	Pulse

VISSR Subsystem Command List
(continued)

Command	Output Characteristics
Visible channel No. 1 gain adjust	Pulse
Visible channel No. 2 gain adjust	Pulse
Visible channel No. 3 gain adjust	Pulse
Visible channel No. 4 gain adjust	Pulse
Visible channel No. 5 gain adjust	Pulse
Visible channel No. 6 gain adjust	Pulse
Visible channel No. 7 gain adjust	Pulse
Visible channel No. 8 gain adjust	Pulse
Visible channel focus, forward	Pulse
Visible channel focus, reverse	Pulse
Thermal channel focus, forward	Pulse
Thermal channel focus, reverse	Pulse
Internal calibrate, on	Relay driver
Primary drive select	Relay driver
Scanner drive No. 2 select	Relay driver
Scanner stepping on	Pulse
Scanner stepping off	Pulse
Scanner stepping direction reverse	Pulse
Normal step rate	Pulse
Rapid step rate	Pulse

SEM SUBSYSTEM

Particle Detector

Command	Output Characteristics
Particle detector on	Latch relay 0.1 amp
Particle detector off	Latch relay 0.1 amp
Particle detector cal on	Pulse
Particle detector cal off	Pulse
Particle detector automatic eclipse	Latch relay 0.1 amp
Particle detector auto eclipse override	Latch relay 0.1 amp

Magnetometer

Command	Output Characteristics
Magnetometer on	Latch relay 0.1 amp
Magnetometer off	Latch relay 0.1 amp
Magnetometer calibrate on	Pulse
Magnetometer calibrate off	Pulse

X-ray Sensor

Command	Output Characteristics
X-ray sensor on	Latch relay 0.1 amp
X-ray sensor off	Latch relay 0.1 amp
X-ray sensor cal on	Pulse
X-ray sensor cal off	Pulse

X-ray Sensor
(continued)

Command	Output Characteristics
X-ray sensor auto eclipse	Latch relay 0.1 amp
X-ray position forward	Latch relay 0.1 amp
X-ray position reverse	Latch relay 0.1 amp
X-ray position "step"	Pulse

VHF Transponder

Command	Output Characteristics
VHF transmitter on	Latch relay 1.0 amp
VHF transmitter off	Latch relay 1.0 amp
Select VHF transmitter 1	Latch relay 1.0 amp
Select VHF transmitter 2	Latch relay 1.0 amp
VHF transmitter automatic eclipse	Latch relay 1.0 amp
VHF transmitter automatic eclipse override	Latch relay 1.0 amp
VHF transmitter low power	Latch relay TBD
VHF transmitter high power	Latch relay TBD

Communications Subsystem

Command	Output Characteristics
S-band RF switch 1, Position 1	Pulse
S-band RF switch 1, Position 2	Pulse
S-band RF switch 2, Position 1	Pulse

Communications Subsystem
(continued)

Command	Output Characteristics
S-band RF switch 2, position 2	Pulse
S-band RF switch 3, position 1	Pulse
S-band RF switch 3, position 2	Pulse
S-band RF switch 4, position 1	Pulse
S-band RF switch 4, position 2	Pulse
S-band RF switch 5, position 1	Pulse
S-band RF switch 5, position 2	Pulse
S-band RF switch 5, position 3	Pulse
S-band RF switch 6, position 1	Pulse
S-band RF switch 6, position 2	Pulse
S-band RF switch 6, position 3	Pulse
S-band RF switch 7, position 1	Pulse
S-band RF switch 7, position 2	Pulse
S-band RF switch 7, position 3	Pulse
S-band RF switch 8, position 1	Pulse
S-band RF switch 8, position 2	Pulse
S-band RF switch 8, position 3	Pulse
S-band transponder on	Latch relay 0.1 amp
S-band transponder off	Latch relay 0.1 amp

Communications Subsystem
(continued)

Command	Output Characteristics
S-band transponder auto eclipse	Latch relay 0.1 amp
S-band transponder auto eclipse override	Latch relay 0.1 amp
S-band transponder select 1	Latch relay 0.1 amp
S-band transponder select 2	Latch relay 0.1 amp
Select S-band power amp 1	Latch relay 5.0 amp
Select S-band power amp 2	Latch relay 5.0 amp
S-band power amp auto eclipse	Latch relay 5.0 amp
S-band power amp auto eclipse override	Latch relay 5.0 amp
Squelch wide band IF amp	Latch relay 0.1 amp
Wide band IF amp normal	Latch relay 0.1 amp

UHF Transponder

Command	Output Characteristics
UHF RF switch 1, position 1	Pulse
UHF RF switch 1, position 2	Pulse
UHF RF switch 2, position 1	Pulse
UHF RF switch 2, position 2	Pulse
UHF RF switch 3, position 1	Pulse
UHF RF switch 3, position 2	Pulse
UHF RF switch 4, position 1	Pulse

UHF Transponder
(continued)

Command	Output Characteristics
UHF RF switch 4, position 2	Pulse
UHF RF switch 5, position 1	Pulse
UHF RF switch 5, position 2	Pulse
UHF RF switch 6, position 1	Pulse
UHF RF switch 6, position 2	Pulse
UHF transponder on	Latch relay 0.1 amp
UHF transponder off	Latch relay 0.1 amp
Select UHF transponder 1	Latch relay 0.1 amp
Select UHF transponder 2	Latch relay 0.1 amp
UHF transponder auto eclipse	Latch relay 0.1 amp
UHF transponder auto eclipse override	Latch relay 0.1 amp
Select UHF power amp 1	Latch relay 0.1 amp
Select UHF power amp 2	Latch relay 0.1 amp
UHF power amp on	Latch relay 0.1 amp
UHF power amp off	Latch relay 0.1 amp
UHF power auto eclipse	Latch relay 0.1 amp
UHF power amp auto eclipse override	Latch relay 0.1 amp
Select UHF local oscillator chain	Latch relay 0.1 amp
Select S-band local oscillator chain	Latch relay 0.1 amp

Power Subsystem

Command	Output Characteristics
ABM safe - AGE only	Latch relay 1.0 amp
ABM arm - AGE only	Latch relay 1.0 amp
ABM ignite	Pulse
ABM separation	Pulse
Uncage passive nutation damper	Pulse
Battery charge on	Latch relay 5.0 amp
Battery charge off	Latch relay 5.0 amp
Boost conv. on	Latch relay 0.1 amp
Undervoltage override	Latch relay 0.1 amp
Boost conv. off	Latch relay 0.1 amp
Undervoltage override	Latch relay 0.1 amp
Boost conv. enable	
Undervoltage override reset	
Sun presence normal	Latch relay 0.1 amp
Sun presence override	Latch relay 0.1 amp
AGE, ADAC, CMD - AGE only	
Auto dummy load override	Latch relay 0.1 amp
Auto dummy load normal (reset)	Latch relay 0.1 amp

Auxiliary Propulsion Subsystem

Command	Output Characteristics
0.5 RT 1 line valve open	Latch relay 0.1 amp
0.5 RT 1 line valve close	Latch relay 0.1 amp
0.5 RT 2 line valve open	Latch relay 0.1 amp
0.5 RT 2 line valve close	Latch relay 0.1 amp
5.0 LB radial thruster #1 fire	Pulse
5.0 LB radial thruster #2 fire	Pulse
0.5 LB radial thruster #1 fire	Pulse
0.5 LB radial thruster #2 fire	Pulse
5.0 LB axial thruster #1 fire	Pulse
5.0 LB axial thruster #2 fire	Pulse
Latch valve 1 open	Pulse
Latch valve 1 close	Pulse
Latch valve 2 open	Pulse
Latch valve 2 close	Pulse

Telemetry and Command Subsystem

Command	Output Characteristics
Select telemetry unit 1	Latch relay 1.0 amp
Select telemetry unit 2	Latch relay 1.0 amp
Telemetry on	Latch relay 0.1 amp

Telemetry and Command Subsystem
(continued)

Command	Output Characteristics
Telemetry off	Latch relay 0.1 amp
Normal mode	Latch relay 0.1 amp
Dwell mode	Latch relay 0.1 amp
Select dwell channel	Pulse
PCM modulation select 1	Latch relay 0.1 amp
PCM modulation select 2	Latch relay 0.1 amp
Real-time modulation select 1	Latch relay 0.1 amp
Real-time modulation select 2	Latch relay 0.1 amp
Ranging mode on	Latch relay 0.1 amp
Ranging mode off	Latch relay 0.1 amp
Temp sense power 1	Latch relay 1.0 amp
Temp sense power 2	Latch relay 1.0 amp
TLM 1 power to ADAC	Latch 1.0 amp
TLM 2 power to ADAC	Latch 1.0 amp

Attitude Determination and Antenna Control (ADAC) Subsystem

Command	Output Characteristics
Sun/earth angle data	Pulse
Sun/earth angle data load cmd	Pulse
Ant control bus 1 array power	Latch relay 5.0 amp

Attitude Determination and Antenna Control (ADAC) Subsystem

Command	Output Characteristics
Ant control bus 1 eclipse power	Latch relay 5.0 amp
Ant control bus 2 array power	Latch relay 5.0 amp
Ant control bus 2 eclipse power	Latch relay 5.0 amp
UHF ant on	Latch relay 0.1 amp
UHF ant off	Latch relay 0.1 amp
S-band ant on	Latch relay 0.1 amp
S-band ant off	Latch relay 0.1 amp
VISSR mux normal	Latch relay 0.1 amp
VISSR mux turn off inhibit	Latch relay 0.1 amp
Active nutation damp manual	Latch relay 0.1 amp
Active nutation damp normal	Latch relay 0.1 amp
Active nutation damp power on	Latch relay 0.1 amp
Active nutation damp power off	Latch relay 0.1 amp

ADAC Subsystem

Command	Output Characteristics
PSEUDO earth pulse (gnd cmd)	Pulse
Earth sensor 1 & 2 on	Latch relay 0.1 amp
Earth sensor 1 & 2 off	Latch relay 0.1 amp
Earth sensor 3 & 4 on	Latch relay 0.1 amp

ADAC Subsystem
(continued)

Command	Output Characteristics
Earth sensor 3 & 4 off	Latch relay 0.1 amp
Select earth sensor 1 (RTD)	Latch relay 0.1 amp
Select earth sensor 2 (RTD)	Latch relay 0.1 amp
Select sun sensor 1 (RTD)	Latch relay 0.1 amp
Select sun sensor 2 (RTD)	Latch relay 0.1 amp
Spacecraft normal	Latch relay 0.1 amp
Spacecraft inverted	Latch relay 0.1 amp
Sensor 1 reference	Latch relay 0.1 amp
Sensor 2 reference	Latch relay 0.1 amp
Sun sensor reference	Latch relay 0.1 amp
Earth sensor reference	Latch relay 0.1 amp
PSEUDO earth pulse reference	Latch relay 0.1 amp
Normal earth pulse reference	Latch relay 0.1 amp
ADAC electronics on	Latch relay 0.1 amp
ADAC electronics off	Latch relay 0.1 amp
Select ADAC elect #1	Latch relay 1.0 amp
Select ADAC elect #2	Latch relay 1.0 amp
Auto eclipse	Latch relay 0.1 amp
Auto eclipse override	Latch relay 0.1 amp

ADAC Subsystem
(continued)

Command	Output Characteristics
Bit 1 one	Latch relay 0.1 amp
Ant bias angle bit 1 zero	Latch relay 0.1 amp
Ant bias angle bit 2	Latch relay 0.1 amp
Ant bias angle bit 2	
Ant bias angle bit 3	Latch relay 0.1 amp
Ant bias angle bit 3	
Ant bias angle bit 4	Latch relay 0.1 amp
Ant bias angle bit 4	
Ant bias angle bit 5	Latch relay 0.1 amp
Ant bias angle bit 5	
Ant bias angle bit 6	Latch relay 0.1 amp
Ant bias angle bit 6	
Load ant bias angle	Pulse